An investigation of the ABA laser cladding process; A new Laser – Direct Energy Deposition (DED) technique.

By

Daniel Koti

Supervisor: Dr. Katy T. Voisey

Co-supervisor: Dr. John Powell

Faculty of Engineering

Department of Mechanical, Materials and Manufacturing Engineering

Research group: Advanced materials

August 2023

Table of contents

List of Figures

List of Tables

List of symbols and abbreviations

A	The entire surface area of the cladding [m^2]
A_c	Cladding area above the substrate [m^2]
AISI	American Iron and Steel Institute
A_s	Substrate area [m^2]
A_{track}	Cross-sectional area of a single track above the original line of the substrate [m^2]
BDMS	Bright drawn mild steel
BPP	Beam Parameter Product
C	Clad height [mm]
CAD	Computer aided design
CNC	Computer numerically controlled
CW	Continuous mode
D	Diameter of the unfocused laser beam [mm]
$D_{(wt\%)}$	Metallurgical dilution [%]
D_{AREA}	Dilution by area measurement [%]
D_{EDX}	Dilution by EDX analysis [%]
D_{HEIGHT}	Dilution by height measurement [%]
d_{foc}	Focal spot diameter [mm]
DED	Directed energy deposition
EDX	Energy Dispersive X-ray spectroscopy
E_{pc}	Powder catchment efficiency [%]
E_{sp}	Specific point energy [J]
f	Focal length of the lens [mm]
F_p	Powder feed rate [g/min]

h	Planck`s constant
HAZ	Heat affected zone
HSI	High Speed Image
$I_{(x,y)}$,	Power density [W/mm^2]
K	Beam quality factor, equal to 1/M^2
LASER	Light Amplification by the Stimulated Emission of Radiation
LC	Laser cladding
LMD	Laser metal deposition
n	The number of the layers
OF	Optical Flow
PIV	Particle Image Velocimetry
P_L	Laser power [W]
r_b	Beam radius [mm]
S	Clad depth [mm]
SEM	Scanning electron microscope
t	The time to cover the surface [h]
T_{area}	Track cross sectional area above the original line of the substrate surface [mm^2]
v	Process speed [m/h]
W_0	Focused beam radius [mm]
$wt\%_c$	The weight percentage of element X in the additive material
$wt\%_{c+s}$	The local weight percentage of element X in the clad region
$wt\%_s$	The weight percentage of element X in the substrate material
y	Inter track distance [mm]
$Z_{Rayleigh}$	Rayleigh distance [mm]

θ	Divergence angle [°]
λ	Wavelength of the laser light [nm]
ρ	Density of cladding material [kg/m^3]
ρ_c	Density of the additive powder [kg/m^3]
ρ_s	Density of substrate [kg/m^3]
τ	Interaction time (s)

Preface

The thesis has been submitted for the degree of Doctor of Philosophy at the University of Nottingham. The research was conducted under the supervision of Dr Katy Voisey and Dr John Powell in the department of Mechanical, Materials and Manufacturing Engineering.

The list of Publications from the work presented in this thesis is listed below:

I. Koti, D., Powell, J. and Voisey, K.T., 2022. Improving laser cladding productivity with 'ABA' cladding. Procedia CIRP, 111, pp.205-209, https://doi.org/10.1016/j.procir.2022.08.048

II. Powell, J., Koti, D., Garmendia, X. and Voisey, K.T., 2023. Assessing the quality and productivity of laser cladding and direct energy deposition: Guidelines for researchers. Journal of Laser Applications, 35(1), p.012024, https://doi.org/10.2351/7.0000897

III. Koti, D., Powell, J., Naesstroem, H. and Voisey, K.T., 2023. Powder catchment efficiency in laser cladding (directed energy deposition). An investigation into standard laser cladding and the ABA cladding technique. Journal of Laser Applications, 35(1), p.012025, https://doi.org/10.2351/7.0000904

IV. Koti, D., Powell, J., Naesstroem, H., Spaccapaniccia, C. and Voisey, K.T., 2023. Laser cladding: A high-speed-imaging examination of powder catchment efficiency as a function of the melt pool geometry and its position under the powder stream. Journal of Laser Applications, 35(4), https://doi.org/10.2351/7.0001199

I declare that the thesis is the product of my own efforts and has been undertaken primarily during my time as a student at The University of Nottingham. I have complied with the 100,000-word limit. In the thesis, references to work other than my own have been properly cited.

Daniel Koti

August 2023

My parents have always believed that if I have arms only 50 cm, I'll never be able to reach anything in my life. Training my mind is just as important as training my body. Although I have 48 cm arms, I can only bench press 200 kg, squat 260 kg, and deadlift 300 kg. As a result of my PhD, they now have something to be proud of.

Daniel Koti

Acknowledgements

I would like to thank the Centre for Doctoral Training in Innovative Metal Processing (IMPaCT) for funding my research.

I genuinely appreciate the opportunity that Dr Katy Voisey and Dr John Powell, my supervisors, granted me. During this time, they always made an effort to support my work and me, and it is thanks to their assistance that I have become the researcher that I am today. Moreover, the invaluable support, advice and mentoring during my three years of doctoral research. I learnt to be critical to ideas, progress logically through the course of an investigation and think rationally from working with them. It has been a life changing experience for me.

The work presented in this thesis would have not been possible without the help of the technical team at Wolfson building (Jason Greaves, Kieran Orange, Richard Homer, Rebecca Saint, Daniel Flower), the Nanoscale and Microscale Research Centre (Martin Roe, Lorelei Roberston) and the Advanced Manufacturing building (Alexander Jackson-Crisp). I will always be grateful to all of them.

I would like to acknowledge the assistance of Professor Alexander Kaplan and Dr Himani Naesstroem in conducting the experiments in Luleå University of Technology.

It is my pleasure to acknowledge the assistance offered by Dr Chiara Spaccapaniccia who patiently guided me through challenging times.

The same can be said about all the colleagues that I had the pleasure to work with. Every single one of the members of the Advanced materials research group, and other teams working at Wolfson. They all provided me with their knowledge and friendship, and these years would have been quite different without them.

My family will always have a special place in my heart. I would like to thank to my father Sandor Koti, my mother Magdolna Feher, my brother David Koti, who supported me, and believed in me throughout the years, allowing me to follow my passion.

Finally, in recognition of my wife Diana Koti, I am incredibly grateful, who always believed in me that I can be real scientist one day. I cannot imagine a better person to share this journey with. Throughout the good and tough times, she is always by my side, offering me her support and encouragement.

Dedicated To my Son Mathias Gabriel Koti.

Abstract

Blown powder directed energy deposition (DED), commonly known as laser metal deposition (LMD), is discussed in this thesis. All industries demand engineering components with required surface characteristics, including suitable wear and corrosion resistance and hardness properties. Thus, in some cases high-grade alloys are essential to achieve the desired surface quality. However, industries are primarily interested in reducing the cost of engineering parts with these surface characteristics. With a cheaper substrate material and the appropriate coating alloy, cost reductions can be achieved very easily. High powder catchment efficiency, deposition rate and coverage rate can enhance productivity and increase cost-effectiveness. Laser cladding is an effective technique for changing the physical and chemical properties of material surfaces.

This thesis starts by providing guidelines and advice for researchers and engineers in the field of laser cladding and related Direct Energy Deposition (DED) techniques, to help establish a standardised approach to quality assessment and productivity metrics. Factors considered are; deposit geometry, porosity, cracking, dilution, deposition rate/coverage rate and powder catchment efficiency. Although there is an exceptionally large body of research work on laser cladding and related Direct Energy Deposition (DED) techniques, there are no clear guidelines about which quality and productivity parameters are important to the relevant branches of industry, nor are there any general rules about what constitutes a high-quality deposit.

The main focus of the work in this thesis concerns investigation of a new laser cladding technique (‘ABA’ cladding) wherein a series of separate, or only slightly overlapping clad tracks are laid down initially (the ‘A’ tracks), and these are later interleaved with tracks which can use different parameters (the ‘B’ tracks). ‘ABA’ cladding was found to have considerable benefits over traditional laser cladding including improved powder catchment efficiency and coverage rates, more predictable metallurgy, and dilution levels. The ‘ABA’ process was studied in order to understand the underlying reasons for the observed benefits. The majority of the study was conducted using high-speed video frames, in conjunction with cross-sectional and surface images of the clad and quantitative analysis of the results. Manufacturing companies could benefit from several of the results generated.

1 Chapter I. Introduction

1.1 Background and problem definitions

Engineering components consider the surface to be the most important part since most failures occur at the surface. Consequently, a field of engineering has been established, called "surface engineering", which mainly focuses on modifying surface properties in accordance with requirements to improve the functionality of surface manufactured products [1, 2]. In addition to fatigue, corrosion and wear resistance are the three primary factors influencing the life expectancy of engineering components [3]. The cost of maintenance, repair, part replacement, and shutdowns caused by these factors has an enormous economic impact on industries. In surface engineering, processes such as surface modification, alloying, and coating, can provide a solution to increased resistance to wear, corrosion and oxidation; improvement in mechanical, electrical, electronic, and thermal properties; improve the lubrication properties and reduce friction coefficients [4]. This treatment may be achieved by deposit of a clad on the substrate surface or by modifying the surface itself [5]. Surface engineering includes a variety of processes used to alter the surface characteristics of material components, ranging from conventional techniques to more advanced coating techniques and surface treatment methods [6].

Lasers have a vital role in modern technology. Due to its versatility, laser manufacturing has become one of the most valuable and versatile tools for material processing. One of its most important characteristics is its ability to achieve very high-power densities when focused. Therefore, it is suitable for heating, melting, evaporating, bringing to a plasma state, and, as a result, it can also be used for heat treatment, labelling, cladding, and cutting. A rapidly growing research area is laser surface engineering, which enhances the performance of a variety of components in many different applications [7, 8]. Laser surfacing technology produces metallurgically bonded coatings rather than mechanically bonded coatings. Often, laser-surfaced coatings have a greater thickness than coatings produced by other surface engineering methods. There are several lasers supported surface modification processes available, including: laser surface melting [9], laser surface alloying [10] and laser surface cladding [11]. There have been a number of approaches that have demonstrated the effectiveness of using lasers to improve surface properties, and laser cladding (LC) may be considered the most versatile method of improving surface properties.

All industries demand engineering components with required surface characteristics, including suitable wear and corrosion resistance and hardness properties. Industries are primarily interested in reducing the cost of engineering parts with these surface characteristics [12]. With a cheaper substrate material and the appropriate coating alloy, cost reductions can be achieved very easily. Laser cladding is an effective technique for changing the physical and chemical properties of material surfaces [7, 13]. The application of laser cladding is one of the different coating methods that offers advantages over other surface engineering technologies. Among them are substantial metallurgical bond at the substrate-coating interface [14, 15], low substrate distortion [16], minimal dilution [17], low porosity and controlled heat input with low heat affected zone (HAZ) [18]. In 1976, AVCO Everett research laboratory in the United States patented the use of lasers for cladding [19]. By melting an additive material and a thin layer of a substrate simultaneously, laser acts as the heat source for creating a meltpool. A track is formed when the laser beam moves relative to the substrate. It is common to refer to the track as a clad bead. As a feedstock material, wire or powder can be used for cladding. Overlapping tracks can be used to cover a component completely. To perform laser cladding, a CO_2 laser, or a variety of Nd:YAG lasers are commonly used. As a result of their greater efficiency, cost savings, and adaptability to various working environments, fibre lasers are rapidly replacing traditional lasers [20, 21]. In contrast to CO_2 lasers, fibre lasers use an integrated optical fibre to deliver their energy, allowing considerable flexibility in how the cladding is designed. Additionally, fibre laser beams provide excellent beam quality as well as the ability to focus to exceedingly small areas [20].

Laser cladding has several applications across a wide range of industries, including aircraft, aerospace, automotive, tooling, and manufacturing [22, 24, 25, 26, 27, 28, 29, 30]. Involves the application of high-quality coat surfaces, reconstructing the damaged surfaces, deposition of hybrid materials [31, 32, 33, 34, 35]. Moreover, laser cladding is a highly effective method of improving abrasive wear resistance, corrosion resistance, erosion wear resistance [36, 37, 38, 39, 40, 41].

Several commercial laser cladding systems have been available in industry, which are based on powder-based technologies. Wire is becoming more popular in laser metal deposition due to several significant advantages: 100% of the material can be deposited, the process is cleaner, the deposition rate can be high, and the wire feeding system is simple, despite this, it is difficult to control the position of the wire [42, 43].

By using laser cladding with wire instead of powder feeding, the process environment can be kept cleaner, the deposition rate can be increased, and the surface quality can be improved. A wire is also more cost-effective than a powder because the cost of manufacturing a wire is lower.

Compared with wire feed and blown powder processes, the powder injection process provides greater flexibility [44, 45, 46]. Powder alloys are more readily available than wire materials [47, 48]. Furthermore, the method is more reliable than wire cladding, as it does not have direct mechanical contact with the interaction zone [49]. Hence, the laser beam can easily irradiate the substrate surface because the laser is not fully blocked by the powder stream. In general, this method has advantages over alternative methods in terms of energy efficiency [50, 51].

Investigations into laser cladding with blown powder has grown to achieve industrial status, particularly with the development of additive manufacturing. Nowadays, the process commonly utilizes a processing head that supplies a stream of the cladding powder alloy coaxially with a defocused laser beam. One of the aims of the process is to melt all the powder which arrives at the laser-material interaction area into the clad track. Unfortunately, complete capture of all the incoming powder is not generally possible, and a certain percentage of powder escapes the process, often by deflection off the solid material beyond the edges of the melt pool or the surface of the melt pool itself. This ‘escaping’ powder is an important feature of the profitability of the cladding process because the powder is expensive and generally cannot be recycled [52].

The powder catchment efficiency of the process has a strong influence on costs and is thus of prime importance to industrial users. This efficiency is simply the percentage of powder provided to the process which becomes part of the laser melted clad layer. The results of a survey of investigations into DED laser cladding over a wide range of process parameters and different laser types, done as part of this work, reveals that powder catchment can often be well below 50%. This is clearly a problem as the powder is expensive and unused powder cannot be recycled into the cladding process, which depends upon high levels of powder uniformity.

Standard laser cladding involves laying down an initial track on the substrate surface and many research investigations simply compare single tracks of this type laid down under different processing conditions. In industrial practice however, single tracks of this type have very limited application as it is much more common to overlap track one with track two, then track three, etc., until the required clad surface is achieved. The clad tracks are ostensibly identical. However, this similarity only becomes apparent once a few tracks have been laid down. In the initial stages of the process, the previous tracks affect the shape of subsequent ones in various ways. This point is rarely discussed in the literature [509] but is clear in the cross-sections of clad layers presented by most researchers in the field [53, 54, 55, 56, 57]. In this area, there can be major differences in local clad track height, cross-section, and metallurgy. For example, because it is the only track laid upon a flat surface, track 1 will have a different melt pool geometry which will affect powder capture and the level of dilution of the cladding alloy with the substrate compared to subsequent tracks.

Although there is an exceptionally large body of research work on laser cladding with blown powder, there are no clear guidelines about which quality and productivity parameters are important to the relevant branches of industry, nor are there any general rules about what constitutes a high-quality deposit. In particular, in the area of blown powder deposition with fibre laser, the data is limited. There is the need to investigate the links between quality and productivity factors in order to gain a better understanding of the process and to be able to apply it successfully in industry.

1.2 Aims and Objectives

The main aim of this thesis is the improvement of blown powder laser cladding by implementation of a new cladding strategy: ‘ABA’ cladding.

Specific objectives are listed below in order to accomplish these aims:

- Completion of a literature review on laser cladding.
- Review of the various current quality measures used in laser cladding to produce relevant guidelines and advice for researchers and engineers in the field of laser cladding and related Direct Energy Deposition (DED) techniques.
- Demonstration of the novel ‘ABA’ cladding strategy.
- Determination of quantitative information on powder catchment efficiency for ‘ABA’ cladding as a function of cladding parameters.
- Utilisation of high-speed filming and associated analysis to understand the powder-melt pool interactions in ‘ABA’ cladding.

It is of course impossible to cover all the potential ground in one thesis, but many major points are covered and directions to be taken by future work are made clear.

1.3 Organisation of the thesis

This thesis is submitted in the Thesis by Papers format. The overall structure of the thesis is as below. Each of the four results chapters is a submitted and/or already published paper. References are given at the end of each individual chapter.

Preface

The list of Publications from the work presented in this thesis is listed below:

I. Koti, D., Powell, J. and Voisey, K.T., 2022. Improving laser cladding productivity with 'ABA' cladding. Procedia CIRP, 111, pp.205-209, https://doi.org/10.1016/j.procir.2022.08.048

II. Powell, J., Koti, D., Garmendia, X. and Voisey, K.T., 2023. Assessing the quality and productivity of laser cladding and direct energy deposition: Guidelines for researchers. Journal of Laser Applications, 35(1), p.012024, https://doi.org/10.2351/7.0000897

III. Koti, D., Powell, J., Naesstroem, H. and Voisey, K.T., 2023. Powder catchment efficiency in laser cladding (directed energy deposition). An investigation into standard laser cladding and the ABA cladding technique. Journal of Laser Applications, 35(1), p.012025, https://doi.org/10.2351/7.0000904

IV. Koti, D., Powell, J., Naesstroem, H., Spaccapaniccia, C. and Voisey, K.T., 2023. Laser cladding: A high-speed-imaging examination of powder catchment efficiency as a function of the melt pool geometry and its position under the powder stream. Journal of Laser Applications, 35(4), https://doi.org/10.2351/7.0001199

Chapter I. Introduction

Presents a brief overview of the thesis, its overall goal, objectives, and structure.

Chapter II. Literature review

Provides a comprehensive literature review of the topics investigated in this thesis. First, a discussion of the laser cladding technique is presented, emphasizing the current knowledge regarding blown powder deposition, the current state of the art, and the research opportunities identified. Secondly, a discussion of the quality and measuring techniques that are available for direct energy deposition coatings is provided.

The third section of the literature review focuses on laser cladding productivity. High-speed imaging is explained in detail in the last section. The literature chapter concludes with an explanation of research gaps and the hypothesis and objectives of the current study.

Chapter III. Experimental procedures

This chapter provides information on all the experimental methods and equipment used in this study are presented. The principles of the experimental techniques are also included so that readers get a better understanding of the experimental activities carried out in this study**.**

Chapter IV-VII. Published papers

The following sections describe that the thesis is submitted in the form of a thesis paper that contains previously published research. Accordingly, each of the next four discussion chapters was written as an individual paper with an abstract, an introduction, an experimental method, a discussion and a conclusion. For this thesis, each of these papers is designed to be self-contained and unique.

Writing the thesis in paper form will result in some degree of repetition. Firstly, each paper is structured as an independent piece of work, which meets all the requirements for publishing in a journal. In addition, sections such as introduction and experimental methods will contain some repetition, since all of these papers are related in some way. This is because of the uniform methodology and overarching narrative utilized throughout the research, despite different concepts yielding different results.

In Chapters 8 and 9, we'll explain how these four papers interrelate. It'll be accomplished by analysing, integrating, and synthesizing the results to build a cohesive, comprehensive story. The goal of these chapters is to explain how each paper's findings contribute to and interact with the overall themes and hypotheses.

A subchapter has been added to the general discussion chapter where updated versions of graphs are included and explained, which were not included in previous papers. This is due to the fact that the last paper contains the correlation position of meltpool and powder stream / laser beam. The papers have, however, already been published and have been accepted by journal editors who are professionals in the field.

Chapter IV. Assessing the quality and productivity of Laser Cladding and Direct Energy Deposition (DED); Guidelines for researchers.

This paper provides guidelines and advice for researchers and engineers in the field in order to help establish a standardised approach to the quantification of quality assessment in laser cladding. Factors considered are; Geometrical quality, porosity, cracking, and dilution.

Chapter V. Improving laser cladding productivity with 'ABA' cladding.

In this work a new cladding technique is investigated wherein a series of separate, or only slightly overlapping clad tracks are laid down initially (the 'A' tracks) and these are later interleaved with tracks which can use different parameters (the 'B' tracks). The influence of the process parameters was examined in the laser cladding of AISI 316L stainless steel powders and using a coaxial powder delivery nozzle. Process speed, laser power, powder flow rate and overlap strategy and were all found to have an important effect on the process.

Chapter VI. Powder catchment efficiency in laser cladding (Direct Energy Deposition). An investigation into standard laser cladding and the ABA cladding technique

This paper investigates the efficiency of powder catchment in blown powder laser cladding (Direct Energy Deposition) for standard 'track by overlapping track' cladding and for 'ABA' cladding. In both these techniques the melt pool surface is the collection area for the cladding powder and the shape of this pool is affected by several parameters including cladding speed, inter-track spacing and which cladding technique is employed. The results presented here are the result of an analysis of high-speed videos taken during processing.

Chapter VII. Laser cladding (DED); A High-Speed-Imaging examination of powder catchment efficiency as a function of the melt pool geometry and its position under the powder stream.

This paper provides quantitative information about the paths taken by powder particles which enter and do not enter the laser generated melt pool during laser cladding (DED). A proportion of the powder is 'wasted' by bouncing off the solid areas surrounding the melt pool. This wastage reduces the productivity of the process. In this paper, specially developed software was used to analyse High Speed Imaging videos of the cladding process, to monitor the directions of powder particle flight towards and away from the melt pool area.

This information has been correlated to the geometry and position of the melt pool zone for three different cladding techniques; single track cladding (A tracks), standard overlapping track cladding (AAA cladding) and a recently developed technique called ABA cladding. The results show that the melt pool geometry, and particularly the overlap between the melt pool and the incoming powder stream, have a strong influence on powder catchment efficiency.

Chapter VIII. General discussion

A summary of the most important results of each chapter of the thesis and a link between them. Throughout this chapter, the main objective is to explain the key concepts and their implications in a more comprehensive and understandable manner.

Chapter IX. General conclusion and Future work

The final chapter summarizes the scientific contributions made during the course of the project, highlighting future directions for research based on the progress presented.

2 Chapter II. Literature review

2.1 Introduction

This chapter provides a comprehensive literature review of the topics investigated in this thesis. The chapter begins by introducing the laser cladding, beginning with surface engineering, expanding into laser surface engineering techniques, followed by laser cladding, discussing laser cladding techniques and focusing on coaxial blown powder, emphasizing the current state of the art, and the identified research opportunities.

2.2 Introduction to laser cladding

As a surface modification technique, laser cladding is gaining increasing attention in the industry for applications of repair and coating, in addition to rapid prototyping [58-61]. The purpose of this section is to provide a brief overview of the laser cladding procedure and discuss its similarities and differences with other surface modification techniques.

2.2.1 Surface engineering

In most engineering components the surface is the most important part since most failures occur at the surface. Consequently, a field of engineering has been established, called "surface engineering", which mainly focuses on modifying surface properties in accordance with requirements in order to improve the functionality of the surface of manufactured products [0]. In addition to fatigue, corrosion and wear resistance are the primary factors influencing the life expectancy of engineering components [3]. The cost of maintenance, repair, part replacement, and shutdowns caused by these factors has an enormous economic impact on industries. An area of surface engineering that involves the modification, alloying, and coating of surfaces, can provide a solution to increased resistance to wear, corrosion and oxidation; improvement in mechanical, electrical, electronic, and thermal properties; improve the lubrication properties and reduce friction coefficients [4]. This treatment may be achieved by applying a coating on the surface or by modifying the surface itself [5].

The formation of surface layers could decrease, leave unchanged or even increase the size of the object (Figure 2.1). Several techniques can be employed to achieve this; therefore they are classified as follows.

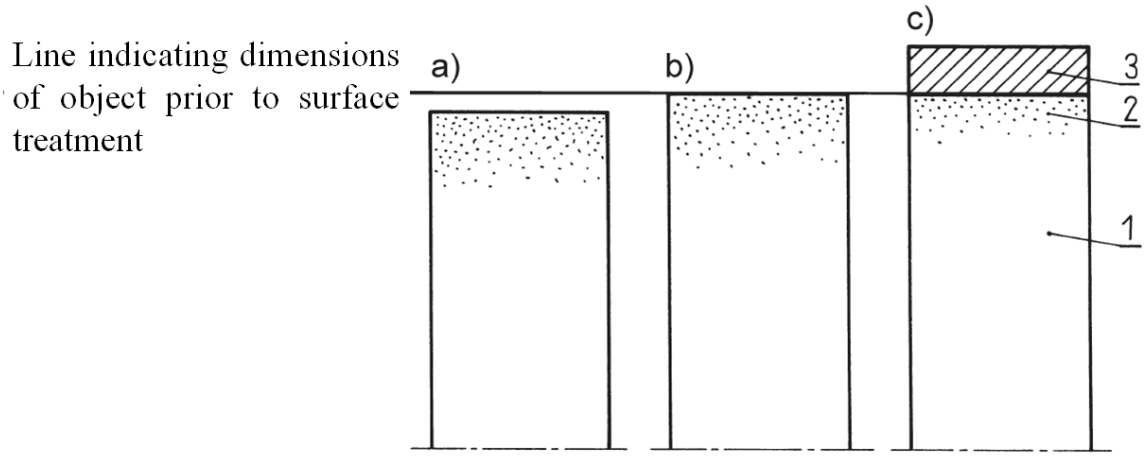

Figure 2.1 An illustration of the surface layers that are produced by various methods: a) decremental; b) non-decremental; c) incremental; 1 - substrate; 2 - superficial layer; 3 - coating [256]

Decremental, involves the reduction of the dimensions of an object by machining. Non-decremental, is achieved without changing the object's dimensions e.g., by ion implantation. Incremental means that the object's dimensions are increased by chemical or thermo-mechanical processes [256]. Laser cladding is incremental process.

Surface engineering includes a variety of processes used to alter the surface characteristics of material components, ranging from conventional techniques to more advanced coating techniques and surface treatment methods [6]. This includes thermal spraying, chemical vapor deposition, physical vapor deposition, mechanical plating, welding, and laser surfacing.

2.2.1.1 Laser surfacing

Laser surface engineering involves modifying a component's surface properties by modifying the microstructure or adding extra materials [7, 8]. Laser surfacing technology produces metallurgically bonded coatings rather than mechanically bonded coatings. Often, laser-surfaced coatings have a greater thickness typically 1-2 mm than coatings produced by other surface engineering methods. Laser surface engineering is concerned with providing superior surface characteristics through laser heating, melting, cladding, alloying. Several industrial applications utilize laser surfacing techniques, such as the aerospace, automobile, maintenance, and repair industries [62, 63].

In summary, surface engineering applies to a wide range of products. Performance can be enhanced, costs reduced, and surface properties can be controlled independently of the substrate.

2.2.2 Laser surface engineering

Surface modification of metallic surfaces using laser surface engineering technologies is an innovative solution to improving their performance in hazardous industrial and environmental conditions. Essentially, laser surface engineering refers to processes in which electromagnetic radiation is emitted by laser sources, followed by absorption by materials, resulting in localized heating [7, 8]. In reality, the energy that is applied to the surface can be directed precisely to the points of application. Consequently, lasers provide a unique opportunity for surface engineering. Among the many advantages of laser surfacing over other surface engineering technologies are: controlled energy input and thermal characteristics, consequently the size and shape of the heat-affected zone; minimal post-processing (if necessary); and automating this process is relatively straightforward [13].

Combining laser power density with laser-material interaction time allows different processes to occur, as illustrated in Figure 2.2. There are significant differences between these processes in terms of absorption, melting, heat conduction, rapid solidification and the addition of powder.

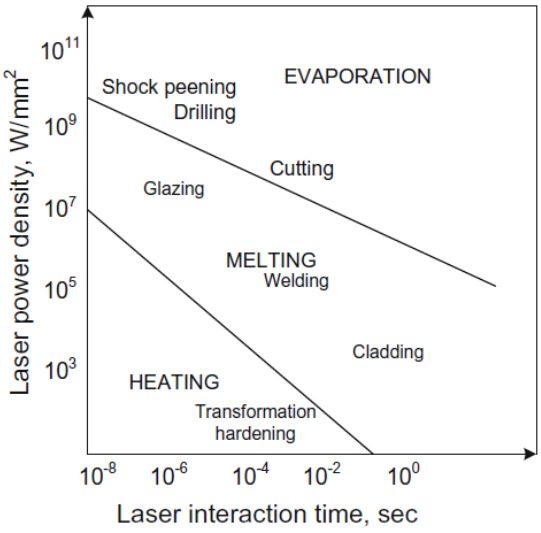

Figure 2.2 Relationship between laser power density and interaction time for a broad range of processes [0]

Thermal cycling occurs in the surface layer due to the effect of the laser beam. An illustration of the physical effects that occur during different types of laser surface engineering processes can be seen in Figure 2.3. Nevertheless, a common characteristic of most laser surface engineering techniques is rapid solidification, resulting in a more refined metallurgical structure.

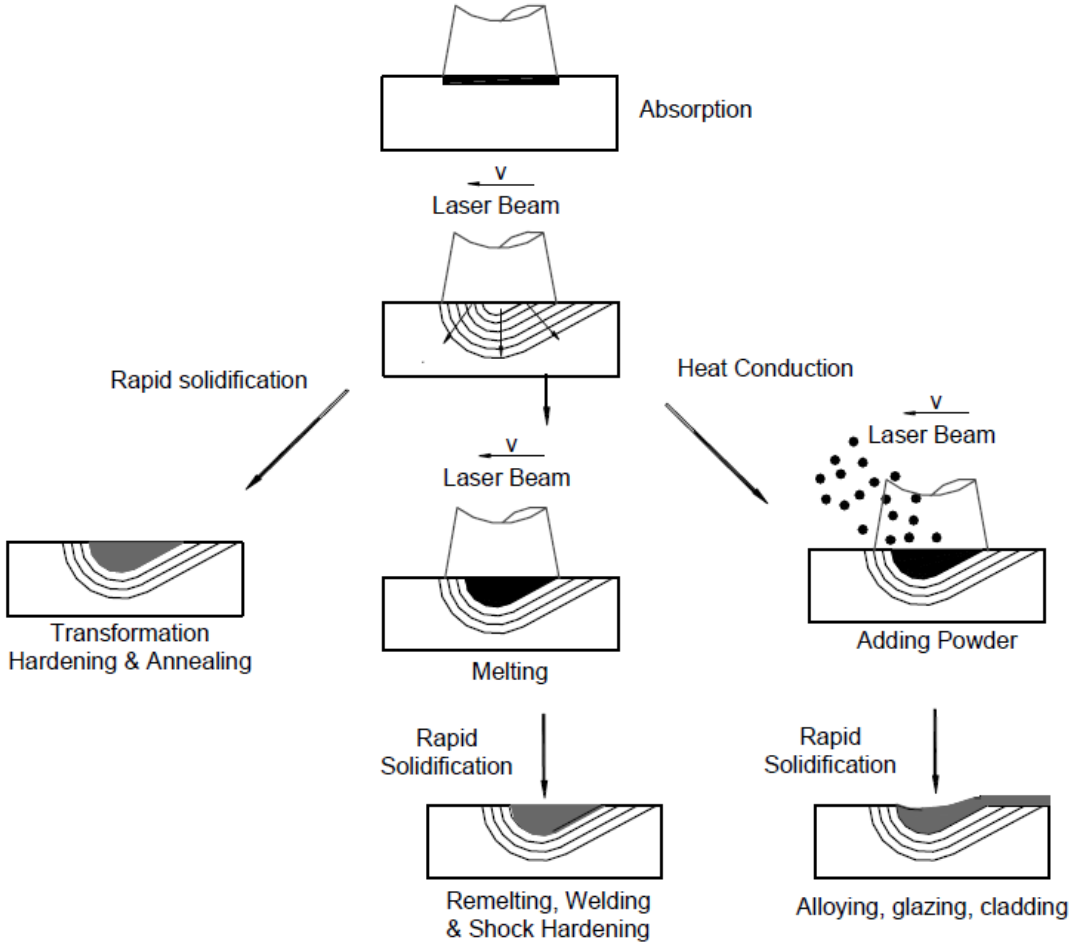

Figure 2.3 An illustration of the physical characteristics associated with different laser surface engineering techniques [256**]**

Laser surface engineering treatments can be categorized into two categories: thermal and thermochemical. The thermal processes such as surface transformation hardening and melting, change the surface characteristics by modifying the surface microstructure [0, 256].

2.2.2.1 Laser transformation hardening

Laser transformation hardening is one of the earliest laser-based methods of improving surface layer properties. During the hardening process of carbon steel, the surface layer is heated up to austenitic temperature level, followed by rapid cooling [0, 256]. In the end, a martensitic transformation is obtained with a very fine grain structure. It has been widely used in the automotive and process engineering industries to increase the wear resistance of components [64, 65].

2.2.2.2 Laser melting

Surface melting involves a similar procedure to transformation hardening, with the exception that in this instance a focused or near focused beam is employed. The process is performed by applying greater power densities in comparison with surface hardening. The process involves rapid melting and quenching, which can lead to an improved microstructure [0, 256, 66]. With enhance tribological and mechanical properties. These melting processes are often used for improving the surface properties of cast irons or tool steels [67, 68].

2.2.2.3 Laser alloying

Thermochemical techniques such as cladding and alloying change the composition of the surface by adding additional materials to a melt pool [0, 256]. An illustration of the chemical composition graph along the coat-substrate interface using thermochemical techniques is shown in Figure 2.4.

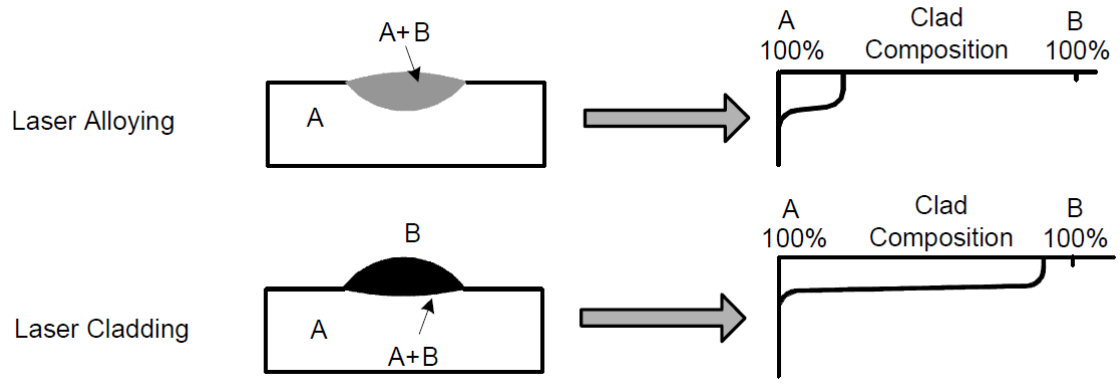

Figure 2.4 Various microstructures associated with laser alloying and cladding [256**]**

Surface alloys and phases are formed with specific characteristics. The laser alloying method involves melting the alloying material and the substrate surface to modify their chemical structure, which leads to increased wear and corrosion protection [0, 256, 66]. Due to Marangoni flow, the mixture of the alloy and the substrate can be almost homogeneous, unless the travel speed exceeds a certain threshold, in which case, insufficient mixing might result [66]. However, the actual mixture of the alloy will be determined by the depth of melt pool. Laser alloying provides the capability of manufacturing a range of alloys. A number of alloys have been investigated for the purpose of alloying steel [69, 70].

2.2.3 Laser cladding

All industries demand engineering components with specific surface characteristics, including suitable wear and corrosion resistance and hardness properties. Thus, in some cases high-grade alloys are essential to achieve the desired surface quality. However, industries are interested in reducing the cost of engineering parts with these surface characteristics [71]. With a cheaper substrate material and the appropriate coating alloy, cost reductions can be achieved very easily. Laser cladding is an effective technique for changing the physical and chemical properties of material surfaces [7, 13].

Unlike previously discussed laser alloying, laser cladding involves a relatively low level of dilution (<10%) and requires a significant amount of material added to the surface, generally in the range of 0.05 to 2 mm thickness [1, 72, 73]. The purpose of cladding is to deposit layers to provide a sufficient metallurgical bond between clad and substrate material while improving the mechanical and chemical properties of the surface layer [**257**, 66, 74]. Early in the 1970s, the technique was first applied for the construction of automobile valves [75]. The laser cladding process requires a laser with a sufficient power density to melt the substrate surface and the additive material above their melting points in order to produce the desired surface structure with pore and crack free coatings [72, 73]. Once the laser beam has passed over the surface, a layer of solid material forms rapidly and provides excellent adhesion bonding at the interface [74]. As part of the laser cladding process, temperature plays a significant role in the interaction of the coating and the substrate material. Whenever the temperature of the interface decreases below a certain point, the coating will exhibit a significant amount of cracks, pores, and poor adhesion bonding. In contrast, excessively high interface temperatures can cause the cladding properties to deteriorate by dilution. The related laser and appropriate process parameters will influence the properties and microstructure of material after laser treatment. By reducing the heat input, the grain structure is refined and dilution is considerably reduced and substrate thermal degradation [76].

In comparison to other methods of coating deposition, laser cladding has the following advantages: a completely dense and metallurgical-bonded coating at the coating-substrate interface is produced [77, 78], low degree of distortion [79, 80], limited defects [61, 63], controlled dilution [81, 82] and minimised heat affected zone [83, 84], high solidification rate [85, 86]. In terms of coverage rate efficiency or cost-effectiveness, laser cladding is not the most suitable technique for the deposition of large surfaces.

Laser cladding has several applications across a wide range of industries; aircraft [21, 22], aerospace [24, 63], automotive [25, 26], tooling [27, 28], manufacturing [29, 30]. Laser cladding involves the application of high-quality coat surfaces on engineering materials [31]. Furthermore, a damaged part can be repaired by reconstructing the damaged surfaces [32, 33]. This method is also suitable for the deposition of hybrid materials, making it more appropriate for certain specialised industrial applications [34, 35]. Moreover, laser cladding is a highly effective method of improving abrasive wear resistance [36, 37], corrosion resistance [38, 39], erosion wear resistance [40, 41] and dealing with environmental conditions that are aggressive, with temperature cycles involving rapid heating and cooling, corrosive gases, extreme heat, abrasive materials, and cavitation erosion, such as are found in nuclear power plant [87, 88]. In recent years, the laser-cladding process has been used in the additive manufacturing industry, where engineering parts can be deposited layer by layer based on computer-aided design (CAD) models. [89, 90].

Generally, laser cladding can be divided into two general categories, Two- and One-step procedures [**256**, **257**]. A schematic diagram of the single- and two-step processes can be found in Figure 2.5.

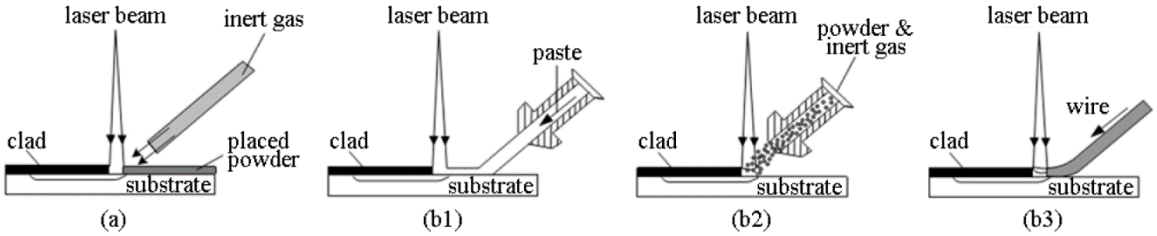

Figure 2.5 Methods of laser cladding: a) two-step, b) single-step, with b1: paste, b2: powder and b3: wire [256**]**

During the two-stage procedure, the additive material is deposited on the substrate surface in the first stage, and afterwards, it is fused by the laser heat source to the substrate as part of the second stage (see Figure 2.5 (a)) [91]. On the other hand, in single-step laser cladding, the coating material is injected dynamically into the interaction zone in various forms: paste, wire or powder (see Figure 2.5 (b)) [92-94]. The advantage of both procedures is that both can be applied to deposit a wide variety of alloys. The following sections will discuss single- and two-step laser cladding.

2.2.3.1 Two step laser cladding

In the two-stage laser cladding method, the coating material is layered over the substrate in the first step, followed by the melting stage to create a fusion bond between the interface of the substrate and the coating material as part of the second stage (see Figure 2.6) [91, 95].

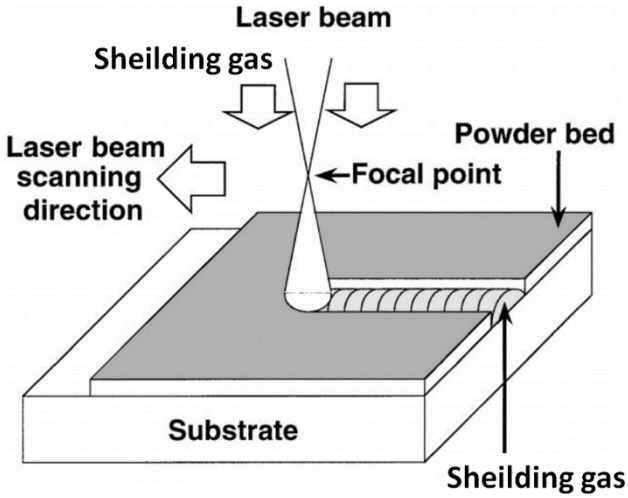

Figure 2.6 Schematic representation of pre-placed laser cladding [95]

The coating material can be delivered in different forms: powder, chip, wire, paste, etc [91, 96, 97]. Probably the simplest and most common two-step method is laser cladding with pre-placed powder [256, 91]. Powder is often mixed with a binder (which is often alcohol) before being layered on the surface [**257**, **256**]. In this way, it is possible to achieve an even accumulation of the powder. Additionally, the combination of the powder and the binder, can eliminate powder being blown away by the shielding gas. During laser melting, the binder is vaporized, which can cause coating defects [**257**, **256**].

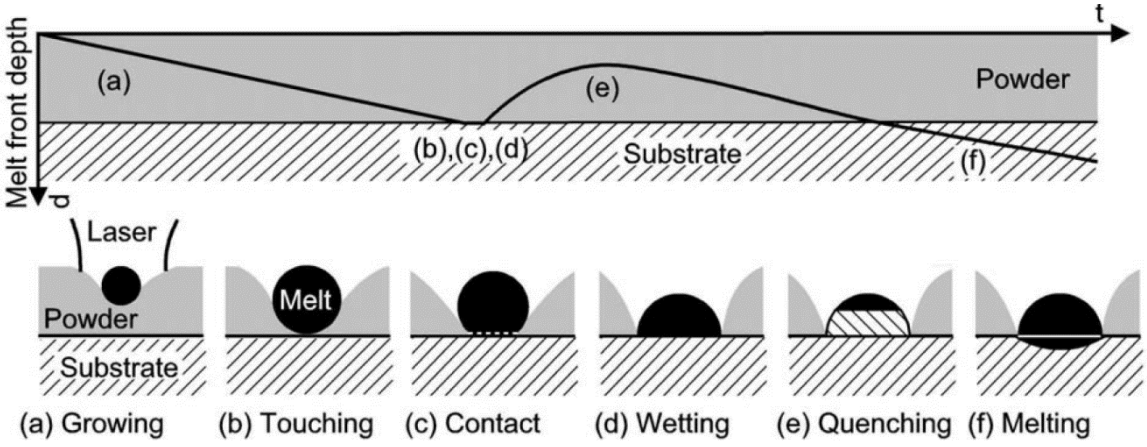

Figure 2.7 A cross-sectional view of the melt-soild contact history (Black = Liquid, Grey = Powder, Shaded = Solid) [98]

The literature has extensively described the physical phenomenon of pre-placed powder laser cladding [91, 98, 99]. As a result of irradiation with a high-density power laser, particles of powder become heated; however, little heat transfer occurs between them since they do not have good conductive contact [91]. Afterwards, the powder particles are melted, and once they are molten, they are capable of conducting heat to nearby material: a resulting liquid layer propagates through the powder film (see Figure 2.7(a)). The moment the melt touches the substrate and subsequently wets it, the substrate cooling effect causes a reversed propagation of the melt front ((see Figure 2.7 (b, c, d)). It begins solidifying but does not penetrate deep into the substrate until sufficient energy and interaction time have been provided ((see Figure 2.7 (e)). As long as the laser energy is high enough, the solid-melt contact can be deepened down into the substrate material ((see Figure 2.7 (f)) [98]. A melt front's final depth indicates how much the cladding material has been diluted. Figure 2.8 illustrates the position of the melted front in relation to the interaction time at different average laser powers. Dilution increases as interaction time and laser power increase [91, 115].

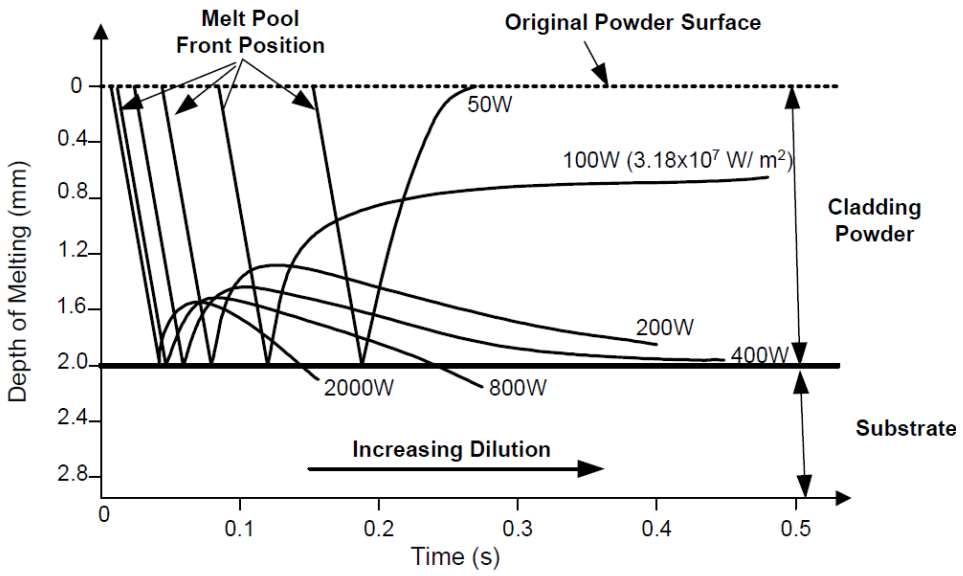

Figure 2.8 Position of the melted front in relation to the interaction time at different average laser powers [91]

Laser cladding with pre-placed powder has some advantages, over other surface engineering methods, including thermal spraying, based on its accuracy, minimal thermal distortion, low diluting effect and minimal powder waste [**257**, **256**].

An increasing number of applications have been developed, including interlocks [100, 101], engines [102], shaft parts [103, 104], valve seats [105, 106], turbine blades [96, 107]. In recent years, rapid prototyping has largely incorporated this process, which involves building up three-dimensional shapes [108, 109]. The technique can also be applied in industry to repair damaged or under dimensioned engineering parts [110, 111], and in rapid prototyping [112, 113]. Among the advantages of this method compared to other processes (wire and powder feeder) it is a suitable choice for surfaces with limited accessibility [114, 115].

Two-step laser cladding is ideal for depositing single layers as well as multiple layers [116]. The principal disadvantages of this method are that it is time-consuming owing to the multistage processes involved, as well as the difficulty in pre-placing powder on complicated shapes [117]. Reproducing accurate powder bed thickness and covering large surfaces can be challenging [1, 91]. In spite of the fact that laser cladding with pre-placed powder ensures superior material efficiency, as compared to blown powder, it requires considerably more energy [118]. Due to these factors, single-step laser cladding is typically the most effective, and most popular, method.

In terms of pre-placed laser cladding, laser requirements can vary depending on the particular application, the materials involved, and the desired outcome. However, there are some general requirements for lasers that need to be considered. For pre-placed laser cladding, high-power solid-state lasers or fiber lasers are typically used. The lasers provide the necessary energy and precision for the process. In order to melt and fuse the pre-placed powder or material onto the substrate, the laser must have sufficient power and energy output. Depending on the application, power levels can range from a few hundred watts to several kilowatts. It is important to ensure a high level of beam quality in order to obtain precise and controlled melting of the material. Generally, a Gaussian beam profile is preferred. Laser wavelengths are selected depending on the type of materials being processed. The most commonly used wavelengths for laser cladding are in the near-infrared spectrum, around 1 micronmeter, which is well suited to a wide range of metallic materials. A laser's pulse duration can vary, however, short pulses (nanoseconds to microseconds) are typically preferred for precise control and minimal heat transfer to the substrate. As an option, the laser beam spot size can also be adjusted in order to control the area of the laser beam affected by heat (HAZ) and to control how deep the laser beam penetrates into the substrate.

For achieving the desired quality and thickness of cladding, this is crucial. Using a scanning or beam delivery system, the laser beam is moved across the surface of the component in a controlled manner. As a result, material and energy are distributed evenly during the deposition process. A powder delivery system is essential for accurate placement of pre-placed powder or material on the substrate. In synchronization with the laser beam, the powder should be delivered precisely where it is needed. To prevent oxidation and ensure proper metallurgical bonding, it may be necessary to control the atmosphere surrounding the cladding area using shielding gases such as argon or nitrogen. Depending on the materials being used, the geometry of the part, and the desired outcome, the specific laser requirements can vary significantly. To achieve the desired quality and properties of cladding, process development and optimization are often required. It is common for manufacturers and researchers to customize the laser parameters and equipment to meet their specific requirements. Listed below are some new relevant papers showing what are the researchers commonly use in terms of laser requirements in preplaced powder laser cladding.

Chen et al. 2024 employed a fiber semiconductor laser system known as LSJG-BGQ-2000, operating at a laser power of 1800 W. The laser beam had a 3mm spot diameter. The metal powder used in the experiment was composed of Co, Cr, Fe, Ni, Nb, and a boron-iron alloy, with particle sizes ranging from 50 to 120 μm and a purity exceeding 99.9% [119].

Chen 2024 used the initial alloy powders, based on iron (Fe), were composed of the following weight percentages: 61.54% pure iron powder, 6.10% graphite powder, and 32.36% FeV50 powder. These powders had varying particle sizes, with the pure iron powder ranging from 28-39 μm, the graphite powder ranging from 18-23 μm, and the FeV50 powder ranging from 75-150 μm. The laser cladding process parameters were as follows: an IPG YLS-10000 fiber laser with a power of 1.0 kW and a spot diameter of 1.7 mm [120].

Zhu et al 2024: In this study, a pivotal component for laser cladding is a high-power direct diode laser with a 2-kilowatt (kW) output, which is carefully focused to create a Gaussian-like distribution. To ensure uniformity and an appropriate beam size during the actual processing, we have established a pitch of 0.5 mm and a radius of 16 mm. For the cladding powder, we have chosen a carbide mixture with a weight ratio of 100:30. The Ni60 powder particles fall within the size range of 80–100 μm, while the WC powder particles, which have an angular shape, range in size from 45 to 100 μm [121].

Ghorbani et al 2024: The starting powders consisted of pure carbon, with an average particle size of 40 μm and a purity of 99.5%, and 15 wt. pct. of pure nickel, with an average particle size of 50 μm and a purity of 99.5%. For the laser cladding process, an IQL-10 Nd:YAG pulsed laser was utilized. This laser had a maximum operating power of 400 W and emitted square pulse shapes in the TEM00 mode. The laser machine predominantly operated in spatial modes TEM00 and TEM01, employing three lenses with a 75 mm focal length and achieving a minimum spot size of 250 μm [122].

Hua et al 2024: The preferred Co-based alloy powder in this case was Stellite 6 powder. All the powders, including Stellite 6, had a high purity level of 99.8%. The particle sizes for all three types of powders ranged from approximately 50 to 90 μm. The laser parameters employed were as follows: a laser power of 1200 W and a beam diameter of 3 mm [123].

Zhang et al 2024: The composition of the newly formulated nickel-based alloy has been provided, with particle sizes ranging from 45 to 150 μm. The laser system used for the process featured a maximum power output of 3000 W, a spot size of 4 mm, and a wavelength of 976 nm [124].

Yi et al 2024: Tantalum (Ta) powder, with a purity exceeding 99.9%, was utilized, featuring a particle size distribution ranging from 5 to 50 μm. Comparatively, the Ta2O5 particles were noticeably smaller, measuring between 2 and 20 μm. To manufacture the Ta and Ta2O5 coatings, a high-power diode laser system was employed, boasting a maximum power output of 4.4 kW and operating within a wavelength range of 978–1025 ± 10 nm. The laser's working distance was adjusted to 138 mm, and the beam size was configured as 4×4 mm² [125].

Feng et al 2024: The fusion cladding material was a mixture of Ni60 powder particles ranging from 45 to 100 microns and WC powder particles ranging from 45 to 150 microns, boasting a purity of 99.9%. The WC powder accounted for 35% of the total weight of the blended powders. For the experiment, a laser spot diameter of 3 mm was used, and the laser system had a maximum power output of 2000 W [126].

Powder particle sizes used in preplaced powder laser cladding can vary according to the application, material being processed, and desired results. As the particle size requirement depends upon factors such as laser power, scanning speed, and substrate material, there is no one-size-fits-all answer. The following is a general guide to particle size considerations in preplaced powder laser cladding. Powder particle size distribution is crucial for laser cladding, which requires a consistent and well-defined particle size distribution. A powder should consist of particles that fall within a certain range of sizes. Depending on the parameters of the process and the material being clad, the specific distribution will vary. A fine powder will melt more readily when exposed to the laser energy, allowing for improved control of the melting and fusion processes. A fine powder can also result in a smoother surface finish in the clad layer. A coarser powder may be used in some cases, especially when higher deposition rates or specific mechanical properties are required. The melting and fusion of coarser particles may require a higher laser power. Preplaced powder particle size should be selected in accordance with the requirements of the laser cladding system and the substrate. As a result, proper bonding is ensured and defects are minimized. A powder particle's size and distribution can have an impact on how it absorbs and distributes laser energy during melting and fusion. A smaller particle may melt more readily than a larger one, while a larger particle may require a greater amount of energy to melt. The surface finish of the clad layer is also affected by the granulometry of the powder. Smaller particles may result in a smoother surface, while larger particles might lead to a rougher finish. Size and distribution of powder particles can affect thermal conductivity and heat transfer within the powder layer and between the powder and substrate. Consequently, the distribution of temperature and the microstructure of the clad layer can be affected. The specific granulometry requirements for preplaced powder laser cladding depend on the material being used, the desired clad layer properties, and the particular application.

2.2.3.2 One step laser cladding

In single-step laser cladding, the coating material is injected dynamically into the interaction zone in various forms: paste, wire or powder (see Figure 2.5 (b)) [92, 93, 94]. These sections focus on laser cladding with wire and powder only, as these are most frequently used.

2.2.3.2.1 Laser cladding with wire

Laser cladding utilizing wire feed first appeared in 1976 [127]. The single-step laser cladding with wire feed begins with creating a melt pool on the substrate surface. Meanwhile, the wire is injected into the interaction zone and melted to ensure a good adhesion bond (see Figure 2.5 (b3)) [128, 129]. For a stable deposition process, it is crucial to establish a balance between the main process parameters, including output laser power, laser spot diameter, wire feed rate, feeding direction, feeding angle and table speed [130, 131]. Establishing a strong fusion bond is possible if these parameters are configured correctly. Numerous scientific publications have examined the effects of feeding angle, direction, and position on this technique [131-135].

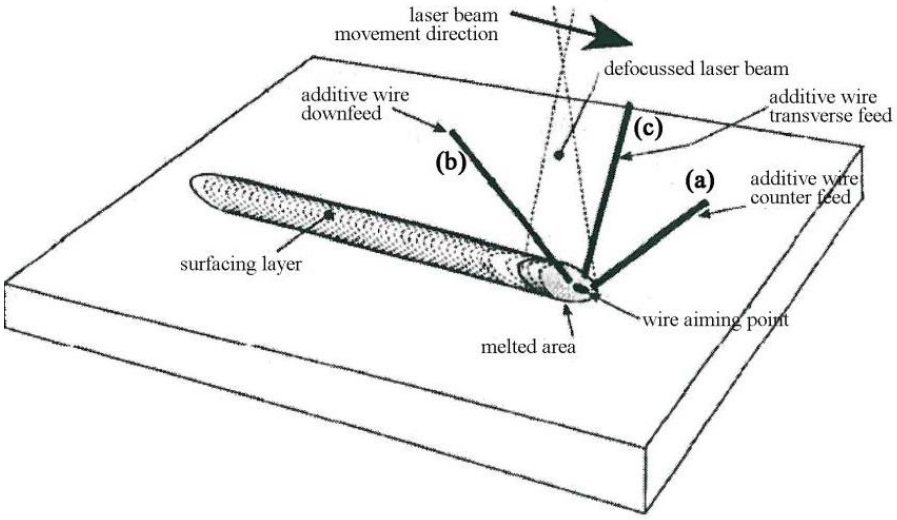

Figure 2.9 Feeding directions for laser cladding using wire: a) leading, b) trailing, c) sideways [129]

Wires can be fed either leading, trailing, or sideways (see Figure 2.9) [129, 132]. In a comparison of feeding directions, it has been shown that using the leading direction can result in smoother surface roughness with improved coating quality since the melt pool is not disturbed [132]. The feed angle, which refers to the angle between the substrate surface and axis of the wire feeder, is also crucial (see Figure 2.10) [133, 134]. For instance, angles less than 20 degrees produce tracks with an asymmetric shape [133], angles between 20 and 60 degrees produce a symmetric shape with an identical height [134] but an angle of 45 degrees may provide the highest volume of wire deposition [133]. In terms of wire tip positions, there are three different options: the centre, the leading edge, and the trailing edge locations [132, 135]. The leading wire tip position produce the most uniform deposition [132].

Several authors have recommended using leading feed direction at a 45-degree angle and placing the wire tip at the leading edge [131, 132].

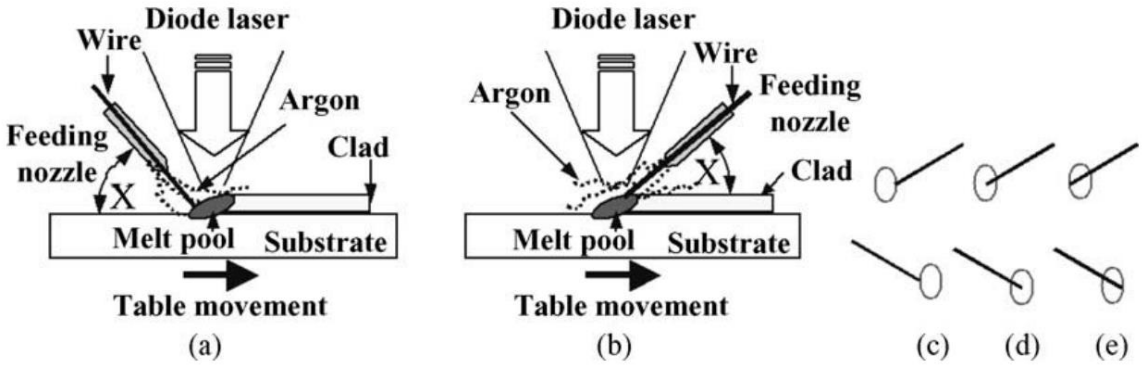

Figure 2.10 Angles and positioning of wire feeding, including wire tip positions: (a) front, (b) rear, (c) leading-edge position, (d) centre position, (e) melting pool trailing edge position. [132]

Laser cladding with wire has been gaining in popularity due to its enhanced process characteristics [129, 136]. Among the advantages of this design are high material efficiency [137], low material waste [138], high cladding efficiency [139, 140], an environmentally friendly (dust-free) [133], cost- and time-effective process [139, 141], It is possible to produce three dimensional engineering parts from CAD models [142, 143], smooth surface roughness (Ra) of 40 to 50 microns also have been reported [134, 144]. There is a large variety of materials obtainable in wire and, in most cases, they are more affordable than metal powders [145, 146]

Laser cladding with wire feeder has been performed with a variety of materials, including, mild steel [147], stainless steel [148, 149], Co-based alloys [150, 151], Ni-based alloys [152, 153], Cu-based alloys [154], Ti-based alloys [155, 156] and Al-based alloys [157, 158]. Laser cladding has several applications across a wide range of industries, aerospace [159, 160], automotive [161, 162], manufacturing [163, 164]. However, as a result of a variety of disadvantages, laser cladding with wire has always occupied a secondary position in single-step laser cladding and laser cladding with powder is the primary industrial process. These disadvantages include sensitive wire delivery system [**256**], direction dependency [129, 132], difficult dilution control [165], poor surface quality, adhesion, coating defects caused by drop transfer [166]. However, this disadvantages are becoming less important because to avoid wire feeding cladding heads are now becoming available [167, 168]. These heads use a hollow coaxial beam [169].

2.2.3.2.2 Laser cladding with blown powder

Laser cladding with powder injection has become the most widely used single-step process for several reasons. A major reason is its well-defined heated region, there is a wide range of materials and alloys available as powders, the laser beam and powder are coupled with good efficiency and low dilution [170], adaptability to automatic processing [171] and provides superior wear and corrosion resistance on certain surfaces [48, 165].

One of the earliest documents discussing the blown powder laser cladding technique dates from the early 1980s and is a Rolls Royce Ltd patent [172].

During the laser clad process with blown powder, the laser beam creates a melt pool on the surface of the substrate, which is entered by the melted powder particles (see Figure 2.11). [173, 174]. Once the laser beam has passed over the surface, a layer of solid material forms rapidly and with excellent adhesion bonding at the interface [74]. An adequate amount of heat must be provided to melt the powder without overheating the substrate [173, 174].

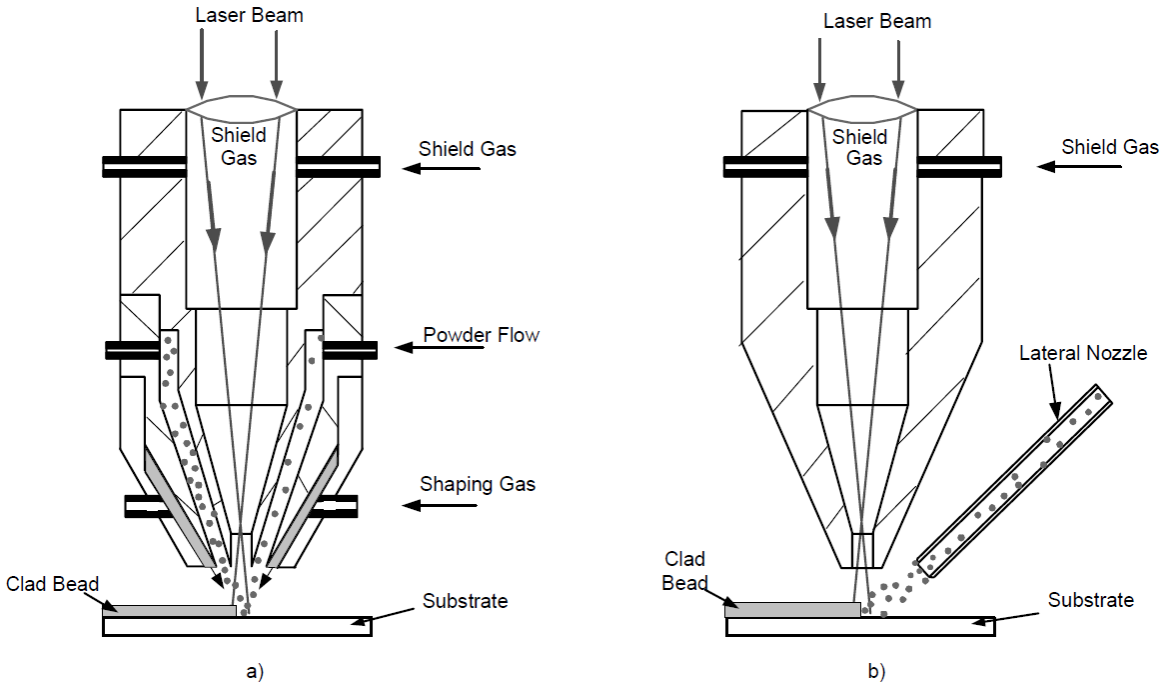

Figure 2.11 Feeding nozzles for laser cladding powder a) Coaxial b) Lateral nozzle [6]

A number of factors influence whether the supplied powder sticks to the melt pool to form a coating. The potential types of interaction are described below, depending on the percentage of laser energy absorbed by the substrate and powder particles:

1. solid powder – solid surface: laser energy cannot be absorbed by either the powder or the substrate in sufficient quantities to cause melting. Cladding does not take place.
2. solid powder – liquid surface: the powder particle, which does not absorb enough energy to melt, is captured by the molten pool formed.
3. liquid powder – solid surface: Powder particles melt during injection, causing them to stick to the solid substrate surface; this causes powder catchment.
4. liquid powder – liquid surface: The substrate as well as the powder particles melt, resulting in catchment

Of these options number 2 is the most common in laser cladding [175-177]. The amount of material efficiently applied depends critically on the size of the melt pool as compared to the size of the powder stream's impact area [178, 179]. Generally, the one-step laser cladding process with powder feeding has a low powder catchment efficiency and this will be discussed in detail in section 2.4.3. In the literature, values typically range between 10 and 90 percent. Studies have shown that using finer grade powder can increase material efficiency and productivity [180], with the added benefit of reducing the roughness of the final coating. However, fine powders are more likely to cause vaporization and aerosol emissions during operations [181, 182]. Moreover, agglomeration of powders and difficulties with powder flow in powder feeders and cladding nozzles may have an adverse effect on the injection of these powders, an essential function of this system.

One of the most important characteristics of the blown powder technique is the powder feeding system. Two primary methods of powder feeding are available, namely off-axis powder feeding and coaxial powder feeding. Catchment efficiency is influenced by the geometry and alignment of nozzles [183]. A high injection angle can increase powder efficiency. Fundamentally, the coating process is either omnidirectional or unidirectional, although designing an off-axis nozzle is easier than designing a coaxial nozzle. [184]. Although, recent advances have made coaxial nozzles commercially available [185]. In-depth review of the off-axis and coaxial techniques is provided in the following sections.

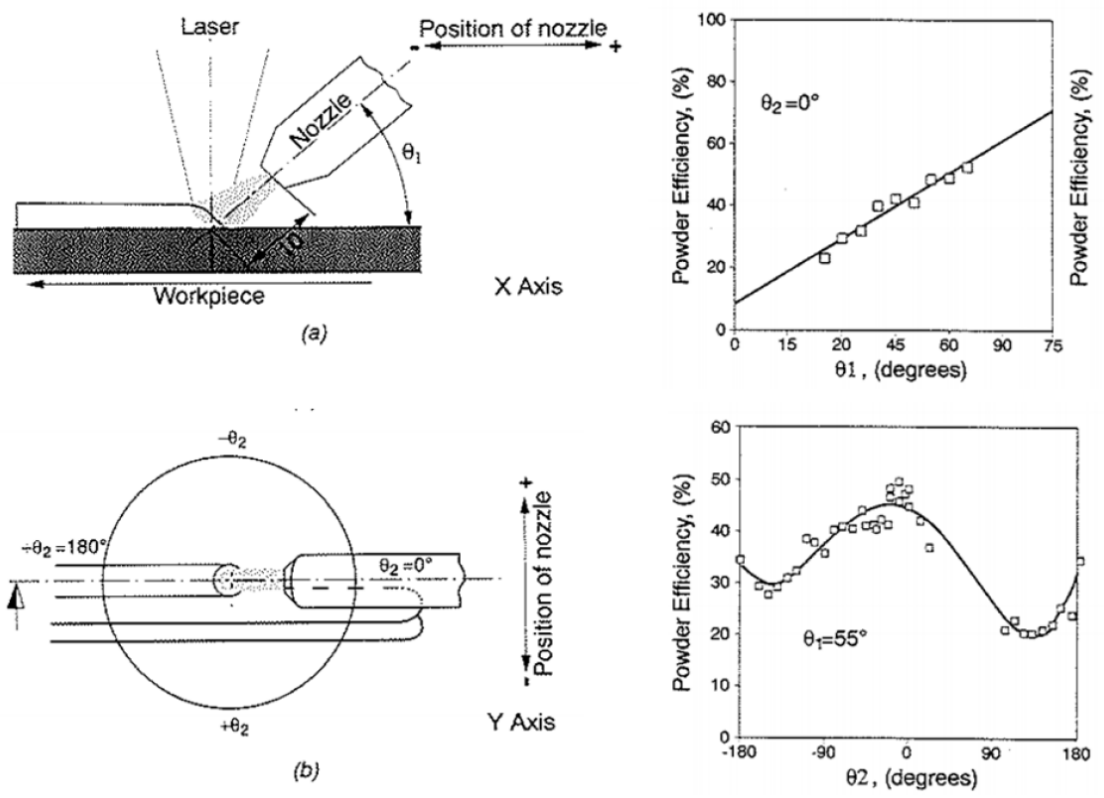

Figure 2.12 Laser cladding using powder injection (a) transverse profile at an angle of θ1 and its impact in terms of powder efficiency and (b) a plan view of the coated surface in accordance with θ2 as well as its effects on powder efficiency [186]

According to the nozzle-workpiece angle (θ_1), the gap between the tip the substrate surface (d) and the feeding direction of the powder (θ_2), the lateral nozzle setup is established [186]. The greater the nozzle angle (θ_1), the smaller the powder stream's cross section on the surface and the greater the effectiveness of powder deposition [186]. Comparing rear and front feeding directions, applying front feeding results in a significant improvement in powder capture efficiency up to around 40%, as shown in Figure 2.12 [134, 186]. Hence, the shape and orientation of the nozzle affect the effectiveness of the material deposition [187, 188].

Laser cladding of blown powder utilizes a high-energy laser beam. Laser requirements are crucial for the successful processing of blown powder laser cladding. This process requires the following laser requirements: For blown powder laser cladding, a high-power laser source is required. Lasers commonly used include CO2 lasers, Nd:YAG lasers, and fiber lasers. The choice of laser type depends on factors like material compatibility. It is imperative that the laser be able to melt both the substrate and the blown powder material with sufficient power. Based on the materials used and the rate at which the cladding is desired, the power requirement will vary. Most commonly, lasers are powered by several hundred watts to several kilowatts. A high-quality laser beam with good focusability is necessary for precise control during the process. A well-focused laser beam ensures that the material is efficiently melted and deposited. Depending on the material being processed, the laser wavelength is selected. There are many lasers in the near-infrared spectrum that can be used for the treatment of metals. Wavelength selection should consider material absorption properties. Spot Size: The laser should be capable of providing a spot size that matches the desired cladding area. The spot size can be adjusted by using appropriate focusing optics. Here are a few instances showcasing laser requirements and particle size considerations in blown powder laser cladding.

Chen at el 2024: The initial alloy powders used were based on iron (Fe) and included the following weight percentages: 61.54% pure iron powder, 6.10% graphite powder, and 32.36% FeV50 powder. These powders had varying particle sizes, with pure iron particles ranging from 28-39 μm, graphite particles ranging from 18-23 μm, and FeV50 particles ranging from 75-150 μm. The laser cladding process was carried out using an IPG YLS-10000 fiber laser with a power output of 1.0 kW [189].

Feng et al 2024: For the experiment, coating materials comprised spherical powders of Co, Cr, Fe, Mn, Ni, and Nb, all exceeding 99.5% purity. These powders had a particle size range of 45–108 μm. The laser system used was a TruDisk 4002 disk laser with a power output of 2000 W and a spot diameter of 3 mm [190].

Jeong et al 2024: a 1 kW continuous wave laser with a wavelength of 1070 nm from IPG Photonics in Oxford, utilizing a Coax-8 nozzle. The metal powder used in this system is Inconel 718, featuring particle sizes ranging from 45 to 106 μm and spherical in shape [191].

Yang et al 2024: The chosen material consists of a blend of AlCoCrFeNi2.1 alloy powder and CeO2 particles. The primary elements, Al, Co, Cr, Fe, and Ni, were acquired through vacuum argon atomization. These elements are in spherical powder form, each with a purity exceeding 98%, and particle sizes ranging from 45 to 125 μm. The laser employed for the process operates at 1200W power with a 3mm spot diameter [192].

The particle size in blown powder laser cladding may fluctuate based on the particular demands of the cladding procedure, the material under treatment, and the machinery in operation. Nevertheless, as a rule of thumb, particle size considerations in blown powder laser cladding usually encompass a spectrum spanning roughly from 20 (μm) to 150 (μm) or potentially even larger. Here are key factors to contemplate regarding particle size: A powder size range is selected based on the material being processed, the desired clad layer characteristics, and the cladding equipment. Distribution of particle sizes within the specified range is critical. It is possible to achieve a more uniform and consistent clad layer by maintaining a narrow and well-controlled particle size distribution. The granulometry of the powder should be selected to match the capabilities of the laser system being used. This includes considerations such as laser power, spot size, and beam quality. The powder size should be suitable for efficient melting and bonding when exposed to the laser beam. Different materials may require different granulometry profiles. For example, metals, ceramics, and polymers may have varying powder size requirements based on their melting points, thermal conductivity, and other material properties. As part of the cladding process, the granulometry should be aligned with the specific goals. If the purpose is to achieve a fine, smooth surface finish, finer powders may be preferred. Coarser powders might be chosen when higher deposition rates are needed. The flowability of the powder is crucial for uniform deposition onto the substrate. The granulometry should ensure that the powder can flow smoothly through the powder feeding system and nozzle without clogging or inconsistent flow. The granulometry of blown powder laser cladding should be carefully selected and controlled so that the powdered material is deposition and fusion effectively by the laser, resulting in a high-quality clad layer with the desired properties. The specific requirements will vary depending on the application and material being processed.

2.2.3.2.2.1 Laser cladding with off-axis powder injection

Utilizing lateral powder feeding, the powder is transferred to the interaction zone using an off-axis nozzle. Essentially, lateral nozzles consist of cylindrical pipes of the appropriate diameter, length, and shape. The lateral powder feeding nozzle set up, as illustrated in Figure 2.13 [186-199].

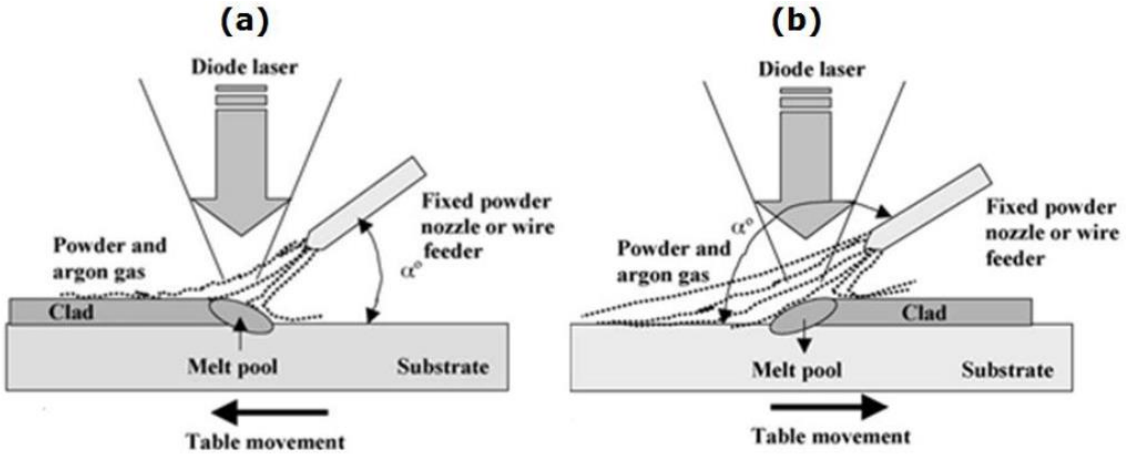

Figure 2.13 Orientations for powder feeding: (a) forward, (b) backward feeding [134]

The off-axis nozzles can be oriented in such a way as to guide the powder steam efficiently to a specific location within the melting pool. Consequently, it is possible to manage the interaction time to maintain the optimal temperature of the powder and minimise coating defects. In general, the design of the lateral nozzles is quite straightforward. Various designs can be developed for difficult-to-reach areas [193, 194].

However, one of the disadvantages of this method is that it is direction dependent. Thus, it is evident that the process with a lateral nozzle is not appropriate for cladding three-dimensional engineering parts [73, 195]. A major disadvantage of the lateral feeding procedure is the difficulty of reproducibility since minor differences in powder distribution in connection with laser beam characteristics can result in significant variations in clad geometric characteristics, material effectiveness, as well as dilution [196, 200].

The process has the capability of modifying the microstructure and chemical composition of a substrate surface by layering a coating, resulting in functionally graded components [199]. Similarly, these advantages also apply to laser cladding with coaxial powder injection.

2.2.3.2.2.2 Laser cladding coaxial powder injection

The laser cladding process has been greatly enhanced by the development of the coaxial powder feeding mechanism, illustrated in see Figure 2.11 a) [201-231]. The powder is transferred to the substrate surface coaxially with the laser beam through a coaxial nozzle giving an approximately Gaussian distribution of powder density (see in Figure 2.14).

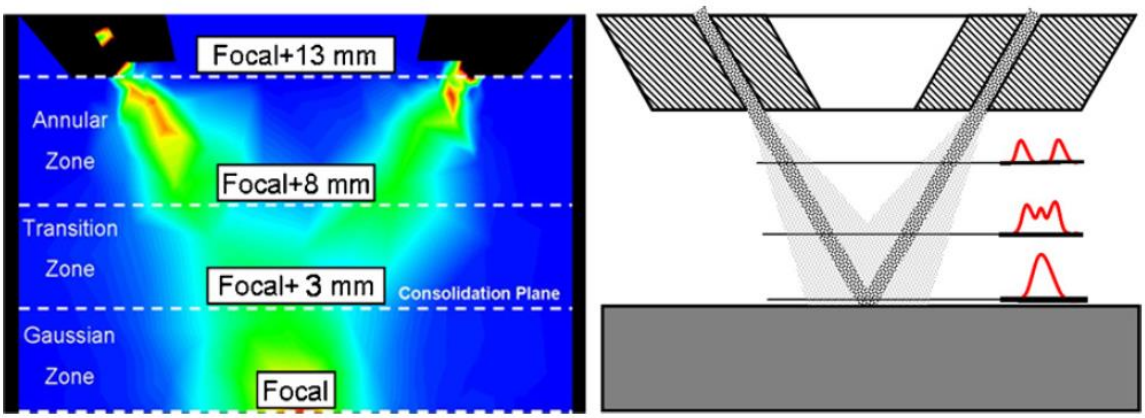

Figure 2.14 Powder concentration distribution through a coaxial nozzle [203]

An understanding of the powder steam properties is crucial to depositing a coating of precise dimensions and good cladding efficiency. In this process, three different streams interact with the material surface: shielding gas, carrier gas and powder stream as shown in Figure 2.11 a). The shielding gas is responsible for two distinct purposes, carrying the powder particles within the nozzle around the laser beam and protecting the coating from the atmosphere to avoid the coating defects. The powder jet must be uniformly dispersed, parallel to the laser beam profile, and in a laminar flow. Moreover, the focus point of the powder jet should be positioned directly over the melt pool [205]. These criteria determine excellent coating quality and high powder catchment efficiency. Compared with a lateral nozzle, the powder jet generated by an axial nozzle experiences a greater amount of heat when it reaches the coating surface since it has been exposed to the laser beam for a longer interaction time [195]. The powder steam partially protects the substrate from laser beam, thus minimizing substrate melting [206]. A wide range of coaxial nozzle designs allows various powder jet configurations and powder focus points.

The major advantage of the coaxial nozzle is its directional independence [207-211]. Regardless of the orientation of the reference substrate, its motion is identical to the axis of the laser beam. The coaxial nozzle system offers a solution for real-time monitoring and process control by allowing for the easy integration of sensors and optical components [209, 212, 213]. Furthermore, the advantages of the axial nozzle are the precise temperature control, greater powder catchment efficiency, and low heat affected zone [214-216]. In view of more prolonged interaction time as well as the occurrence of multiple reflections within the powder steam, the overall energy efficiency is likely to be higher [216].

The process is suitable for fabricating components from CAD designs, thereby broadening the possibilities for its industrial application across a wide range of industries [209, 217]. Nevertheless, coaxial powder nozzles cannot be used for all products, because tilting the nozzle is inherently problematic since powder flow is affected by gravity in tilted nozzles [195, 213]. It has been observed that low deposition rates of powder are encountered in numerous applications, resulting in increased processing times [73]. Furthermore, post-processing operations are frequently necessary because of high surface roughness [218]. Depending on the system and parameters used, material efficiency can also be low [219]. Potentially poor shielding conditions are created in the absence of a sealed environment during the deposition process [220]. Likewise, the optical components of the laser are susceptible to damage from powder particles or electrically conductive materials [209].

The effects of powder flow on-axis and off-axis nozzle applications have been investigated using high-speed images [298] (see in Figure 2.15).

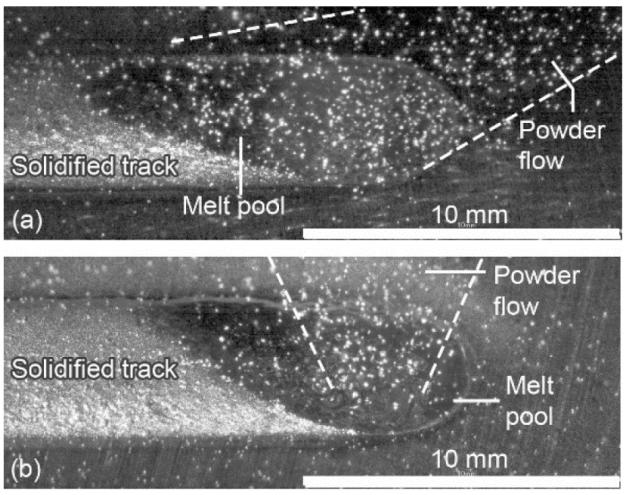

Figure 2.15 Images obtained from high-speed imaging of laser cladding applying (a) off-axis and (b) axis nozzles, indicating powder flow by dashed lines [228]

As opposed to the axial nozzle, the off-axis nozzle distributes powder over a wider area. Therefore, the powder catchment efficiency of the axis nozzles is significantly higher than off-axis nozzles [228].

In addition to the two nozzles described above, several other types of nozzles have been developed. For instance, a specific nozzle has been designed to fabricate and repair parts for turbines and compressors [229], or for complicated parts [230], or for boosting the deposition rate [231].

2.2.3.2.2.3 Comparative advantages of blown powder over other methods of laser cladding

According to publications about laser cladding, the blown powder technique is the preferred method for laser cladding as compared with wire and pre-placed powder feed techniques [51, 145, 232, 233, 234, 235, 236, 237, 238, 239,]. In contrast to pre-placed powder applications, this process offers improved cladding efficiency and a more comprehensive range of processing options and can be applied to deposit complex three-dimensional parts [233, 234].

The primary benefit of cladding with blown powder is the subsequent melting process [235, 236]. In contrast to the method where the powder is pre-placed and the melt pool creation requires more energy since the pre-placed powder has to be melted, blown powder is more efficient [91, 237]. Moreover, in pre-placed laser cladding, when the melted zone approaches the interface of the substrate surface, the melted powder particles start to solidify as a result of higher thermal conduction, which may result in weak adhesion. [91, 238, 239].

Compared with wire feed the powder injection process provides greater flexibility [44-46]. Powder alloys are more readily available than wire materials [47, 48]. Furthermore, the method is more reliable than wire cladding, as it does not have direct mechanical contact with the interaction zone [49]. Hence, the laser beam can easily irradiate the substrate surface because the laser is not fully blocked by the powder stream. In general, this method has advantages over alternative methods in terms of energy efficiency [50, 51]. Wire cladding does, however, have the advantage that cladding material catchment efficiency is 100% because all the wire enters the meltpool [240].

A new laser cladding process called extreme high-speed laser cladding (EHLA), uses synchronized powder feeding to achieve maximum efficiency. According to this technique, by adjusting the orientation of the laser beam and the powder focal plane, when the powder is in contact with the laser beam, it melts and becomes evenly coated. Dilution is extremely low, as the cladding layer solidifies rapidly and limiting substrate melting [250]. One of the main differences between the extreme high speed and conventional laser cladding (CLA) refers to the melting of the powder. In EHLA, melted additive material lands directly on the substrate as opposed to solid powder particles; this could significantly increase the process speed [251, 252]. It has been reported that the cladding speed can reach 200 m/min [242-254]. Additionally, the thickness of the clad is between 25 and 250 μm, although in conventional laser cladding, the clad is typically thicker than 0.5 mm [255]. In other words, EHLA shows great promise for preparing high-quality thin coatings with improved coverage rates.

2.2.3.2.2.4 Laser cladding system

Normally, a laser cladding with a powder injection system consists of three major elements: the laser system, the computer numerically controlled (CNC) robotic system, and the powder feeding system (see in Figure 2.16) [256, 257].

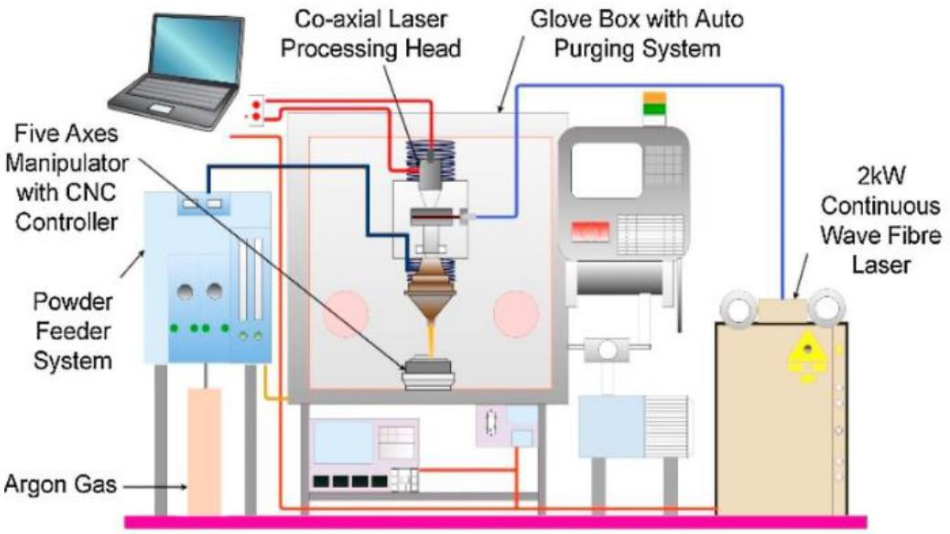

Figure 2.16 Laser cladding system parts [258]

Laser cladding process requires an understanding of the structure of these systems and their functionality in a variety of operating conditions. An overview of the laser cladding systems will be given in chapter 3. In general, the laser system generates the required energy for the operation [256, 257]. The system is controlled by computer numerical control equipment. There are two main types of configurations available: the substrate remains fixed while the laser and feeding system move; or the laser and feeding system is fixed and the substrate moves with CNC table [257]. The powder delivery system needs to provide the appropriate amount of powder to the melt pool.

It is crucial to select a reliable powder system in order to achieve a satisfactory process operation. A powder system is intended to produce a powder flow that is continuous, uniform, and follows a defined powder feed rate. However, customized powder systems based on various powder transportation methods are also being used [256, 259-266]. Powder systems are classified into four categories according to their operating principles: Gravity-based, Mechanical wheel, Fluidized-bed, Vibrating (see in Figure 2.17) [256].

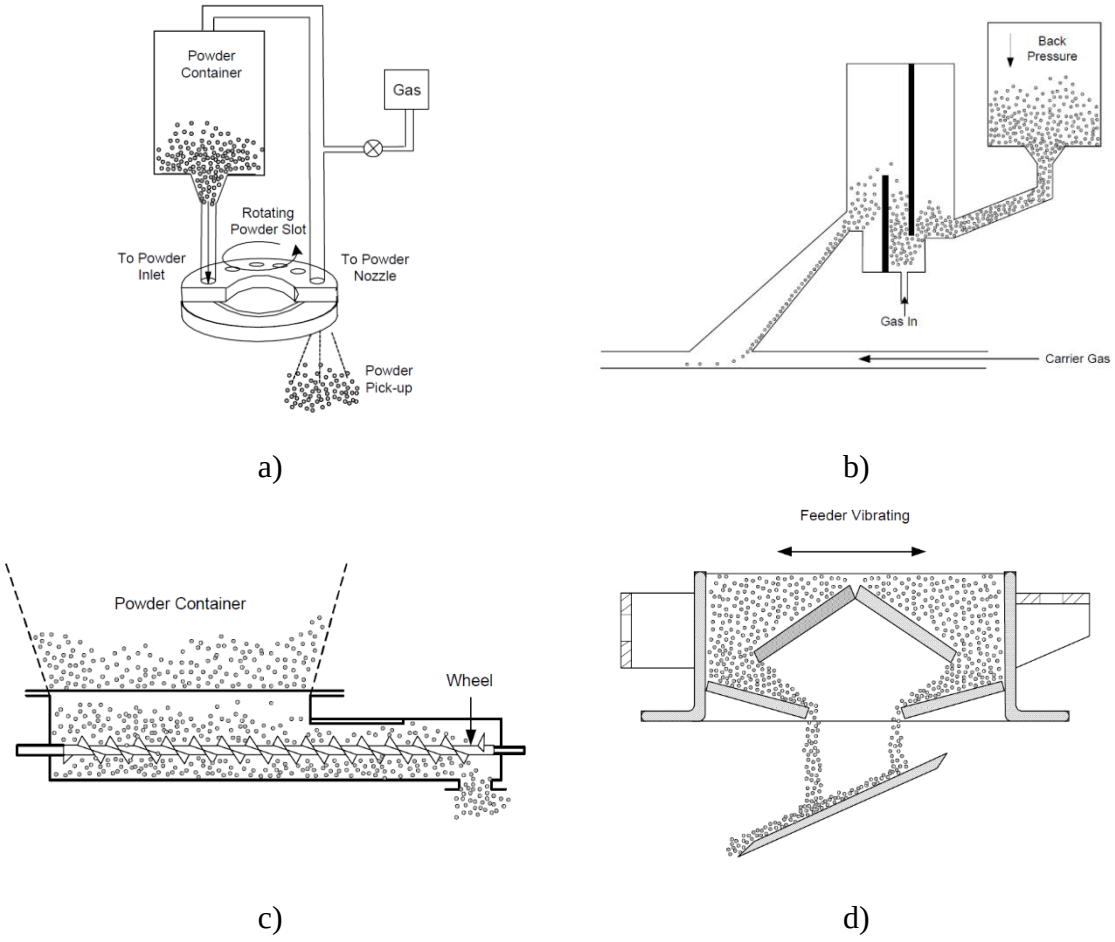

Figure 2.17 A schematic depiction of powder delivery systems: a) Gravity-based, b) Fluidized-bed, c) Mechanical wheel, d) Vibrating [256**]**

It is not uncommon for powder systems to use a mixture of these methods to achieve greater powder transport stability. Any type of powder system requires the use of carrier gas to carry powder particles [256].

The gravity-based powder feeder system contains two main parts: powder storage and a rotational disk (see in Figure 2.17 a)). From the container, the powder is transferred to the rotating disk and delivered to the collection unit using a carrier gas. Furthermore, the powder stream can be stabilized by applying back pressure to the carrier funnel. Several variables affect the volumetric powder feed rate, including the slot size and the disk speed [259-261].

A fluidized bed powder system functions as follows: the carrier gas travels through a filter, spreading through the powder, thus fluidizing it (see in Figure 2.17 b)). Then the fluidized bed solution is transported along the pickup tube through the carrier chamber and is transported to the nozzle by the carrier gas. This kind of system can offer steady, uninterrupted powder feed, allowing for optimal manufacturing process control and enhanced clad quality depending on powder type [264, 265].

A mechanical wheel powder system may also use a screw powder feeder. This system works on the principle of powder being transferred from a container to a powder pickup device and then to the powder nozzle mechanically (see in Figure 2.17 c)). The feed rate is determined depending on the rotation speed and screw diameter. For a consistent flow rate, various screw designs are available. Mechanical wheel powder systems face a disadvantage of abrasive wear when mechanical parts contact solid particles, which can affect the clad quality and increase the cost of maintenance [262, 263].

A vibratory tray system contains a shallow tray with a flat bottom and a vibrating tray with several plates positioned at an angle to achieve enhanced precision and control of powder flow (see in Figure 2.17 d)). This system operates as follows: the powder passes from the hopper outlet onto the tray, and the tray vibrates, sending powder downward, which regulates how much powder is fed into the system [256, 266].

In an overview of the applications of powder feeder systems in laser cladding, it is challenging to determine what type of powder feeder will be ideal for a particular laser cladding application. Since laser cladding is used in various situations in industry, it requires different types of powders of different sizes with varying powder feeding rates [256].

Powder feed systems can be classified into these four types based on their methods of operation. The powder injection method, which means the powder delivery direction, can be performed in two main directions: off-axis (lateral) [187-199] and coaxial [201-231] (see Figure 2.11). In either case, the powder is transported through the laser beam, where it is heated or melted before entering the melt pool. The off-axis nozzle is relatively simple to design, while coaxial nozzles require significant engineering [187].

2.3 Topics of specific interest to this thesis

2.3.1 Dilution in laser cladding

2.3.1.1 Introduction

Laser cladding demands creating a strong adhesion between the substrate and the cladding material. However, the substrate melt depth must generally be kept to a minimum to ensure that the cladding material is not diluted excessively by the base material. Dilution is understood to mean how much mixing of the substrate and clad material has occurred and is reported as a percentage. Dilution is a natural consequence of the cladding process because some substrate melting is necessary in order for there to be a good interfacial weld between the cladding and the substrate. Excessively high dilution decreases the benefit gained from adding the clad material to the surface. Target dilution values vary but tend to be in the range of 10 to 20 percent. In some cases high dilution levels are actually preferred [267-269] but such applications are unusual. There are no clear guidelines on how to measure or analyse the level of dilution in laser clad surfaces. There is a range of dilution measurement and analysis techniques in use, and the following section is an attempt to compare them and identify the most suitable ones for scientific and industrial use.

2.3.1.2 Determining the level of dilution

2.3.1.2.1 Geometric dilution methods

In the most common method of dilution estimation, used by a number of researchers [81, 256, 270-357],dilution is determined from the geometry of the cross section by dividing the cross sectional area of the substrate melt by the area of the whole melt. This gives us a dilution we can call D_{AREA}:

$$D_{AREA} = \frac{A_s}{(A_c + A_s)}$$

Where,

Ac: cladding area above the substrate

As: substrate area

Another method of the dilution measurement, which is the simplest method, is to determine the dilution by dividing the maximum depth of melt penetration into the substrate by the overall melt depth of the clad layer. This gives a dilution estimate we can call D_{HEIGHT}:

$$D_{HEIGHT} = \frac{S}{(S + C)}$$

where (C) is clad height and (S) is depth of substrate melting. This simple estimate of dilution has been used by numerous researchers including [77, 86, 279, 291, 297, 298, 307, 308, 311, 312, 317, 318, 337, 350-350, 352, 358-412]. This measurement requires only two distances to be measured: S the depth of penetration and C the height, both measured with respect to the original substrate surface. This D_{HEIGHT} dilution measurement method has the benefit of being quick and easy. There is however a hidden assumption with this method, which is that S and C are measured in the centre of the clad where both values are at their maximum. For geometries such as that in Figure 2.18 a) this is the obvious place to make the measurements, however this is not the case for all geometries as shown in Figure 2.18 b).

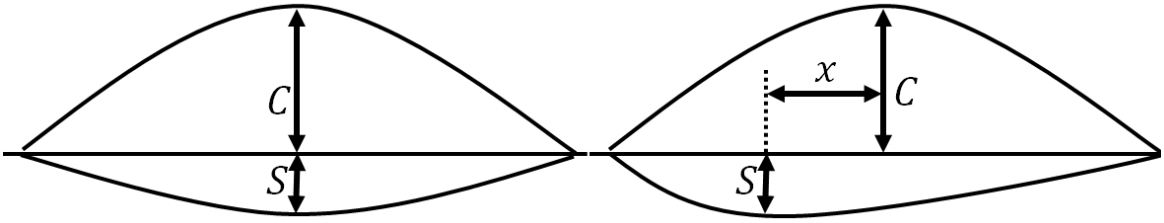

a) b)

Figure 2.18 Possible clad geometries a) symmetric and b) asymmetric

The two different dilution measurement techniques are presented in the Figure 2.19 in order to compare their differences. The figure below demonstrates that D_{HEIGHT} is not always equivalent to D_{AREA}.

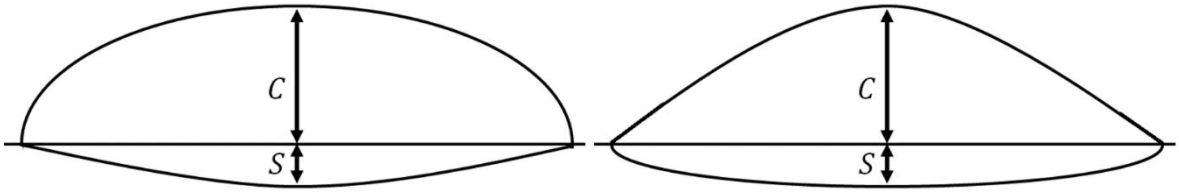

Figure 2.19 Two clad tracks with the same Dheight but different Darea

In above the two clad cross sections have the same width, depth and height and therefore the same D_{HEIGHT}. However, the D_{AREA} of the left hand track is 18.45 % and that of the right hand track is 30.34% These clads will give different dilution results depending on the method used to determine dilution.

All geometrical dilution measurements are made on cross-sections of laser clads. This makes geometrical dilution measurement a necessarily destructive process which is a clear disadvantage. It should however be noted that there is other useful information that can be extracted from examination of such cross-sections, including overall clad shape, quality of the interface, presence or absence of porosity and cracking.

It is important to realise two things about D_{HEIGHT} and D_{AREA};

1. Both methods only give an overall dilution value and give no indication of the dilution gradients which may exist in the clad layer, particularly near the clad-substrate interface.
2. Both methods give only a spatial measurement of dilution levels which do not account for the densities of the alloys involved. D_{AREA} gives a dilution value which can be used to calculate the volumetric proportions (Vol%) of the average content of the diluted clad layer. D_{HEIGHT} is too inaccurate for this calculation.

It is standard metallurgical practice to discuss alloys in the percentage of weight of each of the alloying constituents (wt%) or the atomic percentage (at%). To convert D_{AREA} to wt% we can use the equation below, to give an average dilution value which we can call 'metallurgical dilution' or $D_{wt\%}$.

$$D_{wt\%} = \frac{\rho_s A_s}{(\rho_c A_c + \rho_s A_s)}$$

ρ_c is the density of the additive powder, ρ_s is the density of substrate, As is the cross-sectional area of the substrate melt and Ac is the cross sectional area of the clad area of the clad area above the line of the original substrate surface.

A lot of published work on laser cladding focusses only on single tracks, however industry is almost solely interested in multiple, overlapping clad tracks. This gives rise to two separate issues:

1. How is the dilution measurement process adapted for overlapping tracks?

2. Danger of extrapolating single-track results to overlapping clads.

The majority of geometrical dilution measurement methods are defined with reference to a single track. These need to be redefined for multiple overlapping tracks. This generally results in simplified measurements as more regular shapes need to be measured. The extreme would be an entirely uniform clad where clad height above the original surface and melt depth below the original surface are uniform along the clad. There are well known differences at the start and end of the cladding, where steady state conditions are not obtained.

2.3.1.2.2 EDX chemical analysis of the dilution level

A scanning electron microscope (SEM) enables both the imaging and analysis of bulk samples using a highly focused beam of electrons contained within a vacuum chamber. Electrons are generated through the use of ether a thermionic, Schottky or field-emission type cathode and are subsequently accelerated due to a potential difference applied between the anode and cathode of the electron gun.

The incident electrons that strike the sample surface interact with both the nuclei and the electrons of the sample and result in the emission of electrons, X-rays, heat, and light (cathodoluminescence). These secondary signals can be analysed to gain a wealth of knowledge about the sample.

The elemental composition of a region can be determined by measuring the energy associated with the X-rays produced as a result of the de-excitation that occurs when a low energy electron vacancy is occupied by an electron from a higher energy level. As previously mentioned, these electron vacancies exist due to the inelastic interactions that result in the emission of secondary electrons. The energy and wavelength associated with the X-ray emission is characterised by: the element, the energy level of the shell vacancy and the number of orbital shell jumps made in order to fill the vacant shell. The energy criterion needed to remove an electron from a given shell is known as the critical excitation energy. Therefore, if the incident electron beam has sufficient energy to remove an electron from a

given shell, a characteristic X-ray will be produced due to electron de-excitation. The differences in the critical excitation energy between different elements gives rise to variations in the spatial resolution when analysing different elements. Noncharacteristic X-rays are also produced due to the deceleration of electrons as the enter the coulombic field of an atom and are often referred to as background, continuum or bremsstrahlung X-rays. A collimator, electron trap, window, semiconductor crystal detector and a field effect crystal transistor make up the main constituent components of an EDS detector. The collimator ensures that only X-rays which have been generated due to interactions between the electron beam and sample enter the detector. Preceding the collimator is an electron trap which is aptly named as it prevents the entry of electrons into the detector. The window is simply fitted to the detector to act as a barrier and isolate the semiconductor crystal detector from the chamber of the microscope. However, the window limits the ability to detect low atomic number elements. The semiconductor crystal detector is kept under a high vacuum cold environment and converts incident X-rays into measurable short voltage pulses. This is achieved by applying a large bias voltage across a lithium drifted silicon semiconductor to create a region depleted in electrons. When an X-ray passes through this depleted region a series of electron hole pairs are created; these charge carriers migrate to opposing electrodes thus generating a charge signal. This signal is added to the applied bias voltage and is proportional to the energy of the original X-ray. The voltage pulse from the detector requires amplification and this is partly achieved using a field effect transistor.

A dilution method using EDX was also presented in the literature. EDX dilution analysis is based on the measured values obtained from EDX analysis of the tracks. To perform the dilution analysis, it is required to have knowledge of the density of the substrate and cladding feedstock material and their composition, as well as the composition of the deposited clad. According to the equation below, the dilution can be calculated [256, 272, 275, 293, 295, 313, 319, 324, 331, 332 337, 352, 397, 413-431].

$$D_{EDX} = \frac{\rho_c(wt\%_{c+s} - wt\%_c)}{\rho_s(wt\%_s - wt\%_{c+s}) + \rho_c(wt\%_{c+s} - wt\%_c)} \times 100\ [\%]$$

p_c is the density of the additive material.

p_s is the density of substrate material.

$wt\%_c$ is the weight percentage of element X in the additive material.

$wt\%_s$ is the weight percentage of element X in the substrate material.

$wt\%_{c+s}$ is the local weight percentage of element X in the clad region.

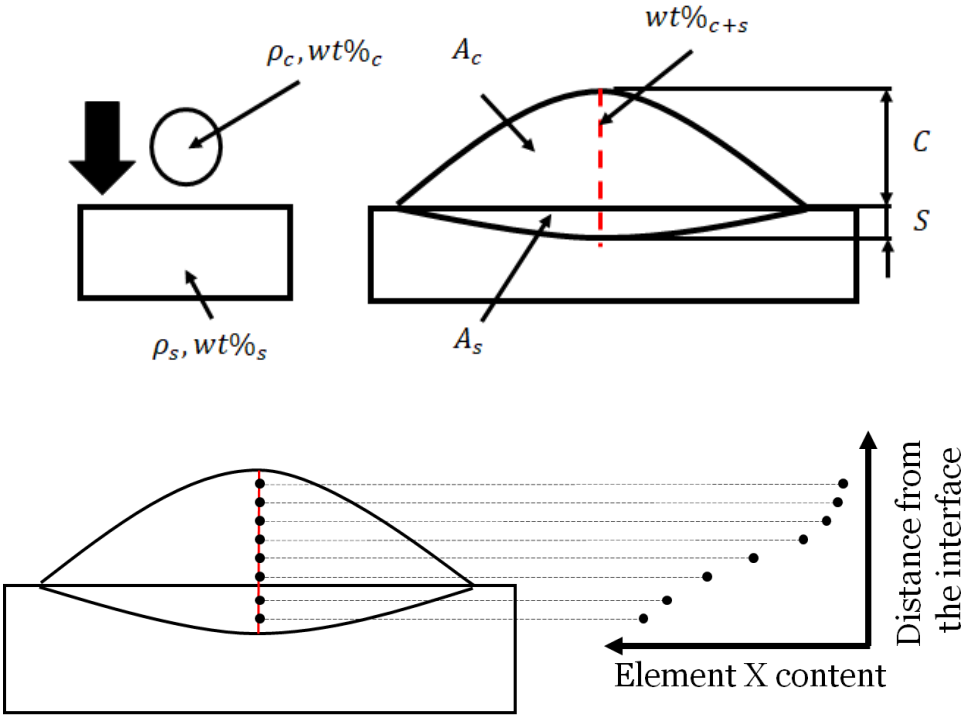

Figure 2.20 Illustration of the cross-sectional areas used to define the dilution with EDX

The dilution can be determined by analysing the X element concentration profile in the cross-section of the clad using EDX analysis. A line profile was collected along the thickness of the clad, starting from the interface and continuing to the external surface. Schematic representation of the cross-sectional areas used to define dilution with EDX, shown in Figure 2.20. Due to the gradient in X element concentration along the clad thickness, an estimating info as a function of position was used to determine the dilution. Using the average will result in the loss of information. A spatial variation can also be determined using EDX mapping, depending on the objectives.

There is a representative example in the paper that presented the EDX chemical analysis of the dilution level [445]. The following Table 2.1 shows the chemical composition of alloys.

Table 2.1 Density ρ (kg/m^3) and chemical composition (wt.%) of Eutroloy 16012 and SS304 steel substrate level [445]

Material	Alloy	kg/m^3	Co	Fe	Cr	W	C	Si	Ni	Mn	Cu
powder	Eutroloy 16012	8520	57.2	1	29.5	8.5	1.6	1.2	1	0	0
substrate	SS304	8000	0	71.2	17.8	0	0.08	0.7	8	1.7	0.6

The dilution in this paper was calculated from both the Fe and Co contents. Below in Table 2.2 represents three different measurements for Fe and Co elements.

Table 2.2 Chemical composition (wt.%) and dilution results

		Measurement 1.		Measurement 2.		Measurement 3.	
		Fe	Co	Fe	Co	Fe	Co
$wt\%_{c+s}$	Clad	7.63	51.79	10.97	49.06	14.34	46.32
$wt\%_s$	Substrate	71.2	0	71.2	0	71.2	0
$wt\%_c$	Powder	1	57.2	1	57.2	1	57.2
	Dilution (%)	9.997	10.011	14.987	15.017	19.991	20.010

Based on the dilution results, it appears that the EDX equation gives the same results for all elements. As a consequence, the general equation for an EDX can be applied to any element present in a clad.

2.3.1.3 Choice of dilution method

Based on a large literature review, which involved more than 200 scientific papers, the researchers' use of each of the dilution techniques has been noted. As the below shows the most common method to determine the dilution is using the ratio between the cross-sectional area of the molten substrate material and the total cross-sectional area of the clad.

Table 2.3 Researchers' use of different dilution techniques

Technique	Researchers' usage rate
D_{area}	47%
D_{height}	37%
D_{EDX}	16%

Based on the research papers, we can conclude that there is no explanation for the choice of dilution technique. Moreover, no previous studies have been conducted to compare dilution techniques. This subject is covered as part of one of the papers published as part of this PhD.

2.3.1.4 Summary of dilution

To briefly summarize the various dilution measurement techniques, geometrical dilution techniques require only optical microscopy measurements, but only provide average chemical content. The most accurate method for determining dilution is EDX analysis. Such a measurement requires expensive equipment, such as scanning electron microscopy, but can give gradient and spatial information as well as average dilution results.

2.4 Productivity in laser cladding

2.4.1 Clad deposition strategies, introducing ABA cladding

2.4.1.1 Introduction

In the early 1980s, researchers embarked on the exploration of laser cladding, a process that has since gained significant industrial significance. Laser cladding involves melting a cladding alloy onto a metal substrate, achieved either through pre-placed or blown powder, with successive tracks deposited side by side to form a clad surface. This technique has proven highly effective in modifying the physical and chemical properties of material surfaces. The primary focus within the engineering sector revolves around cost reduction while maintaining the required surface characteristics of engineering components. Often, cost savings can be realized by employing a more affordable substrate material in combination with a suitable coating alloy. Additionally, improving powder catchment efficiency, deposition rate, and coverage rate can enhance overall productivity and cost-effectiveness. This thesis proposes a new approach to reducing costs by examining different layering techniques and introducing a new possible solution, called ABA cladding.

2.4.1.2 Layering techniques

According to the literature, there are three distinct cladding strategies. The first strategy involves shaping the contour by initially constructing a wall with a square form and then following a spiral path with overlapping square shapes that gradually decrease in size. The second cladding technique consists of creating zigzag tracks by continuously moving back and forth in a parallel direction. This technique can be modified by depositing the first layer in a transversal manner and the second layer longitudinally. The third cladding technique involves depositing the clad layers in parallel, commencing and concluding at the same point [425, 426]. The conventional method for cladding desired surfaces involves the parallel layering technique, commonly referred to as traditional AAA cladding.

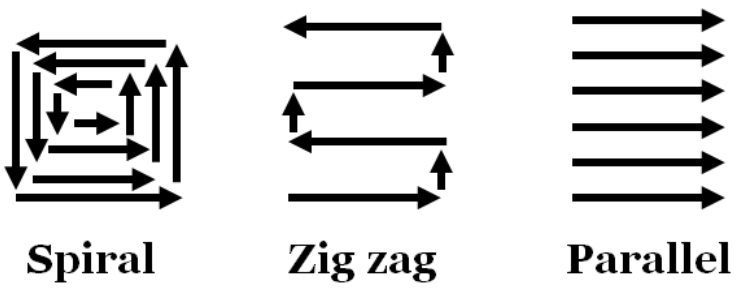

Figure 2.21 Layering methods in laser cladding

2.4.1.3 Problems with traditional AAA cladding

The traditional laser cladding process involves the deposition of a single track on the substrate surface, and researchers often analyse the characteristics of these single tracks under various processing conditions. However, in practical industrial applications, it is more common to overlap multiple tracks until the desired clad surface is achieved.

Despite the initial resemblance of these clad tracks, the traditional cladding process can be termed "AAA cladding" only after several tracks have been laid. The shape of subsequent tracks is influenced in various ways by the preceding tracks during the early stages of the process. While this aspect is not frequently discussed in the literature, most researchers in the field illustrate it in the cross-sections of clad layers. There can be significant variations in the height, cross-section, and metallurgy of clad tracks. Track 1, in comparison to subsequent tracks, exhibits distinct melt pool geometry, impacting powder capture and dilution. A repetitive cladding pattern typically does not establish itself until track 4, as depicted in Figure 2.22. It is important to note that these initial anomalies in starting and finishing tracks pose a significant drawback in the AAA cladding system, leading to localized disturbances in clad surface morphology, dilution, and the presence of heat-affected zones.

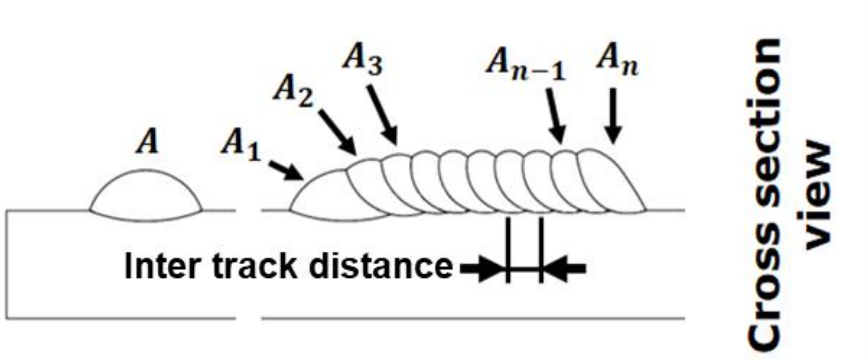

Figure 2.22 Cross-sectional view of initial 'A' track and a standard (AAA) laser clad surface, where the clad surface consists of overlapping 'identical' tracks

The laser cladding process entails a processing head that delivers a cladding powder alloy in conjunction with a defocused laser beam, both coaxially aligned. The objective of this process is to completely melt all the incoming powder within the laser-material interaction area to form the clad track. However, capturing all of the incoming powder within the melt pool is generally unattainable, and a certain portion of the powder escapes from the melt pool. The escape of powder plays a vital role in the cost-effectiveness of the cladding process.

In considering the behaviour of the escaping powder, it's essential to note that due to the diverse escape routes available to powder particles, influenced by the previous track's shoulder and the melt pool's slope, they are directed away from the melt pool. The pathways for powder particle escape are illustrated in Figure 2.23 for both single-track (A cladding) and overlapping-track (AAA cladding) scenarios.

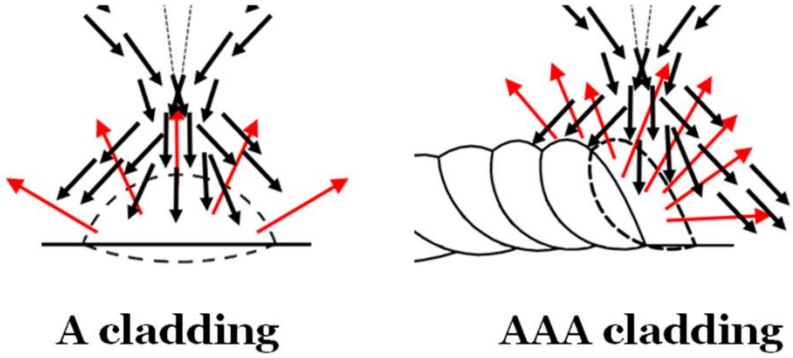

Figure 2.23 An illustration of the powder particle escape pathways in A and AAA claddings.

The efficiency of powder capture within the process holds immense significance for cost control and is a top priority for industrial users. This efficiency can be defined as the percentage of powder supplied to the laser melting process that ultimately contributes to the laser clad layer. According to technical literature, powder capture efficiencies vary widely but often fall significantly below 50%. This presents a substantial challenge due to the high cost of the powder and its limited recyclability.

Despite a substantial body of research on laser cladding with blown powder, there are currently no clear guidelines outlining the critical quality and productivity parameters relevant to various industrial sectors. Likewise, there are no universally accepted criteria for defining a high-quality deposition. It is imperative to investigate the impact of productivity factors to gain a deeper comprehension of the process, enabling its successful application in the industry.

2.4.1.4 Possible solution, introducing ABA cladding.

This thesis explores an innovative cladding technique known as ABA cladding, aiming to establish a more predictable and efficient process. In this approach, clad tracks are initially laid down at wider intervals ('A' tracks), and the gaps between them are subsequently filled with tracks produced under different parameters ('B' tracks). This method results in a more uniform structure, as illustrated in Figure 2.24 Consequently, all 'A' tracks exhibit identical shapes, dilution levels, and other characteristics, and the same applies to all 'B' tracks.

The study in this work conducts a comparison between ABA laser cladding and the traditional AAA cladding method. Specifically, the research evaluates the efficiency of powder capture and the deposition/coverage rates of these two techniques.

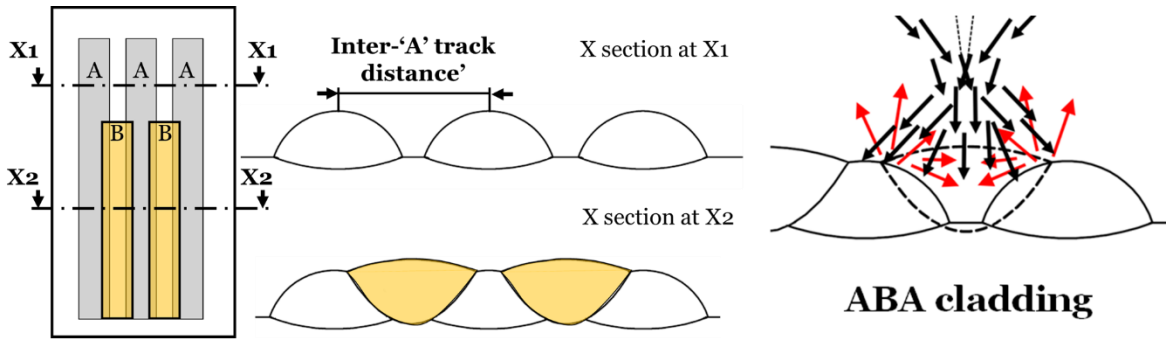

Figure 2.24 A cross-sectional view of ABA cladding, where parallel 'A' tracks are laid first, and the gaps between them are filled with parallel 'B' tracks. A schematic illustration of the powder particle escape pathway in ABA cladding.

Laser cladding, a prominent process within Additive Manufacturing, typically entails building a clad surface by adding parallel, overlapping lines of cladding material onto a substrate. This study explores a novel cladding technique in which initially, a series of separate or slightly overlapping clad tracks (referred to as 'A' tracks) are deposited. Subsequently, these 'A' tracks are interleaved with tracks that can utilize different parameters (referred to as 'B' tracks). The investigation focused on the impact of process parameters in laser cladding, specifically with AISI 316L stainless steel and Stellite 6 powders, utilizing a coaxial powder delivery nozzle. Parameters such as process speed, laser power, powder flow rate, and overlap strategy were found to exert a significant influence on the process.

The ABA cladding technique could offer a potential solution to the challenges posed by AAA cladding:

a) Significant enhancement in powder catchment efficiency.

b) Substantial improvement in deposition and coverage rates.

c) Ability to create flatter clad surfaces, reducing the need for extensive post-processing.

d) Improved predictability of dilution levels and local metallurgy.

e) Capability to clad dissimilar materials in combinations of tracks.

2.4.2 Deposition rate (powder catchment)

2.4.2.1 Introduction

High productivity is crucial in laser metal deposition to make the process economically viable. By improving the deposition rate of the process, it is possible to optimize the productivity of laser cladding. Over the past ten years, research has focused on deposition rate as an important research topic [432, 433, 439, 442, 449, 456, 458, 463, 474]. Typical deposition rates for laser cladding with blown powder are usually around 0.5 kg/h [432, 433, 439, 442, 449, 456]. The deposition rate is determined by: the total amount of powder deposited per unit of time. It is possible to achieve a very high deposition rate, up to 16 kg/h, which can significantly improve the productivity of the process [458].

2.4.2.2 Determining the deposition rate

The deposition rate can be determined by multiplying the cross-section of a single clad track by the processing speed and the density of the cladding material [432, 442, 449, 456, 458, 463, 474].

The deposition rate is therefore defined as:

$$\boldsymbol{Depostion\ rate = A_{track} \cdot v \cdot \varrho \left[\frac{kg}{h}\right]}$$

Where,
A_{track} = Cross-sectional area of a single track above the original line of the substrate (m^2)
v = Process speed (m/h)
ρ = Density of cladding material (kg/m^3)

2.4.2.3 Deposition rate and processing parameters

Laser power

The laser power influences the deposit rate positively. An increased laser power can lead to higher deposit rates. Increasing the laser power produces higher overall absorption of laser energy producing a larger molten pool with a higher temperature. Consequently, more particles collide with, and are captured in, the melt pool [432, 433, 439, 442, 449]. On the other hand, it is important to note that, when the density of the laser power falls below a certain threshold, discontinuous tracks with irregular cross-sections can occur. Additionally, significant substrate melting, leading to excessive dilution of the clad could occur if the laser power density exceeds a specified value. A high level of dilution must generally be avoided [292].

Powder feed rate

Increasing the powder flow rate generally influences deposition rate in a positive manner. In the presence of constant laser power and processing speed, as the powder feed rate increases, the deposition rate will increase linearly up to a critical point. Before the critical point, the increased powder feeding rate resulted in higher deposition rates due to the injection of more particles into the deposited pool [432, 433, 439, 442, 449]. Upon exceeding this critical value, the increase in deposition rate becomes more complicated. The excessive powder flow can block the laser beam and result in insufficient melting of the substrate and the powder, which can lead to poor adhesion to the substrate.

Process speed

The rate of deposition is usually adversely affected by the linear speed of cladding. In general, the faster the cladding speed, the lower the deposition rate, since it is directly related to interaction time. By speeding up the cladding process, less energy is supplied to the melt pool, resulting in a smaller melt pool. By having a smaller melt pool, the powder injected from the nozzle has a smaller surface area to attach to, which reduces the deposition rate [432, 433, 439, 442, 449].

Nozzle design

Under identical experimental conditions, a coaxial nozzle and a three-jet nozzle have been compared [474]. The three-jet nozzle configuration showed a lower deposition rate with higher usage of powder, while the coaxial configuration showed a better deposition rate. With the three-jet nozzle, the majority of powder particles that hit the melt pool surface rebounded. With a coaxial nozzle, almost all of the powder particles were captured and observed. On the basis of these experimental results, it can be concluded that the coaxial powder feeding has the advantage of a higher deposit rate [474].

2.4.2.4 Reported results of deposition rate

A large survey was carried out to identify the range of deposition rates noted in the literature. This resulted in 28 relevant data points which are presented in Table 2.4 in order of increasing deposition rate. In 9 of these papers the deposition rate is directly identified by the authors. In the remaining 19 the deposition rate had to be calculated from the information in the paper and the clad cross section photographs. In Table 2.4 these different types of information are labelled ‘author ID’ and ‘calculated’.

Table 2.4 Reported results of deposition rates

No.	Papers	Paper type	Laser type	Substrate	Powder	Density of the powder	Laser power	Powder feed rate	Process speed	Beam diameter	Cross sectional area	Deposition rate	Powder catch. Eff
				-	-	(g/cm^3)	(kW)	(g/min)	(mm/min)	(mm)	(mm^2)	(kg/h)	(%)
1	[439]	Author ID	3.5 kW CO2	Inconel 625	Inconel 625	8.44	1-1.5	4.55-7.6	300-800	2	-	0.005-0.01	28-40
2	[432]	Author ID	1 kW fiber	Zr alloy	Zr	6.49	0.8	8.8	245	1.4	-	0.05	9.09
3	[457]	Calculated	1 kw Nd:YAG	Ti-6Al-4V	Ti-48Al-2Cr-2Nb	2.3	0.7	2	300	2	2.04	0.084	70.22
4	[433]	Author ID	1.2 kW CO2	AISI 1050	AISI 316L	8	0.8-1	8.16-16.26	288-480	2.2	-	0.06-0.12	12-16
5	[462]	Calculated	2.5 kW diode laser	CuBe alloy	AISI H13	8.4	3.6	3.2	18200	3	0.02	0.153	79.63
6	[469]	Calculated	3.0 kW disk laser	300M	Aermet®100	7.8	3	3.86	750	1.3	0.54	0.191	82.29
7	[461]	Calculated	TruDisk 4002 disk laser	Ti811	Ni60	4.4	0.9	5	500	3	1.79	0.236	78.61
8	[450]	Calculated	3kw solid state laser	Q235	Fe901 + Cr3C2	7.7	1.2	7.3	300	5.4	1.71	0.237	54.19
9	[445]	Calculated	3.3 kW Fiber laser	SS304	Eutroloy 16012	8.2	1	9	300	3	1.83	0.269	49.88
10	[451]	Calculated	3KW Nd:YAG laser	Q235	Fe-based alloy	8.5	1.1	8.5	300	4	1.86	0.285	55.8
11	[449]	Author ID	1 kW fiber	AISI 1050	AISI 316L	8	0.2-0.6	6.9-9.4	200-400	-	-	0.04-0.54	9-95
12	[448]	Calculated	2.7 kW Nd:YAG	BDMS	NiCrBSi	7.8	2	10	1000	2.67	0.66	0.309	51.48
13	[442]	Author ID	2 kW fiber	S235JRC+C	1.4313	7.7	1.2	14-16	800-1000	2	-	0.33-0.35	34-42
14	[456]	Author ID	1 kW fiber	AISI1045	AISI 316L	8	0.2-0.6	7.8-9.4	200-300	-	-	0.23-0.54	44-95
15	[454]	Calculated	6 kW fiber laser	27SiMn	AISI 431	7.8	3.3	13	1500	2	0.69	0.484	62.1
16	[470]	Calculated	6 kW fiber laser	AISI 304	CoCrFeNi HEA	8.2	2	10	480	2.5	2.11	0.499	83.13
17	[471]	Calculated	4 kW Nd:YAG	DIN 2393	Tribaloy T-400	8.9	3	13.2	600	4.8	2.09	0.670	84.65
18	[453]	Calculated	12 kw fiber	Inconel 625	Inconel 625	8.4	2.5	19	636	4	2.16	0.693	60.77
19	[466]	Calculated	8 kW diode laser	SNCrW	EuTroLoy 16006	8.4	4	20	240	2	7.97	0.964	80.34
20	[472]	Calculated	8 kW diode laser	SNCrW	EuTroLoy 16006	8.4	4	20	240	2	8.56	1.035	86.25
21	[465]	Calculated	1 kw Nd:YAG laser	AISI 420	Stellite 6	8	0.72	22	3000	2	0.73	1.057	80.11
22	[443]	Calculated	6.0 kW diode laser	AISI 316L	Inconel 625	4.3	3.2	50.91	24960	5	0.2	1.288	42.16
23	[444]	Calculated	6 kW fiber laser	A45	Ni60	4.4	3.2	50.91	24960	2	0.2	1.318	43.14
24	[473]	Calculated	2.5 kW Nd:YAG laser	Mild steel	Hastelloy C	8.8	2.4	28	1400	4	1.97	1.458	86.78
25	[468]	Calculated	5 kw fiber laser	AISI 1045	Inconel 625	8.4	3.131	40	1545	2	2.53	1.973	82.2
26	[474]	Author ID	12 kW diode	Inconel 718	Inconel 718	8.17	2.9	45	1500	4	-	2.49	92.04
27	[463]	Author ID	15 kW fiber	S235JR	Inconel 625	8.44	15	273	1000	5	-	13.1	79.98
28	[467]	Author ID	15 kW fiber	S235JR	Inconel 625	8.44	15	273-315	750	5	-	14.1-15.6	79-82

The following paragraphs give more experimental details from the papers where the deposition rate was discussed by the authors.

Paul et al. [439], examined laser cladding for components made from Inconel-625. A high-power continuous wave CO2 laser system with a maximum output power of 3.5 kW was used. In terms of processing parameters, the laser power was 1-1.5 kW, powder feed rate 4.55-7.6 g/min and process speed 300-800 mm/min. According to the results obtained, the deposition rate ranged from 0.005-0.01 kg/h with powder catchment efficiency of 28-40%. The highest deposition rate was obtained with 1.5 kW laser power, 6.03 g/min feed rate and 500 mm/min process speed.

Harooni et al. [432], contributed to the development of processing windows for laser cladding of zirconium alloy on zirconium. Laser cladding experiments used a fiber laser with a power output of 1 kW. The effect of laser power, processing speed, laser beam diameter and powder feed rate on the clad quality was investigated. Processing parameters were 0.8 kW, 8.8 g/min and processing speed 24 mm/min. It was possible to deposit zirconium clad at a deposition rate of 0.05 kg/h with a dilution of 50% and powder catchment efficiency

Pinkerton and Li [433], investigated the impact of deposition point standoff variations in multilayer coaxial laser cladding. For the laser cladding experiments, a 1.2 kW CO2 laser was used with the following processing parameters: laser power 0.8-1 kW laser power, 8.16-16.26 g/min feed rate and 288-480 mm/min speed. According to the results obtained, the deposition rate ranged from 0.06-0.12 kg/h with powder catchment efficiency of 12-16%. The highest deposition rate with 12% powder catchment was obtained with 1 kW laser power, 16.26 g/min feed rate and 480 mm/min process speed.

Tabernero et al. [449], worked on optimal parameters for 5-axis laser cladding. For the laser cladding experiments, a 1 kW fiber laser was used with the following processing parameters: laser power 0.2-0.6 kW laser power, 6.9-9.4 g/min feed rate and 200-400 mm/min speed. According to the results obtained, the deposition rate ranged from 0.04-0.54 kg/h with powder catchment efficiency of 9-95%. 0.2 kW laser power, 9.4 g/min feed rate and 200 mm/min process speed, mild steel substrate, and 316 stainless steel powder resulted in the highest deposition rate with 95% powder catchment.

Dalaee et al. [442], optimized deposition rates for laser direct metal deposition on components. The objective was to determine the optimal combination of process parameters in order to make laser cladding economically feasible. In the laser cladding experiments, a fiber laser with a maximum output power of 2 kW was used. In the experiment, mild steel S235JRC+C and stainless-steel powder 1.4313 were used. The main processing parameters were, a laser power of 1.2 kW, powder feed rate 14-21 g/min and process speed 800-1400 mm/min. Based on the results, the deposition rate ranged from 0.33-0.35 kg/h with powder catchment efficiency of 34-42%. The highest deposition rate was obtained with 1.2 kW laser power, 21 g/min feed rate and 1400 mm/min process speed.

Calleja et al. [456], investigated the improvement of strategies and parameters for multi-axis laser cladding. This paper examines how to complete laser cladding operations in 5 axis. The laser cladding experiments used a fiber laser of 1 kW maximum output power. The experiment was conducted with an AISI 1045 mild steel substrate and AISI 316L stainless steel powder material. In terms of main processing parameters, the laser power was changed from 0.2-0.6 kW, powder feed rate 7.8-9.4 g/min and process speed 200-300 mm/min. According to the results, the deposition rate ranged from 0.23-0.54 kg/h with powder catchment efficiency of 44-95%. The highest deposition rate was achieved with 0.2 kW laser power, 9.4 g/min feed rate and 200 mm/min process speed.

Zhong et al. [474] investigated the effect of powder stream on laser metal deposition using Inconel 718. Processing parameters were 12 kW, 45 g/min and processing speed 1500 mm/min. The deposition rate of 2.49 kg/h was achieved with a 92% powder catchment efficiency.

Turichin et al. [463] worked on the technical aspects of laser cladding with high power 15 kW fiber laser using Inconel 625 powder on mild steel. Processing parameters were 15 kW, 273 g/min and processing speed 100 mm/min. It was possible to reach a deposition rate of 13 kg/h with powder catchment efficiency 80%.

Tuominen et al. [467], worked on laser cladding using a 15 kW fiber laser on mild steel using stainless steel 316 powder. Processing parameters: laser power 15 kW laser power, 273-315 g/min feed rate and 750 mm/min speed. It was possible to deposit a clad with deposition rate of 14.1-15.6 kg/h with powder catchment efficiency 79-82%. Accordingly, the highest powder feed rate indicated the highest deposition rate.

From the industry's point of view, it is imperative to control costs. Among the costs associated with laser cladding are electricity, staff, overheads, raw materials, etc. Productivity improvement typically involves minimizing the time spent creating a product, i.e. a higher deposition rate. Also, reducing the wastage of the process, i.e. a high powder catchment efficiency. As well as deposition rate, the powder catchment efficiency represents another significant aspect of productivity, measured as the percentage of the powder fed into the cladding zone that becomes part of the cladding. Deposition rate and powder catchment efficiency are important metrics for the laser cladding industry as they have a direct influence on the cost of the process.

2.4.3 Powder catchment efficiency

2.4.3.1 Introduction

Blown powder laser cladding offers a flexible, robust, and economically advantageous method of supplying coating material thanks to the efficiency and repeatability of the process [475, 476]. Contrary to other laser surface technologies, this technology is characterized by complex interactions among the laser beam and the powder particles, as well as the molten areas of the substrate, making laser cladding challenging to control. Generally, most of the laser energy reaches the workpiece, while only a fraction is absorbed by the powder particles [477-479]. This results from the absorption of the beam by the powder stream, which creates the shadowing effect of the powder particles [478, 479]. Furthermore, only those powder particles hitting the molten pool adhere, whereas particles striking the solid region bounce away [480-485]. In view of the properties of the powder cloud it is problematic to forecast the laser power at which the workpiece and incoming powder will be melted. Creating the cladding layer is a complex process that involves a variety of process variables [486-489]. The morphology and quality of the cladding layer can be affected significantly by these parameters.

It is possible to optimize the performance of laser cladding and reduce waste by improving the powder catchment efficiency. Powder catchment efficiency was among the earliest research topics in laser metal deposition [455, 490]. The focus has been mainly to identify processes that are economically and environmentally feasible [491]. In the case of alloys that are more expensive, such as Ti- and Ni-alloys, the material costs can represent a significant portion of the overall operating costs associated with laser deposition. By optimizing the laser-powder interaction, new high-speed deposition techniques can be developed [492]. The catchment efficiency is defined as: the proportion of powder supplied that is incorporated into the clad. The powder catchment can be evaluated by weighing the substrate before and after cladding [434-438, 440, 441, 446, 447, 452, 455, 460, 464, 467, 490, 493-503]

2.4.3.2 Process parameters and powder catchment efficiency

The effects of each processing parameter on the powder catchment efficiency were investigated in a review of 26 papers [434-438, 440, 441, 446, 447, 452, 455, 460, 464, 467, 490, 493-503]. The parameters considered were the following: laser power, powder feed rate, carrier gas flow rate, cladding speed, melt pool size, powder flow diameter, the inclined angle, standoff distance, preheating, nozzle design (axial and lateral feeding), powder shape and powder density. The results of this review noted below.

Laser power

Increasing laser power generally has a positive effect on powder catchment efficiency. A higher laser power generates a larger molten pool with a higher temperature. More particles are therefore captured and melted to form the clad [434, 436, 446, 447, 452, 460, 467, 493-495].

Powder feed rate

The powder catchment efficiency generally increases as the powder flow rate increases. The increased powder feeding rate could enhanced the efficiency of the powder catchment since more particles were injected into the deposited pool. However, when the feeding rate exceeds a critical point, the catchment efficiency gradually decreases [434, 436-438, 440, 447, 452, 455, 459, 464, 467].

Carrier gas flow rate

There is a negative correlation between carrier gas flow rate and powder catchment efficiency. If the carrier gas flow rate is high enough, particles with a high traveling speed will be bounced off or blown away by the gas flow. Moreover, a too high carrier-gas flow rate affects the convection cooling of the molten pool and may lead to an irregular surface of the deposited clad. A high carrier-gas flow rate leads to irregularities in the deposited surface and has a negative impact on the molten pool geometry [446, 447].

Cladding speed

In many cases, the greater the cladding speed, the lower the powder catchment efficiency. With a faster cladding speed, the reduced energy supplied to the melt pool results in a smaller melt pool, with a smaller melt pool, the powder injected from the nozzle has a smaller area to attach to, which reduces the efficiency of the catchment of the powder [434, 436, 438, 455, 460].

Melt pool size

The size of the molten pool greatly affects powder catchment efficiency. A reduced size of the molten pool reduces the powder catchment efficiency, resulting in a smaller coating width and height [434, 435, 441, 496].

Powder stream diameter

There is a negative correlation between powder stream diameter and powder catchment efficiency. When the powder stream diameter is smaller than the melt pool size, more powder can be captured, thus increasing powder catchment efficiency [455].

Inclined angle of the substrate

When the substrate is inclined between 0◦ and 20◦ degrees and the laser is not perpendicular to the surface. It enlarges the laser irradiation area when the laser spot changes from a circle to an ellipse, which increases the molten pool's powder catchment ability. From 20° to 30°, the melting pool area decreases due to two causes. There is a slight decrease in laser power density. Furthermore, the inclined substrate has a lower laser absorptivity. Secondly, the alloy powders are harder to capture due to the inclined angle. The relative catchment of powders tends to be stable when the pool's inclined angle is between 30° and 50°.The increase of the catchment of alloy powders caused by the larger molten pool is approximately balanced with the decrease of the laser power density and absorption[497, 498].

Preheating the substrate

Powder catchment efficiency is positively affected by preheating. As preheating temperature increases, powder catchment efficiency increases. Preheating the substrate had an effect on improving powder catchment efficiency by increasing the molten pool's size and life-time. The longer trailing part of the molten pool (as it solidifies more slowly in a hot substrate) could enhance the powder catchment efficiency [499].

Nozzle design (axial or lateral nozzle)

For the catchment efficiency, the off-axis configuration showed a lower performance with a higher usage of powder. The coaxial configuration showed better catchment efficiency even when a higher track offset was used. Based on the experimental results it can be concluded that axial powder feeding is very beneficial from the point of view of high powder catchment efficiency [438, 464]. Alternatively, researchers have proposed new nozzle designs to enhance the performance of powder [500-502]

Powder shape

It seems that the powder catchment efficiency is improved by using crushed (non-spherical) powders. This reduction of catchment efficiency of the spherical powders might be explained by the ease of these particles to bounce off out of the melt pool during the process, due to their spherical shape [440, 503].

2.4.3.3 Reported results of powder catchment efficiency

15 papers were reviewed that discussed powder catchment efficiency. All of these powder catchment efficiency results are summarised in Figure 2.25. It can be seen that the powder catchment efficiency ranged between 10-90% [434-438, 440, 441, 446, 447, 452, 455, 459, 460]. Some of the papers reported high powder catchment efficiency above 80% [455, 460, 464]. However, the powder catchment efficiencies noted in the technical literature are frequently substantially below 50%. The range of powder catchment efficiency calculated from the relevant 28 papers is presented in Table 2.4. Overall the range is 9% to 95% with over 46% of the results below 65%. The x axis numbers on this figure refer to the reference numbers of the papers listed. More detail of reviewed papers is presented in Table 2.5, in order of ascending powder catchment efficiency.

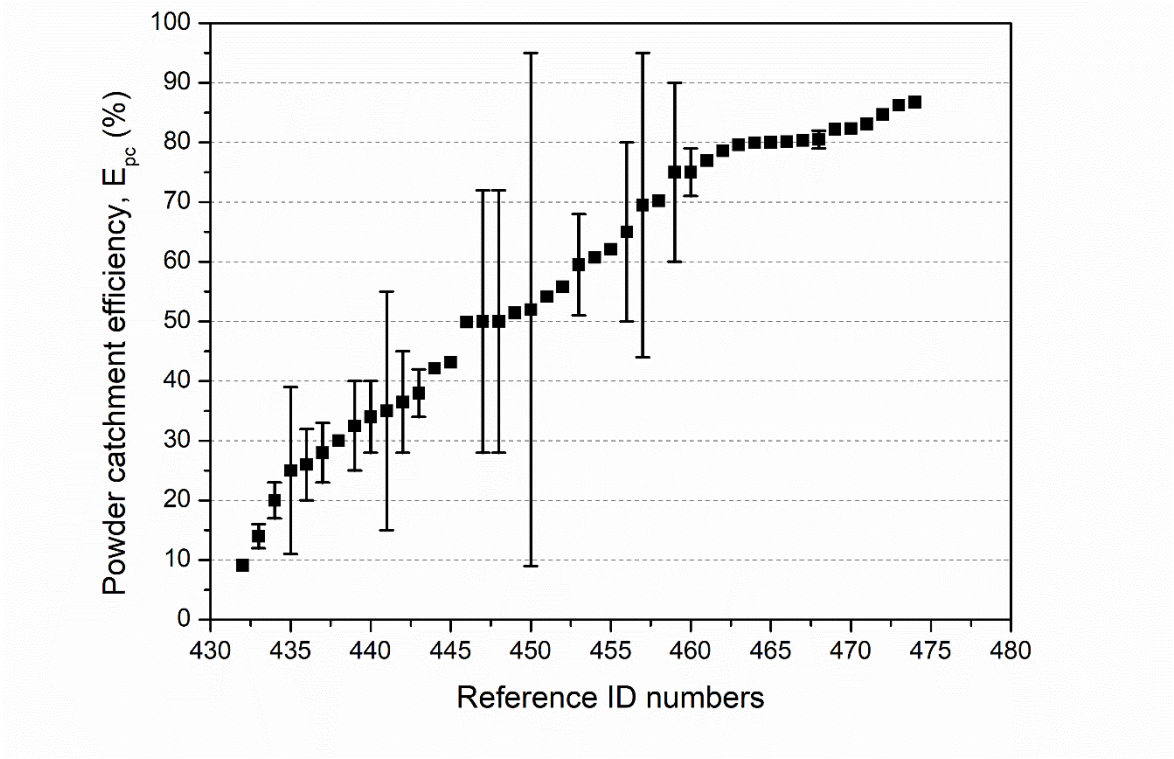

Figure 2.25 Powder catchment results reported and calculated from literature.

Table 2.5 Reported results of powder catchment efficiency (see also Table 2.4)

No.	Papers	Paper type	Laser type	Substrate	Powder	Density of the powder	Laser power	Powder feed rate	Process speed	Beam diameter	Powder catch. Eff
				-	-	(g/cm3)	(kW)	(g/min)	(mm/min)	(mm)	(%)
1	[434]	Author ID	0.5 kW fiber	Stainless steel	Fe-based	7.8	0.39-0.45	5-7.46	240-360	1	17-23
2	[435]	Author ID	-	-	-	-	0.4-2.4	7-42	3000-18000	-	11-39
3	[436]	Author ID	3 kW fiber	AISI 316L	AISI 316L	8	0.525-0.7	6-13	1320-2520	1.2	20-32
4	[437]	Author ID	1 kW CO2	Mild steel	AISI 304L	8	1	3	300	0.3	23-33
5	[438]	Author ID	4 kW Nd:YAG	6082	RotoTec 19850	4.3	0.67-1	-	-	1.6	25-40
6	[440]	Author ID	8 kW diode	A36	Fe-based	8	3.5	30-70	300	3.38	15-55
7	[441]	Author ID	1 kW fiber	Inconel 718	Inconel 718	8.19	0.35-0.55	1.2	600	1	28-45
8	[446]	Author ID	8 kW diode	A36	Fe-based	8	3-4	40-60	300	3.38	28-72
9	[447]	Author ID	8 kW diode	A36	Fe-based	8	3-4	40-60	300	3.38	28-72
10	[452]	Author ID	8 kW diode	A36	Fe-based	8	3-4.5	40-60	180-420	3.38	51-68
11	[455]	Author ID	1 kW CO2	Mild steel	AISI 304L	8	1	-	180-600	-	50-80
12	[458]	Author ID	15 kW fiber	S235JR	Inconel 625	8.44	10-15	150-400	500-1000	5	71-79
13	[459]	Author ID	15 kW fiber	S235JR	Inconel 625	8.44	15	295	750	5	77
14	[460]	Author ID	3 kW Nd:YAG	XC38	MoSi2	6.31	1.2-3	7-13	300-600	4	65-90
15	[464]	Author ID	2 kW diode	AISI 304	AISI 316L	8	1.5-2	8.5-17	300-600	3	80

2.4.3.4 Summary of powder catchment efficiency

High powder catchment efficiency can enhance productivity and increase cost-effectiveness. The catchment efficiency is defined as the percentage of the mass of the clad layers divided by the mass of powder supplied to the process. Following a comprehensive literature review, the interaction between powder catchment and processing parameters was investigated. As stated in literature review, the powder catchment efficiency can be improved by higher laser power, increased powder flow rate, lower carrier gas flow rate, slower process speed, larger melt pool size, narrower powder flow diameter, preheating the substrate, new nozzle designs, using crushed powders. The powder catchment efficiencies noted in the technical literature cover a large range, between 5-95%, but are frequently substantially below 50%. Since these powders are relatively expensive, it is obviously important to maximize their use wherever possible. It is important to note that the process is usually dependent upon the flow characteristics of the powder, and this may be adversely affected by contaminants or particles that have been fused together. For that reason, powders that were not incorporated into the clad cannot be reused.

2.4.4 Coverage rate

2.4.4.1 Determining the coverage rate in laser cladding

For a given clad thickness the coverage rate is defined as the area covered per unit time. The coverage rate can be evaluated by dividing the clad area by the time taken for the cladding [508].

The coverage rate for a given clad thickness is defined as:

$$Coverage\ rate\ \left[\frac{m^2}{h}\right] = \frac{The\ entire\ surface\ area\ of\ the\ cladding\ [m^2]}{The\ time\ to\ cover\ the\ surface\ [h]}$$

The coverage rate can also be approximated from the translational speed and inter-track distance.

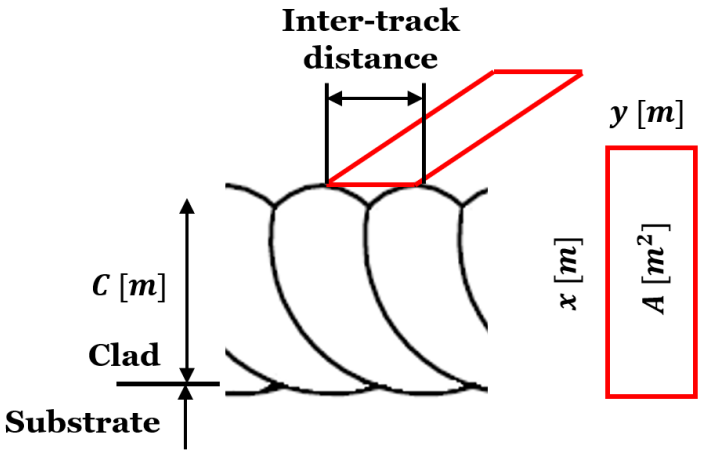

Figure 2.26 Cross-section of multiple clads, the red area represents the top area of the clads

$$Coverage\ rate\ \left[\frac{m^2}{h}\right] = \frac{A}{t} = yv$$

Where,

A = The entire surface area of the cladding [m^2]

t = The time to cover the surface [h]

y = inter track distance [m]

v = process speed [m/h]

C= thickness of the clad [m]

In accordance with the reviewed papers, researchers are interested in how long it takes to cover the substrate area. Usually in cladding, only one layer is used, but in other cases, multiple layers may be necessary to meet the thickness requirement. Taking this into consideration, the same coverage rates can be achieved with different clad thicknesses. Therefore, the thickness of the clad is also an important factor to consider when determining the coverage rate. The volumetric coverage rate can be defined as:

$$Volumetric\ coverage\ rate\ \left[\frac{m^3}{h}\right] = \frac{yvC}{n}$$

Where: n is the number of the layers.

2.4.4.2 Reported results of coverage rate

After conducting a thorough literature review, the coverage rate was calculated based on previous researches. This information is presented in Table 2.6. Based on 20 papers [504, 505, 506, 507, 508, 509, 510, 511, 512, 513, 514, 515, 516, 517, 518, 519, 520, 521, 522, 523] coverage rate ranged between 2.18-208.34 mm^3/s. In [523], the maximum coverage rate was approximately 210 mm^3/s with 2.5 mm effective thickness, process speed 1000 mm/min, 5mm inter track distance using 15kW laser power and 273 g/min powder feed rate. Compared to extreme high speed laser cladding, where 117810 mm/min process speed, 3.6 kW laser power and 3.2 g/min powder feed rate were applied, but only 72.65 mm^3/s volumetric average rate was achieved. Even though there is a wide range of coverage rate noted in technical literature, the average is estimated to be around 60 mm^3/s.

In Table 2.6, papers which reported the coverage rate are marked with ‘R’ and those from which the coverage rate had to be calculated for this PhD are marked with ‘C’.

These coverage rate results are summarized in Figure 2.27. This figure shows the reference numbers of each paper listed on the x axis and the coverage rate on the y axis.

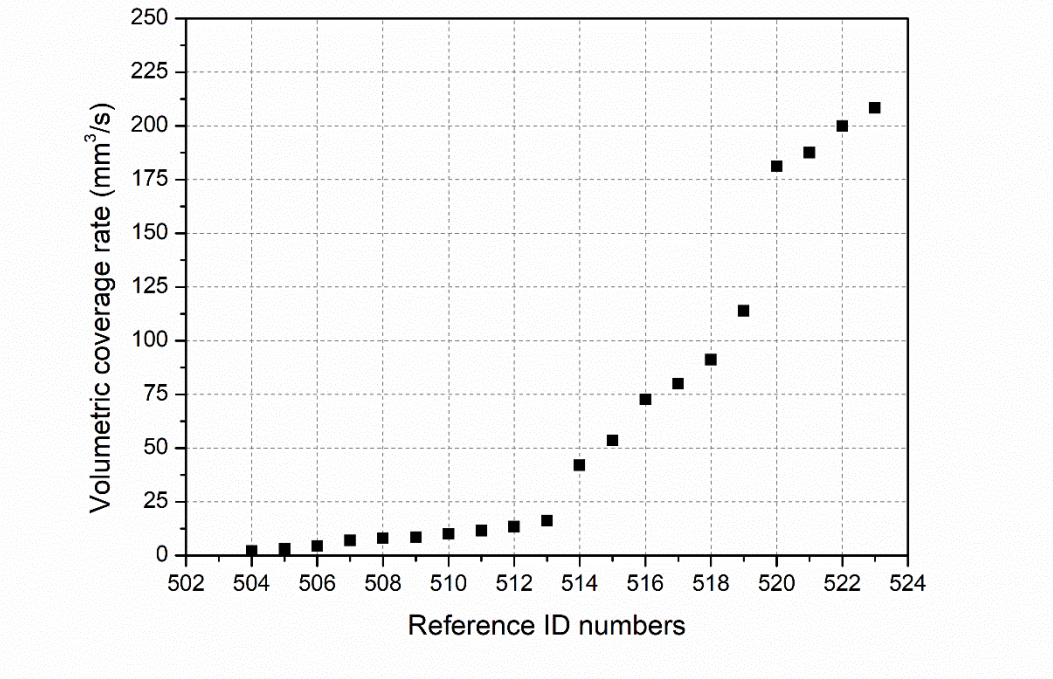

Figure 2.27 Coverage rate results, reported and calculated from literature

The following notes give more detail from the papers where the coverage rate was reported by the authors (papers with marked 'R' in Table 2.6)

In Brandt et al. [508], a new laser coating technique was described that could be used to create wear and corrosion-resistant surfaces. A combination of pre-placed and blown powder methods for production of clad layers was used.

A 500 W Nd: YAG pulsed laser delivered by optical fibers was applied. Nickel-based alloys were bonded to mild steel substrates. In a single pass, layers exceeding 1 mm in thickness can be produced using a 300 W laser power, see in Figure 2.28. The cladding obtained is homogenous, without any cladding defects, and has low dilution (less than 2%). The volumetric coverage rate was 8.125 mm^3/s.

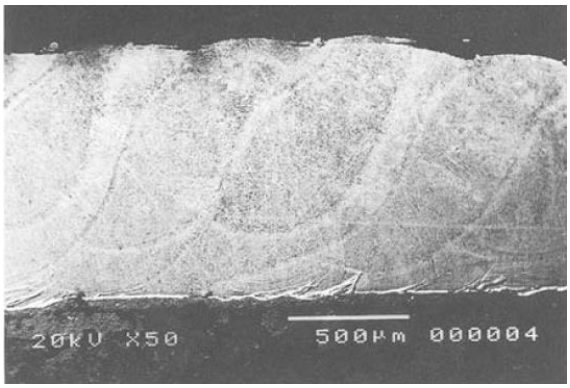

Figure 2.28 Cross-sectional view of overlapping tracks for a typical layer with an average thickness of 1.0 mm, a coverage rate of 8.125 mm^3/s [508]

Yuan et al. [512] investigated the microstructure and properties of traditional laser cladding and high-speed laser cladding of Ni45 alloy coatings. A 2 kW fiber laser was applied. By using Ni45 as additive materials bonded to AISI 1045 steel substrates. These results indicate the volumetric coverage rate of 13.57 mm^3/s with a layer thickness of 0.053 mm.

Lubaszka and Baufeld [518], describe results that were obtained when powder was deposited horizontally using a high-power diode laser. A 15 kW high power diode laser was used to form the clad layers. A powder material of 308L was applied to S355 substrate. The volumetric coverage rate calculated from their data is between 80 and 91.25 mm^3/s with a thickness of 1.5 mm, 1000 mm/min process speed and 3.2-3.6 mm inter track distance.

In Tuominen's work [519], the reported volumetric coverage rate was 114 mm^3/s with the inter-track distance of 9 mm, and process speed of 1900 mm/min with approximately 15% overlap. The effective thickness achieved was 0.4 mm.

Moreover, Tuominen et al. [520] presents a new method of laser strip cladding, suitable for surface treatments, repair, and additive manufacturing. Testing was conducted using a solid Inconel 625 strip width of 30mm on the base material of S235. Figure 2.29 depicts the cross section of the multi clad. Results showed that with 8 kW laser power, with an inter-track distance of 29 mm, the volumetric coverage rate of 181.25 mm^3/s can be reached with 1.5 mm effective coating thickness.

Figure 2.29 Cross-section of multi-clad layered by 8 kW, 250 mm/min, 127 g/min, inter-track advance 29 mm, the volumetric coverage rate of 181.25 mm^3/s. [520]

In a review of more than 200 papers, results of the coverage rate were compiled from only 6 papers. The results are summarized in Table 2.6. It can be seen that the volumetric coverage rate ranged between 8.13-181.25 mm^3/s. Coverage rate of 181.25 mm^3/s was the highest which was reported. However, the coverage rate noted in the technical literature cover a large range but are frequently substantially below 88 mm^3/s.

Table 2.6 Reported (R) results of coverage rate and calculated (C) coverage rate based on people's work

Num.	Papers	Paper type	Laser type	Substrate	Powder	Laser power (kW)	Feed rate (g/min)	Process speed (mm/min)	Inter-track distance (mm)	Beam diameter (mm)	Layer thickness (mm)	Coverage rate (m^2/h)	Volumetric coverage rate (mm^3/s)
1	[504]	C	2 kW CO2 laser	A3	Nickel-based	0.7	4	360	1.3	4	0.28	0.028	2.184
2	[505]	C	1 kW Nd:YAG	AerMet 100	AerMet 100	0.774	12.5	640	1	2.5	0.3	0.038	3.2
3	[506]	C	3 kW fiber laser	Gray cast iron	NiCrBSi	0.5	8.5	300	1.5	1.7	0.6	0.027	4.5
4	[507]	C	1 kW fiber laser	Inconel 718	Inconel 718	0.65	6	500	1.3	-	0.65	0.039	7.042
5	[508]	R	0.5 kW Nd:YAG	Mild steel	Hastelloy C	0.3	5.76	750	0.65	1.5	1	0.029	8.125
6	[509]	C	3.3 kW fiber laser	AISI 304	Höganäs 3533	1.8	-	300	1.35	-	1.27	0.024	8.573
7	[510]	C	1.6 kW HPDL	AISI 4340	Cu15Sn0.4P	1	24	600	1	3	1	0.036	10
8	[511]	C	1.5 kW CO2 laser	Mild steel	Stellite 6	1.38	12	1200	0.66	2	0.87	0.048	11.484
9	[512]	R	2 kW fiber	AISI 1045	Ni45	2	-	76860	0.2	-	0.053	0.940	13.579
10	[513]	C	4 kW diode laser	A45	FeCrMoMn	2.2	38	70000	0.2	0.5	0.07	0.840	16.333
11	[514]	C	3 kW fiber laser	AISI 1045	W6Mo5Cr4V2	1.4	16	420	3	-	2	0.076	42
12	[515]	C	3 kW fiber laser	Cr–Ni-based	AISI 1045	3	450	306	7	-	1.5	0.129	53.55
13	[516]	C	4 kW fiber laser	AISI 1045	TiC/IN625	3.6	3.2	117810	0.5	1	0.074	3.534	72.65
14	[517]	R	15 kW HPDL	S355	308L	4.5	30	1000	3.2	7	1.5	0.190	80
15	[518]	R	15 kW HPDL	S355	308L	5	50	1000	3.65	9	1.5	0.220	91.25
16	[519]	R	4 kW Nd:YAG	S235	Inconel 625	4	60	1900	9	5	0.4	0.900	114
17	[520]	R	10 kW HPDL	S235	Inconel 625	8	127	250	29	13.5	1.5	0.435	181.25
18	[521]	C	6 kW fiber laser	C45	FeCoNiCrAl	6	30	50000	0.5	1	0.45	1.500	187.5
19	[522]	C	4 kW fiber laser	Mild steel	X-M6V	2.4	13	30000	0.8	2	0.5	1.440	200
20	[523]	C	15 kW fiber laser	S235JR	Inconel 625	15	273	1000	5	5	2.5	0.300	208.333

2.4.4.3 Summary of coverage rate

The laser cladding process is intended to provide an excellent defect-free coating, improving surface properties with low dilution and maximum powder catchment efficiency and coverage rate. High coverage rates can improve productivity and reduce costs. The volumetric coverage rate is defined as the area covered per unit time with required thickness. The linear process speed, inter-track distance and the clad thickness can be used to calculate the volumetric coverage rate. Following a comprehensive literature review, the volumetric coverage rates were calculated using data from other people's work. Coverage rate ranged between 2.18-208.34 mm^3/s. The maximum volumetric coverage rate was approximately 208.34 mm^3/s with 2.5 mm maximum thickness. Even though there is a wide range of coverage rate noted in technical literature, the average is estimated to be around 60 mm^3/s.

2.5 Summary of the literature review

According to the above literature review, information for laser cladding with blown powder for high quality and productivity applications can be summarised and consolidated into the below key findings:

Dilution is a natural consequence of the cladding process because some substrate melting is necessary in order for there to be a good interfacial weld between the cladding and the substrate. Excessively high dilution decreases the benefit gained from adding the clad material to the surface. Target dilution values vary but tend to be 5 percent. In some cases high dilution levels are actually preferred but such applications are unusual. There are no clear guidelines on how to measure or analyse the level of dilution in laser clad surfaces. There is a range of dilution measurement and analysis techniques in use. Dilution can be determined using geometrical features and chemical composition.

Geometrical dilution measurements are made on cross-sections of laser clads. This makes geometrical dilution measurement a necessarily destructive process which is a clear disadvantage. It should however be noted that there is other useful information that can be extracted from examination of such cross-sections, including overall clad shape, quality of the interface, presence or absence of porosity and cracking.

Geometrical methods only give an overall dilution value and give no indication of the dilution gradients which will exist in the clad layer, particularly near the clad-substrate interface. Geometrical methods give only a spatial measurement of dilution levels which do not account for the densities of the alloys involved.

A lot of published work on laser cladding focusses only on single tracks, however industry is almost solely interested in multiple, overlapping clad tracks. The majority of geometrical dilution measurement methods are defined with reference to a single track. These need to be redefined for multiple overlapping tracks. This generally results in simplified measurements as more regular shapes need to be measured. The extreme would be an entirely uniform clad where clad height above the original surface and melt depth below the original surface are uniform along the clad. There are well known differences at the start and end of the cladding, where steady state conditions are not obtained.

Based on the research papers, we can conclude that there is no explanation for the choice of dilution measurement technique. Moreover, no previous studies have been conducted to compare dilution techniques. This subject is covered as part of one of the papers published

as part of this PhD. Geometrical dilution techniques require only optical microscopy measurements, but do not provide accurate information regarding chemical properties. The most accurate method for determining dilution is EDX type chemical analysis.

Productivity is crucial in laser metal deposition to make the process economically viable. By improving the deposition rate of the process, it is possible to optimize the productivity of laser cladding. Over the past ten years, research has focused on deposition rate as an important research topic . Typical deposition rates for laser cladding with blown powder are usually around 0.5 kg/h. The deposition rate is determined by: the total amount of powder deposited per unit of time. It is also possible to achieve a very high deposition rate, up to 16 kg/h.

High powder catchment efficiency can enhance productivity and increase cost-effectiveness. The catchment efficiency is defined as the percentage of the mass of the clad layer divided by the mass of powder supplied to the process. Following a comprehensive literature review, the interaction between powder catchment and processing parameters was investigated. As stated in literature review, the powder catchment efficiency can be improved by higher laser power, increased powder flow rate, lower carrier gas flow rate, slower process speed, larger melt pool size, narrow powder flow diameter, preheating the substrate, new nozzle designs, using crushed powders. The powder catchment efficiencies noted in the technical literature cover a large range, between 5-95%, but are frequently substantially below 50%. Since these powders are relatively expensive, it is obviously important to maximize their usage wherever possible. Additionally, it is important to note that the process is usually dependent upon the flow characteristics of the powder, and this may be adversely affected by contaminants or particles that have been fused together. Powders that were not incorporated into the clad cannot be reused.

High coverage rates can improve productivity and reduce costs. The process speed, inter-track distance and the clad thickness can be used to calculate the volumetric coverage rate. Published coverage rates ranged between 2.18-208.34 mm^3/s. The maximum volumetric coverage rate was approximately 208.34 mm^3/s with 2.5 mm maximum thickness. Even though there is a wide range of coverage rate noted in technical literature, the average is estimated to be around 60 mm^3/s.

2.6 Research hypothesis

In this thesis, the principal objective is to improve the quality and productivity of blown powder laser cladding. Based on the literature review on laser cladding powder deposition, the following research hypotheses are proposed:

- Providing guidelines and advice for researchers and engineers in the field of laser cladding and related Direct Energy Deposition (DED) techniques, could help to establish a standardised approach to quality assessment and productivity metrics.
- By using a different cladding deposition technique over the traditional AAA cladding, overall productivity and quality factors could be improved.
- Using high-speed video images and developing a program to detect particles could assist in the understanding of powder catchment behaviour by analysing the meltpool of the clad and the movement of powder particles.
- The quantitative analysis of the powder catchment behaviour of powder grains in laser cladding may be useful in understanding how to improve further the productivity of the process.

3 Chapter III. Experimental procedures

3.1 Introduction

In this chapter, the equipment and experimental procedures are explained. Firstly, the materials used are discussed, including powder chemical analysis. Then, explanation of the preparation of the workpiece and the setup of the laser system for laser cladding experiments, which includes the control system, the powder delivery method, and the nozzle design. All laser cladding experiments are described, including the processing parameters used. Characterisation of deposited coatings as well as sample preparation for the microstructural examination and description of optical microscopy, scanning electron microscopy (SEM) and Energy Dispersive X-ray spectroscopy (EDX) techniques used for both powder and deposit characterisation are detailed. Geometrical characterisation, dilution, microstructural characterisation, identification of cladding defects of the cladding samples are also explained.

Laser cladding experiments were conducted in two different laboratories. The first laboratory is located at the University of Nottingham, United Kingdom. A second one is located at Luleå University of Technology, Luleå, Sweden.

3.2 University of Nottingham

Three major components are required as part of the laser cladding system with powder injection: the laser system, the powder feeding system, and the computer numerically controlled (CNC) robotic system. Understanding the structure of these systems and their functionality under a variety of operating conditions is critical to the laser cladding process. The laser system is generally responsible for generating the required energy. This powder system is designed to produce a continuous, uniform powder flow over a defined rate. Computer numerical control equipment controls the laser coating process.

3.2.1 Laser system

Laser cladding experiments were performed with a 2 kW IPG Ytterbium-doped, continuous-wave fibre laser (YLR-2000), which operates with 1070 nm wavelength, 125 mm collimating lens and 206 mm focusing lens beam delivery system and combined with the Precitec YC 50 cladding head (Laser Trader Ltd., Chesterfield, UK). The maximum output power of the laser used in the experiments was 1.8 kW. A laser can be operated both in continuous mode (CW) and in pulse mode. During the trials conducted within this project, the laser was only operated in continuous mode. The laser system is using a fibre with a diameter of 100 μm, coupled to a fibre with a diameter of 600 μm in order to deliver the light beam. Using an Ethernet cable, the laser is connected to the computer and is controlled using the LaserNetTM software. The laser power can also be controlled externally with analogue signals of 0-10 V DC. The beam was defocused to a round spot measuring about 2.54 mm in diameter and 12 mm away from the focus, which yielded a working distance of 206 mm with approximately Gaussian energy distribution. There is a common practice of operating the laser system out of focus in order to provide a larger circular spot for materials to be placed into the melt pool generated by the laser beam on the substrate. The laser cladding system can be seen in Figure 3.1.

Figure 3.1 Laser cladding system

3.2.2 Powder delivery system

All depositions were carried out using a Miller Thermal, Model 1264 (Praxair Surface Technologies Ltd., Swindon, UK) gravity-based powder feeder (see in Figure 3.2). A gravity-based powder feeder system consists of two major components: a powder storage container and a rotating disk. Powder is transferred from the container to the rotating disk and transported using a carrier gas to the collection unit and finally to the cladding head.

Figure 3.2 Powder delivery system

Argon was used as a carrier gas to pressurize the powder chamber with a constant gas flow rate of 10 L/min. Backpressure was applied to the carrier funnel to stabilize the powder stream. The volumetric powder feed rate can be adjusted according to the slot size and the disk speed. Coaxial powder feeding with 1mm copper nozzle has been employed for laser cladding experiments. Powder feeders have been calibrated for specific powder feeding rates based on changes in the speed of the motor that spins edge-perforated disks in the feeder, and their revolutions per minute (rpm). Powder calibration was accomplished by weighing a series of powder samples delivered over a period of time. Using the coaxial nozzle, powder is applied coaxially to the substrate surface in the case of laser cladding, corresponding to a nearly Gaussian distribution of powder density. Through this process, three streams interact with the material surface: a shield, a carrier gas and a powder stream. Gas is responsible for two distinct purposes, carrying the powder particles within the nozzle around the laser beam and protecting the coating from the atmosphere to avoid the coating defects. In order for the powder jet to be effective, it must be dispersed uniformly, parallel to the laser beam profile, and flowing laminarly.

3.2.3 CNC system

Laser coating is controlled by computer numerical control (CNC) equipment. The laser cladding was carried out on a simple 4 axis CNC table. Both the laser head and the powder feeder nozzles are attached on the z-axis and remain fixed, whereas traversal movement of the substrate is accomplished in the x and y-axes directions, which is accomplished by mounting the substrate plate on the worktable of the CNC machine using a programme written in G-code. As a result of this setup, the work piece is moved relative to the stationary laser beam. High scanning speeds and high positioning accuracy characterize this motion control system. The cladding process generated fumes which were removed using a suction extraction system. The laser beam was defocused to a round spot measuring about 2.54 mm in diameter and 12 mm away from the focus, which yielded a working distance of 206 mm and the standoff distance, distance between the substrate surface and the coaxial nozzle, is 10mm. There were two types of plates utilized in the experiments, sample plates and run-on plates. Run-on plates are used to compensate for slow acceleration of the table. Using clips and screws, the plates were attached to a four axis table. As illustrated in the following figure in Figure 3.3, the left plate is the run-on plate and the right plate is the sample plate, therefore the cladding direction is from left to right. The stage was surrounded by a protective wall in an effort to reduce the powder pollution outside the stage (see in Figure 3.3b)).

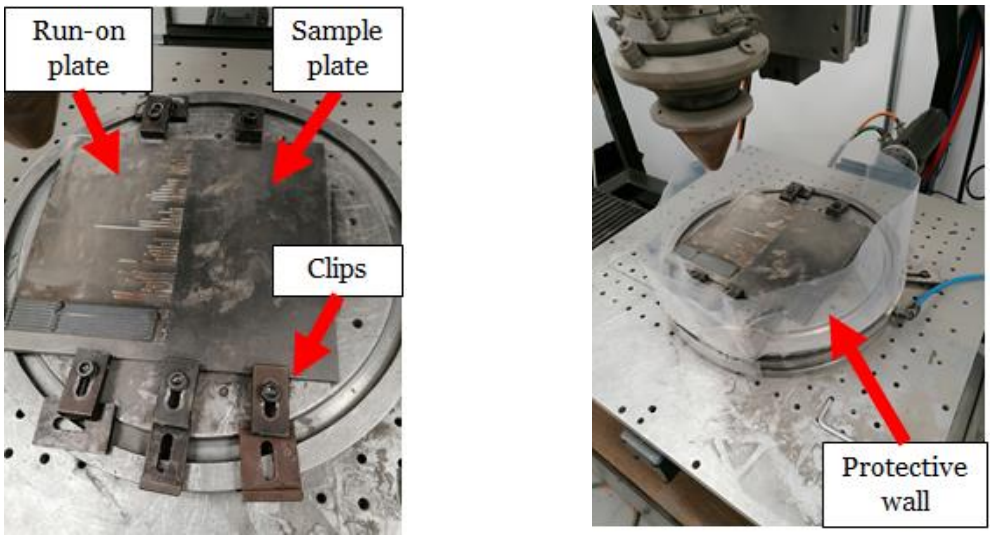

a) b)

Figure 3.3 CNC table setup

3.2.4 Materials

The substrate material was bright drawn mild steel (BDMS) AISI 1023 provided by Smith Metals Nottingham. Plates with dimensions of 100 mm ×180 mm × 6 mm (width × length × thickness) have been prepared and then cleaned with acetone before the cladding procedure to enhance laser absorption on the substrate surface and remove contaminants to decrease the cladding defects. Below in Table 3.1 is summarizing the chemical composition of mild steel derived from energy dispersive X-ray analysis (EDX).

Table 3.1 Chemical composition of bright drawn mild steel AISI 1023

	Chemical Composition (wt%)					
Alloy	**C**	**Si**	**Mn**	**P**	**S**	**Fe**
AISI 1023	0.2	0.25	0.5	0.045	0.03	bal.

As an additive powder, AISI 316 stainless powder, supplied by Hoganas Belgium, and Stellite 6, supplied by LPW Technology, was used. The following Table 3.2 summarizes the chemical composition of the powders based on energy dispersive X-ray analysis (EDX).

Table 3.2 Chemical composition of AISI 316 and Stellite 6 powders

	Chemical Composition (wt%)									
Alloy	**C**	**Si**	**Mn**	**Cr**	**W**	**Mo**	**Ni**	**Fe**	**Co**	**Other**
AISI 316	0.03	1.00	2.00	17.00	-	2.00	12.00	bal.	-	0.175
Stellite 6	0.96	1.47	-	27.00	5.00	-	0.87	0.73	bal.	0.07

According to technical data, 316 powder particles ranged from 40 to 80 μm, while Stellite 6 particles were 20 to 50 μm.

3.2.5 Powder feed rate measurements

Previously, it was explained that the disc speed and slot size can be adjusted to control the volumetric powder feed rate. For the laser cladding experiments, different rotation speeds were used for different powder feed rates. The first thing that should be done prior to every laser cladding session is to measure the powder feed rate. This calibration of powder flow rate was conducted by running system for a known time, collecting and weighing the powder. Particle size also affects the powder feed rate. In the experiments, two different powders were used: 316 with size range of 40-80 μm and Stellite 6 particle size range between 20-50 μm. The measurement of the powder was accomplished using a collector unit, designed to collect the powder without wasting any material (see in Figure 3.4). A 3D printer was used at the university to produce the collector unit.

Figure 3.4 Powder collector device

The device consists of three components, a glass holder, glass beaker container, and an exhaust cap with a fabric filter. This design allows for powder and carrier gas to enter into the collector device and leave the powder inside with the carrier gas exiting. Before the powder feed rate measurement, the device is weighed three times. A feed tube is inserted into the input of a collector after turning on the feed rate and letting it run for a minute. The device was weighed again after the measurement, and the powder feed rate was calculated by subtracting the weight before and after the measurement.

3.2.6 Determining the powder catchment efficiency

Using the cross-section of the clad, this PhD used another method to determine the powder catchment efficiency, defined as:

$$E_{pc}(\%) = \frac{A_{track} \cdot v \cdot \rho}{PFR} \cdot 100 \quad (1)$$

Where,

Epc = powder catchment efficiency (%)

A_{track} = Cross sectional area of a single track above the original line of the substrate (mm^2)

v = Process speed (mm/min)

Ro = Density of cladding material (g/mm^3)

PFR = Powder feed rate (g/min)

3.2.7 Processing parameters

3.2.7.1 Experimental design

3.2.7.1.1 Processing parameters

Numerous factors influence the quality and characteristics of laser cladding coatings. These factors encompass clad geometry, microstructure, dilution, presence of defects, residual stresses, distortion, surface roughness, metallurgical changes in the substrate, and process efficiency. The impact of these factors is mediated by laser cladding process parameters and the physical phenomena occurring during the cladding process.

Process parameters in laser cladding can be categorized based on factors like the type of beam, feeding mechanism, materials, and operational aspects. Some parameters, such as beam and feeding, are typically fixed and contingent on equipment choices like the laser and optics. Material parameters are reliant on the selection of additive material and substrate, encompassing properties of the powder particles (particle size, morphology, chemical composition, thermophysical, and optical properties) and substrate properties (geometry, mass, chemical composition, surface condition, thermophysical, and optical properties). Laser cladding operating parameters can be adjusted by the operator and significantly affect process outcomes. Among these parameters, the three most critical ones that profoundly influence coating characteristics are laser power (P), scanning speed (V), and feeding rate (Q).

Research indicates that increasing laser power, while keeping other parameters constant, results in an increase in bead height [424, 481]. However, the effect of laser power on clad height is minimal. Laser cladding with powder feeding typically exhibits linear correlations between height and feeding rate (Q) and between height and powder feed rate per unit length (Q/V) [285, 325, 380]. Generally, an increase in the feeding rate leads to an increase in clad height ,moreover, the cross-sectional area of the clad (Ac) also increases with increasing Q and Q/V [321, 433].

Reducing scan speed and increasing laser power have been observed to lead to an expansion in clad width [166, 433, 511]. Notably, the primary determinant of this width is the spot size of the laser beam. Surprisingly, it is possible to achieve a width larger than the spot size even with very low processing speeds and very high laser powers [511]. In the context of coaxial laser cladding, these relationships exhibit linearity [285].

One of the key factors influencing substrate melting is the amount of energy available per unit mass of powder, denoted as P/Q. Dilution tends to increase with higher laser power [193, 424] but decreases with an increased feed rate [321, 328, 380]. Moreover, an increase in scanning speed, especially for thin beads, tends to elevate dilution [286, 328, 369]. However, for cladding with greater bead heights, this influence becomes less pronounced [344].

A comprehensive understanding of the interplay between processing parameters and clad characteristics is vital to achieve defect-free coatings with the desired geometry, fusion bond, and low dilution. Essentially, once the additive and substrate materials are chosen, achieving a successful laser cladding process hinges on striking the right balance between the material fed and the laser energy supplied. To identify operational parameters and explore correlations, creating a process map is the most suitable approach [285].

3.2.7.1.2 Clad characteristic

In the preceding section, we established that laser cladding coatings are influenced by a multitude of factors. Now, let's delve into the primary characteristics defining a clad. The Figure 3.5 below illustrates a typical cross-section of a single clad bead, featuring the key parameters associated with clad geometry. These parameters include:

Clad Height (C): This represents the thickness of the clad above the surface of the clad substrate.

Clad Depth (S): It signifies the thickness of the substrate that undergoes melting during cladding and becomes part of the clad.

Clad Width (W): This dimension corresponds to the width of the individual clad.

Clad Cross-Sectional Area (Ac): It denotes the area enclosed within the cross-section of the clad.

Clad Penetration Cross-Sectional Area (As): This parameter represents the area within the penetration cross-section of the clad.

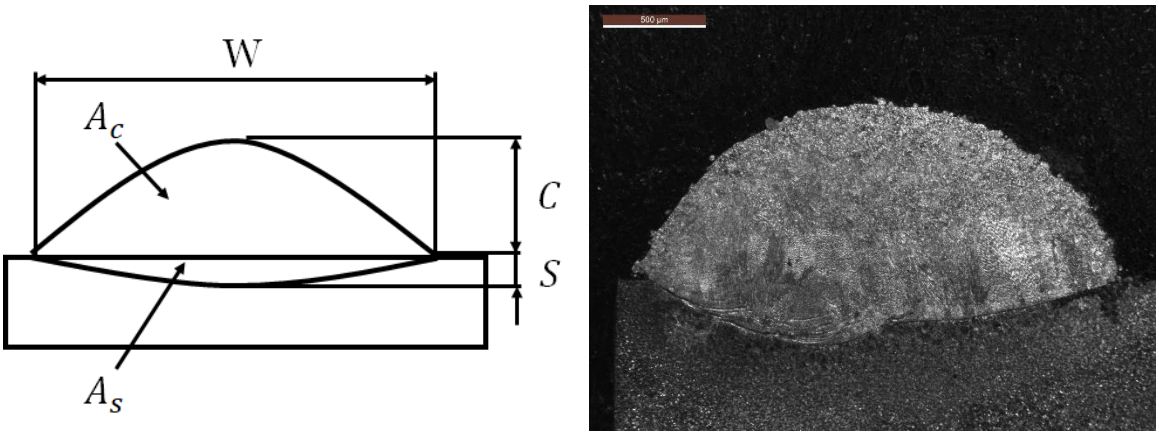

a) b)

Figure 3.5 Clad with specific geometric characteristics a), exemplified by b)

3.2.7.1.3 Parameters for A and B clad

Optimizing cladding parameters for both AAA and ABA cladding involves achieving a single clad with minimal dilution, as well as suitable clad height and width (Figure 3.6)

To fine-tune the single clad, various adjustments were made to the processing parameters, ranging from maximum to minimum settings, in order to obtain a diverse range of single clad shapes. Three primary processing parameters were the focus of this optimization: laser power, powder feed rate, and table speed. In the course of this research, a 2 kW fiber laser was employed; in industrial applications, higher laser power is typically utilized to enhance cladding efficiency. To minimize potential errors from the laser, a 1.8 kW laser power setting was used, with variations made solely to the powder feed rate and process speed.

The beam's movement speed was adjusted within the range of 500 to 2000 mm/min, along with a feed rate spanning from 15 to 30 g/min. It was determined that the most suitable A clad for further investigation could be achieved with the following processing parameters: 1.8 kW laser power, a scanning speed of 1000 mm/min, and a feed rate of 25 g/min.

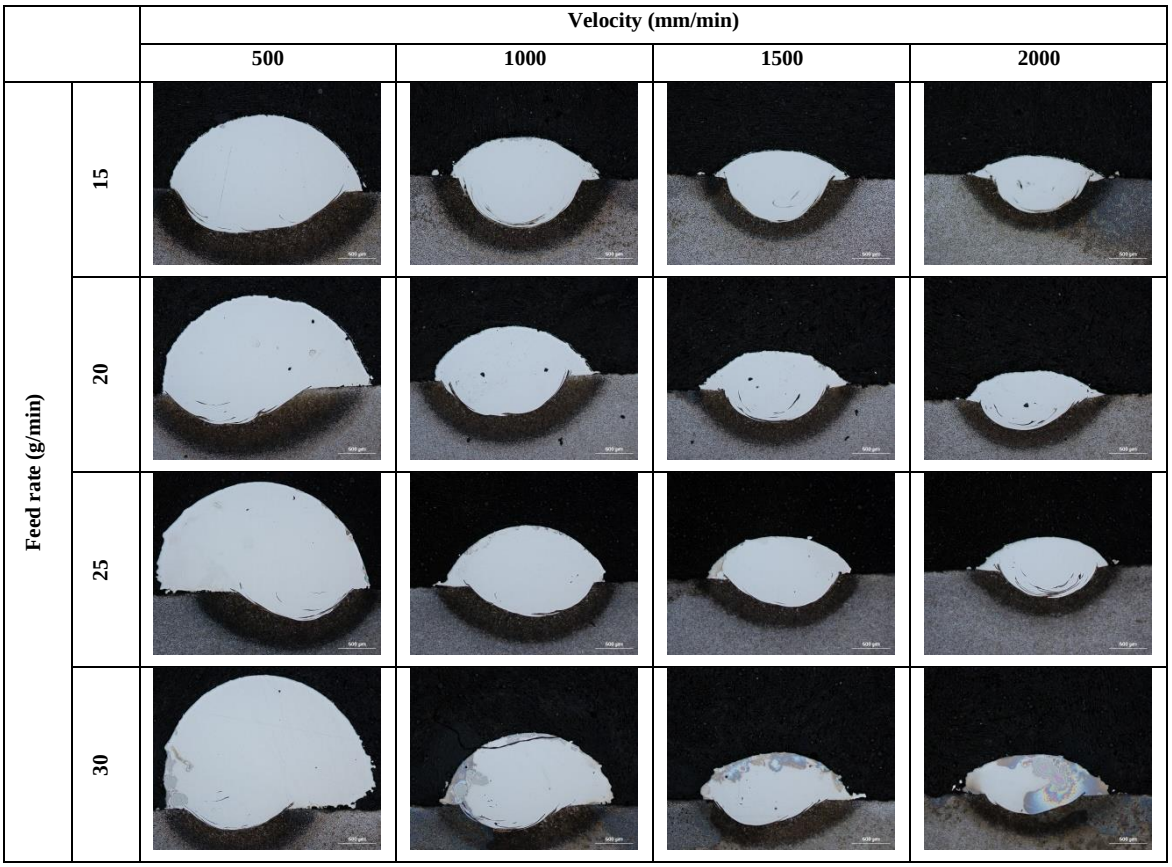

Figure 3.6 A clad cross section geometry for various scanning speed and powder feeding rates.

3.2.7.1.4 Other characteristics

This part of the work does not contain other characteristics, such as: the clad microstructure, which are strongly influenced by laser cladding. The coating defects (cracks and pores/voids) which can occur in laser-clad surfaces. The residual stress (tensile stresses), due to localized heat sources with high intensity and short interaction times. Energetic efficiency, which is influenced by the reflection and absorption of laser irradiation by the surface of the melt pool.

3.2.7.2 Parameters for AAA and ABA cladding

After determining the appropriate processing parameters for A clads, the parameters for B clads can also be selected. The main focus is to achieve maximum efficiency, deposition rate, and powder catchment efficiency. To achieve this, the cladding speed and inter-track distance were adjusted. Increasing the speed could lead to a reduction in production time, while increasing the inter-track distance allows for covering a larger area per unit of time. The laser powder remains constant as used in A cladding, as well as the powder feed rate. This is because changing the powder feed rate is complex and can yield unreliable results. Adjusting the powder feed rate up and down requires multiple measurements to obtain the exact feed rate.

As illustrated in the Figure 3.7 below, A cladding is deposited first with specific speed and inter-track distance, resulting in clad area A, deposition rate DRa, catchment efficiency PCa, and volumetric coverage per unit of time VOLa. By increasing the inter-track distance, the approximate area of B clad can be calculated to be approximately 87% of A clad area. This calculation is crucial when aiming for a flat surface, as it reduces the need for post-processing, thus saving time and material.

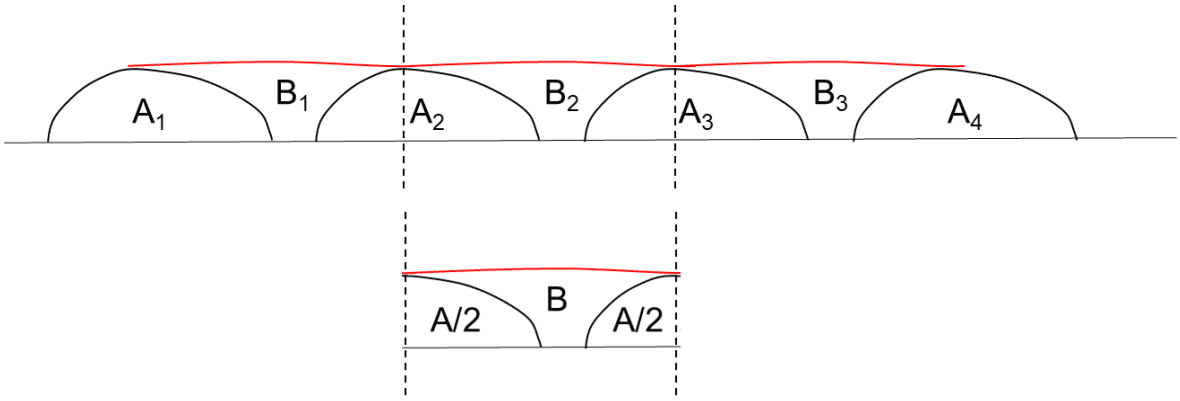

Figure 3.7 ABA cladding concept

Furthermore, when the speed is increased, for example, doubling it compared to A clad, the deposition results for B clad are as follows: the deposition rate and powder catchment efficiency could become 1.75 times that of A clad, and the volume of B clad is also 1.75 times that of A clad. This approach, known as ABA cladding, aims to achieve a flat surface without the need for post-processing machining, reducing material waste and process time. Additionally, this concept can enhance deposition rates and powder catchment efficiency, possibly due to factors such as powder reflection from the shoulders or changes in melt pool geometry.

Table 3.3 An example of ABA cladding data

		A clad	B clad
Speed	V	Va	Vb=2Va
Area of the clad	A	Aa	Ab=0.87Aa
Deposition rate	DR	DRa	DRb=1.75Dra
Powder catchment efficiency	PC	PCa	PCb=1.75PCa
Volumetric cover rate	VOL	VOLa	VOLb=1.75VOLa

Figure 3.8 shows a simplified diagram of 'A', 'AAA' and 'ABA' sample which gives details of how the samples were created and subsequently sectioned. In 'ABA' cladding, the actual samples involved 8 identical, parallel 'A' tracks interspersed with 7 'B' tracks. Tracks were completed with different A-B lateral spacings. The length of "A" clad was 90 mm and for "B" clads 60 mm. For the clad "B", two different processing parameters were changed laser beam scanning speed and inter-track spacings. The process speed (i.e. the movement speed of the CNC table) was varied between 800 mm/min and 3200 mm/min. Samples were created with a variety of inter-track spacings 1.05-1.65 mm (overlapping ratio 20%-80%). The following processing parameters were always used for clad "A": 1.8kW laser power, 1000 mm/min scanning speed, and 25 g/min feed rate. There were 37 samples deposited in total.

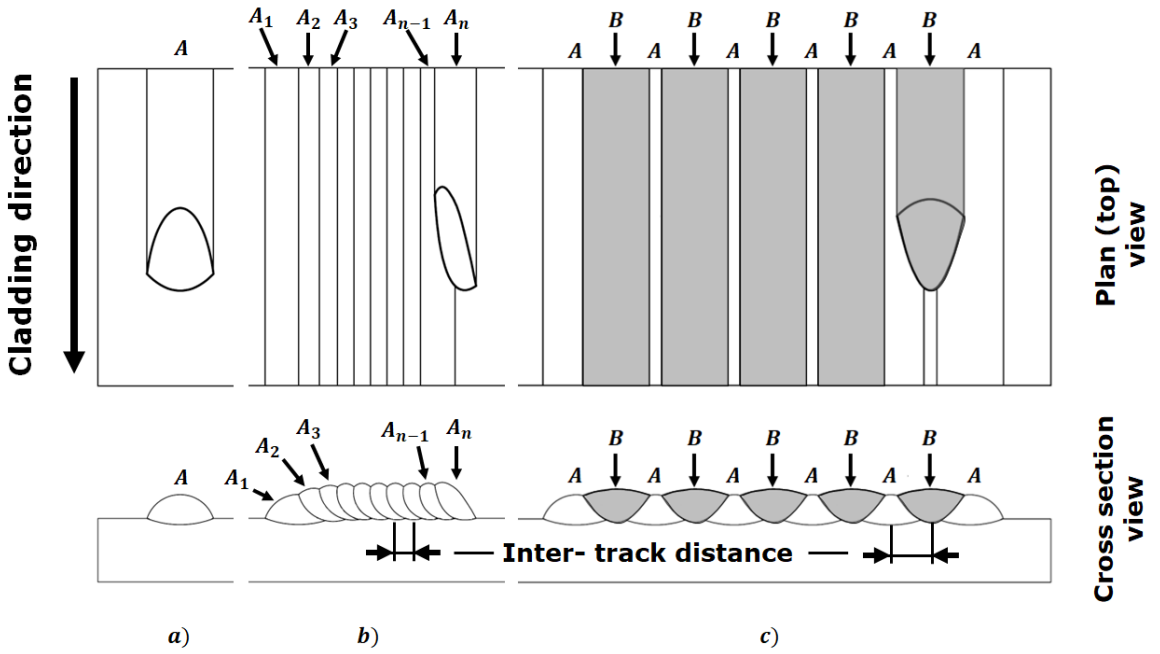

Figure 3.8 a) A solo, or initial, 'A' track, b) In standard (AAA) laser cladding the clad surface is made up of overlapping 'identical' tracks (although a few, early tracks differ from later tracks), c) in ABA cladding a set of widely spaced identical 'A' tracks are laid down first and then the gaps between them are filled with 'B' tracks.

This experiment was designed to compare the deposition rate, powder catchment efficiency, coverage rate, surface roughness, local metallurgy and dilution of the AAA and ABA claddings.

3.3 Luleå University of Technology

The experiment was carried out at the University of Lulea by Dr. Himani Naesstroem. The equipment, such as the laser system, powder feed rate device, and CNC table, and experimental methods were described.

3.3.1 Laser system

Laser cladding measurements were conducted with a 15 kW IPG Ytterbium-doped, continuous-wave fibre laser, which operates with 1070 nm wavelength, 150 mm collimating lens and 250 mm focusing lens beam delivery system and combined with the Precitec YW 50 cladding head. The laser has only been operated in continuous mode during the experiment. The laser system is using a fibre with a diameter of 100 pm, coupled to a fibre with a diameter of 400 µm. The laser output was 3 kW. The beam was defocused into a round spot measuring approximately 4 mm in diameter and having a Gaussian energy distribution and stand-off distance of 13mm. Figure 3.9 illustrates a laser cladding system.

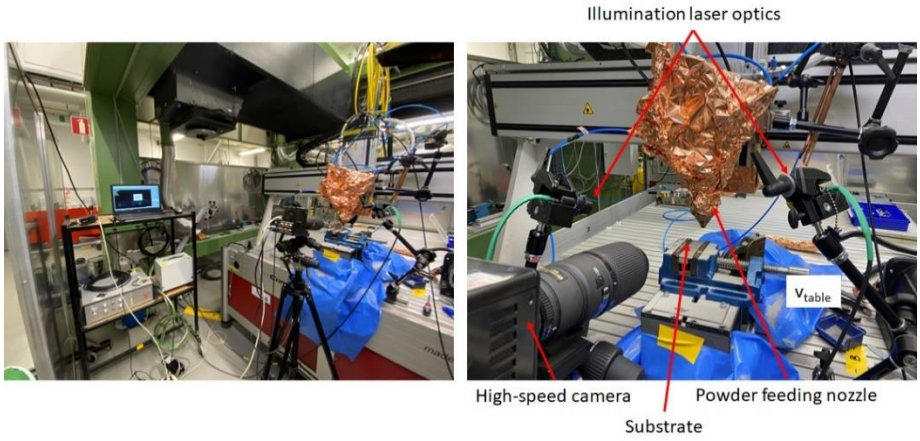

Figure 3.9 Laser cladding system in Lulea university

3.3.2 Powder delivery system

A blown powder directed energy deposition process was used for the cladding. A coaxial COAX 14V5 (Fraunhofer IWS) continuous nozzle (also known as a ring-slit nozzle) was employed, where the carrier gas and the powder were fed through the slit, and the laser beam and shielding gas passed through the central hole. This produced a focussed powder feeding stream with a diameter of approximately 2mm at the melt pool surface. The argon gas was used for shielding and as a carrier gas. Powder was fed through a commercial gravity-based powder feeder. The carrier gas flow was 8 l/min and shielding gas flow was 15 l/min. Powder feeders have been calibrated for specific powder feeding rate. This feed rate was checked experimentally twice by collecting the powder in a specially designed container over a five-minute period, with a standard deviation on 26g/min of 0.08.

3.3.3 Materials

AISI 304 austenitic stainless steel was used as the substrate material. Plates with dimensions of 50 mm ×180 mm × 5 mm (width × length × thickness) have been prepared, then grinded and cleaned with acetone before the cladding procedure. A powder of austenitic stainless steel AISI 316L was used as an additive powder. Table 3.4 summarizes the chemical composition of the substrate and the powder as determined by energy dispersive X-ray analysis (EDX).

Table 3.4 Chemical composition of the applied materials

	Chemical Composition (wt%)						
Alloy	**C**	**Si**	**Mn**	**Cr**	**Mo**	**Ni**	**Fe**
AISI 316L	0.01	0.8	1.5	17.00	2.6	12.7	bal.
AISI 304L	0.07	1.00	2.00	18.50	-	9.00	bal.

Microscopy measurements revealed that the 316L powder particles ranged from 50 to 150 microns in size.

3.3.4 Powder feed rate measurements

Powder calibration was accomplished by weighing a series of powder samples delivered over a period of time. The measurement of the powder was accomplished using a collector unit (see in Figure 3.10).

Figure 3.10 Powder collector device in Lulea university

Before the powder feed rate measurement, the device is weighted. A feed tube is inserted into the input of a collector after turning on the feed rate and letting it run for 5 minutes. The device was weighed again after the measurement, and the powder feed rate was calculated by subtracting the weight before and after the measurement. The powder feed rate was 26 g/min for the experiment and remain unchanged.

3.3.5 CNC system

Laser cladding is controlled by computer numerical control (CNC) equipment. The laser cladding was carried out on a simple a 3-axis ISEL FlatCOM L150 CNC system with test plates clamped to a linear motion table. Both the laser head and the powder feeder nozzles are attached on the z-axis and remain fixed, whereas traversal movement of the substrate is accomplished in the x and y-axes directions. The cladding process generated fumes which were removed using a suction extraction system.

3.3.6 High speed camera and image processing

3.3.6.1 Introduction

A high-speed video characterization section is divided into four subchapters, each with a specific research objective and technical aspect:

I. Objectives and Tasks

A brief introduction to the research employing high-speed video characterization is provided in this introductory subchapter. To provide a comprehensive understanding of the objectives and specific tasks, we outline its primary objectives.

II. Hardware Setup

The next chapter goes over the hardware configuration used for the research. There's a detailed description of the hardware components selected, their placement within the laser cladding system, and any modifications or adaptations made to facilitate high-speed video data acquisition.

III. Software Implementation

This subchapter focuses on the software aspect of the methodology. Provides a comprehensive overview of the software architecture and programming paradigms used to control and capture high-speed video. During the experimental phase, it provides insights into the selection of programming languages, platforms, and specialized software tools.

IV. Video Analysis Concept

The final subchapter within this section explores the fundamentals of video analysis. Based on the high-speed video data collected and processed, this chapter explains how to calculate, measure, and analyze errors. An in-depth look at how analytic techniques were applied to capture meaningful insights from the high-speed video frames.

With this structure, readers can follow a logical progression, starting with a detailed explanation of research objectives, then understanding hardware and software configurations. Ultimately, it explores video data analysis methods in depth.

3.3.6.2 Objectives in high-speed image processing

An objective of image processing is to achieve the following key goals: Analyze and describe the meltpool and interaction zone in the cladding process. Analyze high-speed images of powder particles by isolating and identifying individual particles. Calculation and documentation of particle velocity vectors for each powder particle during cladding will provide insight into how the particles move. Analyze directional trends in powder loss to determine governing mechanisms of powder dispersion. Evaluation of Powder Capture Efficiency: Evaluate the efficiency of powder capture, providing insight into the ability of the cladding process to retain powder particles. Quantify Powder Flow Rate: Use high-speed images to determine precisely how much powder is flowing through the system. Collectively, these objectives form a comprehensive framework for image processing, allowing us to investigate powder dynamics and interaction within laser cladding systems in depth.

3.3.6.3 Hardware setup

The procedure was captured using a high-speed imaging (HSI) camera operating at 8000 frames per second. The lighting was provided by a continuous wave diode illumination laser with a wavelength of 808 nm. To filter out extraneous process light, a narrow bandwidth filter precisely matching the illumination laser's wavelength was employed. The configuration of the process is depicted in Figure 3.11, with the camera positioned at an 11° angle from the horizontal axis. A total of 2000 frames were acquired throughout the processing. High-speed imaging videos were played back at reduced frame rates to facilitate the observation of powder catchment behavior and the geometry of the melt pool. Specifically developed software was employed for the analysis of the High-Speed Imaging videos, enabling the monitoring of powder particle trajectories towards and away from the melt pool region.

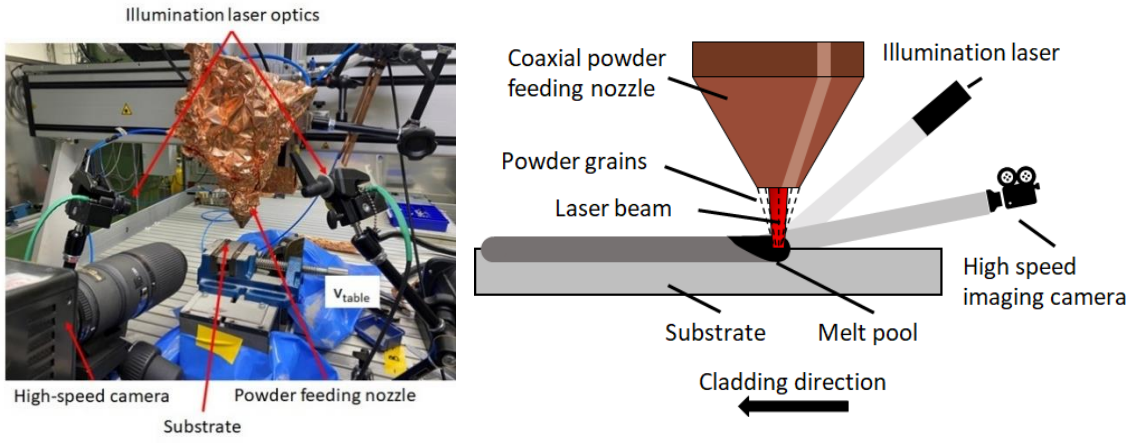

a) b)

Figure 3.11 High speed imaging a) experimental setup, b) an illustration of the side view

3.3.6.4 Software setup

A Python code was developed using libraries such as numpy, OpenCV, and OpenPIV to perform a sequence of operations, which are organized into the following steps:

- Particle Detection: This step involves the detection of particles within individual images.
- Velocity Computation: The code calculates the velocity of particles.
- Association of Directional Vectors: It associates directional vectors with individual particles.
- Computation of Flow Rates: This step involves the computation of flow rates.

Each of these steps is explained in detail in its respective section. The code processes individual images for particle detection and utilizes pairs of consecutive images to compute displacement vectors.

3.3.6.4.1 Particle detection

The objective of this stage is to generate a binary image in which only the droplets are clearly visible. The original images (in Figure 3.12-a) exhibit noise with high-frequency, low-intensity patterns stemming from electronics, particularly noticeable in the darker regions. Additionally, there are high-intensity signals arising from particles (in Figure 3.12-b) and from the deposition zone. Despite excluding the deposition area from the calculations due to the particles reaching zero velocity and melting in that region, the reflections originating from this area contribute to the overall noise in the surrounding environment. Consequently, a background intensity removal process is executed, involving the subtraction of a blurred image derived from the original.

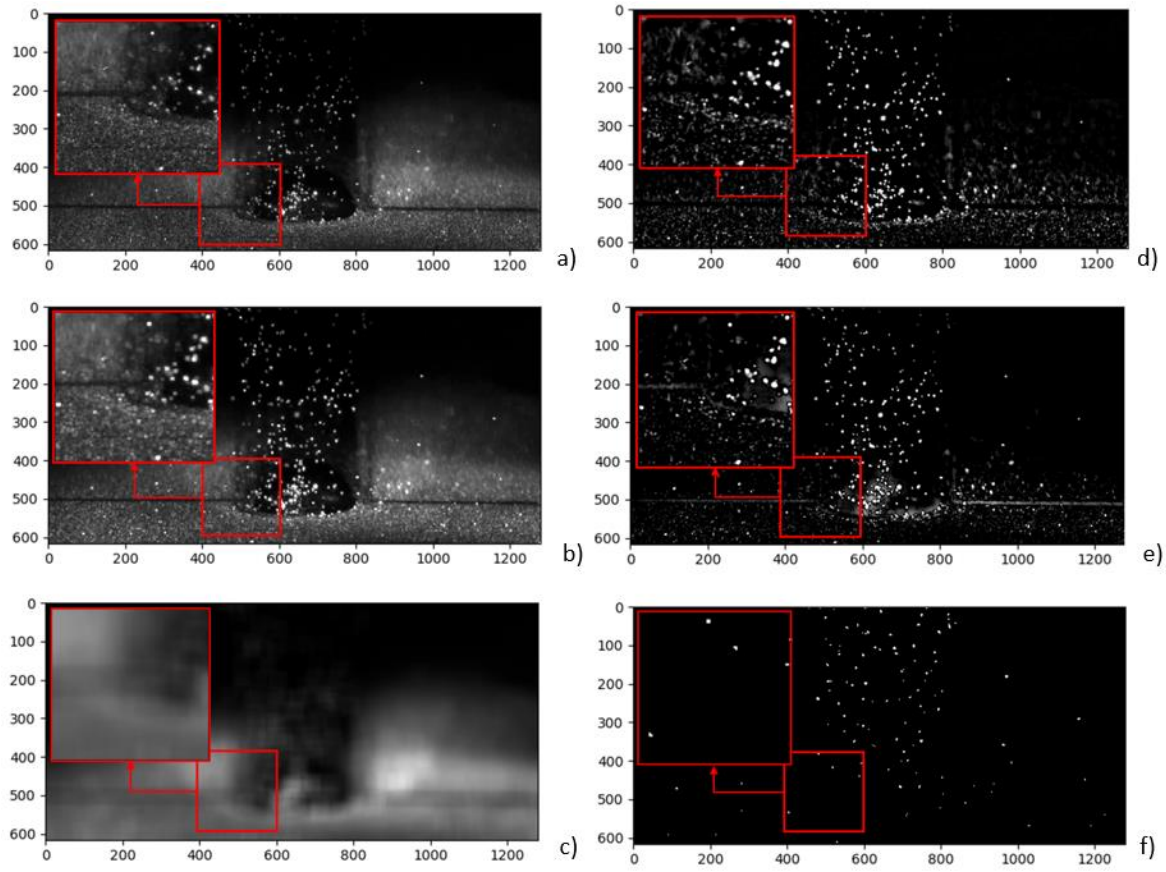

Figure 3.12 Intensity processing

Blurring an image involves the process of smoothing the image until it resembles Figure 3.12-c, where all the intensity peaks (representing particles) have been effectively eliminated, leaving behind the background intensity distribution. To provide a more intuitive understanding of these operations, consider the following 1D analogy (Figure 3.13): The red curve represents the original data, while the green curve represents the smoothed data. In the context of images, this smoothing or blurring is accomplished through convolution of the image with a Gaussian filter. When the smoothed data is subtracted from the original data, only the peaks remain, as illustrated in Figure 3.12-d for 2D data, which are images.

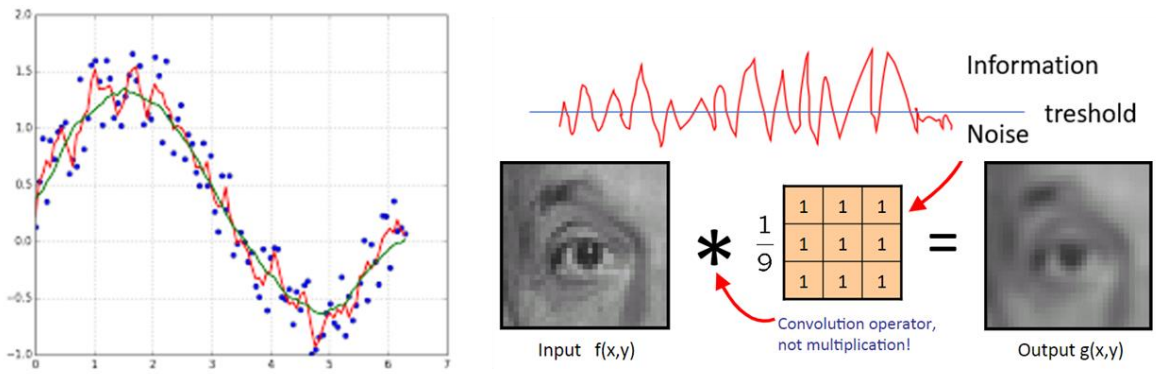

Figure 3.13 Image blurring

Figure 3.12-c displays the computed background intensity distribution for the image shown in Figure 3.12-a. The outcome of subtracting this background (Figure 3.12-c) from the original image (Figure 3.12-a) is depicted in Figure 3.12-d. In Figure 3.12-d, it is evident that, following background subtraction, what remains consists of the particle signals and high-frequency noise. To eliminate the high-frequency noise, a low-pass filtering operation is performed on the Fourier spectrum of the image, as illustrated in Figure 3.12-e.

As the initial background subtraction process alone cannot effectively eliminate high-frequency noise, an additional step is required. In the context of a 1D data frequency spectrum, it becomes evident that the implementation of a low-pass filter is indispensable for the removal of high-frequency components (Figure 3.14).

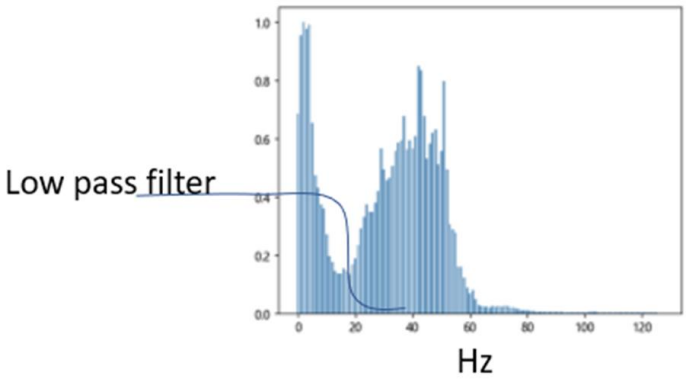

Figure 3.14 As an illustration, consider the frequency spectrum of 1D data, where it becomes evident that the utilization of a low-pass filter is essential to filter out high frequencies.

In the context of 2D data analysis, a frequency spectrum is also present. Leveraging previous experience of the characteristic distribution spectrum associated with particles. In order to retain this crucial information while reducing high-frequency noise, the application of a low-pass filter is chosen (Figure 3.15). However, it should be noted that precise frequency values are not available for this purpose. Nevertheless, the initial frequency filtering step, while beneficial, may not completely eliminate all noise. Therefore, It was found that it is necessary to conduct a secondary round of background subtraction and frequency filtering to further enhance the data quality.

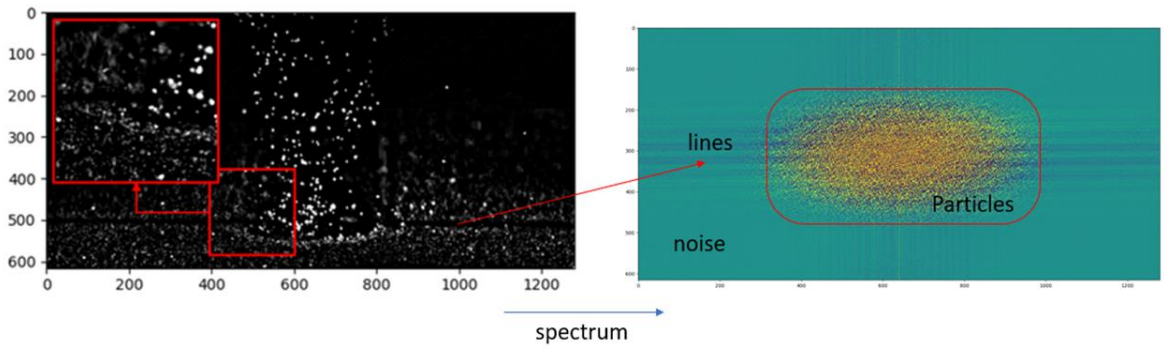

Figure 3.15 Background elimination through low-pass filtering

The process of background subtraction, in which the background image is computed from the filtered image as depicted in Figure 3.12-e, is iterated until the particle signal becomes the dominant feature within the image. This iterative process aims to achieve a clear threshold that can be applied to binarize the image effectively. The outcome of this binarization process is illustrated in Figure 3.12-f. Subsequently, following the processes of background subtraction and frequency filtering, obtaining an image that facilitates the identification of a clear threshold. The particles or droplets within the image exhibit distinct peaks of high intensity, enabling the utilization of a relatively conservative threshold value. In summary, it's worth noting that once this process is successfully applied to one image, it can be consistently and effectively replicated for all other images. The binary image depicted in Figure 3.12-f serves as the initial reference for the particle counting process, which is executed utilizing structural analysis tools within OpenCV. This tool proves effective in not only identifying particles but also determining their centers of gravity and establishing their coordinates within the image plane. It forms the foundation for particle counting. However, for the subsequent step involving the computation of particle motion direction and speed, the original image is employed. This choice is made because employing a binarized image can introduce errors in the cross-correlation-based algorithm.

The algorithm employed for detecting and categorizing objects within the binary image is known as "cv2.connectedComponentsWithStats," a component of the OpenCV package. This algorithm not only counts the droplets but also provides valuable information about their size in terms of pixels and their respective coordinates. To refine the results, a second step is implemented to filter out objects that are deemed too small. A pixel size of 5 corresponds to an approximate diameter of 44 microns, considering the particle size distribution ranging from 45 to 180 microns. Based on careful examination of the images and the particle distribution data sheet, a threshold of 5 pixels is chosen. Consequently, any object with a size smaller than 5 pixels is disregarded in the computations.

3.3.6.4.2 Velocity computation

Two distinct algorithms, Particle Image Velocimetry (PIV) and Optical Flow (OF), are employed for vector calculation. PIV relies on a cross-correlation-based approach to assess the spatial displacement of a group of particles or features. It proves invaluable when the time gap between frames is too significant to track the continuous positional changes of individual particles or features over time. Conversely, Optical Flow (OF) operates based on the differential equation of intensity distribution and is ideally suited for scenarios where an object can be unambiguously identified between consecutive frames. In the case of small objects such as particles, successful OF implementation demands a very low particle density. Both algorithms are applied to the entire image and require two successive frames to deduce particle displacement. It has been observed that PIV is particularly effective in computing vectors within high-speed regions of the image (e.g., jet), while OF demonstrates greater reliability in regions with low-speed particles.

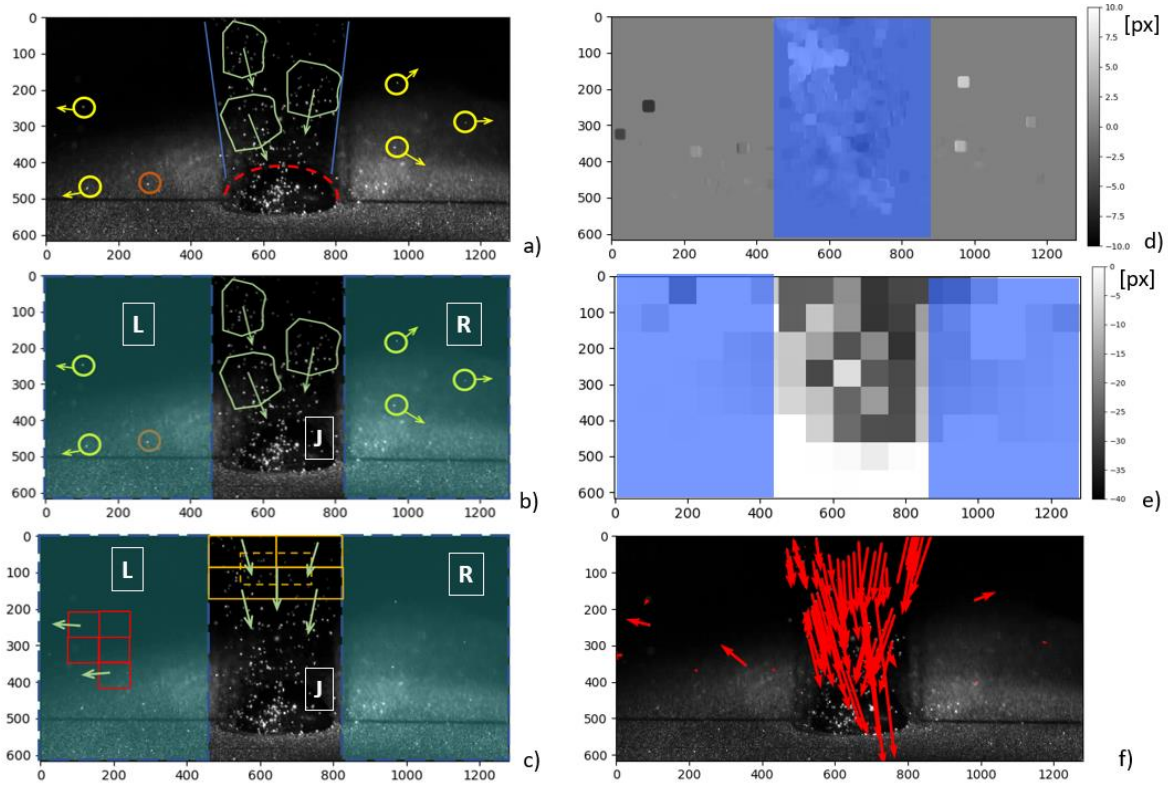

Figure 3.16 Calculation of directional vectors

In Figure 3.16-a, distinct regions of the cladding process are discernible: at the core, clusters of rapidly moving metal droplets are confined within a conical shape, progressing towards the deposition zone. Flanking the central region are slower-moving, solitary particles that escape the deposition area and reach the image borders. Figure 3.16-b provides an illustrative schematic of the partitioning of these regions within the image: 'J' designates the central jet, 'L' and 'R' represent the left and right areas surrounding the jet. It's worth noting that particles eluding the melting area can be present throughout the vicinity of the jet, although they may not be visible due to the limited depth of field of the camera lens. As mentioned earlier in this paragraph, PIV is employed to compute velocity vectors in region 'J' of Figure 3.16-b, while OF is utilized in regions 'L' and 'R'. Figure 2-c illustrates the distinct schemes employed to create search windows for the two different methods: PIV employs overlapping windows measuring 100x100 pixels, whereas OF utilizes 24x24 pixel regions of interest. Subsequently, Figure 3.16-c and-b respectively depict the outcomes of applying OF and PIV to two consecutive images acquired using the OF method.

3.3.6.4.3 Merging particle detection and velocity vectors

Nonetheless, distinguishing the high-frequency noise caused by pixelization from the tiny liquid metal droplets proved to be a challenging task. The code was designed to address this issue by implementing a filtering cascade that encompasses the following filters: Thresholding the particle signal, as demonstrated in step 1, Figure 3.12-e. Eliminating droplets with a size smaller than 6 pixels in the binary image of Figure 3.12-f. Excluding displacement values obtained with Optical Flow at the order of magnitude of 1 pixel. As elucidated in the preceding section, direction and velocities are calculated within regions of interest rather than for individual particles. To assign a vector to each particle, a simple procedure involves overlaying the binary image derived from step 1 with the velocity maps generated in step 2, ensuring that all velocity maps are appropriately transformed into images of 1200x1400 pixels (replace with the correct values). An exemplification of the outcomes of this process is presented in Figure 3.16-f. It is crucial to emphasize that the Optical Flow (OF) velocity maps are superimposed onto particles exclusively in regions R and L, while Particle Image Velocimetry (PIV) vector maps are superimposed onto particles detected in region J. Consequently, slow and scattered particles have their vectors computed via OF, whereas fast and densely grouped particles have their vectors computed using PIV.

An illustrative frame (Figure 3.17) extracted from a high-speed image sequence, featuring identified components such as the powder stream (highlighted in red), the meltpool (depicted in white), entering powder particles accompanied by velocity vectors (indicated in green), and escaping powder particles with their respective velocity vectors (shown in yellow).

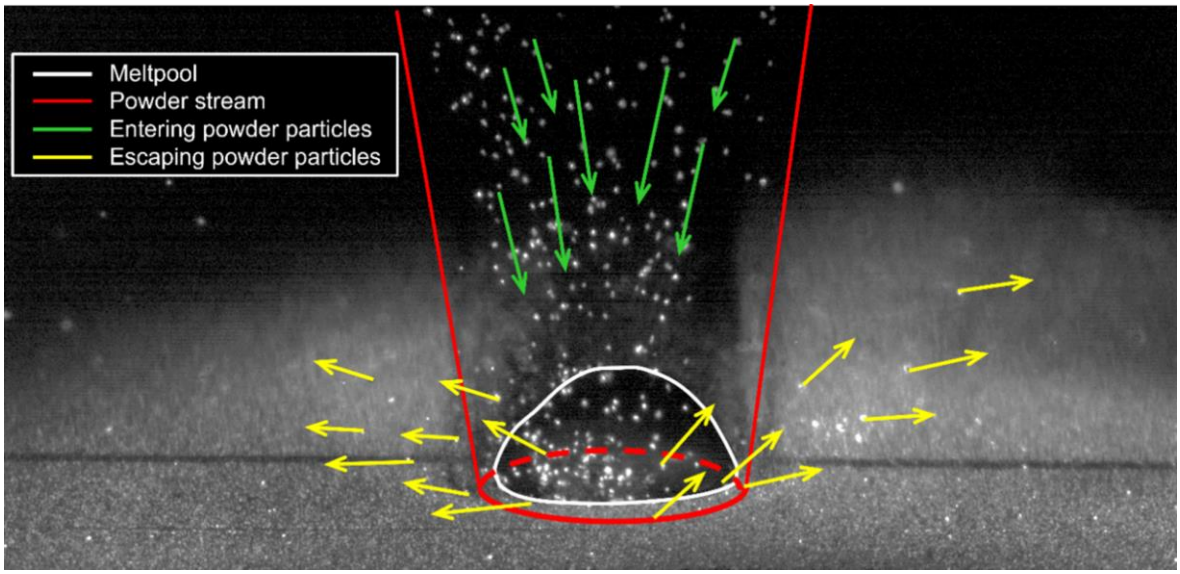

Figure 3.17 A sample frame featuring the identified powder stream (in red), the meltpool (in white), entering powder particles with velocity vectors (in green), and escaping powder particles with velocity vectors (in yellow).

3.3.6.5 Video analysis concept

3.3.6.5.1 Mapping the geometry of the melt pool

The plan view geometry of the weld pool was accurately identified from the HSI videos. Prior to that, it was necessary to identify the meltpool contour based on the frames of the image. To create the final image for processing, brightness and contrast were adjusted in order to clearly distinguish the meltpool. The Figure (a) below shows as-received video frame, (b) the adjusted final image and (c) final image with meltpool mark up with red line. To further process the data, meltpool interface dimensions were collected using ImageJ with 10 repeats for error calculation and then exported to Excel. As the video was captured at an angle of 11, the plain view of the meltpool and the area could be determined.

a)

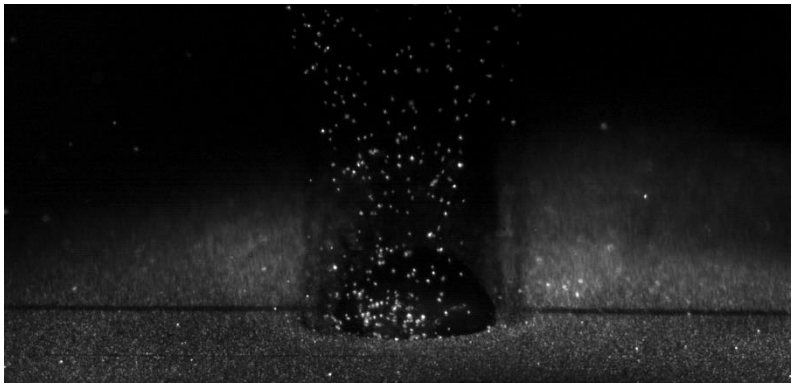

b)

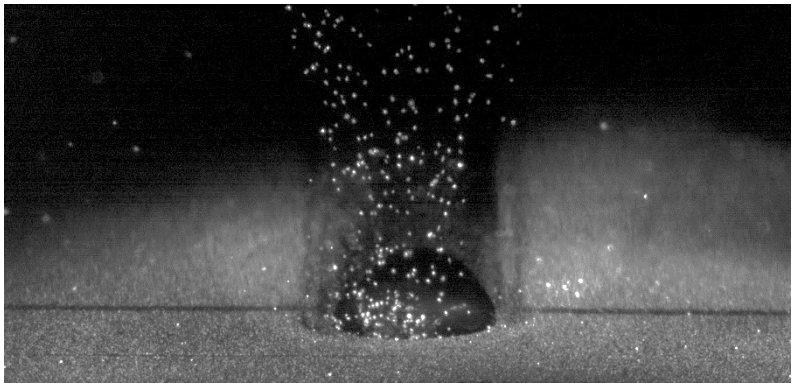

c)

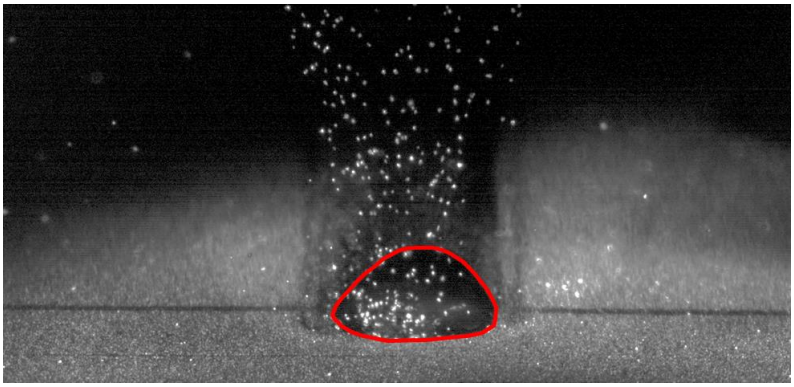

Figure 3.18 HIS video frames as-received video frame, (b) the adjusted final image and (c) final image with meltpool mark up with red line.

Figure 3.19 shows how the plan view maps of the melt pools were extracted from the video data (in this example for a solo ‘A’ track). The maximum width of the melt pool can be measured directly from the video, but its length L needs to be calculated using equation below.

$$L = \frac{D - H \cdot cos(\theta)}{\sin \theta}$$

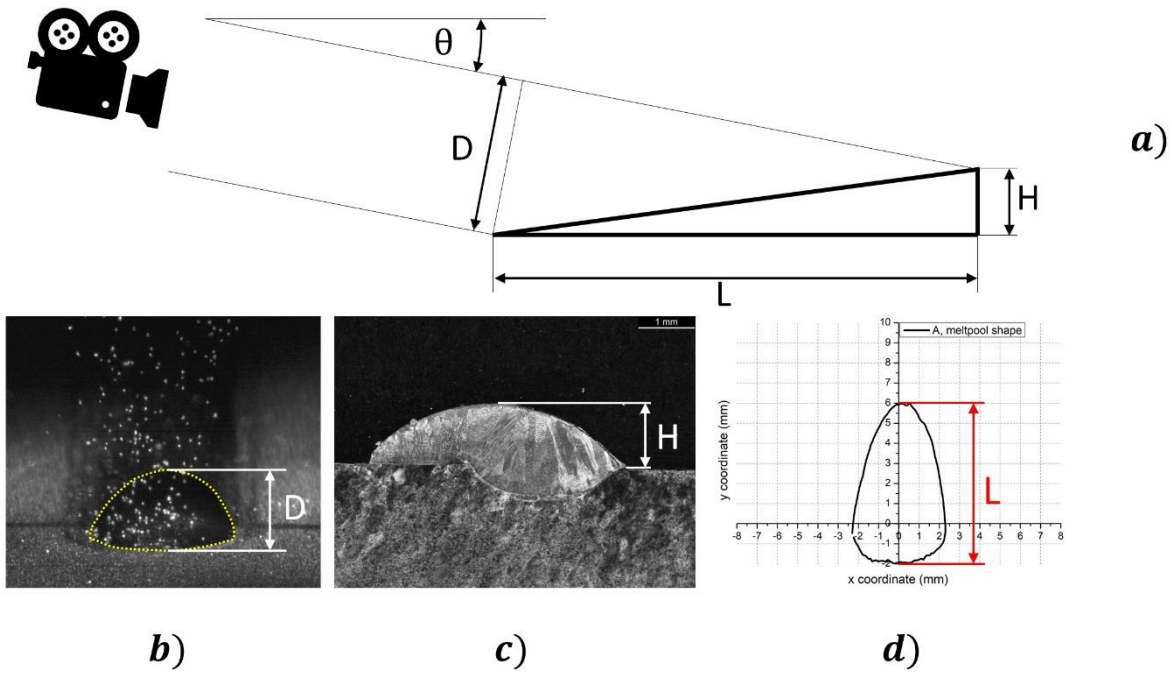

Figure 3.19 a. A schematic of the video capture geometry. b. A typical single frame from the video (‘A’ track). c. A typical ‘A’ track cross section. d. A typical calculated melt pool geometry (plan view ‘A’ track).

Once L and the maximum width are known, then the overall shape of the pool perimeter can be taken from the video data and the plan (top) view of the melt pool mapped. The plan view was preferred to the view perpendicular to the melt surface because the powder can be assumed to be falling vertically downwards.

3.3.6.5.2 Location, diameter, and area of the powder stream

To analyse particle behaviour, high-speed video frames were utilized to identify entry points into the meltpool (Figure 3.20-a) or contact with the substrate. By marking these particle points, the maximum diameter of the powder stream was determined through 12 measurements, along with associated errors (Figure 3.20-b). The powder stream's area and error were calculated from the diameter and its error using the provided equations. Additionally, the distance between the meltpool and the powder stream was measured 10 times, assuming both were centered on the vertical axis (Figure 3.20-c).

a)

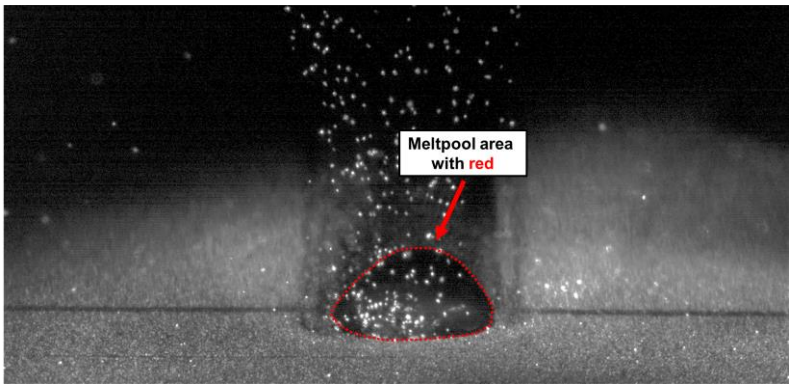

b)

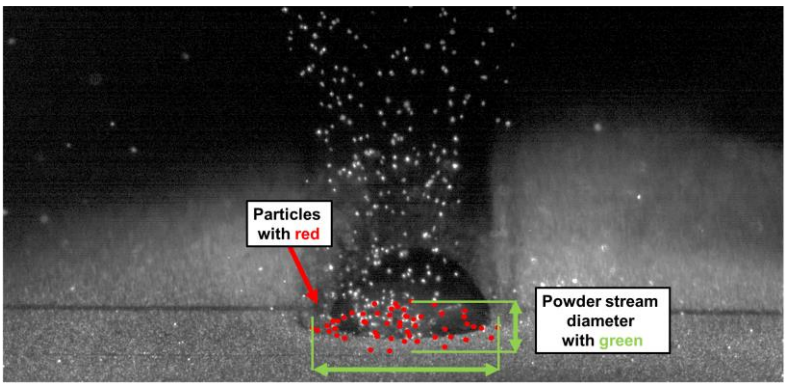

c)

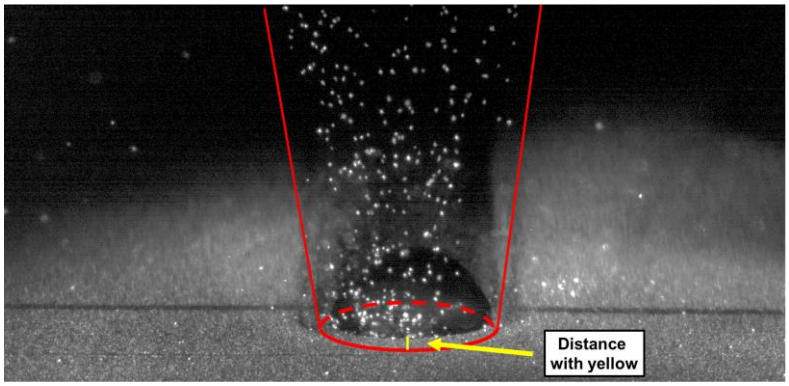

Figure 3.20 High-speed video frames: a) Image with meltpool outlined in red, b) Particles marked for identification, c) Powder stream marked with its location relative to the meltpool.

3.3.6.5.3 Powder catchment efficiency: meltpool and powder stream overlap

Meltpool graphs are plotted with 10 distinct powder stream locations in Origin. For each powder stream location and meltpool area, ImageJ was used to measure the catchment area and determine the pixel ratio of the image (Figure 3.21). In the calculation of the powder catchment area, the meltpool error was not considered. Using the powder catchment area and the powder stream area, both the powder catchment efficiency and its associated error was computed.

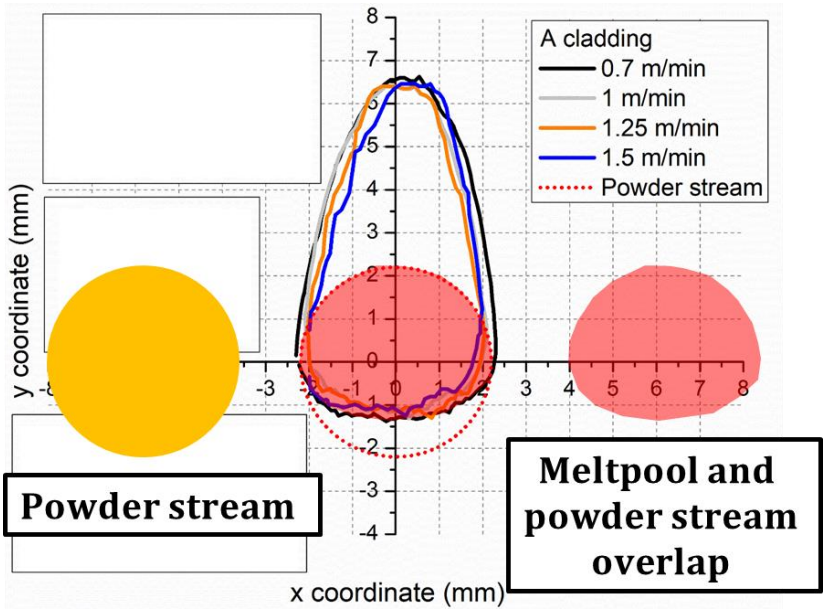

Figure 3.21 Powder catchment efficiency: meltpool and powder stream overlap

3.3.6.5.4 Particle size and powder feed rate

To ascertain particle size, I analysed the high-speed video frames, which consisted of 2000 frames. I adopted a sampling approach, selecting one frame for every 200 frames, resulting in ten sample frames in total (Figure 3.22). A dedicated program identified the particles within each of these frames, revealing approximately 100 particles within the predefined cylinder. With the particle sizes measured in pixels, I determined the diameter of each individual particle. This diameter information allowed me to calculate the mass of each particle. By summing the masses of all particles, I calculated the total powder mass, repeating this process ten times with associated errors. Subsequently, I computed the powder feed rate and its error using the total particle mass, particle velocities, cylinder height, and the error of the total mass over ten frames. Then the average powder feed rate and with error determined.

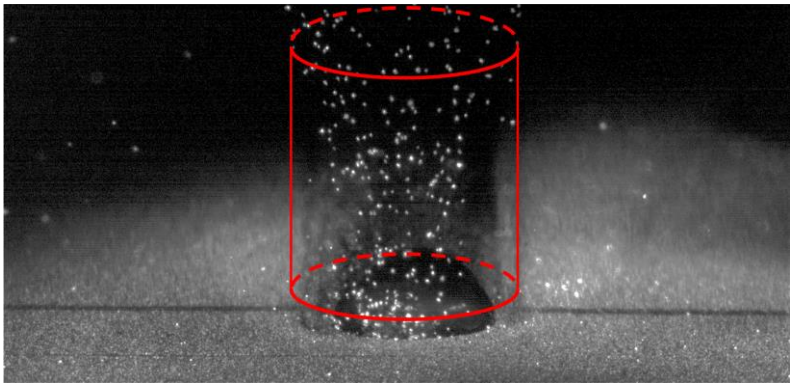

Figure 3.22 Sample frame with the predefined cylinder

3.3.6.5.5 Particle distribution and particle size

By analysing all the particles in each frame along with their respective sizes, the particle size distribution can be determined. The primary objective was to compare these computed results with the manufacturer-provided datasheet, thereby establishing a correlation between the two datasets. The computed results exhibit a high degree of correlation with the datasheet results, characterized by minimal error (Table 3.5).

Table 3.5 Comparison of Powder Size Distribution: Evaluating Calculated Results Against Manufacturer-Provided Data

µm from	µm to	Datasheet %	Calculated %	Error %
150	180	0.1	0.08	0.27
125	150	5.1	4.49	1.60
106	125	15.3	14.58	2.14
75	106	51	53.05	3.64
63	75	18.6	18.47	2.11
53	63	8.9	8.14	1.66
45	53	1	1.19	0.71

3.3.6.5.6 Powder catchment efficiency from particle mass

To assess powder catchment efficiency based on particle mass, high-speed video frames were used comprising 2000 frames each. Within this dataset, the program systematically identified particles that entered the meltpool as well as those that escaped in both left and right directions (Figure 3.23). The diameter of each particle was measured in pixels, enabling the calculation of individual particle masses. Consequently, weight percentages of all particles were determined, encompassing those entering the meltpool and those directed in either the left or right directions. Subsequently, the average powder catchment, powder escape to the left, and powder escape to the right were computed based on this extensive dataset.

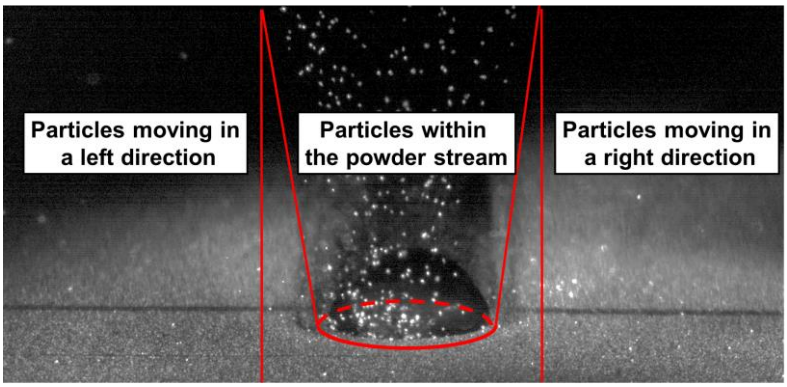

Figure 3.23 High-speed video frame: An illustrative example for explaining the directions of particle escape.

3.3.6.5.7 Powder catchment from the cross-sectional area of the clad

The cross-sectional area ten times was measured, from which I derived the average cross-sectional area and its associated error. Using this cross-sectional area, in conjunction with data on cladding speed, powder density, and the powder feed rate, the powder catchment based on the cross-sectional area was calculated. The powder catchment error was determined using the error associated with the cross-sectional area and the powder flow rate error. An example of a single clad cross-section with the cross-sectional area highlighted in red shown in Figure 3.24.

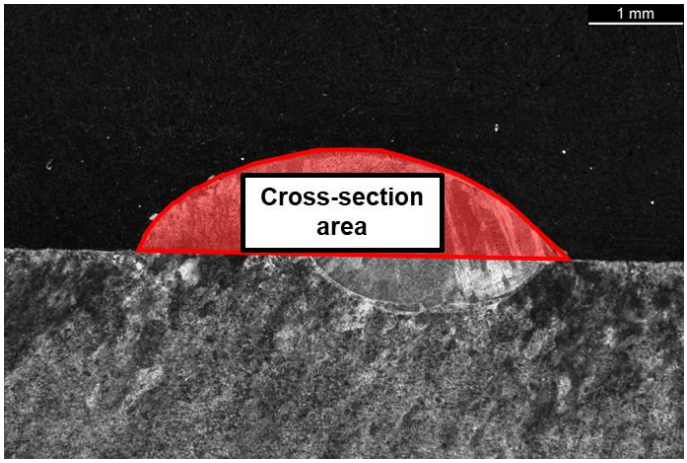

Figure 3.24 Example of a cross-section of a single clad, with the cross-sectional area highlighted in red.

3.3.6.5.8 Comparing powder catchment efficiency calculations and measurements

Three distinct methods for determining powder catchment have been discussed in previous sections: powder catchment efficiency based on particle mass, powder stream and meltpool overlap, and cross-sectional area of the clad. An example of a single A-clad meltpool at various cladding speeds is provided (Figure 3.25). All three calculations for powder catchment efficiency are in agreement with each other.

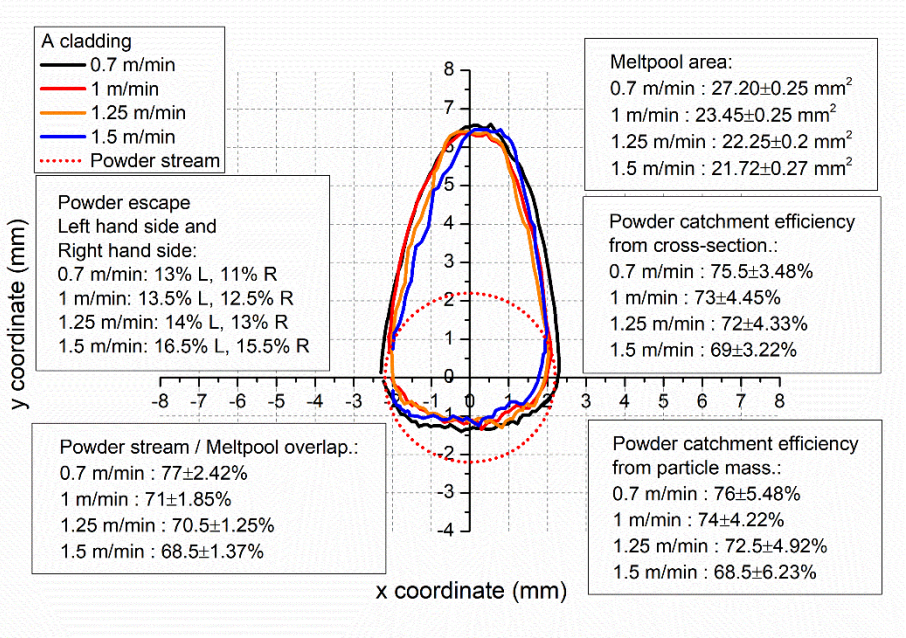

Figure 3.25 Example of a single A-clad meltpool at different cladding speeds with powder catchment efficiency calculations

3.3.7 Processing parameters

3.3.7.1 Process parameter for AAA and ABA cladding

A total of 24 samples were deposited. The unchanged processing parameters: 3kW laser power and 26 g/min feed rate were used. Tracks were created using both the AAA and ABA techniques. The actual samples involved 3 identical, parallel ‘A’ tracks interspersed with 2 ‘B’ tracks. Tracks were completed with different A-B lateral spacings. The length of "A" clad and “B” clad was 90 mm. Two different processing parameters were changed laser beam scanning speed and inter-track spacings. Samples were created with a variety of inter-track spacings 2-4 mm (overlapping ratio 0%-50%). The tracks comparing ‘AAA’ and ‘ABA’ clads were carried out at 700 mm/min. For further investigation into ABA cladding, the process speed was varied between 700 mm/min and 1500 mm/min. A series of solo ‘A’ tracks were also made over this range to investigate pool shape changes as a function of process speed. This experiment was designed to compare the quality and the productivity parameters of the AAA and ABA claddings.

3.4 Sample preparation and metallographic techniques

All specimens were subjected to standard specimen preparation techniques, particularly cutting, mounting, grinding, polishing and etching. Subsequently microstructural analysis was performed.

3.4.1 Sample preparation

3.4.1.1 Sample cutting

Following the laser cladding experiment, the next step was cutting the sample. When selecting the location for authentic measurements, it is essential to select a location where the process has already stabilized. Therefore, it is far enough from the points at which the welds start and also at a sufficient distance from the points at which the beam exits. Cuts were made approximately midway along the track, since it has been observed that laser deposition takes 2-3 seconds to become stable. A sample of 8 mm in length was cut from the plate. For instance, the selected location corresponds to the image below (see in Figure 3.26), which demonstrates laser cladding “AAA” and “ABA” experiment samples.

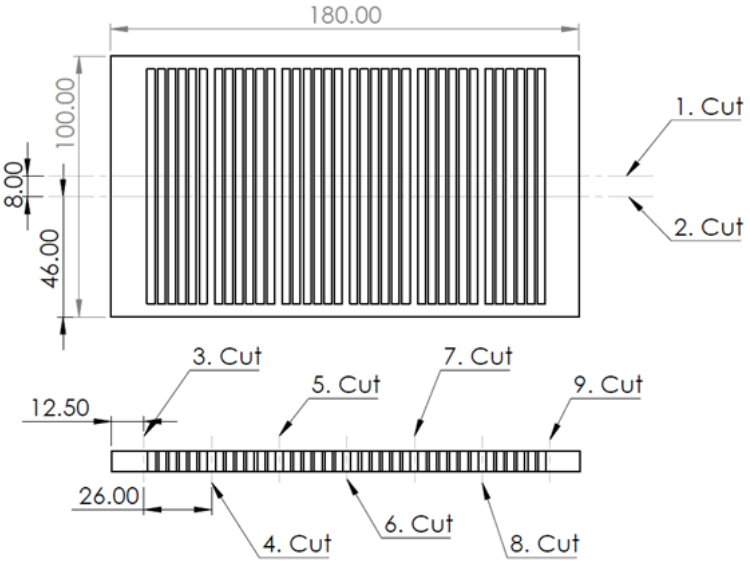

Figure 3.26 Samples with cutting location

Cutting was performed using the AbrasiMatic 300 band saw, which is shown in Figure 3.27. For the successfully separated pieces, manual deburring followed by manual cleaning was done.

Figure 3.27 AbrasiMatic 300 band saw

3.4.1.2 Hot mounting

Prior to grinding, the cut samples were hot mounted in phenol-based resin using a hot embedding device. Sample quality and structure are unaffected by the temperature of the hot mount procedure. Samples were mounted in specimens with a diameter of 30mm. As shown in Table 3.6, the following setup parameters were used for the hot mounting.

Table 3.6 Mounting system setup parameters

System parameters	Notation	Unit	
Heating temperature	T_h	°C	180
Heating time	t_h	min	9
Cooling time	t_c	min	2.5
Container pressure	P_c	bar	3

The purpose of the hot mount was to facilitate handling during sample preparation. As a result of sample preparation, such as grinding and polishing, a surface will be created on the sample that is suitable for microscopic structure studies. Metaserv Automatic Mould Press hot mounting system was used for the moulding process, which is shown in Figure 3.28. After successful mounting, the pieces were cleaned manually.

Figure 3.28 Metaserv Automatic Mould Press system

3.4.1.3 Grinding

Grinding is the next step in sample preparation. P 240, P400, P600, P1000, and P1200 SiC sandpapers were used in the wet environment for grinding. The number on the sandpaper indicates the fineness of the paper - e.g. P240 = 240 pieces of SiC / mm^2 – i.e. the number of SiC particles per 1 mm^2. Water was used to reduce frictional heat during the operation, thus preventing overheating. A smooth surface was required for polishing. For the grinding process, Struers LaboPol-21 grinding system was utilized, which is shown in Figure 3.29. The next step for the successfully ground pieces was to clean them with water and ethanol, followed by a full drying of the sample face.

Figure 3.29 Struers LaboPol-21 grinding system

3.4.1.4 Polishing

The next step involved polishing the sample surface to achieve a scratch-free, glossy appearance. Each sample will therefore require a different amount of polishing time. During the polishing process, fluids and cloths containing the polishing machine and diamond grains of varying sizes (6, 1μm) were used. To reduce friction, a suspension solution was added every minute. The purpose of polishing is to create a scratch-free surface for etching. Struers LaboPol-20 polishing system was used in the polishing process, as shown in Figure 3.30.

Figure 3.30 Struers LaboPol-20 polishing system

3.4.1.5 Etching

In the laser cladding experiments, bright mild steel, austenitic stainless steel and Stellite 6 materials were used, as a result aqua regia etching liquid was chosen as the etchant. The samples were etched with an aqua regia (10 ml HNO_3 + 30ml HCl) solution for 10 seconds 3 times to allow the clad to be etched, followed by an alcohol wash and drying. Etching is performed in order to generate contrast so that the microstructure is visible and measurements can be made.

3.4.2 Metallographic techniques

Microstructural and metallographic examinations were conducted using both optical microscopy and scanning electron microscopy (SEM). The following section introduces the optical and scanning electron microscope systems.

3.4.2.1 Optical microscopy

The optical microscopy pictures discussed in this dissertation were captured using a Nikon Eclipse LV100ND system (see in Figure 3.31) which contains five objectives providing magnifications of 5x, 10x, 20x, 50x and 100x. The recording of optical images was carried out by a Nikon DS-Ri1 high-resolution microscopy camera, which was connected to computer NIS Elements software for viewing, capturing, recording, and storing the micrographs of the samples electronically. The microstructure of the samples was revealed using optical microscopy. For optimal resolution of the track microstructures, contrast was optimized. Analysing images with ImageJ was employed to measure the major geometrical characteristics of the clad.

Figure 3.31 Nikon LV100ND optical microscope with Nikon DS-Ri1 camera

3.4.2.2 Scanning electron microscopy

A Philips XL30 Scanning Electron Microscope (SEM), working in low and high vacuum atmosphere with 1KV-30KV and 10X-100,000x magnification. Its maximum resolution under optimal conditions is 3.5nm. The scanning electron microscope contains an Energy-Dispersive X-ray Spectroscopy (EDX) device, which has been used to observe the microstructures, details of the solidification process and microstructural details investigation and for the study of dilution. The scanning electron microscope is illustrated in Figure 3.32.

Figure 3.32 Philips XL 30 Scanning Electron Microscope

4 Chapter IV. Assessing the quality and productivity of Laser Cladding and Direct Energy Deposition (DED); Guidelines for researchers

The main body of this section is reproduced from the paper:

Powell, J., Koti, D., Garmendia, X. and Voisey, K.T., 2023. Assessing the quality and productivity of laser cladding and direct energy deposition: Guidelines for researchers. Journal of Laser Applications, 35(1), p.012024, https://doi.org/10.2351/7.0000897

4.1 Abstract

This paper provides guidelines and advice for researchers and engineers in the field of laser cladding and related Direct Energy Deposition (DED) techniques, to help establish a standardised approach to quality assessment and productivity metrics. Factors considered are; deposit geometry, porosity, cracking, dilution, build-up/coverage rate and powder catchment efficiency.

4.2 Introduction

Although there is a very large body of research work on laser cladding and related Direct Energy Deposition (DED) techniques, there are no clear guidelines about which quality and productivity parameters are important to the relevant branches of industry, nor are there any general rules about what constitutes a high-quality deposit. It is the aim of this paper to provide such guidelines for researchers in the area.

The great majority of laser Direct Energy Deposition (DED)/cladding research concentrates on the comparison of individual clad tracks like the one marked ‘A’ on the left hand side of Figure 4.1 [1-4]. Although such research is interesting and informative, it has minimal industrial relevance, as the commercial applicability of individual deposited tracks is very low. It is therefore not obvious whether the geometry of any particular single track is a better than another. However, the eventual aim of the process is usually the production of surfaces covered in overlapping tracks (like those labelled A1 to An on the right of Figure 4.1 and presented in cross section in Figure 4.2), which require minimal machining to create a flat surface (In a limited number of cases a rough, ‘as clad’ surface is required rather than a flat, machined one).

Some initial guidelines about what to aim for can be stated which are true for single or multiple tracks;

- Minimal fluctuations in track height (to minimise post cladding machining and areas with insufficient clad material).
- No porosity or undercut (undercut can lead to trapped pores between tracks).
- No cracks.
- An acceptable level of substrate-cladding dilution.
- Maximum coverage or build-up rate (for maximum productivity).
- Maximum powder capture (for minimum powder recycling and optimum process efficiency).

The following sections discuss these points in detail, dividing them into quality and productivity considerations.

4.3 Quality Considerations

4.3.1 Deposit Geometry

Figure 4.1 outlines a fundamental problem found when trying to produce a flat clad surface from ostensibly identical overlapping tracks. Before the second track is laid down, the first track (A) is a solo clad track with a cross section which is approximately a segment of a circle. Subsequent tracks have a different cross-sectional geometry as they are laid down on the 'shoulder' of the previous track. This means that several tracks need to be laid down before a repeating cross sectional track geometry is established. The final track of a layer also has a different geometry because it is not partially remelted by a subsequent track.

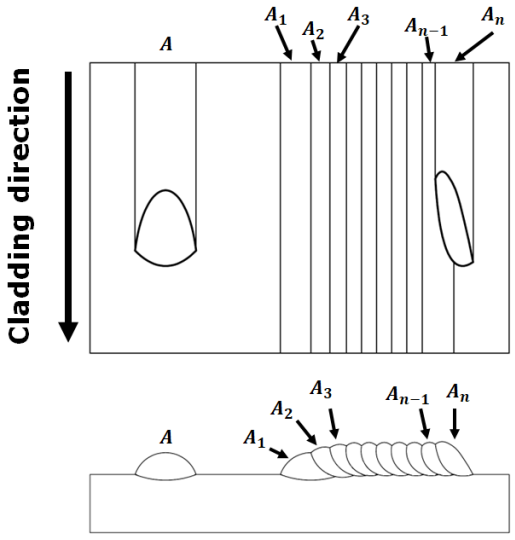

Figure 4.1 Schematic plan views and cross sections of a single clad track and a set of overlapping tracks making a clad surface.

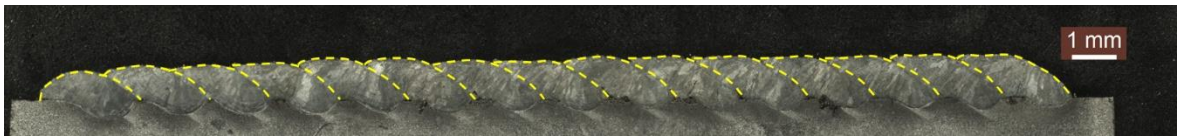

Figure 4.2 A macroscopic cross section of a typical clad layer made from overlapping tracks.

Laser clad surfaces usually need to be machined to a flat surface before use and this will involve the removal of part of the clad deposit. The amount of material which needs to be removed should be minimised because machining is an expensive process in itself, and the wasted powder and energy used to create the discarded layer is also costly. Post-cladding machining is minimised by creating clad surfaces which have a minimum fluctuation in cross sectional height.

One important consideration when looking at multiple, overlapping tracks is that the maximum fluctuation in clad height often occurs between tracks rather than along the length of the individual tracks (see Figure 4.3). For this reason, the maximum height variation of the surface needs to be measured over a substantial area, or at least in two orthogonal directions (for several tens of millimetres if possible). Maximum height variation in roughness is usually given as Rz but roughness measurement devices often give a value for local Rz, which ignores macroscopic waviness of the sample surface. For this reason, we suggest that waviness (Wz) is the appropriate roughness metric for clad surfaces and similar DED products. It should be noted however that in some industrial applications where a rough surface is preferred, the as-deposited surface is used without post-cladding machining.

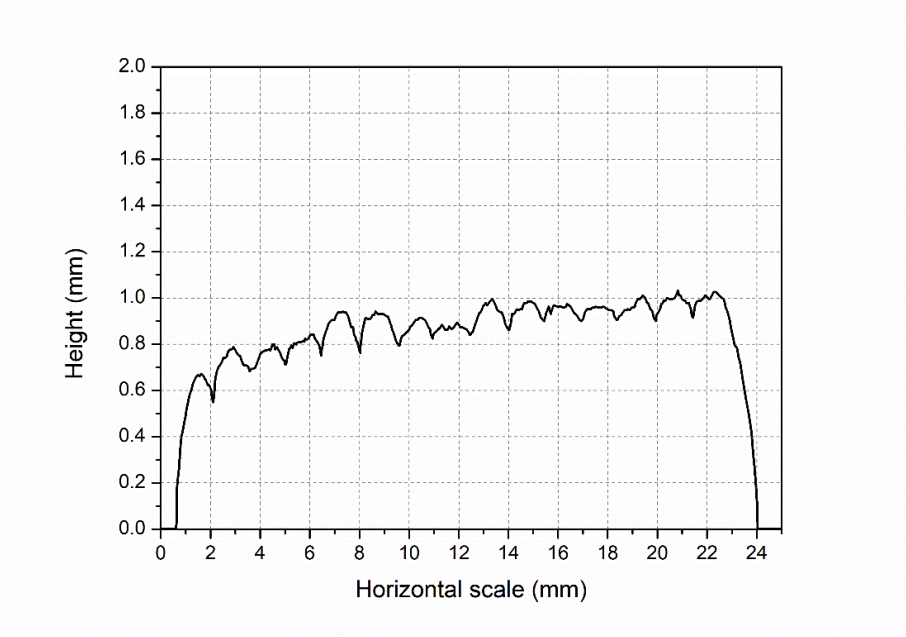

Figure 4.3 A typical example clad layer cross section profile. The biggest variation in clad height is the macroscopic waviness between tracks rather than along the length of any single track.

4.3.2 Porosity

Pores in clad tracks are negative features which need to be minimised or avoided altogether. Pores within the body of the clad layer can be revealed during post-cladding machining and give rise to an open pored, rough surface rather than the generally required smooth one. Open pores of this type can also be stress raisers which can have a deleterious effect on the tensile strength and fatigue life of the clad component [5].

The sources of porosity in laser cladding and DED include; Moisture in the powder or powder feed gas, a melt pool with too short a lifetime, excessive powder flow or powder feed gas, and impurities in the cladding material or the substrate. Problems can be reduced or eliminated by the following control measures [6]:

- Remove scale, rust, paint, grease, oil and moisture from the substrate.
- Eliminate moisture from the powder and gas.
- Keep the cladding pool molten for long enough (eg. by preheating) for gas to escape.
- Minimise the sulphur content of the substrate to prevent generation of hydrogen sulphide.
- Reduce cladding speed or increase laser power.

The distribution of pores in clad layers may be aligned, clustered, or uniformly scattered [7] and the present authors recommend a two-part porosity metric which indicates overall porosity as a percentage of the solidified melt, followed by an average pore diameter. For both numbers a reduction in their value can be taken as an indication of an improvement in clad quality. Levels of porosity can be assessed by Radiography, and computer interpretation of the X ray images is now an established technique [8].

As porosity is never a required feature of a clad track, we recommend that porosity should be zero in cladding and related DED processes.

4.3.3 Cracks

Cracks can form in laser deposited single tracks or surfaces for all the usual reasons associated with welding. As clad surfaces tend to be thin compared with the substrate they are attached to, cladding/DED is susceptible to cold cracking mechanisms associated with the restraint of cooling weld material [9]. Hot cracking, caused by the presence of low melting point constituents which fail in tension during solidification, can also be a problem. Alloys which have a wide solidification temperature range are particularly susceptible to hot cracking [6].

The natural tendency to use high process speeds to maximise productivity can increase levels of cracking. The incidence of cracking can be reduced by; reducing process speeds, increasing laser power and the use of preheating/post heating. It is also important that the substrate surface is completely free of contaminants.

The number of cracks in a clad layer can be reduced by changes in process parameters or by changing the cladding alloy [10]. In some cases this change in alloy can be brought about by increasing or decreasing the amount of dilution in the clad layer (see next section). Another option is to add a 'butter' layer of an alloy which is compatible with both the substrate and the outer clad layer. 'Cracks' can also be created as sharp interfacial flaws between the substrate and the deposited layer and this is sometimes associated with poor wetting between tracks or at the lateral edges of individual tracks [11].

Cracks of any type can compromise the mechanical stability of a clad layer and the present authors would like to suggest that the presence of cracks is so deleterious to the clad product that their presence should be eliminated. If cracks are unavoidable in a particular application, then they should be minimised. It is important to remember that reducing the size of cracks does not necessarily improve the performance of a product. Several small cracks can be a worse outcome than a few larger cracks.

Surface cracks can be identified by several non-destructive testing techniques including Visual inspection, Magnetic Particle inspection and Liquid penetrant inspection [12, 13]. Subsurface and surface defects can be identified by Ultrasonic testing [14], Radiography [8] and Thermography [15].

4.3.4 Dilution

Dilution is widely used as a measure of quality in laser cladding and is generally understood to mean how much of the substrate has been melted into the final clad layer. Cladding materials are expensive and designed to offer high levels of hardness or corrosion resistance to the surface. Excessive dilution usually diminishes the surface hardness or corrosion resistance. For this reason low levels of dilution are generally preferred in laser cladding, though some dilution is unavoidable, as some interfacial mixing of the substrate and clad material is required to make the welded bond. Target dilution values vary but tend to be in the range of 3-5% [16]

However, in some cases high dilution levels might be beneficial to the properties of the clad layer by lowering hardness, increasing ductility and reducing, or eliminating, cracking and porosity. Some applications also demand relatively high levels of dilution to ensure a good substrate-cladding material bond.

For example, the surface properties of Aluminium alloys can be enhanced by laser cladding with other metals or superalloys. Researchers in the field recommend a dilution of at least 10 percent to create a successful bond in some cases [17, 18]. Laser cladding High Entropy Alloys (HEA) is another application where high dilution levels can be useful. HEA coatings with low dilution levels usually have poor formability and this can be improved by increasing the level of substrate melting [19].

Dilution is usually expressed as a percentage, where, for example, 20% dilution indicates that the solidified clad melt is made up of a mixture of 80% cladding alloy and 20% substrate alloy by volume.

However, it should be borne in mind that dilution levels generally give an indication of the overall percentage of substrate melted into the clad and do not indicate the steep dilution gradients which may exist within the clad layer. If a sample has, for example, an estimated 10% dilution, then the local dilution level 0.1mm from substrate-clad interface might be 60% but on the clad outer surface the level might be 2% or lower. At any melt-solid interface such gradients will be very steep in the transition from clad layer to substrate. Also, samples created under different processing parameters might exhibit widely different dilution gradients dependant on the level of stirring forces generated in the melt. Given these complications it is not surprising that most researchers only present overall dilution levels, which can be useful in comparing results within a parameter set.

The most common method of estimating overall, or average, dilution used by researchers [20-25], divides the cross-sectional area of the substrate melt by the area of the whole melt. This gives us a value we can call D_{AREA}:

$$D_{AREA} = \left(A_s / \left(A_c + A_s \right) \right) \times 100$$

Where:

As is the cross-sectional area of the melted substrate,

Ac is the cross-sectional area of the clad layer above the original top surface of the substrate.

Another common method of estimation [26-30] simply divides the maximum depth of melt penetration into the substrate by the overall melt depth of the clad layer (see Figure 4.4). This gives a value we can call D_{HEIGHT}:

$$D_{HEIGHT} = (S/(S+C)) \times 100$$

However, Figure 4.4 demonstrates that, in some cases, D_{HEIGHT} is not equivalent to D_{AREA}.

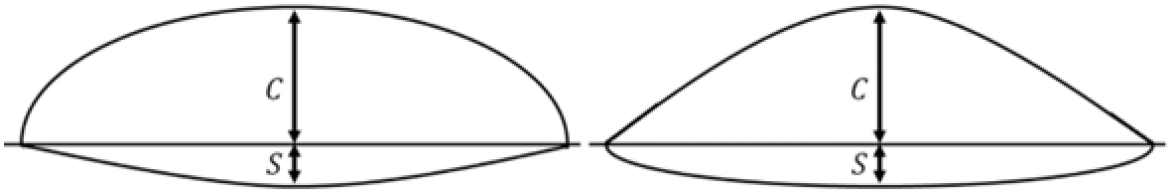

Figure 4.4 Two clad tracks with the same D_{HEIGHT} but different D_{AREA}

In Figure 4.4 the two clad cross sections have the same width, depth, height and therefore the same D_{HEIGHT}. However, the differences in geometry mean that the D_{AREA} of the left-hand track is 18% and that of the right-hand track is 30%.

From this observation it is clear that D_{HEIGHT} does not give a reliable estimation of overall dilution levels for single tracks. Differences between D_{HEIGHT} and D_{AREA} will also exist, but to a lesser extent, for any clad layer of overlapping tracks, as the clad layer is not rectangular in cross section.

We therefore recommend that D_{AREA} should be used in preference to D_{HEIGHT}. It is also worthy of note that D_{AREA} only gives an average volumetric measurement. In the field of metallurgy alloy combinations are usually given in weight %. If average wt% results are required, then the D calculation needs to take the relative densities of the substrate and the cladding feedstock into account.

Detailed chemical dilution analysis is based on measured values created by spectrographic (e.g. EDX) analysis of the samples [31-34]. EDX and related techniques can give information about dilution gradients in cases where the average dilution measurement needs clarification.

4.4 Productivity considerations

4.4.1 Coverage, or build-up rate

From the manufacturing engineer's point of view there is a requirement to minimise costs. The costs of laser cladding and related DED processes include the expenditure on; electricity, staff, overheads and raw materials (powder etc). An increase in productivity is usually associated with a reduction in the time spent creating a product and thus a reduction in some, or all of these costs. Researchers are usually primarily concerned with analysing the process itself, often comparing KPI's between several process parameters. Industrial users are interested in quality and productivity, wishing to optimise both.

Coverage rate, or build up rate, is a measure of productivity which describes how quickly the required clad surface is created. Obviously, this is heavily dependent on the required thickness of the finished, machined, clad layer. Coverage rate might therefore be measured in several ways;

a) Area of substrate covered per unit time (mm2/min)
b) Volume of clad layer per unit time (mm3/min)
c) Mass of clad layer applied per unit time (g/min)

An increase in any of these would imply an increase in productivity, but a rapidly applied rough surface (high Wz) might have a lower coverage rate than a slowly applied smoother one, as the extra post-cladding machining required would reduce the thickness of the final clad layer.

Researchers are often interested in improving industrial performance so the present authors suggest that any comparative measure of cladding processes should take into account the thickness of the final, machined surface.

As researchers generally do not know the required thickness of the clad layer, they cannot state that, for example, sample A, a 0.2mm thick layer laid at 10mm3/s is a better or worse result than sample B, a 0.4mm layer also laid at 10mm3/s. However, a distinction between the two is important and would not be supplied by a mass or volume per unit time metric. The present authors therefore suggest that the area covered is not multiplied by the clad thickness in any such measurement of coverage rate. From an industrial point of view the two figures (area/time and thickness) are more usefully presented as a compound metric as follows;

Coverage rates;

- Sample A. 50mm2/s x 0.2mm
- Sample B. 25mm2/s x 0.4mm

With the thicknesses being the final, machined flat thickness (i.e.. maximum clad height minus surface waviness).

4.4.2 Powder Catchment Efficiency

Although some laser cladding and DED processes use wire as a feedstock, the majority use powder. The powder used in these processes generally has a carefully controlled chemistry and specific physical properties (spherical particles with a certain size distribution) and is therefore expensive. The powder catchment efficiency of the process is simply the percentage of the powder fed into the cladding zone which becomes part of the cladding (in this case we are talking about the pre-machined clad). Powder catchment efficiency is an important metric for the laser cladding industry as it has a direct influence on the cost of the process. It is therefore surprising that it is only rarely mentioned in research papers.

For technical investigations the powder catchment efficiency (Epc) can be calculated using cross sections of the clad layer and knowledge of the process parameters as follows;

$$E_{pc}(\%) = \left(\left(T_{area} \times v \times \rho \right) / F_p \right) \times 100$$

Where,

E_{pc} = powder catchment efficiency (%)

T_{area} = Cross sectional area of the track above the original line of the substrate surface (mm^2)

v = Process speed (mm/min)

ρ = Density of cladding material (g/mm^3)

F_p = Powder feed rate (g/min)

Work by the present authors has analysed the powder catchment efficiency achieved in a large number of published experimental papers and the results are presented in Figure 4.5 [35-78]. In some publications the powder catchment values were explicitly noted by the authors but in many cases the catchment efficiency had to be calculated from the given process parameters and cross section images. The x axis numbers on this figure refer to the reference numbers of the papers listed at the end of this paper.

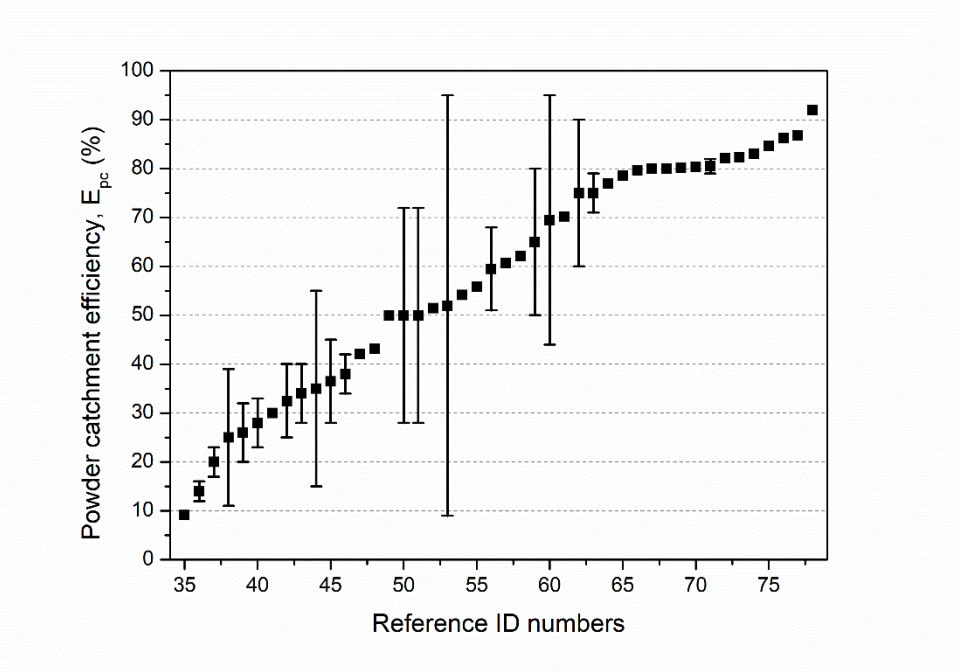

Figure 4.5 The powder catchment efficiency results calculated from published experimental results

It is clear from Figure 4.5 that the range of results of Epc is very large – from below 10% to above 90%. Bearing in mind the cost of these powders it is obviously important to maximise this value wherever possible. It is also worth noting that the process usually depends on the flow characteristics of the powder, and this can be badly affected by contaminants or powder particles which have been fused together. This greatly restricts the re-use of powders which were not incorporated into the clad.

It is the view of the present authors that Epc should become an important, basic metric of any cladding/DED research or industrial work and values below 50% should trigger concern about the industrial viability of the specific application in question.

4.5 Conclusions

The present authors suggest the following guidelines for laser cladding and related DED processes;

4.5.1 Quality Guidelines

- Research into individual clad tracks is of minimal industrial relevance.
- Fluctuations in clad surface height should be as small as possible to minimise post cladding machining and areas with insufficient clad material. Height fluctuations should be measured in two orthogonal directions to find the waviness (Rw).
- Porosity should be minimised and, if possible, eliminated.
- Cracks should be eliminated (small cracks are generally no better than large cracks).
- Measure average dilution by the area method.
- Average dilution should usually be in the target range 3-5% but there are case-specific exceptions.

4.5.2 Productivity guidelines

- Production time should be minimised within the constraints of adequate quality.
- Coverage or build-up rate should be maximised within the constraints of required clad thickness.
- Coverage rates should be given as a compound metric of the form X mm^2/unit time x Y mm (thickness)
- Powder capture efficiency (Epc) should be maximised and should be a major metric for industrial process validity.

4.6 List of references

1. Kumar, S., Mandal, A. and Das, A.K., 2022. The effect of process parameters and characterization for the laser cladding of cBN based composite clad over the Ti6Al4V alloy. Materials Chemistry and Physics, 288, p.126410.
2. Kiehl, M., Scheid, A., Graf, K., Ernst, B. and Tetzlaff, U., 2022. Coaxial Laser Cladding of Cobalt-Base Alloy Stellite™ 6 on Grey Cast Iron Analysis of the Microstructural and Mechanical Properties Depending on the Laser Power. Journal of Materials Engineering and Performance, pp.1-18.
3. Chen, L., Yu, T., Chen, X., Zhao, Y. and Guan, C., 2022. Process optimization, microstructure and microhardness of coaxial laser cladding TiC reinforced Ni-based composite coatings. Optics & Laser Technology, 152, p.108129.
4. Gots, A.N., Lyukhter, A.B., Kochuev, D.A., Frolov, K.A. and Rumyantcev, I.V., 2021. Influence of laser power and scanning speed on the formation of single tracks formed by laser cladding. In Solid State Phenomena (Vol. 313, pp. 15-21). Trans Tech Publications Ltd.
5. Yamaguchi, T., Tanaka, K. and Hagino, H., 2022. Porosity reduction in WC-12Co laser cladding by aluminum addition. International Journal of Refractory Metals and Hard Materials, p.106020.
6. Becker WT, Shipley RJ, Lampman SR, Sanders BR, Anton GJ, Hrivnak N, Kinson J, Terman C, Muldoon K, Henry SD, Scott Jr WW. ASM handbook. Failure analysis and prevention. 2002;11:107.
7. Lippold JC. Welding metallurgy and weldability. John Wiley & Sons; 2014 Nov 24.
8. Zahran O, Kasban H, El-Kordy M, Abd El-Samie FE. Automatic weld defect identification from radiographic images. Ndt & E International. 2013 Jul 1;57:26-35.
9. Gao, Z., Wang, L., Wang, Y., Lyu, F. and Zhan, X., 2022. Crack defects and formation mechanism of FeCoCrNi high entropy alloy coating on TC4 titanium alloy prepared by laser cladding. Journal of Alloys and Compounds, 903, p.163905.
10. Shi, B., Li, T., Guo, Z., Zhang, X. and Zhang, H., 2022. Selecting process parameters of crack-free Ni60A alloy coating prepared by coaxial laser cladding. Optics & Laser Technology, 149, p.107805.

11. Ferreira, A.A., Amaral, R.L., Romio, P.C., Cruz, J.M., Reis, A.R. and Vieira, M.F., 2021. Deposition of nickel-based superalloy claddings on low alloy structural steel by direct laser deposition. Metals, 11(8), p.1326
12. Zolfaghari A, Zolfaghari A, Kolahan F. Reliability and sensitivity of magnetic particle nondestructive testing in detecting the surface cracks of welded components. Nondestructive Testing and Evaluation. 2018 Jul 3;33(3):290-300.
13. de la Yedra AF. Alcance y aplicabilidad de la sentencia del Tribunal de Justicia de la Unión Europea de 20 de diciembre de 2017 (caso Uber). Lan Harremanak-Revista de Relaciones Laborales. 2019 Jun 28(41).
14. Lopez AB, Santos J, Sousa JP, Santos TG, Quintino L. Phased array ultrasonic inspection of metal additive manufacturing parts. Journal of Nondestructive Evaluation. 2019 Sep;38(3):1-1.
15. Dorafshan S, Maguire M, Collins W. Infrared thermography for weld inspection: feasibility and application. Infrastructures. 2018 Oct 9;3(4):45.
16. Garmendia, X. Personal Communication.
17. Siddiqui AA, Dubey AK, Paul CP. A study of metallurgy and erosion in laser surface alloying of AlxCu0. 5FeNiTi high entropy alloy. Surface and Coatings Technology. 2019 Mar 15;361:27-34.
18. Fogagnolo JB, Rodrigues AV, Sallica-Leva E, Lima MS, Caram R. Surface stiffness gradient in Ti parts obtained by laser surface alloying with Cu and Nb. Surface and Coatings Technology. 2016 Jul 15;297:34-42.
19. Wen X, Cui X, Jin G, Zhang X, Zhang Y, Zhang D, Fang Y. Design and characterization of FeCrCoAlMn0. 5Mo0. 1 high-entropy alloy coating by ultrasonic assisted laser cladding. Journal of Alloys and Compounds. 2020 Sep 15;835:155449.
20. Abe N, Tanigawa D, Tsukamoto M, Hayashi Y, Yamazaki H, Tatsumi Y, Yoneyama M. Dynamic observation of formation process in laser cladding using high speed video camera. InInternational Congress on Applications of Lasers & Electro-Optics 2013 Oct 1 (pp. 448-452). AIP Publishing..
21. Aghakhani, M. “Parametric Optimization of Gas Metal Arc Welding Process by Taguchi Method on Weld Dilution.” International Journal of Modeling and Optimization, 2011, pp. 216–220., doi:10.7763/ijmo.2011.v1.38.
22. Alizadeh-Sh M, Marashi SP, Ranjbarnodeh E, Shoja-Razavi R, Oliveira JP. Prediction of solidification cracking by an empirical-statistical analysis for laser

cladding of Inconel 718 powder on a non-weldable substrate. Optics & Laser Technology. 2020 Aug 1;128:106244..

23. Bax B, Rajput R, Kellet R, Reisacher M. Systematic evaluation of process parameter maps for laser cladding and directed energy deposition. Additive Manufacturing. 2018 May 1;21:487-94.
24. Bin L, Heping L, Xingbin J, Yuxin L, Peikang B. The effect of laser process parameters on microstructure and dilution rate of cladding coatings. InIOP Conference Series: Materials Science and Engineering 2018 Feb 1 (Vol. 307, No. 1, p. 012035). IOP Publishing.
25. Caneda CM, Fogagnolo JB, Kiminami CS, Afonso CR. Ultrafine eutectic coatings from Fe-Nb-B powder using laser cladding. Materials characterization. 2020 Feb 1;160:110080.
26. Alvarez P, Montealegre MÁ, Pulido-Jiménez JF, Arrizubieta JI. Analysis of the process parameter influence in laser cladding of 316L stainless steel. Journal of Manufacturing and Materials Processing. 2018 Aug 15;2(3):55.
27. Ansari M, Razavi RS, Barekat M. An empirical-statistical model for coaxial laser cladding of NiCrAlY powder on Inconel 738 superalloy. Optics & Laser Technology. 2016 Dec 1;86:136-44.
28. Barekat M, Razavi RS, Ghasemi A. Nd: YAG laser cladding of Co–Cr–Mo alloy on γ-TiAl substrate. Optics & Laser Technology. 2016 Jun 1;80:145-52.
29. da Silva MD, Partes K, Seefeld T, Vollertsen F. Comparison of coaxial and off-axis nozzle configurations in one step process laser cladding on aluminum substrate. Journal of Materials Processing Technology. 2012 Nov 1;212(11):2514-9.
30. Erfanmanesh M, Abdollah-Pour H, Mohammadian-Semnani H, Shoja-Razavi R. An empirical-statistical model for laser cladding of WC-12Co powder on AISI 321 stainless steel. Optics & Laser Technology. 2017 Dec 1;97:180-6.
31. Erfanmanesh M, Shoja-Razavi R, Abdollah-Pour H, Mohammadian-Semnani H. Influence of using electroless Ni-P coated WC-Co powder on laser cladding of stainless steel. Surface and Coatings Technology. 2018 Aug 25;348:41-54.
32. Abioye TE, McCartney DG, Clare AT. Laser cladding of Inconel 625 wire for corrosion protection. Journal of Materials Processing Technology. 2015 Mar 1;217:232-40.

33. Feng K, Chen Y, Deng P, Li Y, Zhao H, Lu F, Li R, Huang J, Li Z. Improved high-temperature hardness and wear resistance of Inconel 625 coatings fabricated by laser cladding. Journal of Materials Processing Technology. 2017 May 1;243:82-91.
34. Lai Q, Abrahams R, Yan W, Qiu C, Mutton P, Paradowska A, Fang X, Soodi M, Wu X. Effects of preheating and carbon dilution on material characteristics of laser-cladded hypereutectoid rail steels. Materials Science and Engineering: A. 2018 Jan 17;712:548-63.
35. Nurminen J, Riihimäki J, Näkki J, Vuoristo P. Comparison of laser cladding with powder and hot and cold wire techniques. InPacific International Conference on Applications of Lasers and Optics 2006 Oct 1. AIP Publishing.
36. Nurminen J, Riihimäki J, Näkki J, Vuoristo P. Comparison of laser cladding with powder and hot and cold wire techniques. InInternational Congress on Applications of Lasers & Electro-Optics 2006 Oct (Vol. 2006, No. 1, p. 1006). Laser Institute of America.
37. Dalaee M, Cerrutti E, Dey I, Leinenbach C, Wegener K. Parameters development for optimum deposition rate in laser Dmd of stainless steel En x3crnimo13-4. Lasers in Manufacturing and Materials Processing. 2021 Dec:1-7.
38. Harooni A, Nasiri AM, Gerlich AP, Khajepour A, Khalifa A, King JM. Processing window development for laser cladding of zirconium on zirconium alloy. Journal of Materials Processing Technology. 2016 Apr 1;230:263-71.
39. Maniewski P, Laurell F, Fokine M. Laser cladding of transparent fused silica glass using sub-µm powder. Optical Materials Express. 2021 Sep 1;11(9):3056-70.
40. Maniewski P, Laurell F, Fokine M. Laser cladding of transparent fused silica glass using sub-µm powder. Optical Materials Express. 2021 Sep 1;11(9):3056-70.
41. Pinkerton, Andrew J., and Lin Li. “The Significance of Deposition Point Standoff Variations in Multiple-Layer Coaxial Laser Cladding (Coaxial Cladding Standoff Effects).” International Journal of Machine Tools and Manufacture, vol. 44, no. 6, 2004, pp. 573–584., https://doi.org/10.1016/j.ijmachtools.2004.01.001.
42. Tabernero I, Calleja A, Lamikiz A, De Lacalle LL. Optimal parameters for 5-axis laser cladding. Procedia Engineering. 2013 Jan 1;63:45-52.

43. Tuominen J, Näkki J, Pajukoski H, Peltola T, Vuoristo P, Kuznetsov M, Turichin G. Laser cladding with 15 kW fiber laser. InProceedings of the 13th NOLAMP Conference in Trondheim 2011 Jun (pp. 27-29). Trondheim: Norwegian University of Science and Technology.
44. Turichin GA, Zemlyakov EV, Pozdeeva EY, Tuominen J, Vuoristo P. Technological possibilities of laser cladding with the help of powerful fiber lasers. Metal Science and Heat Treatment. 2012 Jul;54:139-44.
45. Zhong C, Pirch N, Gasser A, Poprawe R, Schleifenbaum JH. The influence of the powder stream on high-deposition-rate laser metal deposition with inconel 718. Metals. 2017 Oct 20;7(10):443.
46. Barr C, Da Sun S, Easton M, Orchowski N, Matthews N, Brandt M. Influence of macrosegregation on solidification cracking in laser clad ultra-high strength steels. Surface and Coatings Technology. 2018 Apr 25;340:126-36.
47. Bergant Z, Batič BŠ, Felde I, Šturm R, Sedlaček M. Tribological properties of solid solution strengthened laser cladded NiCrBSi/WC-12Co metal matrix composite coatings. Materials. 2022 Jan 4;15(1):342.
48. Bloemer PR, Pacheco JT, Cunha A, Veiga MT, Filho OC, Meura VH, Teixeira MF. Laser cladding of Inconel 625 on AISI 316L: Microstructural and mechanical evaluation of parameters estimated by empirical-statistical model. Journal of Materials Engineering and Performance. 2022 Jan;31(1):211-20.
49. Cárcel B, Serrano A, Zambrano J, Amigó V, Cárcel AC. Laser cladding of TiAl intermetallic alloy on Ti6Al4V-process optimization and properties. Physics Procedia. 2014 Jan 1;56:284-93.
50. Gao W, Zhao S, Liu F, Wang Y, Zhou C, Lin X. Effect of defocus manner on laser cladding of Fe-based alloy powder. Surface and Coatings Technology. 2014 Jun 15;248:54-62..
51. Ge T, Chen L, Gu P, Ren X, Chen X. Microstructure and corrosion resistance of TiC/Inconel 625 composite coatings by extreme high speed laser cladding. Optics & Laser Technology. 2022 Jun 1;150:107919.
52. Han B, Chen Y, Tan C, Jiang M, Bi J, Feng J, Chen X, Chen L, Zhang L, Liu X, Cao L. Microstructure and wear behavior of laser clad interstitial CoCrFeNi high entropy alloy coating reinforced by carbon nanotubes. Surface and Coatings Technology. 2022 Mar 25;434:128241.

53. Heigel JC, Gouge MF, Michaleris P, Palmer TA. Selection of powder or wire feedstock material for the laser cladding of Inconel® 625. Journal of Materials Processing Technology. 2016 May 1;231:357-65.
54. Kim JD, Lee EJ, Whang JG. Comparison of clad layer characteristics with overlapping criterion in multi pass laser cladding. Journal of Advanced Marine Engineering and Technology. 2016;40(9):768-73.
55. Kim, Jong Do, Eun Jin Lee, and Cheol Gyu Kim. "Study on Laser Cladding of Heat Resisting Steel Using EuTroLoy 16006 Powder (II)-Characteristics of Alloying Elements Distribution of Multi Pass Clad Layer." Transactions of the Korean Society of Mechanical Engineers A 41, no. 4 (2017): 307-312.
56. Yang L, Yang X, Zhang T, Sun R. Optimization of microstructure and properties of composite coatings by laser cladding on titanium alloy. ceramics International. 2021 Jan 15;47(2):2230-43.
57. Ocelík V, Eekma M, Hemmati I, De Hosson JT. Elimination of Start/Stop defects in laser cladding. Surface and Coatings Technology. 2012 Jan 15;206(8-9):2403-9.
58. Pellizzari M, Zhao Z, Bosetti P, Perini M. Optimizing direct laser metal deposition of H13 cladding on cube alloy substrate. Surface and Coatings Technology. 2022 Feb 25;432:128084.
59. Salehi, D., and M. Brandt. “Melt Pool Temperature Control Using Labview in Nd:YAG Laser Blown Powder Cladding Process.” The International Journal of Advanced Manufacturing Technology, vol. 29, no. 3-4, 2005, pp. 273–278., https://doi.org/10.1007/s00170-005-2514-3.
60. Shen F, Tao W, Li L, Zhou Y, Wang W, Wang S. Effect of microstructure on the corrosion resistance of coatings by extreme high speed laser cladding. Applied Surface Science. 2020 Jul 1;517:146085.
61. Sun S, Durandet Y, Brandt M. Parametric investigation of pulsed Nd: YAG laser cladding of stellite 6 on stainless steel. Surface and Coatings Technology. 2005 May 1;194(2-3):225-31.
62. Meng L, Sheng P, Zeng X. Comparative studies on the NI60 coatings deposited by conventional and induction heating assisted extreme-high-speed laser cladding technology: Formability, microstructure and hardness. Journal of Materials Research and Technology. 2022 Jan 1;16:1732-46.

63. Ya W, Pathiraj B, Matthews DT, Bright M, Melzer S. Cladding of Tribaloy T400 on steel substrates using a high power Nd: YAG laser. Surface and coatings technology. 2018 Sep 25;350:323-33.
64. Zhou C, Zhao S, Wang Y, Liu F, Gao W, Lin X. Mitigation of pores generation at overlapping zone during laser cladding. Journal of materials processing technology. 2015 Feb 1;216:369-74.
65. Lin, Jehnming. “A Simple Model of Powder Catchment in Coaxial Laser Cladding.” Optics & Laser Technology, vol. 31, no. 3, 1999, pp. 233–238., https://doi.org/10.1016/s0030-3992(99)00046-8.
66. Chen L, Zhao Y, Song B, Yu T, Liu Z. Modeling and simulation of 3D geometry prediction and dynamic solidification behavior of Fe-based coatings by laser cladding. Optics & Laser Technology. 2021 Jul 1;139:107009.
67. Donadello S, Furlan V, Demir AG, Previtali B. Interplay between powder catchment efficiency and layer height in self-stabilized laser metal deposition. Optics and Lasers in Engineering. 2022 Feb 1;149:106817.
68. Ignat S, Sallamand P, Nichici A, Vannes B, Grevey D, Cicalã E. MoSi2 laser cladding—elaboration, characterisation and addition of non-stabilized ZrO2 powder particles. Intermetallics. 2003 Sep 1;11(9):931-8.
69. Liu, Shuang, and Radovan Kovacevic. “Statistical Analysis and Optimization of Processing Parameters in High-Power Direct Diode Laser Cladding.” The International Journal of Advanced Manufacturing Technology, vol. 74, no. 5-8, 2014, pp. 867–878., https://doi.org/10.1007/s00170-014-6041-y.
70. Liu S, Farahmand P, Kovacevic R. Optical monitoring of high power direct diode laser cladding. Optics & Laser Technology. 2014 Dec 1;64:363-76.
71. Sohrabpoor, Hamed. “Analysis of Laser Powder Deposition Parameters: ANFIS Modeling and ICA Optimization.” Optik, vol. 127, no. 8, 2016, pp. 4031–4038., https://doi.org/10.1016/j.ijleo.2016.01.070.
72. Govekar E, Jeromen A, Kuznetsov A, Levy G, Fujishima M. Study of an annular laser beam based axially-fed powder cladding process. CIRP annals. 2018 Jan 1;67(1):241-4.
73. Liu S, Zhang Y, Kovacevic R. Numerical simulation and experimental study of powder flow distribution in high power direct diode laser cladding process. Lasers in Manufacturing and Materials Processing. 2015 Dec;2:199-218.

74. da Silva MD, Partes K, Seefeld T, Vollertsen F. Comparison of coaxial and off-axis nozzle configurations in one step process laser cladding on aluminum substrate. Journal of Materials Processing Technology. 2012 Nov 1;212(11):2514-9.
75. Lee, Y. S., M. Nordin, S. S. Babu, and D. F. Farson. "Influence of fluid convection on weld pool formation in laser cladding." Weld. J 93, no. 8 (2014): 292-300.
76. Partes, Knut. “Analytical Model of the Catchment Efficiency in High Speed Laser Cladding.” Surface and Coatings Technology, vol. 204, no. 3, 2009, pp. 366–371., https://doi.org/10.1016/j.surfcoat.2009.07.041.
77. Lin, J., and W.M. Steen. “An in-Process Method for the Inverse Estimation of the Powder Catchment Efficiency during Laser Cladding.” Optics & Laser Technology, vol. 30, no. 2, 1998, pp. 77–84., https://doi.org/10.1016/s0030-3992(98)00007-3.
78. Tuominen J, Naekki J, Pajukoski H, Peltola T, Vuoristo P. High deposition rate laser cladding—Recent advancements. In5th Laser additive manufacturing workshop (LAM13), Housten 2013 Aug.
79. Tuominen J, Näkki J, Pajukoski H, Peltola T, Vuoristo P. Recent developments in high power laser cladding techniques. InInternational Congress on Applications of Lasers & Electro-Optics 2012 Sep 1 (Vol. 2012, No. 1, pp. 192-196). Laser Institute of America.

5 Chapter V. Improving laser cladding productivity with ‘ABA’ cladding.

The main body of this section is reproduced from the paper:

Koti, D., Powell, J. and Voisey, K.T., 2022. Improving laser cladding productivity with ‘ABA’cladding. Procedia CIRP, 111, pp.205-209, https://doi.org/10.1016/j.procir.2022.08.048

5.1 Abstract

Laser Cladding is one of several processes within Additive Manufacturing and usually involves the production of a clad surface by adding parallel, overlapping lines of clad material to the surface of a substrate. In this work a new laser cladding technique (‘ABA’ cladding) is investigated wherein a series of separate, or only slightly overlapping clad tracks are laid down initially (the ‘A’ tracks), and these are later interleaved with tracks which can use different parameters (the ‘B’ tracks). The influence of the process parameters was examined in the laser cladding of AISI 316L stainless steel and Stellite 6 powders using a coaxial powder delivery nozzle. ‘ABA’ cladding was found to have considerable benefits over traditional laser cladding including: Improved powder catchment efficiency and coverage rates, more predictable metallurgy and dilution levels, and the ability to clad combinations of different alloys on the substrate surface.

5.2 Introduction

Laser cladding dates back to the 1970s [1,2] and involves the melting of a cladding alloy onto a metal substrate using pre-placed [3,4] or blown [3,5-7] powder which is laser melted to create a clad track. Traditionally, successive tracks are overlapped side by side to create a clad surface like the one shown in cross-section in Figure 5.1. This process has been used to coat a range of metals with expensive wear, abrasion or corrosion-resistant alloys.

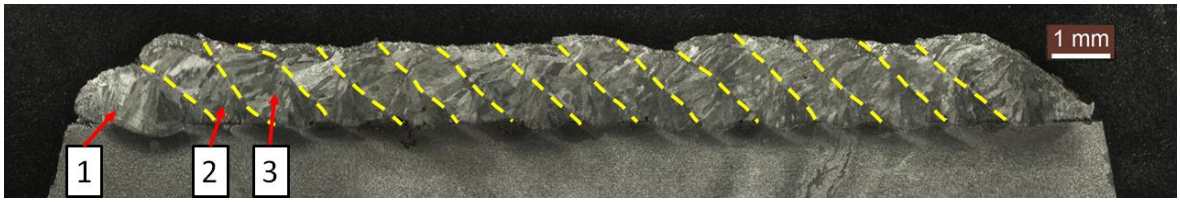

Figure 5.1 A cross-section of a typical ‘AAA’ clad surface is created by laying down parallel, overlapping tracks.

Laser cladding is also a cornerstone of many Additive Manufacturing (AM) production processes, the term "laser cladding" refers to the process of directed energy deposition, a method of additive manufacturing in which focused thermal energy is used to fuse materials by melting as they are being deposited (ISO/ASTM 52900).

For the purposes of this paper, the traditional cladding process could be called ‘AAA’ cladding because the clad tracks are ostensibly identical. However, this similarity only becomes apparent once a few tracks have been laid down. In the early stages of the process, the previous tracks affect the shape of subsequent ones in various ways. This point is rarely discussed in the literature [8] but is clear in the cross-sections of clad layers presented by most researchers in the field [9 - 13]. This point is apparent when comparing the cross-sectional morphology of tracks 1, 2 and 3 on the left of Figure 5.1, and is illustrated schematically in Figure 5.2. In this area, there can be large differences in local clad track height, cross-section and metallurgy. For example, because it is the only track laid upon a flat surface, track 1 will have a different melt pool geometry which will affect powder capture and the level of dilution of the cladding alloy with the substrate compared to subsequent tracks.

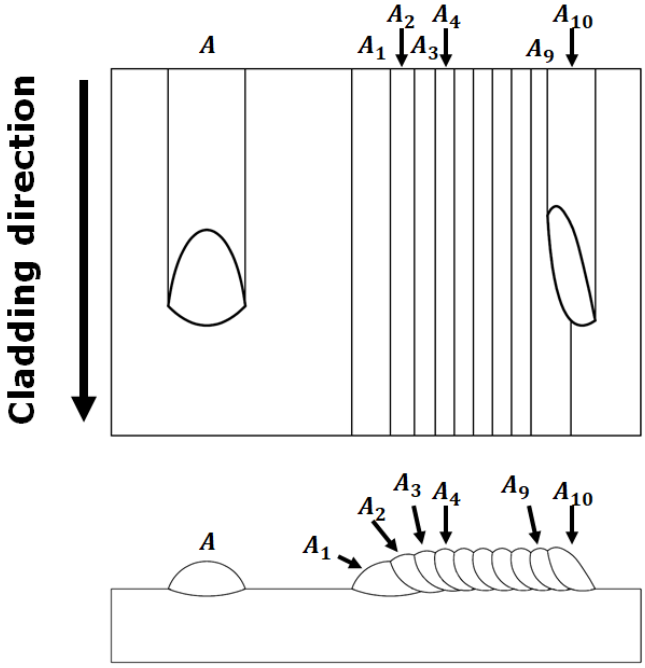

Figure 5.2 Schematic showing how ‘AAA’ cladding builds up a surface by adding subsequent tracks to an initial A track.

In general, several tracks need to be laid down before a repeating cross-section is created and the final track also has a unique morphology because it does not undergo secondary melting by the partial overlay of a subsequent melted track. In the illustration in Figure 5.2 a repeating pattern of cladding is not established until track A4. Tracks A4 to A9 are identical and A10 is the final track.

These start and finish anomalies are one of the drawbacks of 'AAA' cladding because they give rise to local perturbations in clad surface morphology, dilution and heat-affected zones [8-12].

A more major commercial consideration, however, is the powder catchment efficiency of the process. The metal powder which is propelled towards the melt pool interacts with the shoulder of the previous track (see Figure 5.2). The pool is inclined in one direction and there are a considerable number of escape routes for the ricocheting powder particles.

Powder catchment efficiencies noted in the technical literature cover a large range but are frequently substantially below 50% [14-19].

In order to establish a more controllable and efficient process, this paper investigates the concept of laying down more widely spaced clad tracks using one set of parameters ('A' tracks), and then filling in the gaps between these tracks with ones made with a different set of parameters (the 'B' tracks). In this way, all 'A' tracks will be identical in shape and dilution etc. and the same will be true of all 'B' tracks.

This work investigates the possible advantages of 'ABA' laser cladding compared to traditional 'AAA' cladding. In particular the work compares the performance of the two techniques as regards powder catchment efficiency and deposition/coverage rates.

Also, the possibility of cladding dissimilar metals as the 'A' and 'B' tracks is investigated.

5.3 Experimental methods

Laser cladding was performed using an IPG Ytterbium-doped, continuous-wave fibre laser with a maximum peak power of 2 kW operating with a coaxial nozzle powder feeder. In most of the experiments, the powder was AISI 316L stainless steel and the substrate was AISI 1023 bright drawn mild steel. Additional experiments were carried out which utilized Stellite 6 for the 'B' tracks. The powder feed rate was 25g/min in all cases.

The powder catchment efficiency was calculated by comparing this feed rate with the number of grams per minute deposited, see equation below.

$$E_{pc}(\%) = \left(\left(T_{area} \times v \times \rho \right) / F_p \right) \times 100$$

Where,

E_{pc} = powder catchment efficiency (%)

T_{area} = Cross sectional area of the track above the original line of the substrate surface (mm^2)

v = Process speed (mm/min)

ρ = Density of cladding material (g/mm^3)

F_p = Powder feed rate (g/min)

The process speed (i.e. the movement speed of the CNC table) was varied from a value of 1.0m m/min to 3.2 m/min. Samples were created with a variety of inter-track spacings. Clad samples were sectioned, polished, and etched in aqua regia.

Figure 5.3 shows a simplified diagram of an 'ABA' sample which gives details of how the samples were created and subsequently sectioned. The actual samples involved 8 similar, parallel 'A' tracks interspersed with 7 'B' tracks made in the same direction. Tracks were completed with different A-B lateral spacings. In the interests of brevity, only a selection of results is presented here.

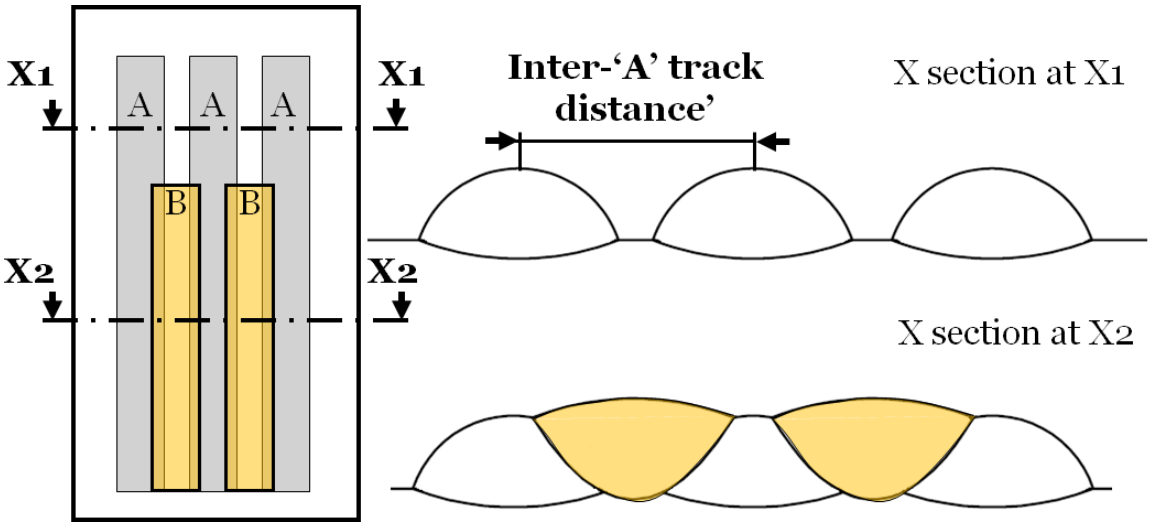

Figure 5.3 ABA clad sample design

5.4 Results and discussion

5.4.1 Improvements in powder catchment efficiency

Figure 5.4 shows the powder catchment efficiency for a sequence of tracks which made up 'AAA' cladding with the following parameters;

- Laser Power: 1800W
- Cladding speed: 1.0 m/min
- Powder feed rate: 25g/min
- Inter-track spacing:1.5mm

It is clear that, for 'AAA' cladding, the initial 'A' track has a higher powder catchment efficiency (57%) than any of the subsequent tracks. The second track has an efficiency of only 35% and, after the first four tracks, the process becomes stable, with an average powder catchment efficiency of 45% (11.3g/min). This figure is considerably below the powder catchment efficiencies measured for 'ABA' cladding using similar parameters for the 'A' tracks.

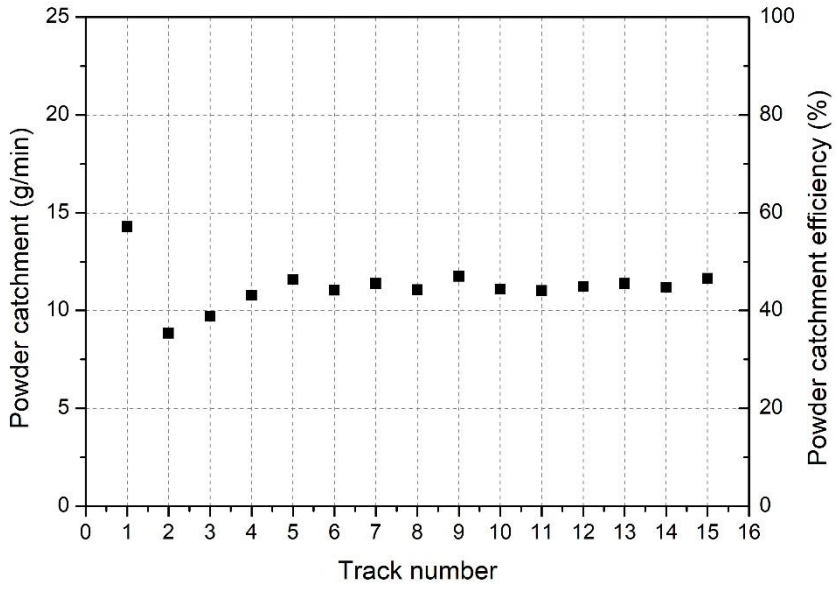

Figure 5.4 Powder catchment efficiency for 'AAA' cladding. The efficiency was calculated from the cross-sectional area of each track as compared to the expected cross-section if 25g/min of powder was melted.

For ‘ABA’ cladding, there is no need to establish a build-up to a stable track geometry because all the ‘A’ tracks have the same melt pool geometry. This is also true of the ‘B’ tracks although in almost all cases of ‘ABA’ cladding it was found that the powder catchment efficiency when laying down the ‘B’ tracks was much higher than it was for the ‘A’ tracks.

‘ABA’ cladding presents the incoming powder cloud with a very effective powder catchment geometry for the ‘B’ tracks as the melt pool is effectively held in a valley between two previously deposited ‘A’ tracks, see Figure 5.5 and Figure 5.6.

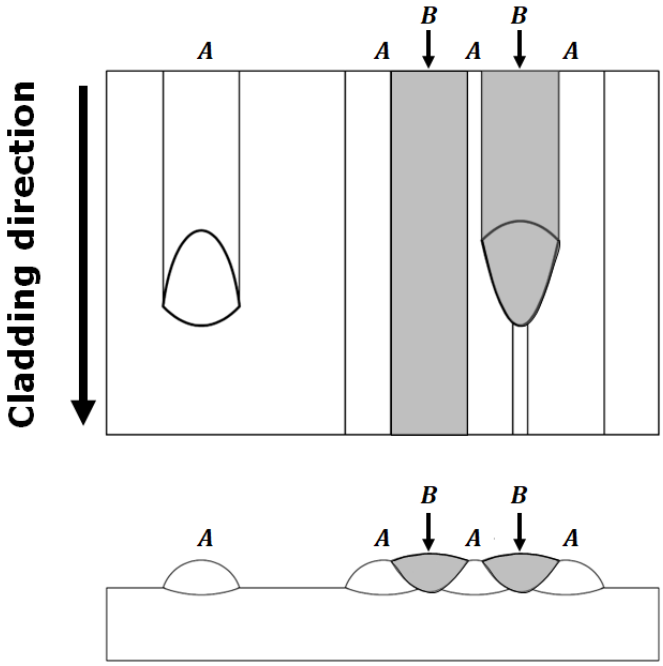

Figure 5.5 A schematic of ABA cladding demonstrating the absence of start/finish anomalies and the pool geometry which results in improved powder capture.

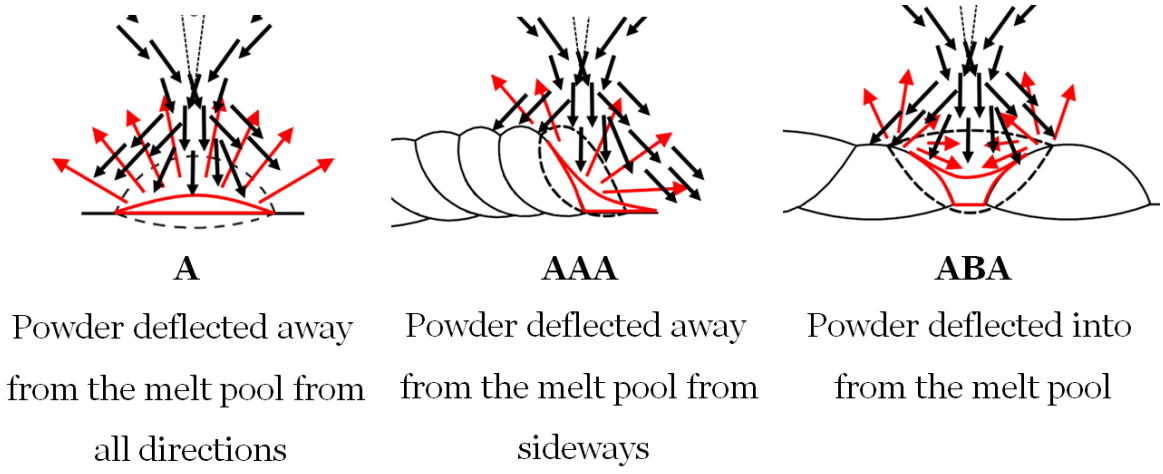

Figure 5.6 In the case of A and AAA cladding a considerable proportion of the powder can be deflected away from the melt pool. In the case of ABA cladding more powder is deflected into the melt pool.

The improved powder catchment of the ‘B’ tracks of ‘ABA’ cladding means that ‘B’ tracks will have a greater cross-section than ‘A’ tracks if the same process parameters are used for both types of track. This can result in an uneven, ridged, clad surface, as shown in Figure 5.8a. An optimized cladding process should result in a level clad surface which minimizes any post-processing costs. In order to level out the surface, the cladding speed for the ‘B’ tracks was increased. This strategy also increases the coverage rate of the overall cladding process.

Figure 5.7 presents powder catchment efficiency results for ‘ABA’ cladding produced with increasing ‘B’ track speeds at the following parameters:

- Laser Power: 1800W
- Cladding speed (‘A’ tracks): 1.0 m/min
- Cladding speed (‘B’ tracks): 1.0 – 2.0 m/min
- Powder feed rate: 25g/min
- Inter-track spacing: 2.1mm and 3mm

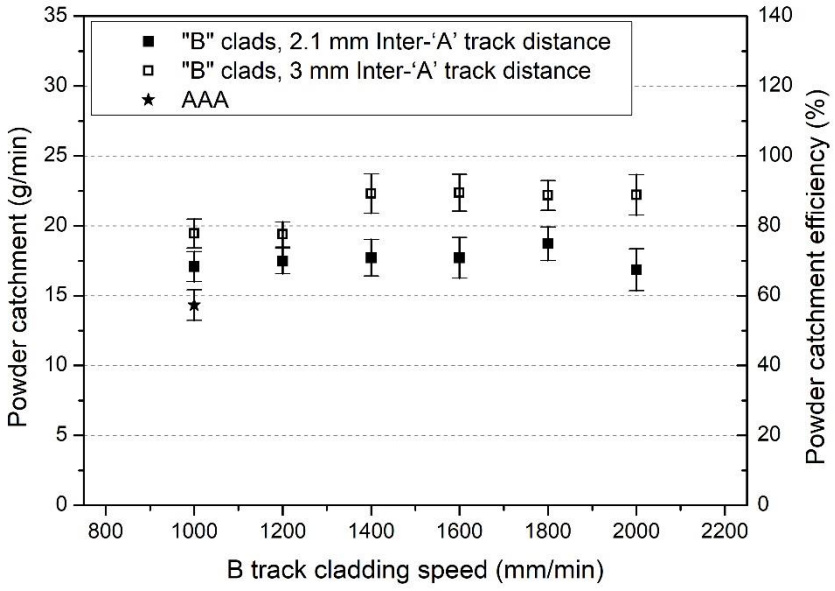

Figure 5.7 Powder catchment efficiency for the ‘B’ tracks of ‘ABA’ cladding at various cladding speeds (powder feed rate is 25g/min in all cases).

The 1.0 m/min results in Figure 5.7 include the catchment efficiency for the eight ‘A’ tracks laid down before the ‘B’ tracks were added at a range of cladding speeds. This value (57%) is the same as for the first track of the ‘AAA’ sample discussed in Figure 5.6, as these ‘A’ tracks were laid down with the same parameters. The rest of the data in Figure 5.7 give details of the powder catchment efficiency of the ‘B’ track weld pools at different processing speeds for two inter-track distances. The powder catchment enhancement for ‘ABA’ cladding is clear in these results. For an ‘A’ track inter-track spacing of 2.1mm the average powder catchment efficiency for the ‘B’ tracks over this range of cladding speeds was 70%, with a range from 67% to 75%. For a larger ‘A’ track inter-track spacing of 3mm, the average powder catchment efficiency for the ‘B’ tracks was 85% over a range from 77% to 89%.

As the ‘B’ track maximum average, in this case, was 85% and the ‘A’ track average was 57% this gives an average powder catchment efficiency for the process of 71%. This figure is a substantial improvement on the average value of AAA cladding of 45% (see Figure 5.6.).

Figure 5.6 and Figure 5.7 support the idea that, within limits, a broadening of the separation between the ‘A’ tracks will result in better powder capture.

5.4.2 Improvements in coverage rate

As Figure 5.8 demonstrates, an improved, flat clad surface was achieved in this case when the cladding speed of the ‘B’ tracks was double that of the ‘A’ tracks. This increase in speed for half of the tracks involved obviously improves the coverage rate. It is difficult to produce precisely similar clad surfaces from both techniques so direct comparison is not possible but, taking Figure 5.6 and Figure 5.7 as an example, the average powder catchment efficiency of the ‘ABA’ technique (with ‘A’ track separation of 3mm) is approximately one and a half times that of the ‘AAA’ method and a similar increase in general cladding productivity could also be expected in this case. It is worth noting that the ‘ABA’ technique is applicable to spiral cladding of rods and tubes as well as other surface geometries.

a)

b)

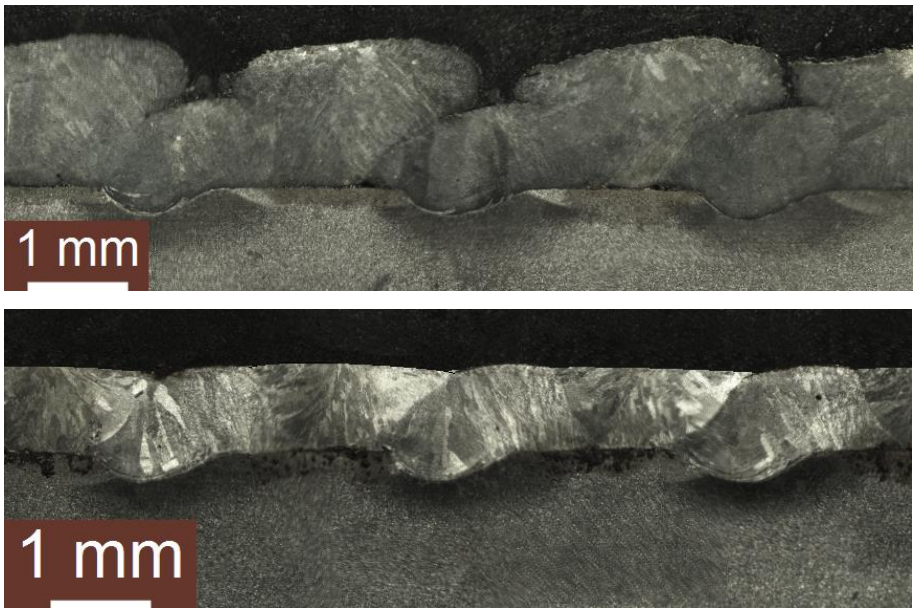

Figure 5.8 ABA cladding with a) 'A' and 'B' tracks clad with the same parameters, b) 'A' tracks at 1m/min, 'B' tracks at 2m/min.

Productivity might also be improved by the point that, because of the nature of the process, 'ABA' cladding could involve wider spacing between the tracks compared to 'AAA' cladding. This means that fewer tracks could be needed to cover a particular surface area.

One further point in favour of 'ABA' cladding is that improved powder catchment reduces the need for powder recycling and minimizes the wastage of expensive alloy powders.

5.4.3 ABA cladding with different materials

In the early days of laser hardening, it was quickly realized that a continuous, hard surface was not always the most cost-effective way to use the technology. Individual stripes of the hardened zone were much faster (and cheaper) to produce and any softened (annealed) areas to each side of the hardened areas can wear away to provide conduits for lubricants [20,21]. The hardened stripes then locate the movement of the parts and minimize general wear. The same principle can be applied to 'ABA' cladding. Figure 5.9 presents cross-sections of 'ABA' clad surfaces where the 'A' tracks are 316 stainless steel and the 'B' tracks are Stellite 6.

a)
1.8 (m/min)

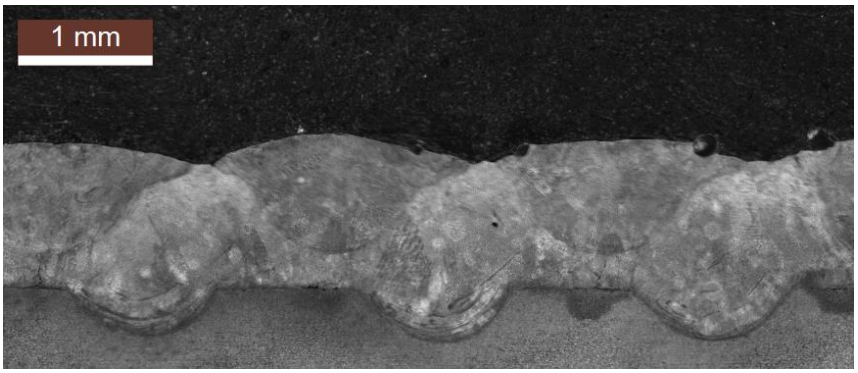

b)
2.2 (m/min)

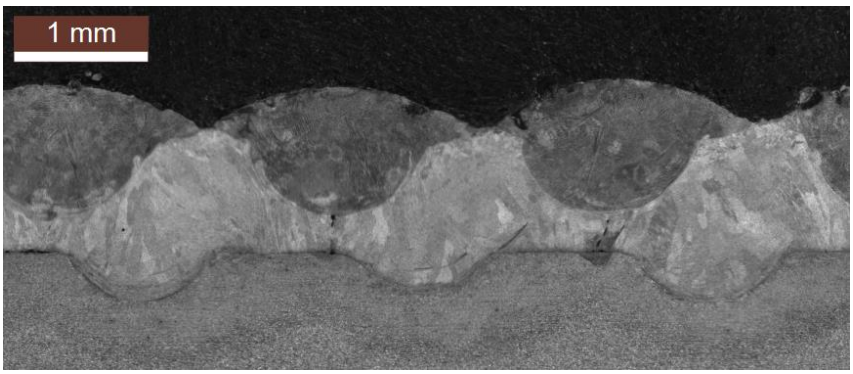

Figure 5.9 ABA cladding with different materials. In this case, the 'A' tracks were 316 stainless steel, the 'B' tracks were Stellite 6.

This technique could be used to save costs on expensive superalloys or to allow incompatible clad/substrate combinations to be clad where an intermediate layer of 'A' material separates tracks of 'B' material from the substrate.

5.5 Conclusions

- 'ABA' cladding offers new opportunities to the cladding process as regards powder usage, coverage rates and cladding of different combinations of materials.
- In the case presented here powder catchment efficiencies were increased from an average of approximately 45% to 71%.
- Coverage rates in the above work were substantially improved using ABA cladding. Speeds of coverage were increased to 150% of their AAA cladding equivalent, although it is difficult to quantify the different clad surfaces generated.
- Different metals can be clad as an ABA sandwich. In this case, Stellite 6 'B' tracks were interspersed between 316 stainless steel 'A' tracks. This technique may have technical and commercial advantages which have yet to be explored.
- A further advantage of ABA cladding over the standard AAA technique is that there is no initiation phase to the process before repeatable tracks are laid down. This means that track morphology, dilution and local metallurgy will be more predictable and evenly distributed over the clad layer.

5.6 References

1. Gnanamuthu DS. Laser Surface Treatment. Proc. Conf. Applications of lasers in materials processing. 1979. American Society for Metals.
2. Steen WM, Powell J. Laser Surface Treatment. Materials in Engineering. Vol.2 No3. 1981.
3. Powell J. Laser Cladding. (PhD thesis. Imperial College, London University) 1983.
4. Kaplan AFH, Powell J, Gedda H. Laser:Powder:substrate interactions in laser cladding and casting. Int. J. of Microstructure and materials properties 5 (2/3):164 – 177 (Oct 2010). DOI: 10.1504/IJMMP.2010.035937
5. Gedda H, Powell J, Kaplan AFH. A process efficiency comparison of Nd:YAG and CO2 laser cladding. Proc. ICALEO 2002: 21st International Congress on Laser Materials Processing and Laser Microfabrication DOI: 10.2351/1.5066172.
6. Siva Prasad H, Brueckner F, Kaplan AFH. Powder incorporation and spatter formation in high deposition rate blown powder directed energy deposition. Additive Manufacturing 35 (2020): 101413 doi:j.addma.2020.101413.
7. Naesstroem H. Phenomena in laser based material deposition. PhD thesis Lulea University of Technology May 2021. ISBN: 978-91-7790-820-3.
8. Ocelík V, Nenadl O, Palavra A, De Hosson JT. On the geometry of coating layers formed by overlap. Surface and Coatings Technology. 2014 Mar 15;242:54-61.
9. Li Y, Ma J. Study on overlapping in the laser cladding process. Surface and Coatings Technology. 1997 Mar 15;90(1-2):1-5.
10. Gao W, Zhao S, Liu F, Wang Y, Zhou C, Lin X. Effect of defocus manner on laser cladding of Fe-based alloy powder. Surface and Coatings Technology. 2014 Jun 15;248:54-62.
11. Nenadl O, Ocelík V, Palavra A, De Hosson JT. The prediction of coating geometry from main processing parameters in laser cladding. Physics Procedia. 2014 Jan 1;56:220-7.
12. Barr C, Da Sun S, Easton M, Orchowski N, Matthews N, Brandt M. Influence of macrosegregation on solidification cracking in laser clad ultra-high strength steels. Surface and Coatings Technology. 2018 Apr 25;340:126-36.
13. Ya W, Pathiraj B, Matthews DT, Bright M, Melzer S. Cladding of Tribaloy T400 on steel substrates using a high power Nd: YAG laser. Surface and coatings technology. 2018 Sep 25;350:323-33.

14. Lin J, Steen WM. An in-process method for the inverse estimation of the powder catchment efficiency during laser cladding. Optics & Laser Technology. 1998 Mar 1;30(2):77-84.
15. Partes K. Analytical model of the catchment efficiency in high speed laser cladding. Surface and Coatings Technology. 2009 Oct 25;204(3):366-71.
16. da Silva MD, Partes K, Seefeld T, Vollertsen F. Comparison of coaxial and off-axis nozzle configurations in one step process laser cladding on aluminum substrate. Journal of Materials Processing Technology. 2012 Nov 1;212(11):2514-9.
17. Lee YS, Nordin M, Babu SS, Farson DF. Influence of fluid convection on weld pool formation in laser cladding. Weld. J. 2014 Aug;93(8):292-300.
18. Chen L, Zhao Y, Song B, Yu T, Liu Z. Modeling and simulation of 3D geometry prediction and dynamic solidification behavior of Fe-based coatings by laser cladding. Optics & Laser Technology. 2021 Jul 1;139:107009.
19. Donadello S, Furlan V, Demir AG, Previtali B. Interplay between powder catchment efficiency and layer height in self-stabilized laser metal deposition. Optics and Lasers in Engineering. 2022 Feb 1;149:106817.
20. Gnanamuthu DS, Shankar VS. Laser Heat treatment of iron-base alloys.in; Laser Heat Treatment of Metals eds; Draper CW, Mazzoldi P. NATO ASI series E. Applied sciences No 115. pp 413-433
21. Eberhardt G. Survey of high power CO2 industrial laser applications and latest laser developments. Proc. First Int. Conf. on Lasers in Manufacturing. Brighton UK 1983 pp 13-19 pub; IFS publications.

6 Chapter VI. Powder catchment efficiency in laser cladding (Direct Energy Deposition). An investigation into standard laser cladding and the ABA cladding technique

The main body of this section is reproduced from the paper:

Koti, D., Powell, J., Naesstroem, H. and Voisey, K.T., 2023. Powder catchment efficiency in laser cladding (directed energy deposition). An investigation into standard laser cladding and the ABA cladding technique. Journal of Laser Applications, 35(1), p.012025, https://doi.org/10.2351/7.0000904

6.1 Abstract

This paper investigates the efficiency of powder catchment in blown powder laser cladding (a Directed Energy Deposition technique). A comparison is made between standard ‘track by overlapping track' cladding (‘AAA’ cladding) and ‘ABA’ cladding where the gaps left between an initial set of widely spaced tracks (‘A’ tracks), are filled in by subsequent ‘B’ tracks. In both these techniques the melt pool surface is the collection area for the cladding powder and the shape of this pool can be affected by several parameters including cladding speed, inter-track spacing and type of cladding technique. The results presented here are derived from of an analysis of high-speed videos taken during processing, and cross sections of the resultant clad tracks. The results show that the first track in AAA cladding has a different melt pool shape to subsequent tracks, and that the asymmetry of the subsequent track melt pools results in a reduction in powder catchment efficiency. In contrast to this, the geometry of the ‘B’ track melt pools between their adjacent ‘A’ tracks results in an enhanced powder catchment efficiency.

6.2 Introduction

Investigations into laser cladding (a Directed Energy Deposition [DED] technique) began in the late 1970s and early 1980s [1-3] and the process has grown to achieve industrial status, particularly with the development of additive manufacturing. Nowadays the process commonly utilizes a processing head which supplies a stream of the cladding powder alloy coaxially with a defocused laser beam [4]. One of the aims of the process is to melt all of the powder which arrives at the laser-material interaction area into the clad track.

Unfortunately, complete capture of all the incoming powder is not generally possible and a certain percentage of powder escapes the process, often by deflection off the solid material beyond the edges of the melt pool or the surface of the melt pool itself [5].

The powder catchment efficiency of the process has a strong influence on costs and is thus of prime importance to industrial users. This efficiency is simply the percentage of powder provided to the process which becomes part of the laser melted clad layer.

For technical investigations the powder catchment efficiency (E_{pc}) of any individual clad track can be calculated using cross sections of the clad layer and knowledge of the process parameters as follows;

$$E_{pc}(\%) = \left(\left(T_{area} \times v \times \rho \right) / F_p \right) \times 100$$

Where,

E_{pc} = powder catchment efficiency (%)

T_{area} = Cross sectional area of the track above the original line of the substrate surface (mm^2)

v = Process speed (mm/min)

ρ = Density of cladding material (g/mm^3)

F_p = Powder feed rate (g/min)

Table 6.1 presents a small, but typical, sample of the results of a survey of investigations into DED laser cladding over a wide range of process parameters and different laser types, which reveals that the E_{pc} can often be well below 50%. This is clearly a problem as the powder is expensive and unused powder cannot generally be recycled into the cladding process, which depends upon high levels of powder uniformity.

Table 6.1 Powder catchment efficiencies calculated from published results in the literature.

Papers	Substrate	Powder	Laser power (kW)	Powder feed rate (g/min)	Process speed (m/min)	Beam diameter (mm)	Powder catch. Eff (%)
[6]	Zr alloy	Zr	0.8	8.8	0.245	1.4	9.09
[7]	AISI 1050	AISI 316L	0.8-1	8.16-16.26	0.288-0.48	2.2	12-16
[8]	AISI 316L	AISI 316L	0.525-0.7	6-13	1.32-2.52	1.2	20-32
[9]	Inconel 625	Inconel 625	1-1.5	4.55-7.6	0.3-0.8	2	28-40
[10]	Inconel 718	Inconel 718	0.35-0.55	1.2	0.6	1	28-45
[11]	S235JRC+C	1.4313	1.2	14-16	0.8-1	2	34-42
[12]	AISI 316L	Inconel 625	3.2	50.91	24.96	5	42.16
[13]	A45	Ni60	3.2	50.91	24.96	2	43.14
[14]	SS304	Eutroloy 16012	1	9	0.3	3	49.88
[15]	Q235	Fe-based alloy	1.1	8.5	0.3	4	55.8
[16]	A36	Fe-based	3-4.5	40-60	0.18-0.42	3.38	51-68
[17]	Inconel 625	Inconel 625	2.5	19	0.636	4	60.77
[18]	S235JR	Inconel 625	15	295	0.75	5	77
[19]	Ti811	Ni60	0.9	5	0.5	3	78.61
[20]	CuBe alloy	AISI H13	3.6	3.2	18.2	3	79.63
[21]	S235JR	Inconel 625	15	273	1	5	79.98
[22]	AISI 304	AISI 316L	1.5-2	8.5-17	0.3-0.6	3	80
[23]	AISI 420	Stellite 6	0.72	22	3	2	80.11
[24]	SNCrW	EuTroLoy 16006	4	20	0.24	2	80.34
[25]	AISI 1045	Inconel 625	3.131	40	1.545	2	82.2
[26]	SNCrW	EuTroLoy 16006	4	20	0.24	2	86.25
[27]	Mild steel	Hastelloy C	2.4	28	1.4	4	86.78
[28]	Inconel 718	Inconel 718	2.9	45	1.5	4	92.04

Standard laser cladding involves laying down an initial track on the substrate surface (an ‘A’ track - see fig 1a) and many research investigations simply compare single tracks of this type laid down under different processing conditions (in this paper we will refer to this type of deposit as a ‘solo ‘A’ track’). In industrial practice however, single tracks of this type have very limited application as it is much more common to overlap track one with track two, then track three etc. until the required clad surface is achieved, as shown in Figure 6.1b (For obvious reasons we can refer to this technique as ‘AAA cladding’). Recent work by the authors [29] has shown that there are E_{pc} benefits to be gained if a new laser cladding technique, which we have called ‘ABA laser cladding’, is employed.

In ABA cladding the coverage strategy is to lay down a sequence of widely separated, identical tracks (the ‘A’ tracks), and then fill the gaps between them with ‘B’ tracks (see figure 1c).

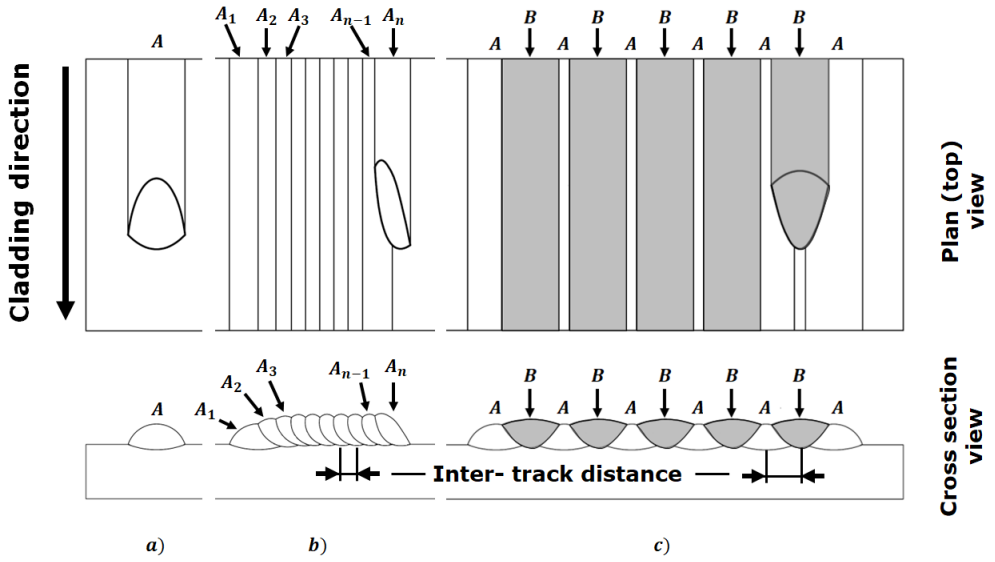

Figure 6.1 a) A solo, or initial, ‘A’ track, b) In standard (AAA) laser cladding the clad surface is made up of overlapping ‘identical’ tracks (although a few, early tracks differ from later tracks), c) in ABA cladding a set of widely spaced identical ‘A’ tracks are laid down first and then the gaps between them are filled with ‘B’ tracks

Early work on ABA cladding [29] has revealed that several benefits can arise from utilizing the technique, including; improved powder catchment efficiency (E_{pc}), the avoidance of a ‘start up zone’ for the process (see Figure 6.1b) and the fact that different alloys could be used for the ‘A’ and ‘B’ tracks. The improvement in E_{pc} (see Figure 6.2) results in less powder wastage and increased coverage rates for the process, and therefore reduced costs.

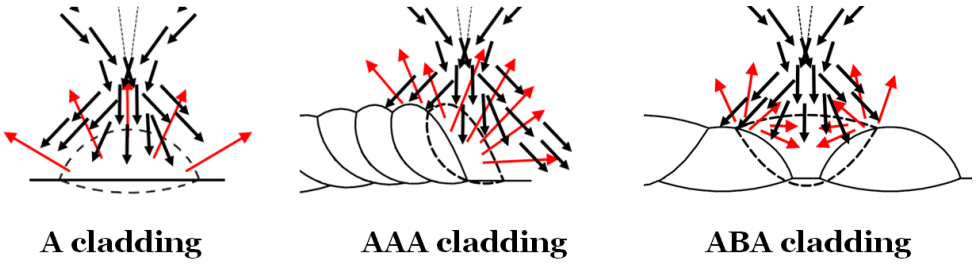

Figure 6.2 . In AAA cladding a considerable percentage of the powder can be deflected away from the melt pool. ABA cladding geometry is more favourable to powder capture.

The E_{pc} of the laser cladding process is fundamentally governed by how much powder enters the cladding melt pool, which is, in turn, influenced by the size and shape of the melt pool surface. The size and shape of the melt pool surface can be affected by laser power, cladding speed, powder feed rate etc. In this work we investigate, for a single clad layer, the influence of cladding technique (AAA or ABA), inter-track spacing and cladding speed on melt pool surface geometry and the effect of that geometry on E_{pc}.

6.3 Experimental details

6.3.1 Cladding parameters

Laser cladding measurements were conducted with a 15 kW IPG Ytterbium-doped, cw fibre laser, (1070 nm wavelength, 150 mm collimating lens and Kugler mirror optics (Kugler LK390F) with a 250mm focussing mirror). The laser system used a fibre with a diameter of 100 µm, coupled to a fibre with a diameter of 400 µm. The laser power used during the experiments was 3 kW. The beam was defocused into a circular spot measuring approximately 4 mm in diameter with a Gaussian energy distribution and a stand-off distance of 13mm.

A coaxial COAX 14V5 (Fraunhofer IWS) 8mm diameter continuous nozzle (also known as a ring-slit nozzle) was employed. The carrier gas and the powder were fed through the ring-shaped slit, and the laser beam and shielding gas passed through the central nozzle. This produced a focussed powder feeding stream with a diameter of approximately 4 mm at the melt pool surface. Argon was used for shielding and as the carrier gas. 316L stainless steel powder with a size range from 50 to 150 microns diameter was fed from a gravity-based powder feeder. The carrier gas flow was 8 l/min and shielding gas flow was 15 l/min. The powder feeder was calibrated, and the feed rate was set at 26 g/min throughout the experiment. This feed rate was checked experimentally twice by collecting the powder in a specially designed container over a five-minute period, with a standard deviation on 26g/min of 0.8. The laser cladding was carried out on a 3-axis ISEL FlatCOM L150 CNC system with the substrate plates (5 mm thick 304S15 stainless steel) clamped to a linear motion table. Both the laser head and the powder feeder nozzle were attached to the z-axis and remained fixed.

Tracks were created using both the AAA and ABA techniques with a range of inter-track (centre to centre, see figure 1) spacings of between 2mm and 4 mm. The tracks comparing ‘AAA’ and ‘ABA’ clads were carried out at 700 mm/min.

For further investigation into ABA cladding, the process speed was varied between 700 mm/min and 1500 mm/min. A series of solo ‘A’ tracks were also made over this range to investigate pool shape changes as a function of process speed. The clad samples were sectioned, polished, and etched in aqua regia.

6.3.2 High speed imaging

The process was recorded using a high-speed imaging (HSI) camera at 8000 frames per second. Illumination was provided by a continuous wave diode illumination laser with a wavelength of 808 nm. A narrow bandwidth filter matching the wavelength of the illumination laser was used to block out the process light. The process setup is illustrated in Figure 6.3. The camera was inclined at 11° from the horizontal. High speed imaging videos were played back at low frame rates to observe powder catchment behaviour and melt pool geometry.

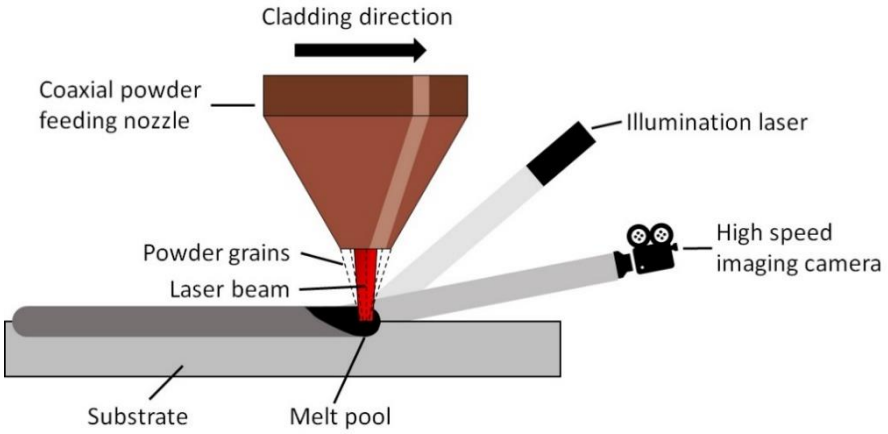

Figure 6.3 High speed imaging experimental setup

Figure 6.4 shows how the plan view maps of the melt pools were extracted from the video data (in this example for a solo ‘A’ track). The maximum width of the melt pool can be measured directly from the video, but its length L needs to be calculated using equation below (refer to Figure 6.4).

$$L = (D - (H \times cos(\theta))) / sin(\theta)$$

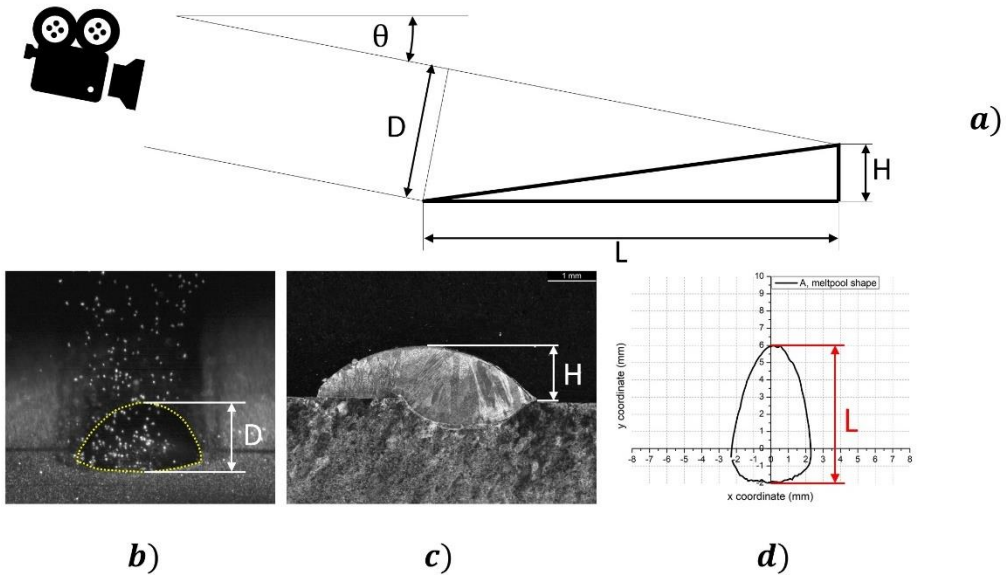

Figure 6.4 a. A schematic of the video capture geometry. b. A typical single frame from the video ('A' track). c. A typical 'A' track cross section. d. A typical calculated melt pool geometry (plan view 'A' track)

Once L and the maximum width are known, then the overall shape of the pool perimeter can be taken from the video data and the plan (top) view of the melt pool mapped. The plan view was preferred to the view perpendicular to the melt surface because the powder can be assumed to be falling vertically downwards.

6.4 Results and Discussion

6.4.1 Differences in melt pool shape between A, AAA and ABA cladding techniques.

Figure 6.5 provides interesting information about the differences in melt pool shape as a function of cladding technique. The information labelled 'A' refers to; solo 'A' tracks, any of the 'A' tracks in ABA cladding, and also to the initial track in AAA cladding. These 'A' tracks are laid down upon the flat substrate surface and therefore have the simplest melt pool geometry (see Figure 6.1). The information labelled 'AAA' refers to any one of the tracks which follow the initial track in AAA cladding. In this experiment we measured and made a high-speed video of track A_3 (see Figure 6.1). The information labelled 'ABA' refers only to the 'B' tracks in ABA cladding.

The cladding process speeds and inter-track distances (see Figure 6.1) for the tracks compared here are given in the figure.

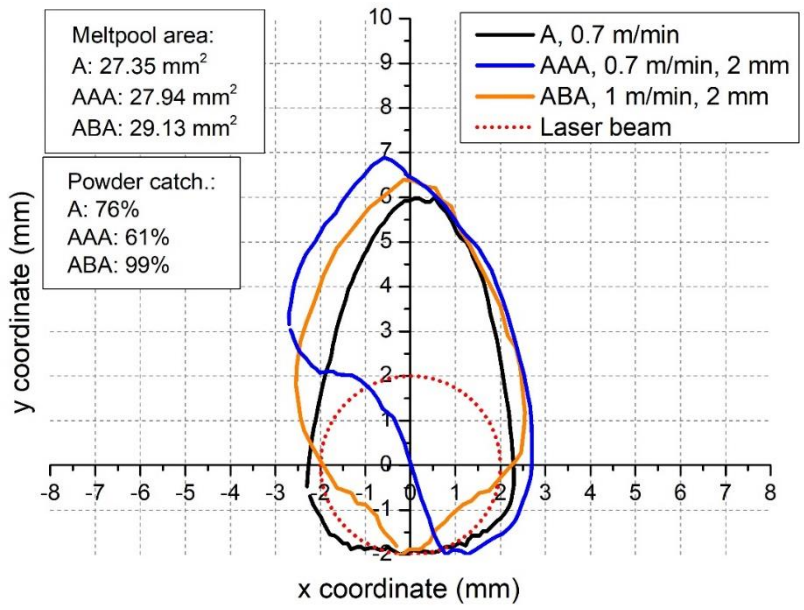

Figure 6.5 Melt pool shapes (plan, or top view i.e. mapped in the plane parallel to the substrate surface) for different laser cladding interaction types. In these maps the part of the melt pool at the bottom of the figure is the front, or leading edge, of the melt pool. (i.e.. The melt pool is portrayed as moving downwards along the y axis in this figure). The laser beam (shown as a dotted circle) is centred on the x,y 0,0 point. The information on the top right gives details of the process speed and inter-track separation distance.

The melt pool associated with single clad tracks produced on a flat surface (the 'A' tracks) is, as we would expect, symmetric about the central axis in the direction of cladding. It is also broadest near the front, in the vicinity of the laser beam, and tapers off behind the laser beam as the melt pool solidifies from the outside edges towards the middle. This melt pool shape is the one created in all the A tracks laid down in ABA cladding and the initial track in AAA cladding.

The melt pool associated with the tracks which follow this initial track in AAA cladding (labelled 'AAA' in Figure 6.5) has a completely different shape to the initial A track pool. At the leading edge, on the side of the pool which is on the flat substrate surface (the bottom right-hand side in the figure), the melt pool shape is similar to (but slightly wider than) the single A track pool. On the left-hand side of the leading edge however, the melt front is initiated a few millimetres later in the laser – material interaction. This is because, on this side, the melt is being generated on the 'shoulder' of the previous track. The geometry of this shoulder means that the intensity of the incident beam is reduced in this area because it is incident on a sloping, curved surface (see Figure 6.6b) and, because of this, the melting takes more time to initiate.

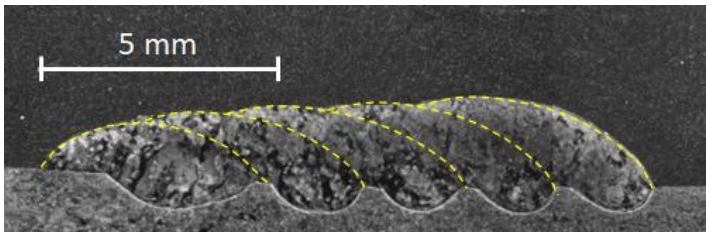

a)

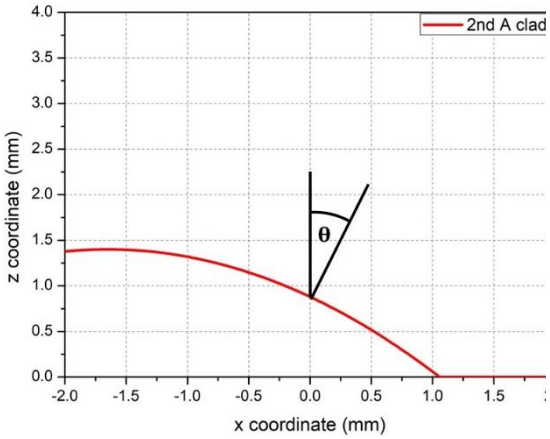

b)

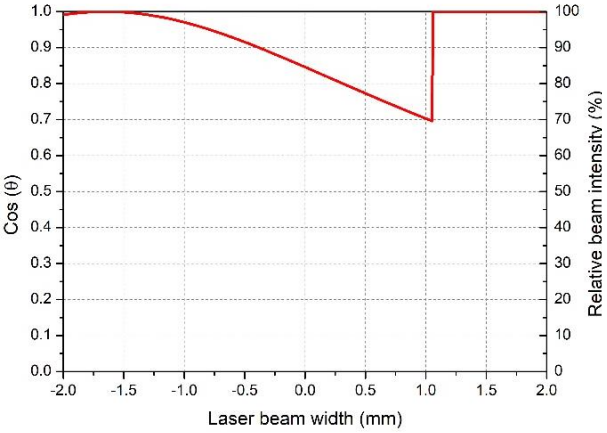

c)

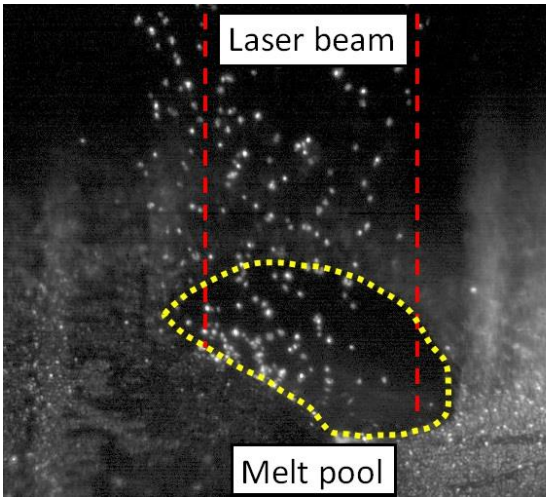

d)

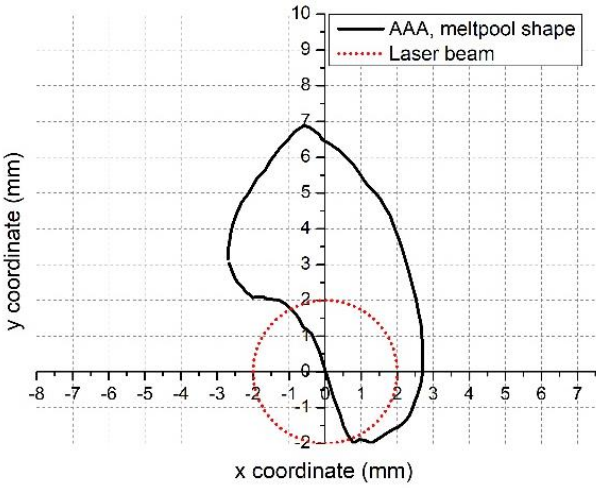

e)

Figure 6.6 Laser energy intensity is dependent on angle of incidence on the 'shoulder' of the previous track. a. The videoed track was the third from the left in this cross section (i.e. A3 in Figure 6.1.b). b. The slope of the 'shoulder' of the previous track (A2 in Figure 6.1.b). c. The relative beam intensity in the laser-material interaction area (proportional to the cosine of the angle of incidence, θ). d. A frame taken from the High-Speed Imaging video. e. The plan view of the perimeter of the melt pool calculated from the video.

Figure 6.6 demonstrates how the relative beam intensity varies as a function of the slope of the previous track, but the situation has been simplified to assume a square cross section laser beam with a top hat mode. In reality, the beam has a Gaussian energy distribution and a circular cross section. Both of these points mean that the reduction of energy absorbed by the sloping surface will be accentuated. A full model of the situation would also have to take into account the temperature of the substrate (as absorptivity can be temperature dependant). To add to the complication of such a model, the absorption coefficient of the laser beam is also dependent on angle of incidence, although this will tend to reduce rather than accentuate the trend shown in Figure 6.6. This reduction will, however, be a minor influence, and figure 6 gives a rough approximation of the laser intensity trend involved with absorption onto the curved surface of a previous clad track.

The ‘ABA’ melt pool shape given in Figure 6.7 is the shape of the ‘B’ track melt pools only (the ‘A’ melt pools in ‘ABA’ cladding would all be similar to the initial ‘A’ track of ‘AAA’ cladding discussed above). In this case the melt front also begins later than for an ‘A’ track, but this effect happens on both sides of the leading edge of the melt because the melt is being generated between two previously laid ‘A’ tracks (see Figure 6.1 and Figure 6.2). There being two ‘shoulders’ involved means that the relative intensity reduction discussed above happens on both sides of the melt pool, see Figure 6.7.

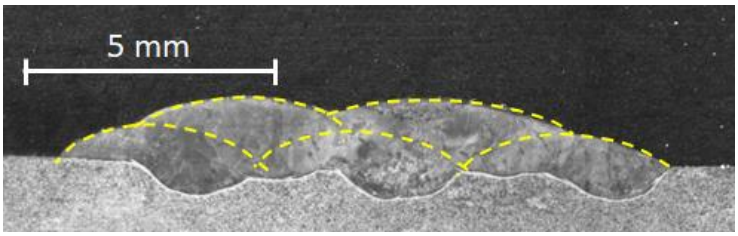

a)

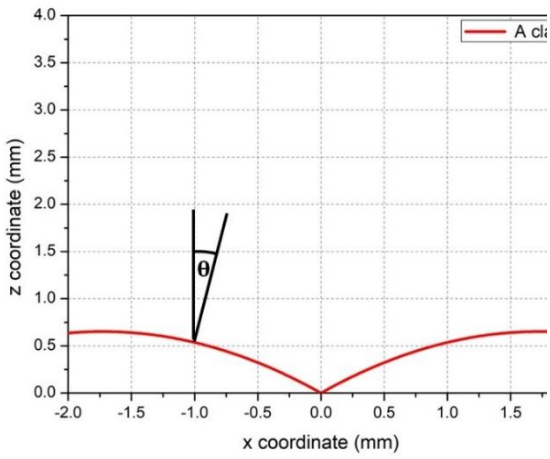

b)

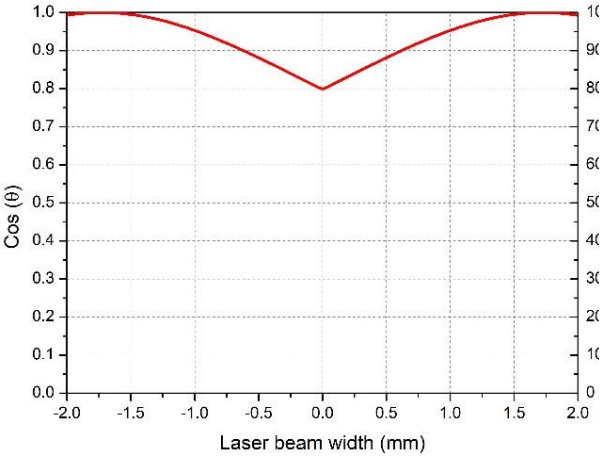

c)

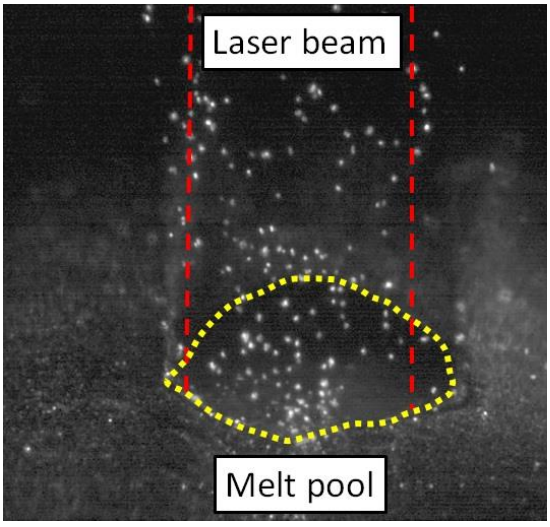

d)

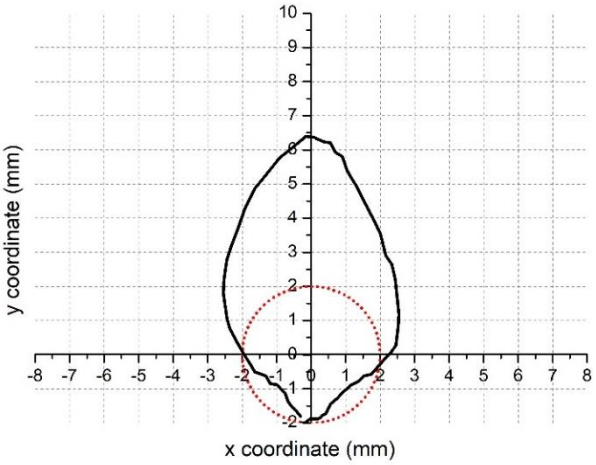

e)

Figure 6.7The results for 'B' tracks in ABA cladding. a. The cross section of the ABA clad layer, b. The cross sectional geometry of the two adjacent 'A' tracks, c. The relative beam intensity reduction as a result of the 'A' track curvature, d. A single frame of

6.4.2 Powder catchment efficiency as a function of cladding technique

Figure 6.5 raises points which concern the total area of the melt pool surfaces and the powder catchment efficiency for each type of cladding technique.

In the case shown in figure 5 for the AAA cladding, the tracks created after the first one has a similar melt pool surface area to the initial track (27.94 mm^2 compared with 27.35 mm^2 for the initial track). However, the powder catchment efficiency of the initial track is higher than for these subsequent melt pools (76% for the initial track, 67% for subsequent tracks in this case). The inferior powder catchment efficiency of the subsequent tracks is probably related to three effects;

a) The delayed melt front on the 'shoulder' side of the melt means that incoming powder would be impinging on more unmelted material and would ricochet away from the interaction zone off the solid shoulder of the previous track,
b) The steeper, 3D sloping nature of the melt makes it less effective for powder catchment than the more straight-forward 2D slope of the melt for initial track (fig 1) i.e.. a more inclined melt surface could deflect incoming particles more effectively.
c) The incoming gas flow and any entrained particles would be deflected only forwards off the 2D sloping melt of the initial track, where they might be reabsorbed by the moving melt. However, for subsequent tracks, the gas and any entrained particles would be deflected forwards and sideways, out of the laser-material interaction zone by the 3D slope of the melt surface.

It should be noted that the 'B' track described in Figure 6.6 was carried out at 1.0 m/min whereas the 'A' tracks for both 'A' and AAA cladding were carried out at the lower speed of 0.7 m/min. It is therefore very interesting that the melt pool size was slightly larger for this track than it was for 'A' or AAA tracks (29.13 mm^2), and the powder catchment efficiency was substantially increased to 99% (see Figure 6.5). This is the catchment efficiency for the 'B' tracks using these parameters, the overall catchment efficiency for the ABA process in this case would be the average of both the 'B' track (99%) and the 'A' track (76%) i.e. 87.5%. The overall catchment efficiency for AAA cladding would, however, be close to the value for tracks subsequent to the initial track, because there are usually a large number of them attached to a single initial track. The overall catchment efficiency for the AAA sample under discussion would therefore be only slightly over 67%.

Pre-heating from the deposition of the adjacent pair of ‘A’ tracks and/or internal reflection of the edges of the laser beam towards the melt explains why the melt pool is larger for the ‘B’ tracks. The increased powder catchment efficiency is explained in Figure 6.2, as the result of improved powder capture, because the incoming powder stream rebounds off the ‘shoulders’ of the previous tracks into the ‘valley’ containing the melt pool [28]. Thus the favoured direction for rebounding particles in ABA cladding is back into the melt pool, whereas in AAA cladding the particles which rebound tend to leave the laser-material interaction zone.

6.4.2.1 The effects of changing the inter-track distance.

In laser cladding the area coverage rate of the process can be increased by increasing the process speed or by decreasing the number of tracks per unit area, which involves an increase in inter-track distance (although other parameters may have to be increased to maintain clad layer thickness). It is therefore of interest to see if an increase in inter-track distance results in an improvement in powder catchment efficiency.

Figure 6.8 presents the melt pool maps for both AAA and ABA cladding at a process speed of 700mm/min with centre-to-centre track spacings of 2, 2.8, 3.6 and 4mm. The individual tracks were approximately 4mm wide in cross section at the substrate surface, so a 2mm centre-to-centre distance means that there was a 50% overlap of one track on the previous one. The AAA melt pool maps show that the late start of the melt front on the track overlap side of the pool (discussed above) is most pronounced when the track-to-track overlap is largest (i.e., at smaller inter-track distances). As the inter-track spacing is increased this effect is diminished because the melt pool is exposed to more of the flat substrate surface and the melt geometry becomes more like a solo ‘A’ track. The ABA melt pool maps present similar information for the late start of the melt (compared with solo ‘A’ tracks) on both sides of the leading edge of the pool.

Figure 6.9 presents the melt pool surface areas and the powder catchment efficiency for each case shown in Figure 6.8 (the result for the initial ‘A’ track in AAA cladding and the ‘A’ tracks in ABA cladding are given as a horizontal dotted line in Figure 6.9 a and b). It is clear that for the AAA cladding process there is a gradual increase in melt pool area as the inter-track distance is increased and the melt pool initiation delay caused by the slope of the previous track diminishes.

For the more symmetrical ABA cladding B pools, there is no clear trend in pool size with increasing inter-track distance although the B pools are generally larger than their AAA counterparts. The B tracks of this data set also have better deposition rates than either the initial or the subsequent 'A' tracks.

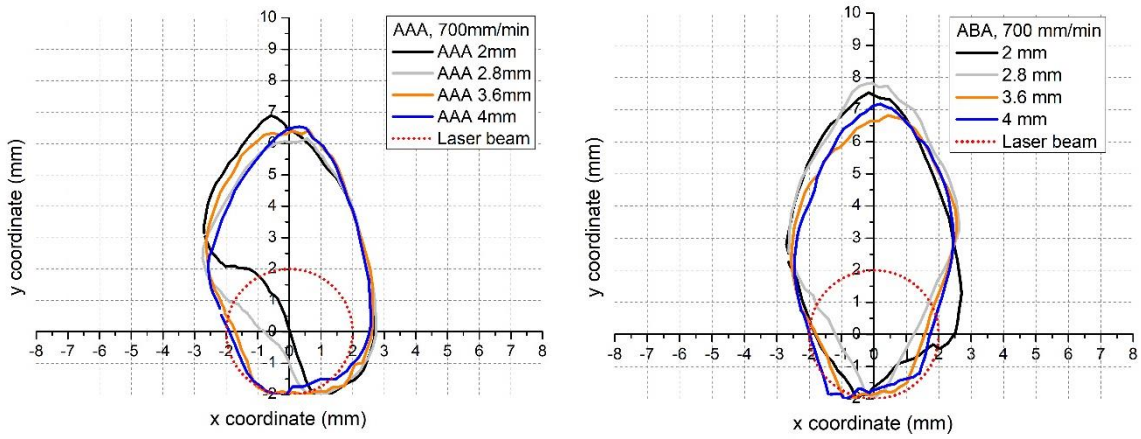

a) b)

Figure 6.8 Melt pool maps for AAA and ABA cladding with increasing inter-track distance.

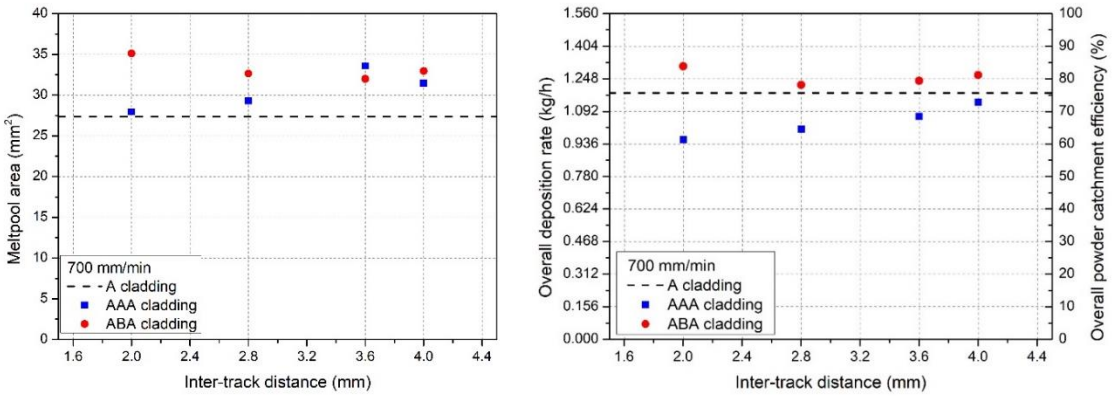

a) b)

Figure 6.9 The melt pool areas (from figure 8) and their associated powder catchment efficiencies

However, when considering the effect of inter-track distance on the process, a very important consideration is any effect on the thickness and waviness of the clad layer. This thickness and waviness determine how much useful clad layer will remain on the surface after the clad layer has been machined to a flat surface.

Figure 6.10 presents cross sections of the AAA and ABA samples and it is evident that, under these process parameters, both the 2mm inter-track distance (50% track overlap) and the 4mm distance are inappropriate choices for producing a flat clad deposit. In the 2mm case the clad surface is oversupplied with powder and in the 4mm case the gap between tracks is insufficiently supplied.

Although both cladding techniques would result in an array of solo 'A' tracks if the inter-track distance were wide enough, it is clear that an inter-track distance which is approximately equal to the melt width (4mm) is not large enough for this to happen. The ABA process retains its superior powder catchment efficiency at this large inter-track distance because escaping powder particles are still directed back into the melt by deflection off the adjacent 'A' tracks.

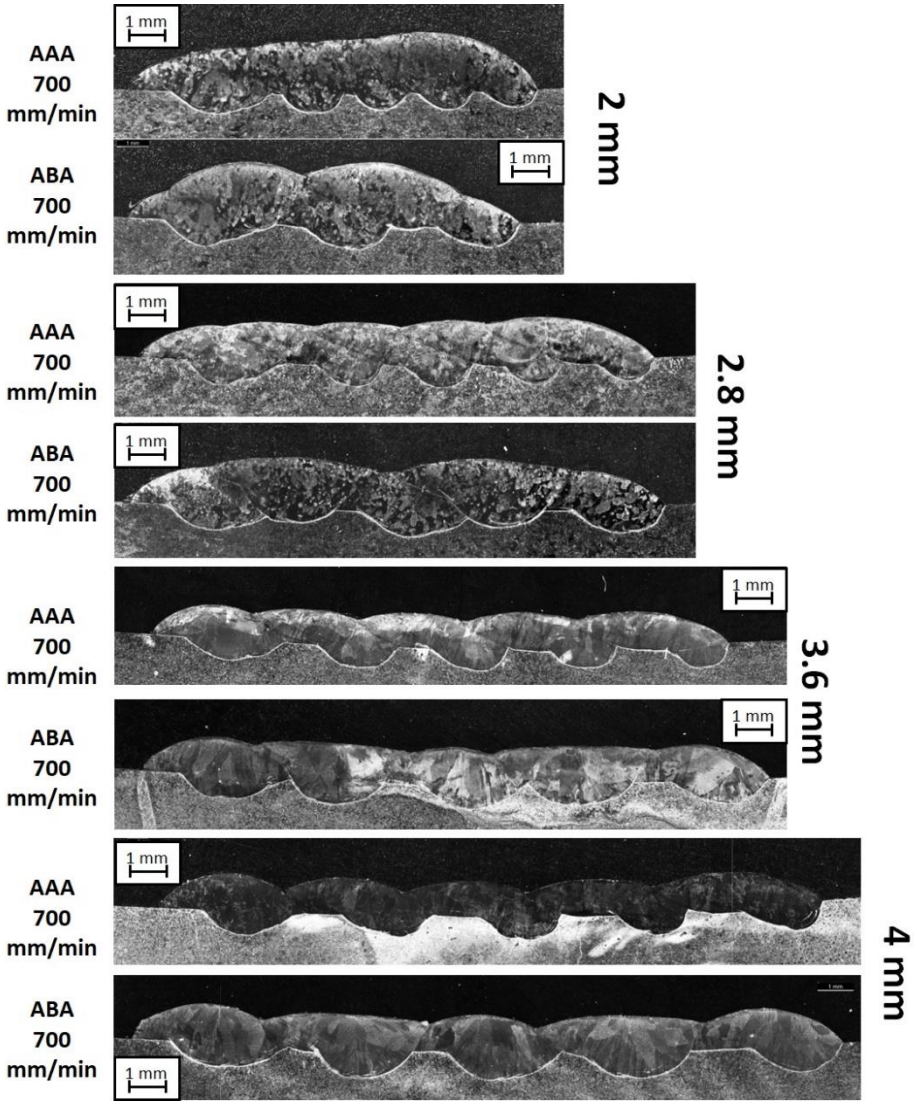

Figure 6.10 Cross sections of AAA and ABA clad deposits produced with the same parameters over a range of inter-track (centre to centre) spacings

6.4.3 The effect of process speed on ‘A’ tracks.

For ‘A’ clad tracks (either solo ‘A’ tracks or the ‘A’ tracks in ABA cladding), an increase in cladding speed from 0.7m/min to 1.5m/min had the expected result of reducing the size of the melt pool surface, as can be seen in Figure 6.11.

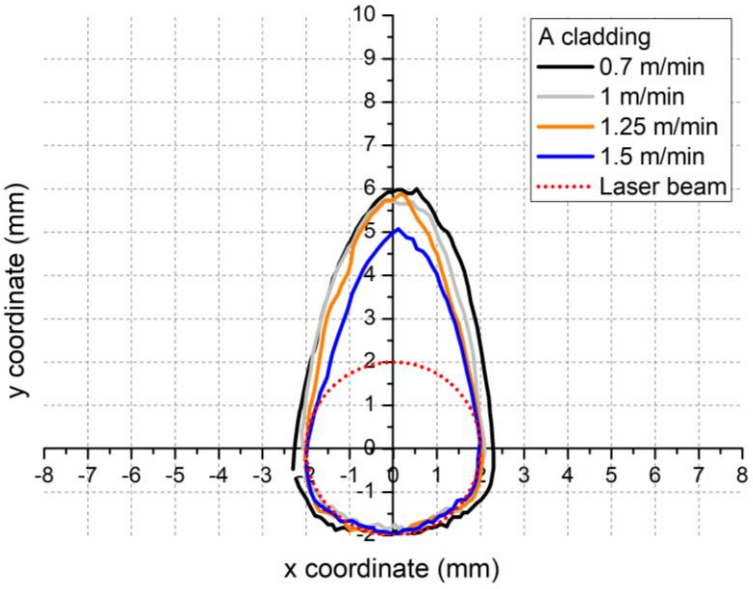

Figure 6.11 Melt (plan view) for ‘A’ tracks as a function of process speed

Although the results shown in Figure 6.11 represent changes over a 214% increase in process speed the associated (linear) reduction in melt pool surface area was only 30% (from 27mm^2 to 19mm^2) and the (linear) reduction in powder catchment efficiency was only 9% (from 76% to 69%). At higher speeds the laser energy produces shallower melt pools with only a limited reduction in melt pool surface area. The minor reduction in powder catchment efficiency over this large speed range clearly indicates that the melt pool surface is large enough throughout this parameter set to interact with most of the incoming powder stream. Small reductions in pool size therefore result in even smaller reductions in powder catchment efficiency.

6.4.3.1 The effect of process speed on ABA cladding.

Figure 6.12 and Figure 6.13 show cross sections of ABA clad specimens created at different process speeds, with inter-track distances of 2.8 and 3.6mm respectively. It is clear that the thickness of the clad layers decreases with increasing cladding speed, as would be expected.

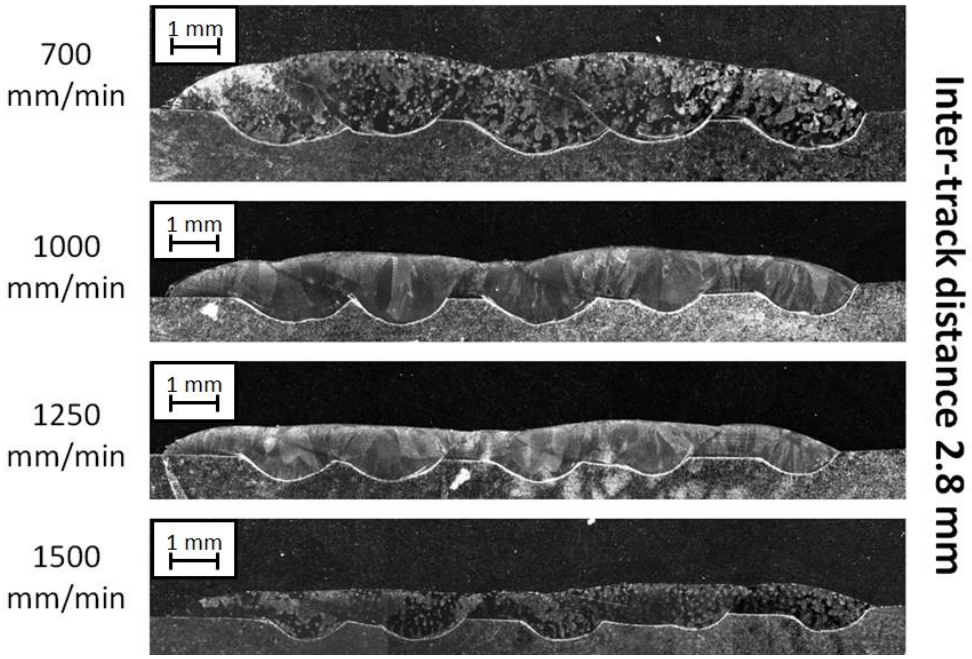

Figure 6.12 Cross sections of ABA clads made at different speeds with an inter-track distance of 2.8mm

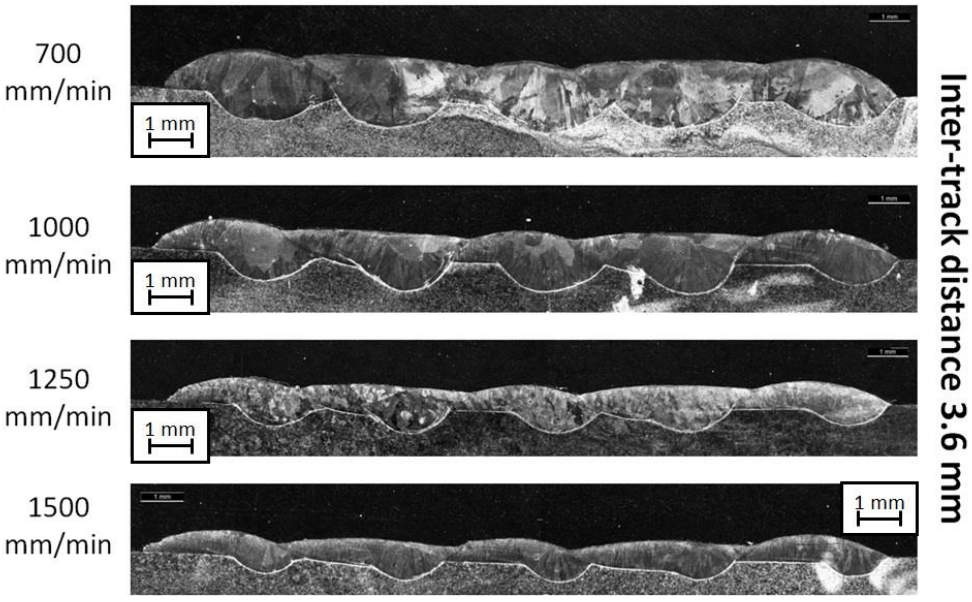

Figure 6.13 Cross sections of ABA clads made at different speeds with an inter-track distance of 3.6mm

Figure 6.14 gives the details of the melt pool shapes, areas and catchment efficiencies for the examples presented in Figure 6.12 and Figure 6.13.

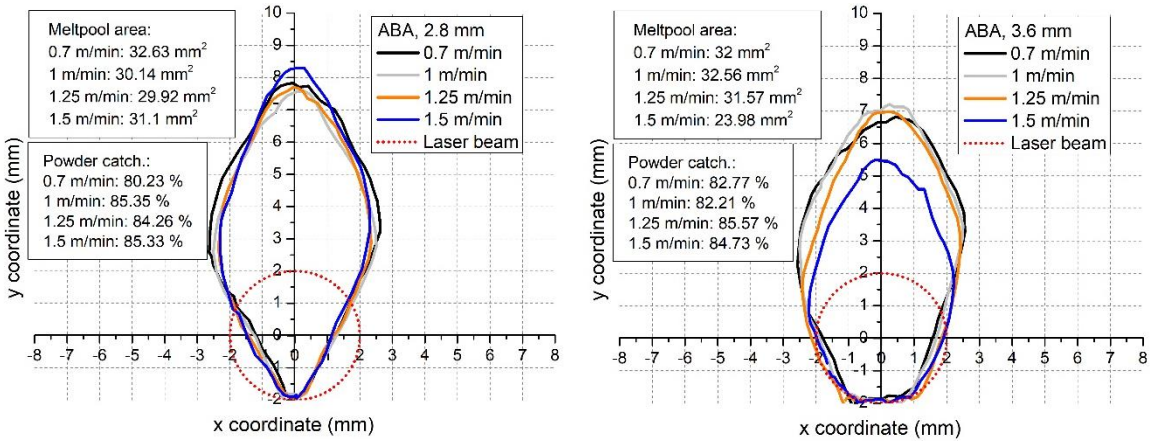

a) b)

Figure 6.14 The melt pool shapes, areas and powder catchment efficiencies for the samples shown in Figure 6.12 and Figure 6.13.

It is surprising that, over a 214% increase in cladding speed in for both inter-track distances, the shape, area and catchment efficiencies vary only slightly. The only outlier is the size of the melt pool for the fastest speed (1.5m/min) and largest inter-track distance (3.6mm). Apart from this result the melt pool areas vary by less than 10% (29.92 – 32.63mm^2).

The powder catchment efficiencies for this group of results (including the melt pool size outlier) only vary by less than 5% (80-85%). All of these ABA powder catchment efficiencies are above those of the solo 'A' or multiple AAA tracks, and this demonstrates that the most important influence on powder catchment efficiency is the choice of cladding technique used, with ABA cladding giving better results than AAA.

6.4.4 A comparison of powder catchment efficiencies for AAA and ABA cladding.

Many of the experimental results for ABA cladding presented so far have been dealing with 'B' tracks in isolation, and an experimental data set for powder catchment efficiency for these tracks is given in Figure 6.15a.

The improvement over AAA cladding is quite clear, with one result showing a 99% powder catchment efficiency (see Figure 6.5). However, this gives an exaggerated view of the powder catchment efficiency of the ABA cladding process, which is, as discussed earlier, the average of the solo 'A' track efficiency for those parameters and the 'B' track results shown in Figure 6.15a. These average powder catchment efficiencies for ABA cladding are presented in Figure 6.15b and, although these values are lower than those shown in Figure 6.15a, they are still a substantial improvement over the AAA results.

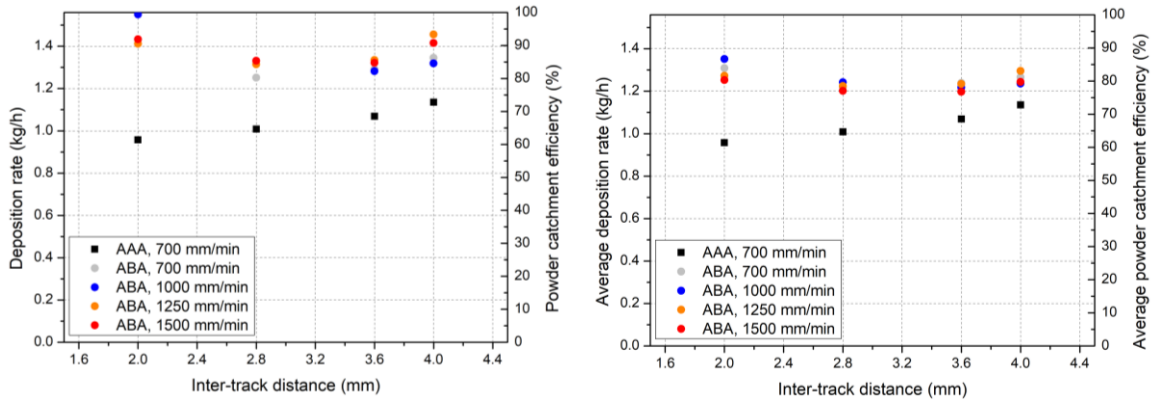

a) b)

Figure 6.15 Deposition rate/powder catchment efficiency results over a wide range of cladding speeds and inter-track distances for: a. 'B' tracks only, b. ABA cladding (average of 'A' and 'B' tracks).

6.5 Conclusions

The experimental and analytical work presented here confirms the following conclusions within the parameter set used:

- Powder catchment efficiency is an important metric for laser cladding and associated DED processes.
- There is a substantial difference between the melt pool shape and the powder catchment efficiency of the initial track and subsequent tracks in AAA cladding.
- The 'subsequent' tracks in AAA cladding have an asymmetrical melt pool shape as a result of the overlap of one track with the previous one. This asymmetry exposes more solid material to the incoming powder stream which decreases the powder catchment efficiency of the process.
- 'B' tracks in ABA cladding have an enhanced powder catchment efficiency primarily because the edges of the powder stream are reflected back into the melt pool off the 'shoulders' of the adjacent 'A' tracks.
- An increase in inter-track distance can improve powder catchment for AAA cladding but has no clear effect on ABA cladding powder catchment.
- Increasing cladding speed has a surprisingly small effect on weld pool size or powder catchment efficiency, although it has a substantial effect on clad layer cross section (reduced speeds result in thicker clad layers).
- ABA cladding offers a substantial improvement in powder catchment efficiency over AAA cladding and also eliminates the initiation anomalies common to AAA cladding.

6.6 References

1. Mazumder, J. Singh, J.I. “Laser Surface Alloying for Corrosion and Wear.” J. High temperature materials and processes. 7 (2-3) 101-106 July 1986
2. Steen, W.M., Powell, J. “Laser Surface Treatment.” J. Materials in Engineering Vol. 2. March 1981. pp 157-162.
3. Powell, J. “Laser Cladding.” PhD Thesis. Imperial college. London University 1983.
4. Naresstroem, H. “Phenomena in laser based material deposition” PhD thesis. Lulea University of Technology. May 2021. ISBN 978-91-7790-819-7
5. Prasad HS, Brueckner F, Kaplan AF. Powder catchment in laser metal deposition. InInternational Congress on Applications of Lasers & Electro-Optics 2018 Oct 1. AIP Publishing.
6. Harooni A, Nasiri AM, Gerlich AP, Khajepour A, Khalifa A, King JM. Processing window development for laser cladding of zirconium on zirconium alloy. Journal of Materials Processing Technology. 2016 Apr 1;230:263-71.
7. S.-W. Bahk, P. Rousseau, T. A. Planchon, V. Chvykov, G. Kalintchenko, A. Maksimchuk, G. A. Mourou, and V. Yanovsky, "Generation and characterization of the highest laser intensities (10^{22} W/cm2)," Opt. Lett. 29, 2837-2839 (2004)
8. Pinkerton, Andrew J., and Lin Li. “The Significance of Deposition Point Standoff Variations in Multiple-Layer Coaxial Laser Cladding (Coaxial Cladding Standoff Effects).” International Journal of Machine Tools and Manufacture, vol. 44, no. 6, 2004, pp. 573–584., https://doi.org/10.1016/j.ijmachtools.2004.01.001.
9. Donadello S, Furlan V, Demir AG, Previtali B. Interplay between powder catchment efficiency and layer height in self-stabilized laser metal deposition. Optics and Lasers in Engineering. 2022 Feb 1;149:106817.
10. Paul CP, Ganesh P, Mishra SK, Bhargava P, Negi JA, Nath AK. Investigating laser rapid manufacturing for Inconel-625 components. Optics & Laser Technology. 2007 Jun 1;39(4):800-5.
11. Lee, Y. S., M. Nordin, S. S. Babu, and D. F. Farson. "Influence of fluid convection on weld pool formation in laser cladding." Weld. J 93, no. 8 (2014): 292-300.
12. Dalaee M, Cerrutti E, Dey I, Leinenbach C, Wegener K. Parameters development for optimum deposition rate in laser Dmd of stainless steel En x3crnimo13-4. Lasers in Manufacturing and Materials Processing. 2021 Dec:1-7.

13. Bloemer PR, Pacheco JT, Cunha A, Veiga MT, Filho OC, Meura VH, Teixeira MF. Laser cladding of Inconel 625 on AISI 316L: Microstructural and mechanical evaluation of parameters estimated by empirical-statistical model. Journal of Materials Engineering and Performance. 2022 Jan;31(1):211-20.
14. Meng L, Sheng P, Zeng X. Comparative studies on the NI60 coatings deposited by conventional and induction heating assisted extreme-high-speed laser cladding technology: Formability, microstructure and hardness. Journal of Materials Research and Technology. 2022 Jan 1;16:1732-46.
15. Ocelík V, Eekma M, Hemmati I, De Hosson JT. Elimination of Start/Stop defects in laser cladding. Surface and Coatings Technology. 2012 Jan 15;206(8-9):2403-9.
16. Gao W, Zhao S, Liu F, Wang Y, Zhou C, Lin X. Effect of defocus manner on laser cladding of Fe-based alloy powder. Surface and Coatings Technology. 2014 Jun 15;248:54-62.
17. Liu S, Farahmand P, Kovacevic R. Optical monitoring of high power direct diode laser cladding. Optics & Laser Technology. 2014 Dec 1;64:363-76.
18. Heigel JC, Gouge MF, Michaleris P, Palmer TA. Selection of powder or wire feedstock material for the laser cladding of Inconel® 625. Journal of Materials Processing Technology. 2016 May 1;231:357-65.
19. Tuominen J, Näkki J, Pajukoski H, Peltola T, Vuoristo P. Recent developments in high power laser cladding techniques. InInternational Congress on Applications of Lasers & Electro-Optics 2012 Sep 1 (Vol. 2012, No. 1, pp. 192-196). Laser Institute of America.
20. Yang L, Yang X, Zhang T, Sun R. Optimization of microstructure and properties of composite coatings by laser cladding on titanium alloy. ceramics International. 2021 Jan 15;47(2):2230-43.
21. Pellizzari M, Zhao Z, Bosetti P, Perini M. Optimizing direct laser metal deposition of H13 cladding on cube alloy substrate. Surface and Coatings Technology. 2022 Feb 25;432:128084.
22. Turichin GA, Zemlyakov EV, Pozdeeva EY, Tuominen J, Vuoristo P. Technological possibilities of laser cladding with the help of powerful fiber lasers. Metal Science and Heat Treatment. 2012 Jul;54:139-44.
23. Govekar E, Jeromen A, Kuznetsov A, Levy G, Fujishima M. Study of an annular laser beam based axially-fed powder cladding process. CIRP annals. 2018 Jan 1;67(1):241-4.

24. Sun S, Durandet Y, Brandt M. Parametric investigation of pulsed Nd: YAG laser cladding of stellite 6 on stainless steel. Surface and Coatings Technology. 2005 May 1;194(2-3):225-31.
25. Kim JD, Lee EJ, Whang JG. Comparison of clad layer characteristics with overlapping criterion in multi pass laser cladding. Journal of Advanced Marine Engineering and Technology. 2016;40(9):768-73.
26. Ge T, Chen L, Gu P, Ren X, Chen X. Microstructure and corrosion resistance of TiC/Inconel 625 composite coatings by extreme high speed laser cladding. Optics & Laser Technology. 2022 Jun 1;150:107919.
27. Kim, Jong Do, Eun Jin Lee, and Cheol Gyu Kim. "Study on Laser Cladding of Heat Resisting Steel Using EuTroLoy 16006 Powder (II)-Characteristics of Alloying Elements Distribution of Multi Pass Clad Layer." Transactions of the Korean Society of Mechanical Engineers A 41, no. 4 (2017): 307-312.
28. Salehi, D., and M. Brandt. “Melt Pool Temperature Control Using Labview in Nd:YAG Laser Blown Powder Cladding Process.” The International Journal of Advanced Manufacturing Technology, vol. 29, no. 3-4, 2005, pp. 273–278., https://doi.org/10.1007/s00170-005-2514-3.
29. Zhong C, Pirch N, Gasser A, Poprawe R, Schleifenbaum JH. The influence of the powder stream on high-deposition-rate laser metal deposition with inconel 718. Metals. 2017 Oct 20;7(10):443.
30. Koti, D., Powell, J. and Voisey, K.T., 2022. Improving laser cladding productivity with ‘ABA’cladding. Procedia CIRP, 111, pp.205-209.

7 Chapter VII. Laser cladding (DED); A High-Speed-Imaging examination of powder catchment efficiency as a function of the melt pool geometry and its position under the powder stream.

The main body of this section is reproduced from the paper:

Koti, D., Powell, J., Naesstroem, H., Spaccapaniccia, C. and Voisey, K.T., 2023. Laser cladding: A high-speed-imaging examination of powder catchment efficiency as a function of the melt pool geometry and its position under the powder stream. Journal of Laser Applications, 35(4), https://doi.org/10.2351/7.0001199

7.1 Abstract

This paper provides quantitative information about the paths taken by powder particles which enter and do not enter the laser generated melt pool during laser cladding (DED). A proportion of the powder is 'wasted' by bouncing off the solid areas surrounding the melt pool. This wastage reduces the productivity of the process. In this paper, specially developed software was used to analyse High Speed Imaging videos of the cladding process, to monitor the directions of powder particle flight towards and away from the melt pool area. This information has been correlated to the geometry and position of the melt pool zone for three different cladding techniques; single track cladding (A tracks), standard overlapping track cladding (AAA cladding) and a recently developed technique called ABA cladding. The results show that the melt pool geometry, and particularly the overlap between the melt pool and the incoming powder stream, have a strong influence on powder catchment efficiency. ABA cladding was found to have considerably better powder catchment efficiency than standard AAA cladding and this improvement can explained by consideration of the geometries and positions of the melt pools and surrounding solid material in each case. As powder costs are an important factor in industrial laser cladding, the adaption of the ABA technique, and/or control of pool/powder stream overlap (for example by making the powder stream not coaxial with the laser beam) could have a beneficial effect on the profitability of the process.

7.2 Introduction

Laser cladding is a Directed Energy Deposition (DED) technique which involves melting a blown stream of metal powder onto a substrate surface to provide a coating which has good wear or corrosion properties [1-3]. Unfortunately, a proportion of the powder fed into the process misses the melt pool and is not incorporated into the clad layer [4]. This 'escaping' or 'wasted' powder is an important feature of the profitability of the cladding process because the powder is expensive and generally cannot be recycled [5]. This paper describes the results of an experimental program designed to identify the total amount of powder which escapes, and the directions taken by the escaping powder particles under various process parameters as a function of melt pool geometry.

The process parameters investigated included cladding speed, inter-track distance and cladding technique. Three cladding techniques were compared; Single track cladding ('A' cladding), Standard, overlapping track cladding (AAA cladding) and a recently developed technique called ABA cladding [6, 7]. These three techniques are described in Figure 7.1. High Speed Imaging (HSI) videos were taken of the laser-material interaction area during cladding, and specially designed software was employed to identify the flight vectors of the individual particles towards, and away from, the melt pool.

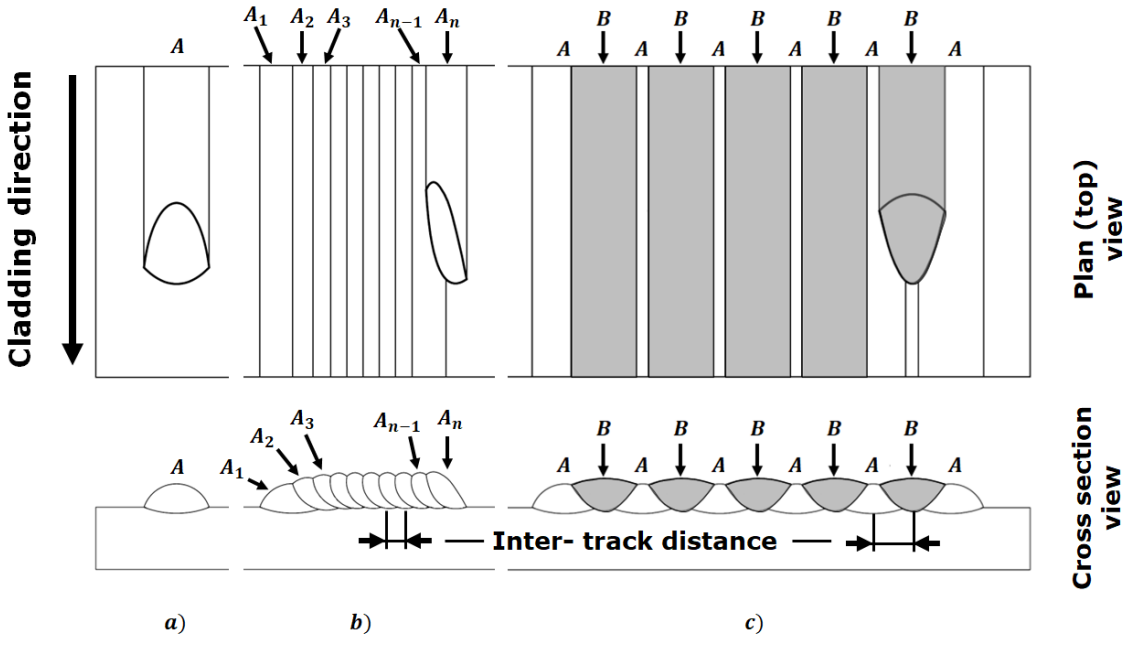

Figure 7.1 a) A solo, or initial, 'A' track, b) In standard (AAA) laser cladding the clad surface is made up of overlapping 'identical' tracks (although a few, early tracks differ from later tracks), c) in ABA cladding a set of widely spaced identical 'A' tracks are laid down first and then the gaps between them are filled with 'B' tracks.

7.3 Experimental Details

7.3.1 Cladding parameters

Laser cladding experiments were conducted with the following parameters; 15 kW IPG Ytterbium-doped, cw fibre laser, (1070 nm wavelength), 3 kW power. 150mm collimating lens and Kugler mirror optics with a 250mm focussing mirror. Fibre diameter; 100µm, coupled to a 400µm fibre. Beam diameter on substrate surface; 4mm (Gaussian energy distribution), Stand-off distance; 13mm.

The powder was fed through an 8mm diameter coaxial COAX 14V5 (Fraunhofer IWS) continuous nozzle (also known as a ring-slit nozzle). This produced a focussed powder stream with a diameter of approximately 4mm at the melt pool surface. Argon was used as the shielding and carrier gas.

The carrier gas flow was 8 l/min and shielding gas flow was 15 l/min. 316L stainless steel powder with a size range from 50 to 150 microns diameter was fed from a gravity-based powder feeder. The powder feeder was calibrated, and the feed rate used (26g/min) was checked experimentally and found to have a standard deviation of 0.8g/min. A 3-axis ISEL FlatCOM L150 CNC system was used, with the substrate plates (5mm thick 304S15 stainless steel) clamped to a linear motion table. Both the laser head and the powder feeder nozzle remained fixed.

Tracks were created using both the AAA and ABA techniques with a range of inter-track (centre to centre, see figure 1) spacings of between 2 mm and 4 mm. The tracks comparing ‘AAA’ and ‘ABA’ clads were carried out at 0.7 m/min. For the solo ‘A’ track cladding experiments, the cladding speed was varied between 0.7 m/min and 1.5 m/min, to investigate pool shape changes as a function of process speed.

7.3.2 Powder particle trajectory image processing.

High Speed Imaging (HSI) videos were taken of the cladding zone, and diagnostic code was written in Python using numpy, opencv, and openPIV. The code’s operations were divided into the following steps: 1. particle detection, 2. velocity computation, 3. association of directional vectors to individual particles, 4. computation of flow rates in different directions. The code was applied to individual HSI frames for particle detection, and pairs of consecutive images were used for the computation of displacement vectors.

The initial step is to achieve a binary image where only the particles are visible. As well as the information on particle positions, the individual frames from the HSI contain high intensity, low-frequency signals from the deposition area and high-frequency low-intensity electronic noise. The first was attenuated through background intensity removal, while the latter was removed by low pass filtering of the Fourier spectrum of the image.

The operation was repeated twice, until the particle signal became predominant, and a clear threshold could be used to binarize the image. Finally, particle counting was performed on the binary image using Open CV structural analysis toolbox.

The algorithms used to calculate the particle vectors were PIV (Particle Image Velocimetry) and OF (Optical Flow). Both algorithms were applied to the whole image and required two consecutive frames to analyse the displacement of the particles. PIV was very effective in computing vectors in high-speed regions of the image, while OF was more reliable for the regions of low particle speed. It is important to mention that the original images are used to compute displacement vectors, since using a binarized image leads to errors in the cross-correlation-based algorithm.

The steps above identify the direction and velocities in the regions of interest but do not link them to the individual particles. In order to associate a vector to every particle, it is necessary to overlap the binary image obtained in step 1 with the velocity maps obtained in step 2.

7.3.3 Mapping the geometry of the melt pool and its overlap with the powder stream.

Using techniques developed in earlier work [7] the plan view geometry of the weld pool was accurately identified from the HSI videos. In each case this could then be mapped onto the circular cross section of the vertically incident powder stream. From this information it was possible to calculate the percentage of the powder stream which landed in the liquid pool and the proportion which landed on the surrounding solid material.

The powder stream was co-axial with the laser beam, and both were circular in cross section. However, it is important to point out that the melt pools were not circular, and there was generally a lag between the front edge of the melt pool and the front edge of the powder stream.

7.4 Results and Discussion

7.4.1 Single ‘A’ track cladding at different speeds

Figure 7.2 presents a single frame from the HSI video of the laser-material interaction zone in single ‘A’ track cladding. The cladding process is moving towards the viewer in this photo. Flight vectors, calculated as described above, have been added to some particles (depicted as arrows, the length of which are proportional to speed).

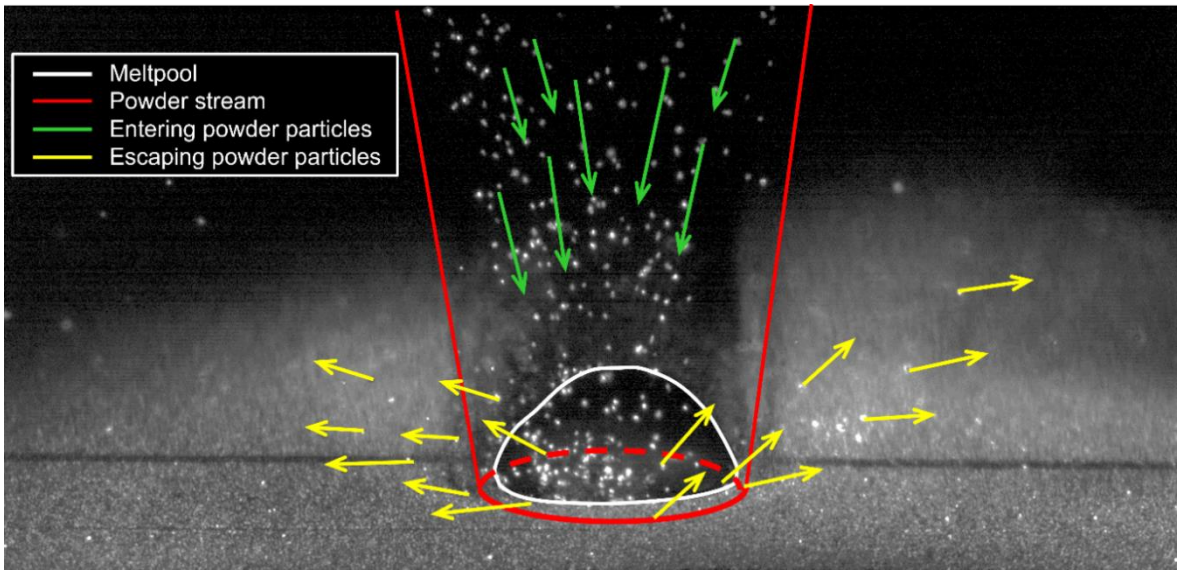

Figure 7.2 A frame from the HSI video of the cladding a single ‘A’ track. Selected particle vectors are shown as arrows (arrow length is proportional to speed).

It is clear from Figure 7.2 that most of the descending powder stream is entering the melt pool. However, a small proportion of the particles are flying away from the area after rebounding off the solid material which surrounds the melt. From the software analysis of the HSI video it was possible to identify the mass of incoming powder entering the melt pool as a percentage of the total powder feed rate, and this can be expressed as the powder catchment efficiency [7]. Figures for powder catchment efficiency can also be calculated from measuring the cross section of the clad tracks and thus the mass per unit time laid down in the clad layer. Both sets of results are presented in Figure 7.3 and subsequent figures.

Single track ‘A’ cladding was carried out at a range of speeds. Figure 7.3 shows the plan view of the shape of the cladding melt pools for single ‘A’ tracks at various process speeds (measured from the HSI videos) with a dotted circle identifying the position and area of the incident powder stream. Plan views of the melt pools were chosen because the input powder is effectively a vertical stream. It is interesting to note that, although the range of process speeds shown here is from 0.7m/min to over double that value (1.5m/min), the reduction in the surface area of the pool is only 20% (from 27.2 mm2 to 21.72 mm2). It is clear that there is a gradual decrease in powder catchment efficiency with increasing cladding speed.

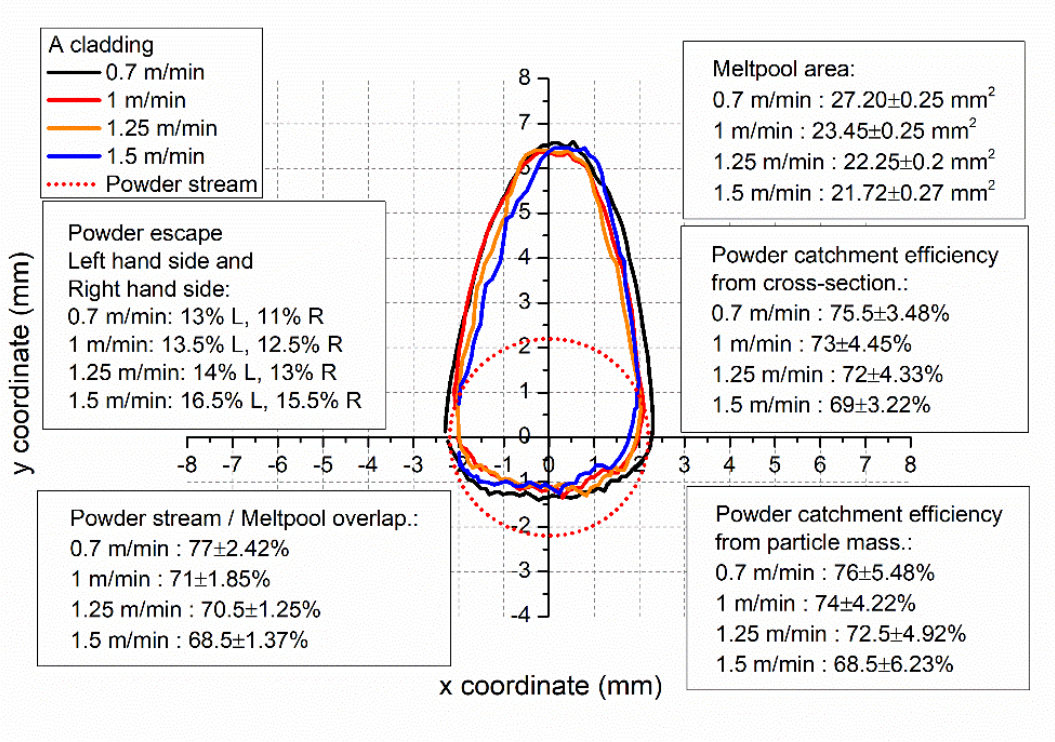

Figure 7.3 Plan views of melt pools in single track ‘A’ cladding as a function of cladding speed. The position and size of the powder stream is indicated as a dotted circle. ‘Powder catchment efficiency from particle mass’ figures is taken from the HSI video anal

In Figure 7.3 the position of the powder stream for each cladding speed melt pool was established directly from the HSI video. The figure gives details of the meltpool area, the powder catchment efficiency and the percentage area overlap between the powder stream and the melt pool. It can be seen that, in every case, melt pool front lags the front of the powder jet slightly. In some processing conditions this would be expected because the powder jet and laser are aligned, and the cold, flat substrate would need some time/distance under the laser beam before melting is initiated.

It is interesting to note that there is a very good match between the percentage overlap (powder/pool) and the powder catchment efficiency. The area overlap between the melt pool and the powder stream matches the powder catchment efficiency to within 2% on average, over this range of processing parameters. This extremely close fit was also evident in the other experiments carried out in this study (see section 3.5). Given this remarkably accurate result, a great deal of care was employed to establish the error range of the results for the melt pool area measurements, the powder catchment efficiencies (cross section and particles mass) and melt pool/powder stream overlap. Each of the underlying measurements was repeated at least ten times, the standard deviations calculated and regarded as the error on each measurement. These were then combined to produce the overall errors given using standard combination of errors equations. The resulting errors are presented in the data boxes in Figure 7.3 and other, appropriate figures.

Figure 7.2 suggests that particles escape the melt pool to the right and left of the cladding path. From the HSI analysis described earlier it was possible to quantify the proportions of particles travelling in each direction. The results of this measurement are presented in figure 4 and show that the two general directions of travel (left and right) were evenly matched. This is not an unexpected result as the clad track and melt pool are axi-symmetric about the axis of travel, as in the case of solo ‘A’ clad tracks.

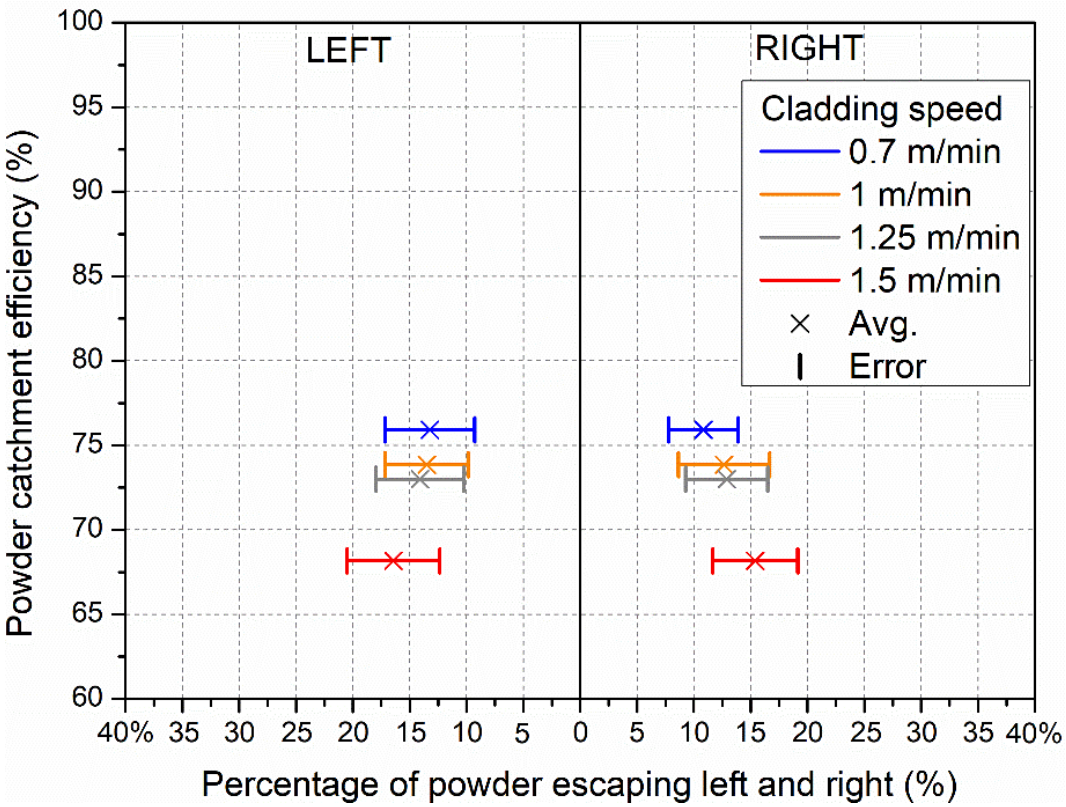

Figure 7.4 Measurements of the powder catchment efficiency of single track 'A' cladding as a function of cladding speed, and the proportions of particles escaping from the cladding zone in the general left and right directions.

7.4.2 'AAA' cladding with different inter-track spacing.

Standard 'AAA' cladding (see Figure 7.1) was carried out at a cladding speed of 0.7m/min with inter-track spacings varied between 2 and 4 mm. Figure 5 shows a typical HSI single frame taken from the video recordings. In this case it can be seen that the track is being overlapped with the previous one, which means that the melt pool and the surrounding area are not axially symmetrical on either side of the axis of movement as they were in the case of the single 'A' track.

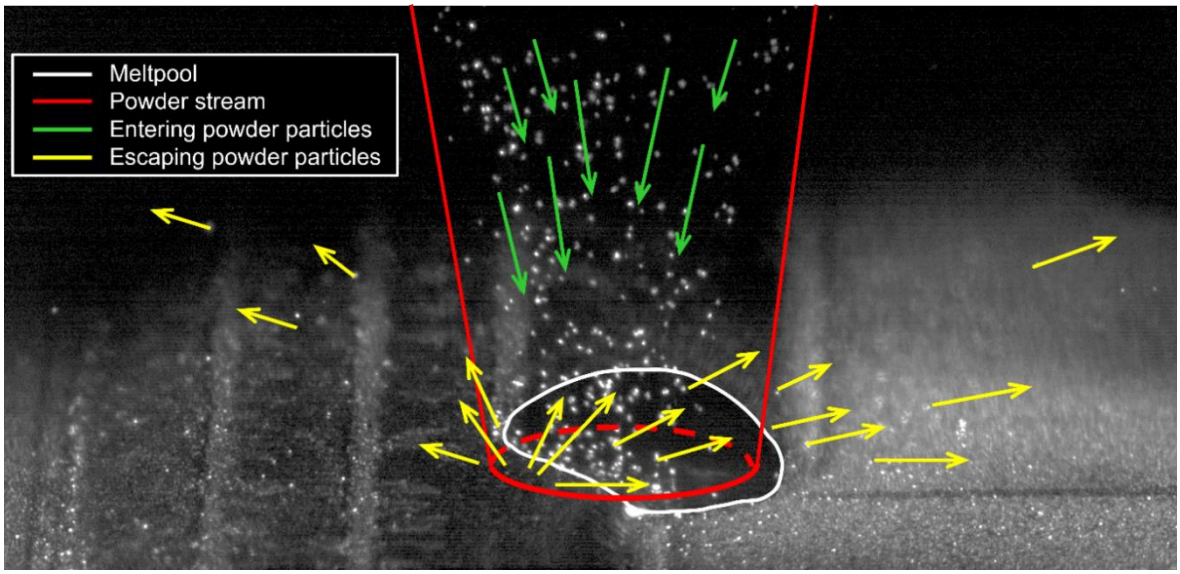

Figure 7.5 A typical view of 'AAA' cladding (in this case the inter-track spacing was 2.8 mm)

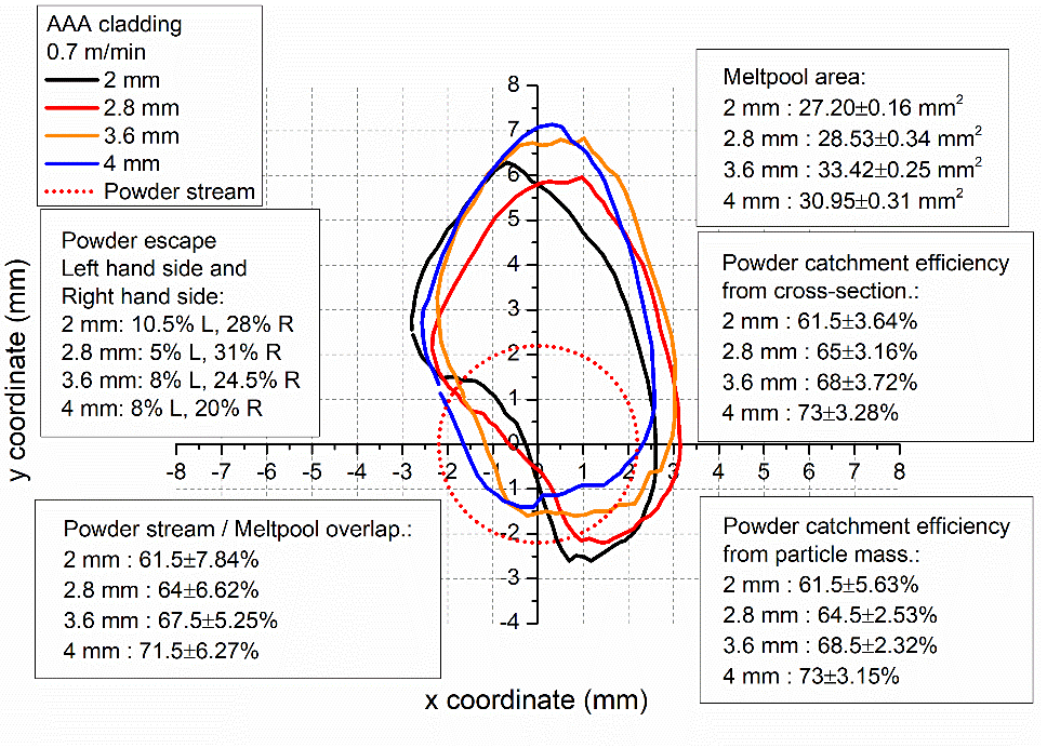

Figure 7.6 Plan views of melt pools for 'AAA' cladding as a function of inter-track distance. The position and size of the powder stream is indicated as a dotted circle.

Figure 7.6 shows that, at the minimum inter-track distance (2 mm) the melt front is slightly ahead of the powder jet on the right-hand side where the flat surface of the substrate is being clad. This could be attributed to pre-heating of the area from the cladding of the previous track, as well as the effect of melt pouring downwards and forwards from the sloping melt pool. As the inter-track distance is increased, this pre-heating effect is weaker, and the melt front lags the powder stream on the right-hand side as the chilling effect of the substrate becomes dominant.

On the left the melt front substantially lags the powder stream in every case. Earlier work by the present authors [7] suggested that this is due to the laser interacting with the curved, sloping 'shoulder' of the previous track which means that the projected beam has a lower energy density (also, other factors such as angular dependence of absorption need to be taken into account).

This distortion of the shape of the melt pool results in an increase of the percentage of powder which impacts the surrounding solid material. This reduces the melt pool/powder stream overlap and thus the powder catchment efficiency. Figure 7.6 demonstrates once more that these two measurements are almost exactly matched. The figures for melt/powder overlap for this set of parameters match the powder catchment efficiency within 1.5% on average for this set of parameters.

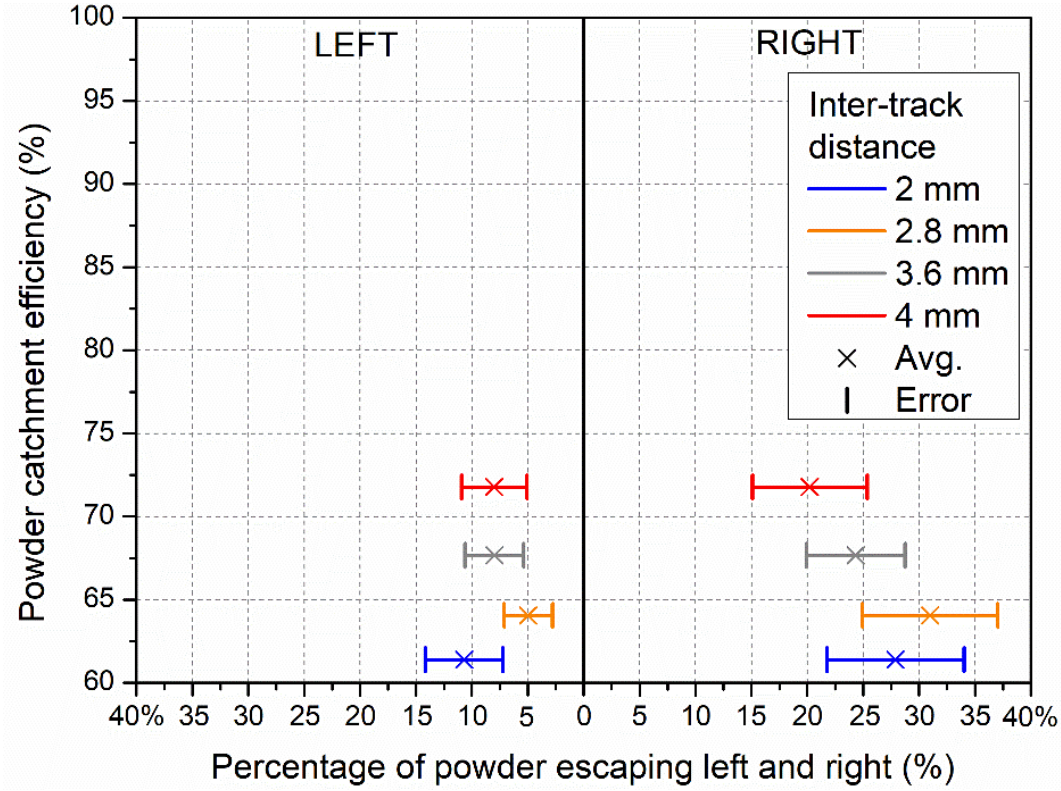

Figure 7.7 Measurements of the powder catchment efficiency of 'AAA' cladding as a function of inter-track distance, and the proportions of particles escaping from the cladding zone in the general left and right directions.

From Figure 7.3 and Figure 7.6 it is clear that the powder catchment efficiency of the 'AAA' process (61.5% - 73%) is lower than that of single track 'A' cladding (75.5% - 76%) at the same cladding speed (0.7m/min). It can also be seen in Figure 7.7 that the direction of travel of the 'wasted' powder particles is heavily biased towards the right-hand side. This makes sense because the 'shoulder' of the previous solidified track is an inclined surface will tend to deflect particles towards the right.

7.4.3 'ABA' cladding with different inter-track spacing.

'ABA' cladding (see Figure 7.1) was also carried out at a cladding speed of 0.7m/min with inter-track spacings varied between 2 and 4 mm.

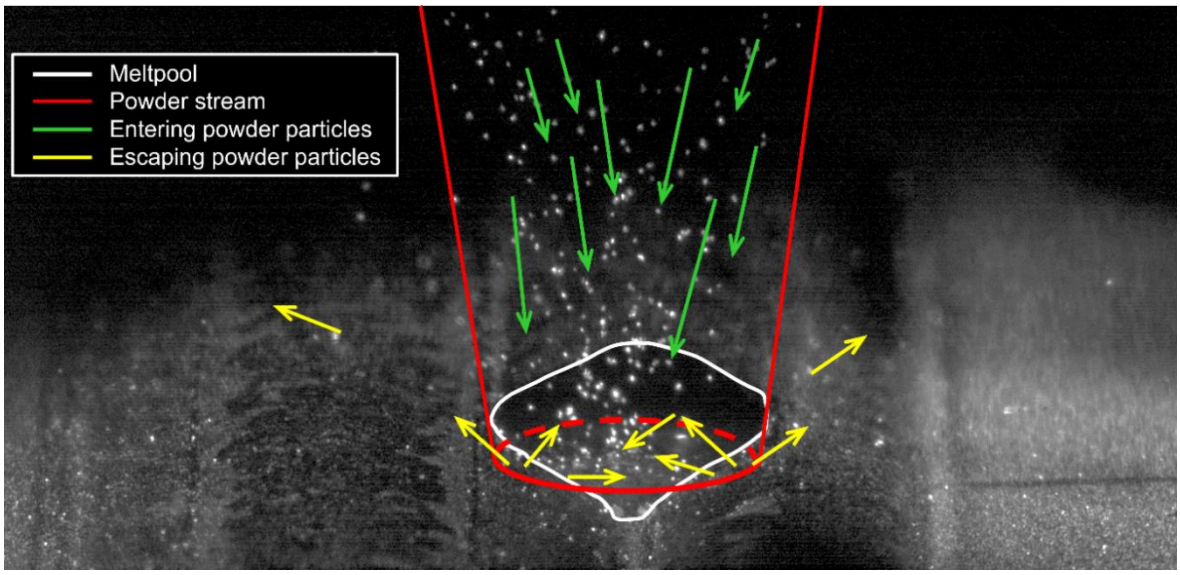

Figure 7.8 A typical view of 'ABA' cladding (in this case the inter-track spacing was 2.8mm)

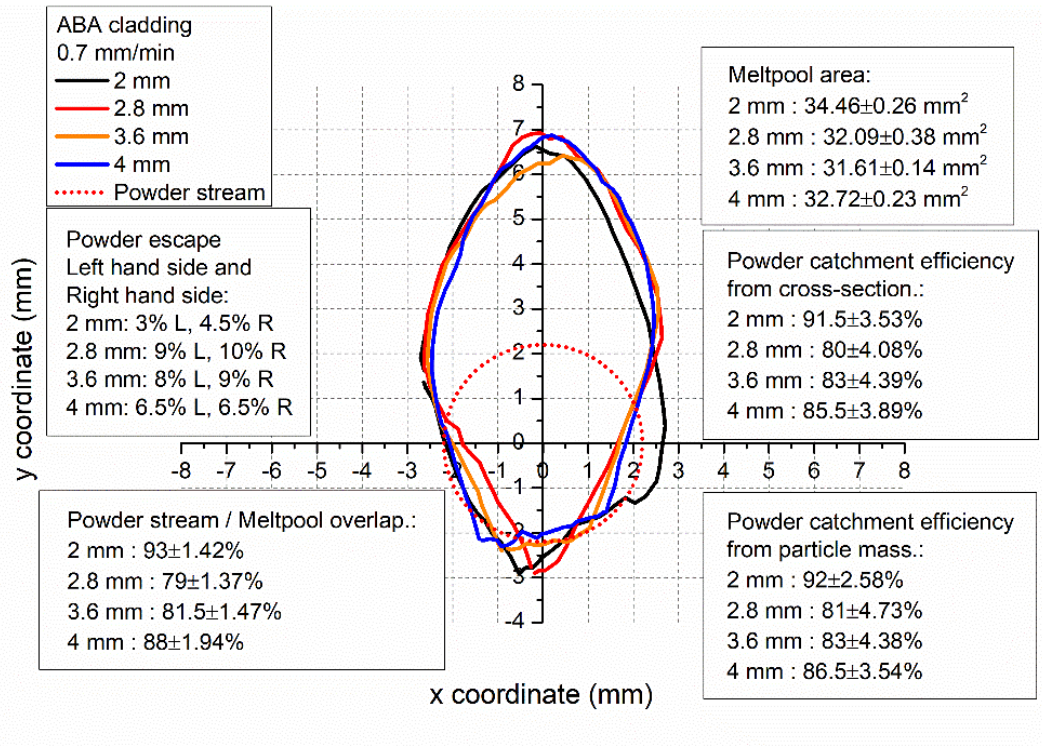

Figure 7.9 Plan views of melt pools for the 'B' tracks in 'ABA' cladding as a function of inter-track distance. The position and size of the powder stream is indicated as a dotted circle.

Figure 7.9 shows that the central part of the melt front for the ‘B’ tracks is slightly ahead of the powder stream for ABA cladding with these parameters. This is probably because the geometry of the melt pool (caught between the two ‘A’ tracks and sloping forwards), tends to pour liquid into the ‘valley’ between the adjoining ‘A’ tracks. Behind this central section the melt pool front lags behind the powder stream slightly. As was the case for AAA cladding this lag is probably caused by a reduction in laser power density of the projected beam on the sloping surfaces of the ‘A’ tracks. Note: In ABA cladding pre-heating effects are reduced compared to in ‘AAA’ cladding. This is because, in many examples of ‘AAA’ cladding, the previous track was laid down only a few seconds earlier. In ‘ABA’ cladding all the ‘A’ tracks need to be laid down before the first ‘B’ track is clad, which gives the material time to cool down before the ‘B’ track part of the process.

It is important to point out that Figure 7.9 only gives information relating to the “B’ Tracks in ABA cladding. The ‘A’ tracks were identical to those presented in Figure 7.3 for a cladding speed of 0.7m/min. Once more we have a very accurate correlation between the powder/pool overlap (79% - 93%) and the powder catchment efficiency (80% - 92%), both of which are very high in the case of the ‘B’ tracks. In the case of ABA cladding these values are within 2% of each other on average in the cases shown here.

The powder catchment efficiency and direction of travel for ABA cladding is presented in Figure 7.10 for the ‘B’ tracks (coloured lines), and it is clear that the left- and right-hand directions of powder travel are evenly balanced as a result of the symmetry of the melt pool and surrounding solid geometry (which is similar to a valley between two identical hills). Combining these results with those for the ‘A’ tracks gives us the average values for ABA cladding and these are presented in Figure 7.10 (coloured dots).

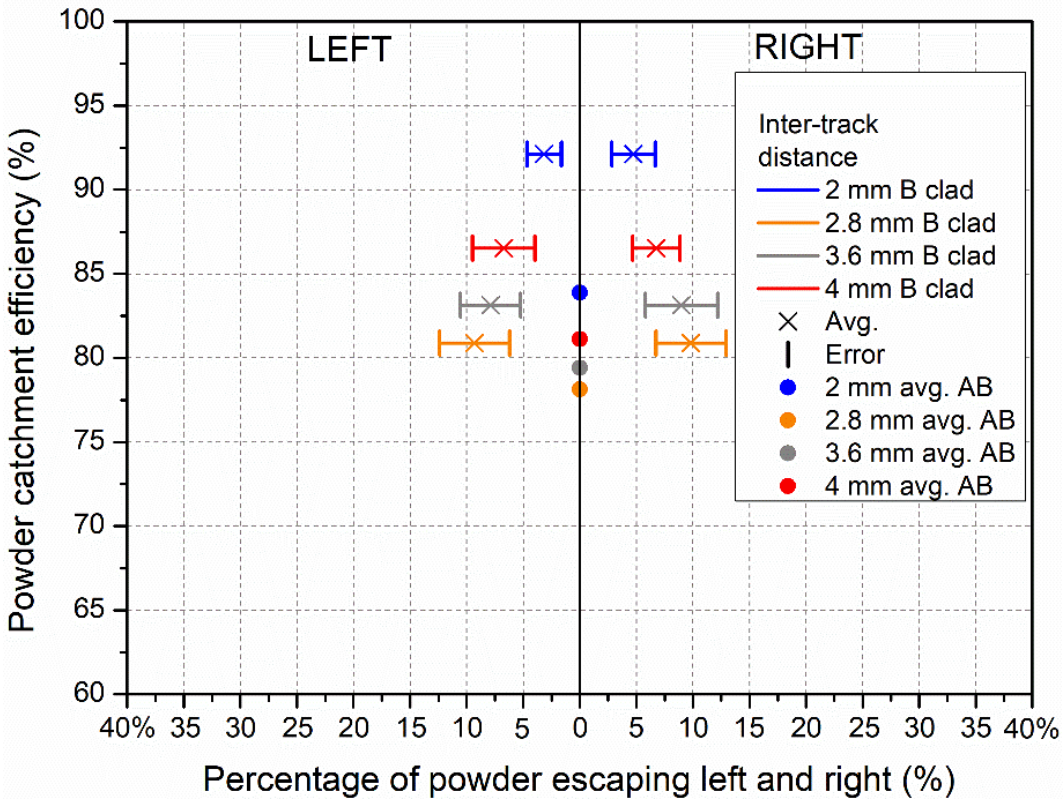

Figure 7.10 Measurements of the powder catchment efficiency of 'ABA' cladding as a function of inter-track distance, and the proportions of particles escaping from the cladding zone in the general left and right directions. Results for 'B' tracks only (coloured lines). Average results for the 'ABA' process, 'B' tracks plus 'A' tracks, (coloured dots).

One important feature to note from Figure 7.10 is the fact that even the average powder catchment efficiency of the ABA process is considerably higher (78-83%) in the case of ABA cladding than it is for standard 'AAA' cladding (61.5-72%).

7.4.4 A comparison of the ‘A’, ‘AAA’ and ‘ABA results.

Figure 7.11 presents the data for the proportion of powder escaping the process zone and direction of travel taken, for all three types of cladding (‘A’, ‘AAA’ and ‘ABA’). The information here is presented as a semicircular histogram of proportion of powder wasted as a function of direction of flight. For example, for ‘AAA’ cladding 6% of the particles rebounded at angles between 10 and 20 degrees to the horizontal. These results demonstrate:

A. The symmetrical flight patterns of the particles escaping from the symmetrical melt pools associated with solo ‘A’ track and ‘ABA’ cladding.

B. The asymmetry of the escape paths for ‘AAA’ cladding.

C. That more powder is escapes from ‘AAA’ cladding process than from solo ‘A’ tracks, and the most powder efficient process is ‘ABA’ cladding.

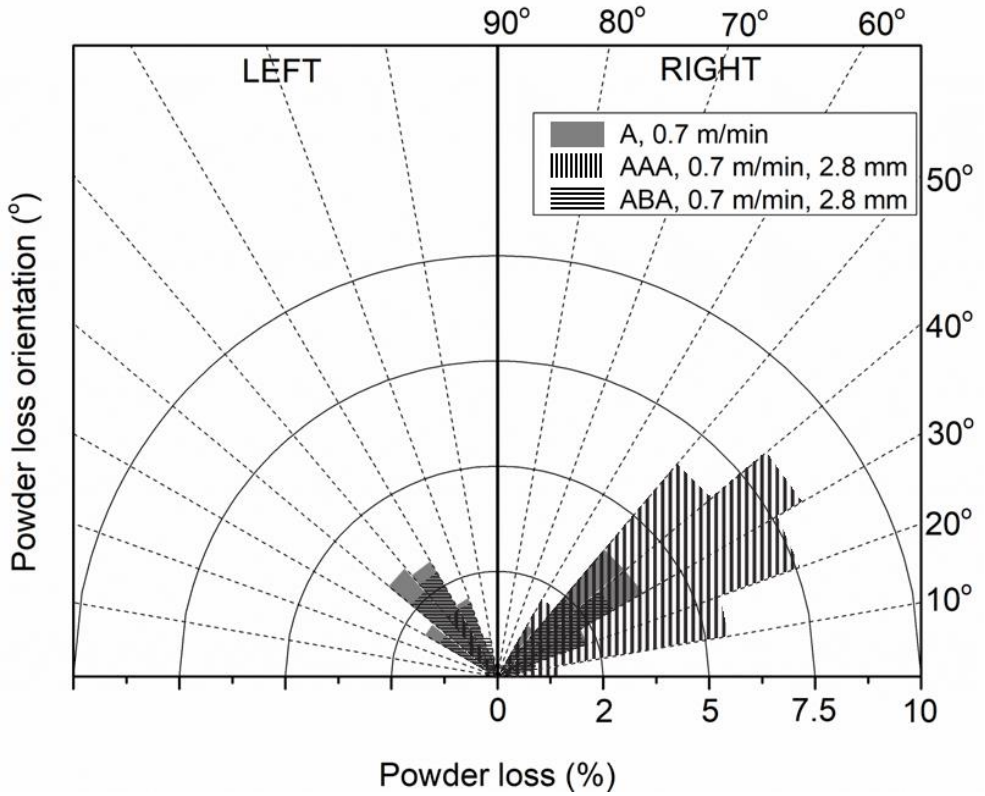

Figure 7.11A comparison of the wasted powder amounts and flight directions for ‘A’, ‘AAA’ and ‘ABA’ cladding.

7.4.5 A summary of the 'powder stream/melt pool overlap' results.

Figure 7.12 gathers together all the experimental results above with regards to powder catchment efficiency as a function of the overlap of the powder stream and the melt pool. It is clear from this figure that the correlation between the overlap and the powder catchment efficiency is very close to 100% over the range of process parameters presented here. This is an important result for the laser cladding industry as, in many cases, the process is unidirectional. This being the case, and the coaxial laser/powder stream nozzles presently in use may not be the optimum solution.

When cladding in different directions is required, coaxial systems are the obvious choice. However, for unidirectional cladding (eg. spiral cladding on tubes), the front of the melt pool can lag slightly behind the front of the laser (and the powder stream). In these cases, higher powder catchment efficiency may be achieved by employing ABA cladding or by directing the powder stream slightly backwards so that it overlaps the melt pool more completely. This strategy is likely to be particularly useful at high cladding speeds where the laser/melt lag could be substantial.

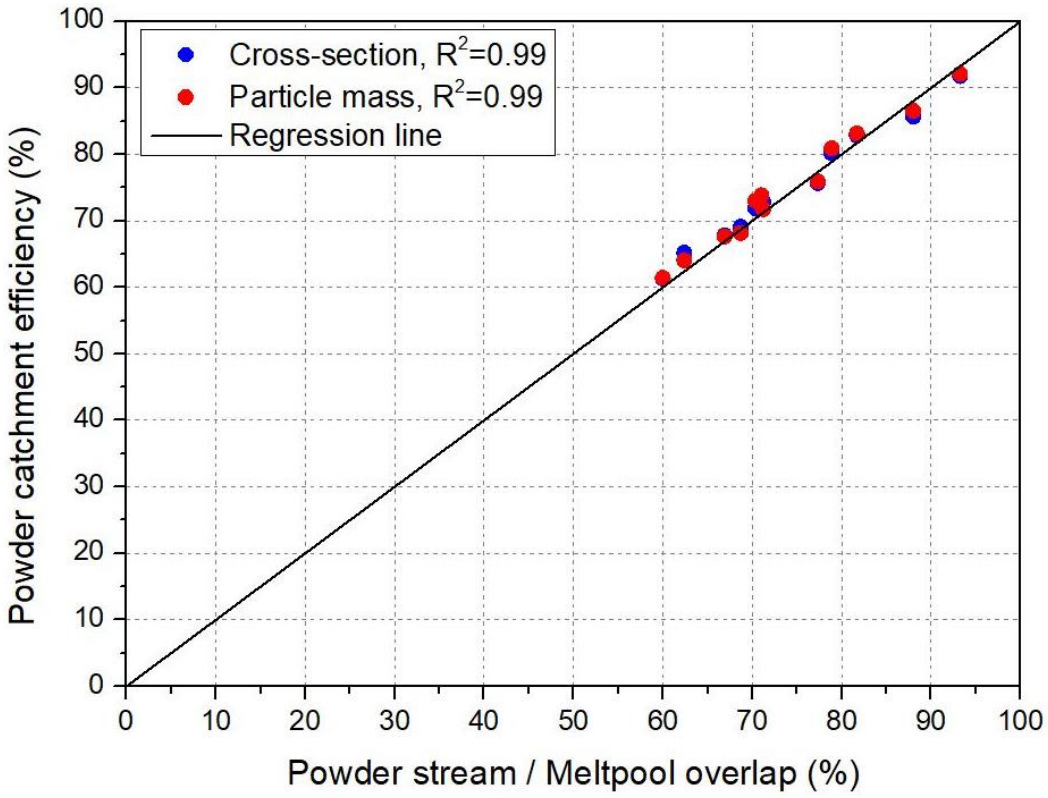

Figure 7.12 The powder catchment efficiency as a function of powder stream/meltpool

7.5 Conclusions

Within the parameter set presented here, and probably more generally;

- There is an almost exact 1:1 relationship between the powder stream/melt pool overlaps and the powder catchment efficiency in laser cladding.
- Powder catchment efficiency is maximised, for a coaxial powder feed/laser beam, by employing the ABA cladding process rather than the traditional AAA technique.
- The routes taken by particles which ‘escape’ the cladding process by missing the melt pool and bouncing out of the area are determined by the shape of the solid material surrounding the melt.
- To maximise profitability, laser cladding firms should maximise powder catchment efficiency by maximising powder stream/melt pool overlap. This optimisation could be achieved by techniques such as ABA cladding or by introducing a lag between the powder stream front and the front of the laser beam.

7.6 References

1. Steen, W. M., and Powell J. "Laser surface treatment." Materials & Design 2.3 (1981): 157-162.

2. Powell, J. “Laser Cladding.” PhD Thesis. Imperial college. London University 1983.

3. Cavaliere, P., ed. “Laser cladding of metals.” Berlin/Heidelberg, Germany: Springer, 2021.

4. Prasad, H. S., Brueckner F., and Kaplan A.F. "Powder catchment in laser metal deposition." International Congress on Applications of Lasers & Electro-Optics. AIP Publishing, 2018.

5. Prasad, H. S., Brueckner F., and Kaplan A.F. "Powder incorporation and spatter formation in high deposition rate blown powder directed energy deposition." Additive Manufacturing 35 (2020): 101413.

6. Koti, D., Powell J., and Voisey K. T. "Improving laser cladding productivity with ‘ABA’cladding." Procedia CIRP 111 (2022): 205-209.

7. Koti, D., Powell, J., Naesstroem, H., and Voisey, K. T. “Powder Catchment Efficiency in Laser Cladding (Directed Energy Deposition). an Investigation into Standard Laser Cladding and the ABA Cladding Technique.” Journal of Laser Applications, vol. 35, no. 1, 2023, p. 012025.

8 Chapter VIII. General discussion

8.1 Introduction

Researchers began investigating laser cladding in the early 1980s; the process has now reached a level of industrial importance. Laser cladding requires the melting of a cladding alloy onto a metal substrate using a pre-placed or blown powder by depositing successive tracks side by side to create a clad surface. Laser cladding has been shown to be an excellent method for altering the physical and chemical properties of material surfaces. The primary concern of the engineering industry is to reduce the cost of engineering parts with the required surface characteristics. In most cases, cost reductions can be achieved by using a cheaper substrate material and a suitable coating alloy. It is possible to increase productivity and cost-effectiveness by enhancing powder catchment efficiency, deposition rate, and coverage rate.

8.2 Problems with traditional AAA cladding

The traditional laser cladding procedure deposits a single track on the substrate surface. The researchers compare the characteristics of single tracks under a variety of processing conditions. However, in industrial practice, the use of single tracks is limited, since it is more common to overlap tracks until the required clad surface is obtained.

Due to the ostensible similarity of the clad tracks, the traditional cladding process could be called AAA cladding. Nevertheless, the similarity becomes apparent only after a few tracks have been laid. The shape of the subsequent tracks is affected in various ways by the previous tracks in the early stages of the process. In spite of the fact that this point is rarely discussed in the literature, most researchers in the field demonstrate it in their cross-sections of clad layers. There can be considerable variation in the height, cross-section, and metallurgy of clad tracks. In comparison with subsequent tracks, Track 1 will have a different melt pool geometry which will affect powder capture and dilution. A repeating pattern of cladding is not usually established until track 4 as shown in Figure 8.1. It is noteworthy that these start and finish anomalies are a significant drawback of the AAA cladding system, as they cause local perturbations in the morphology and dilution of the clad surface, as well as heat-affected zones.

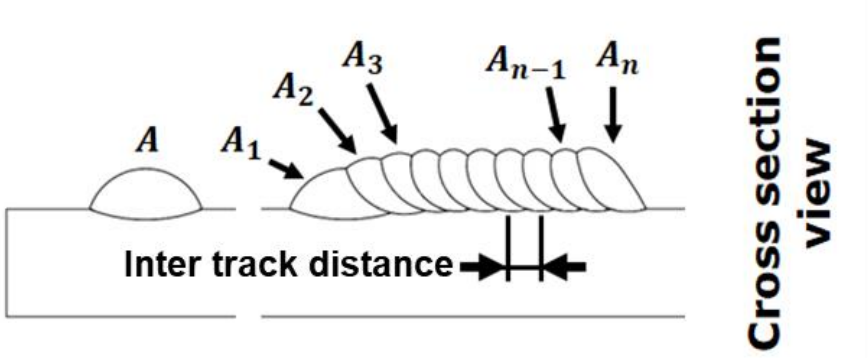

Figure 8.1 Cross-sectional view of initial 'A' track and a standard (AAA) laser clad surface, where the clad surface consists of overlapping 'identical' tracks

The laser cladding process involves a processing head that supplies a stream of the cladding powder alloy coaxially with a defocused laser beam. The purpose of the process is to melt all of the powder that arrives at the laser-material interaction area into the clad track. It is generally not possible to capture all the powder entering the meltpool, and a certain percentage of powder escapes from the meltpool. The 'escape' of powder is a critical component of the profitability of the cladding process. As part of the consideration of the escaping behaviour, it is important to keep in mind that since the powder particles have a wide range of escape routes as a result of the shoulder of the previous track and the slope of the melt pool, they are directed away from the melt pool. The powder particle escape pathways in single track, A, cladding and overlapping track, AAA, cladding is illustrated in Figure 8.2

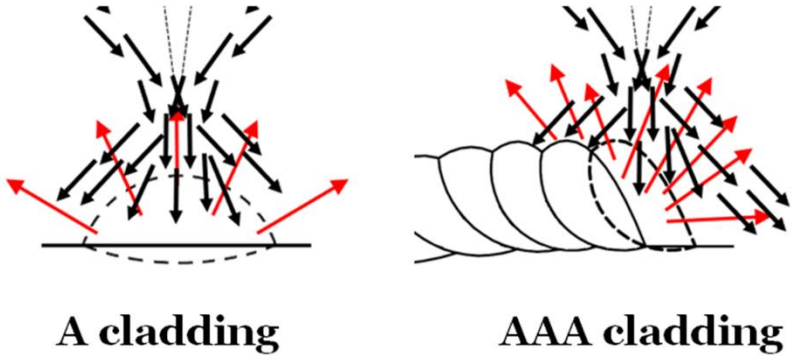

Figure 8.2 An illustration of the powder particle escape pathways in A and AAA claddings.

The efficiency of powder catchment in the process has a significant impact on costs and is therefore of paramount importance to industrial users. The efficiency of this process can be defined as the percentage of powder that is fed to the laser melting process and becomes part of the laser clad layer. According to the technical literature, powder catchment efficiencies

range widely, but are frequently substantially below 50%. As a result of the powder's high cost and inability to be recycled, this poses a significant problem.

Although there is a very large body of research work on laser cladding with blown powder, there are no clear guidelines about which quality and productivity parameters are important to the relevant branches of industry, nor are there any general rules about what constitutes a high-quality deposit. There is the need to investigate the influence of productivity factors in order to gain a better understanding of the process to be able to apply it successfully in industry.

8.3 Possible solution, introducing ABA cladding.

An innovative cladding technique, ABA cladding, is investigated in this thesis with the aim of establishing a more predictable and efficient process. By laying down clad tracks with more widely spaced intervals ('A' tracks), and then filling in the gaps between these tracks with those made with different parameters ('B' tracks), a more uniform structure can be achieved, as shown in Figure 8.3. Consequently, all 'A' tracks will be identical in shape, dilution, etc., and the same will be true for all 'B' tracks. A comparison of ABA laser cladding to traditional AAA cladding is presented in this work. Particularly, the study compares the efficiency of powder catchment and the deposition/coverage rates of the two techniques.

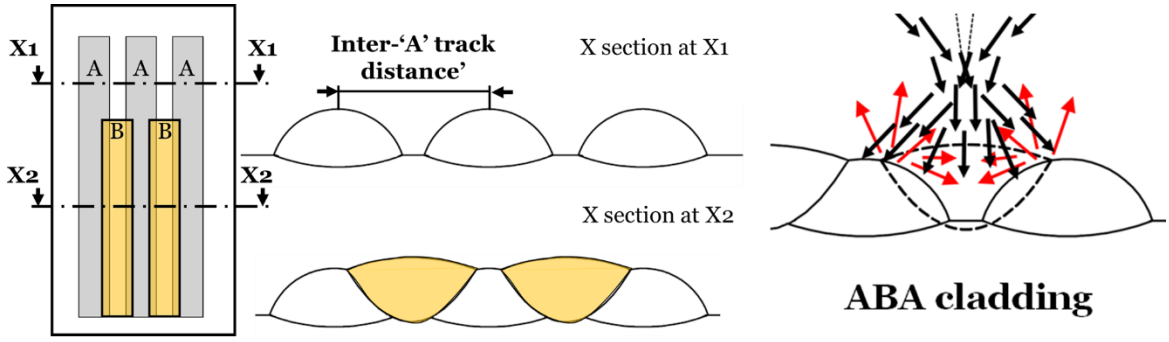

Figure 8.3 A cross-sectional view of ABA cladding, where parallel 'A' tracks are laid first, and the gaps between them are filled with parallel 'B' tracks. A schematic illustration of the powder particle escape pathway in ABA cladding.

8.4 Productivity in ABA laser cladding

During the laser cladding process, powder catchment is fundamentally determined by the amount of powder that enters the cladding melt pool and becomes a clad track. Throughout this section, quantitative information is presented concerning the paths taken by powder particles as they enter or exit from the melt pool. Some of the powder will inevitably bounce off the solid material surrounding the melt pool, resulting in 'waste.' As a result of this waste, the process is less productive. To monitor the directions of flight of powder particles away from the melt pool area, high speed imaging videos of the cladding process were analysed using specially developed software. Laser power, cladding speed, powder feed rate, and other factors can affect the size and shape of the melt pool surface. For three different cladding techniques, such as single-track cladding (A tracks), standard overlapping track cladding (AAA cladding), and ABA cladding, a comparison has been made between melt pool shape and escaping powder particles. It is important to note that, the melt pool surface is the collection area for the cladding powder, and the shape of the pool and the movement of the powder particle can be affected by a number of parameters, including cladding speed and inter-track spacing. Tracks were created with an inter-track spacing ranging from 2 mm up to 4 mm. In order to compare clads of A, AAA, and ABA, were conducted at a speed of 0.7 m/min and inter-track distance of 2.8 mm. In order to further investigate ABA cladding, the ‘B’ clad processing speed was varied between 0.7 and 1.5 m/min.

8.4.1 A study of powder catchment behaviour by detecting powder particles

Single frames from the HSI video illustrates (Figure 8.4) the laser-material interaction zone in single 'A' cladding, traditional AAA cladding, and ABA cladding. The cladding process appears to be moving towards the viewer in this photograph. The program developed is used to identify powder particles, as well as powder particle velocity vectors. Using software analysis of the HSI video, the percentage of powder entering the melt pool can be determined, which is known as the powder catchment efficiency. It is evident from the figure that the majority of the powder stream is entering the melt pool and a small proportion of the particles are, however, flying away from the area after bouncing off the solid material surface.

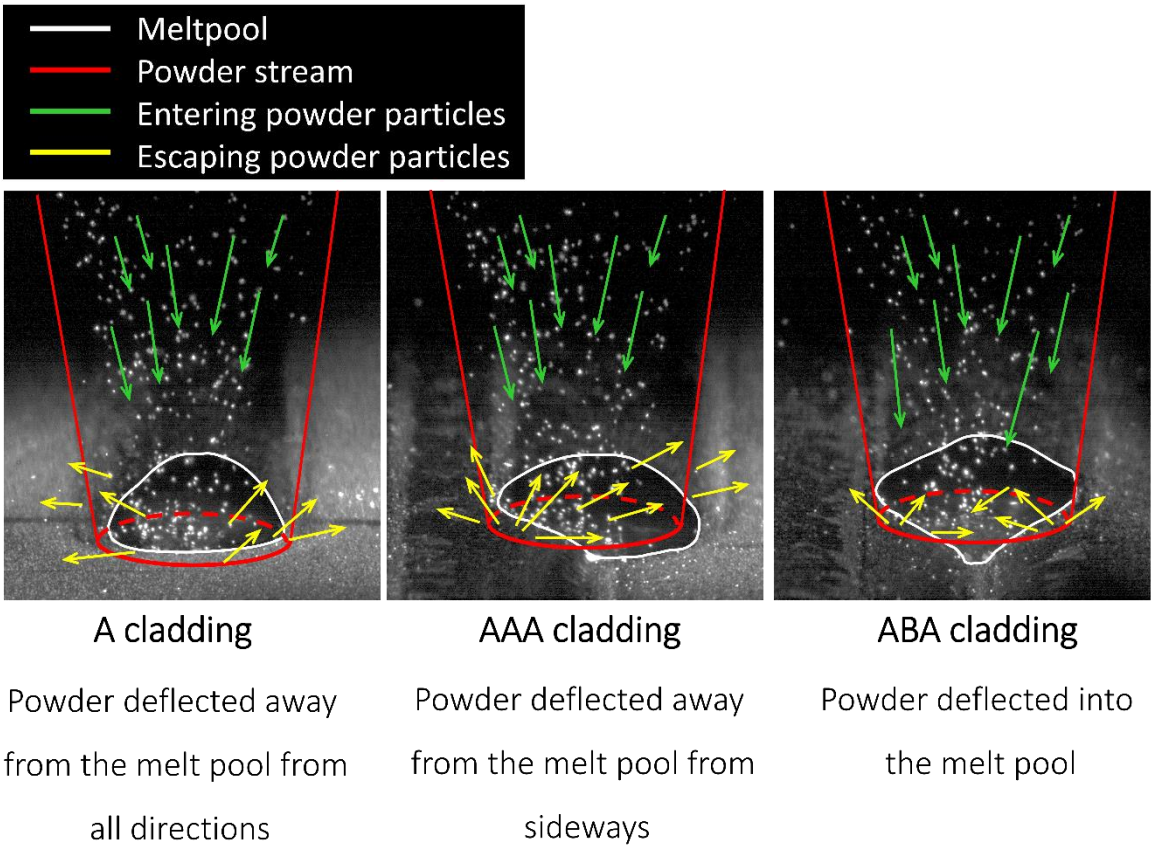

Figure 8.4 The behaviour of powder escape in single A, traditional AAA and the new ABA cladding

In the case of clad tracks produced on a flat surface, A cladding, the melt pool is symmetric about the central axis in the direction of the cladding. Likewise, its width is greatest near the front, near the laser beam, and narrows behind it as the melt pool solidifies inwards from its outer edges. It is the shape created in all the A tracks laid down in the ABA cladding as well as the first track in the AAA cladding. In consequence of the track being deposited on a flat surface, powder particles are seen to escape in all directions.

It has been observed that the melt pools of the tracks following this single track in AAA cladding have a completely different shape. In this instance, the track has overlapped with the previous one (being generated on the ‘shoulder’ of the previous track) and it is evident that the melt pools are not axially symmetrical. On the right-hand side of the flat surface of the substrate, the melt front is slightly ahead of the powder jet. A possible explanation for this could be that melt pours downwards and forwards from the sloped melt pool. Consequently, the melt pool's shape is distorted, resulting in a higher proportion of powder impacting the solid material surface. Also, the melt pool/powder stream overlap is reduced as well as the powder catchment efficiency. The figure also shows that the direction of travel of the 'wasted' powder particles is heavily biased towards the right.

In Figure 8.5, the ABA melt pool shape represents only the B track melt pools. In this case, the geometry of the pool is symmetrical but has a greater degree of complexity than in the case of the single 'A' track. As can be seen from the figure, the melt front is slightly ahead of the powder stream for ABA cladding in the central part of the melt front. Due to the geometry of the melt pool, liquid tends to flow into the valley between the adjoining 'A' tracks, and downhill to extend the melt pool into the region yet to be irradiated by the laser. Because of the symmetry of the melt pool and surrounding solid geometry, the left- and right-hand directions of powder escaping are equally balanced. It should be noted that, for ABA cladding only, bouncing off of either of the A clad shoulders may cause the powder particles to be re-directed into the meltpool, instead of being lost from the process. This mechanism could result in higher powder catchment efficiency.

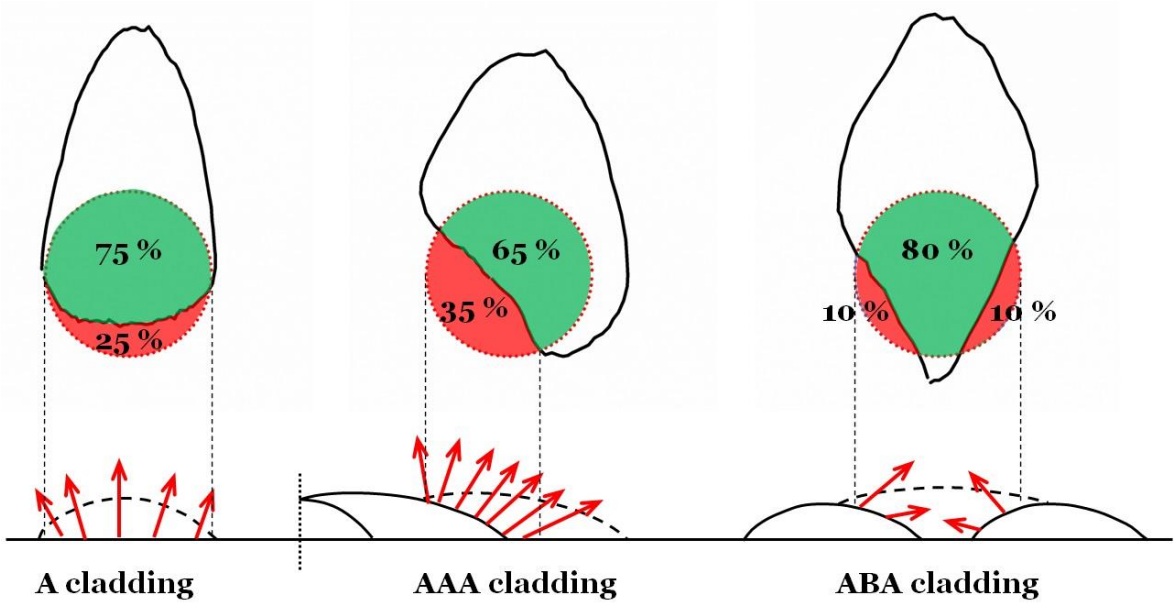

Figure 8.5 The following plan views show melt pools in single 'A', traditional 'AAA' and 'ABA' claddings in relation to the powder streams. Measurement of powder catchment efficiency (green) and the proportion of particles escaping from the cladding zone (red).

The Figure 8.5 shows the plan view of the cladding melt pools in A, AAA and ABA cladding, with dotted circles indicating the location and area of the incident powder stream. Based on the figure, information is provided regarding the percentage overlap between the powder stream and the melt pool. Those particles that enter the meltpool are designated as green, while those that exit its meltpool are designated as red. Since the input powder is effectively a vertical stream, plan views of the melt pools were chosen. For all three types of cladding ('A', 'AAA', 'ABA'), Figure 8.6 illustrates the proportion of powder escaping the process zone and the direction of travel taken. The information presented here is presented as a semicircular histogram of powder wasted based on flight direction.

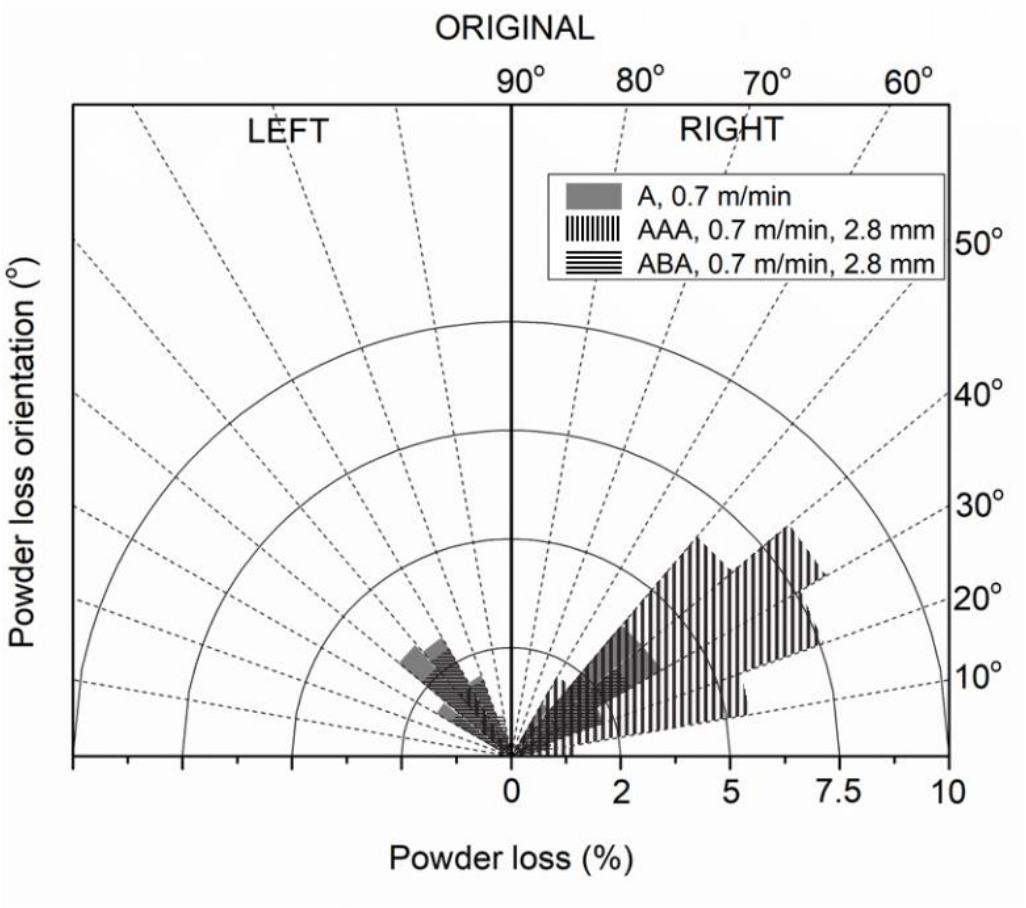

Figure 8.6 Wasted powder amounts and flight directions for cladding types 'A', 'AAA', and 'ABA'.

The main results from Figure X and Y are listed as follows:

- A cladding, the powder particles spread out in all directions (symmetry).
- AAA cladding, the powder deflected away mainly in one direction (asymmetry).
- ABA cladding, the powder particles spread evenly sideways and deflected most of the powder into the meltpool (symmetry).
- That more powder is escapes from ‘AAA’ cladding process than from solo ‘A’ tracks, and the most powder efficient process is ‘ABA’ cladding.

The Figure 8.7 shows the results of this measurement and shows the general directions of travel left and right. Based on the figures, it is clear that the powder catchment efficiency of the AAA process (64.61%) is lower than that of single track ‘A’ cladding (76.03 %) at the same cladding speed (0.7 m/min), as well as lower than the ABA cladding process (80.23 %) at the same cladding speed (0.7 m/min) and inter-track distance (2.8 mm). There is equal exposure of powder in each direction in A cladding, and the altered cladding speed has no effect on the direction of escaping powder particles.

In AAA cladding, the powder particles disposed of as 'wasted' travel in a direction heavily skewed towards to one direction. Because the 'shoulder' of the previous solidified track is an inclined surface, particles are likely to be deflected more likely to one direction. Since the melt pool does not have an axi-symmetric shape, this is not an unexpected result. By increasing the intertrack distance, the AAA clad shape will more resemble a single A clad shape and by depositing the clad track on a flat surface, the directionality of the escapee powder particles will return to symmetry.

In the case of ABA cladding, the improvement over AAA cladding is quite evident, with one result demonstrating a powder catchment efficiency of 92%. Due to the symmetry of the melt pool and surrounding solid geometry, the left- and right-hand directions of powder travel are equally balanced. As a result, rebounding particles in ABA cladding tend to return to the melt pool, whereas in AAA cladding, particles tend to leave the area of laser-material interaction. Increased overlap between the power stream and meltpool area can explain the improved powder catchment efficiency, as a higher proportion of particles impact the meltpool as opposed to surrounding solid material.

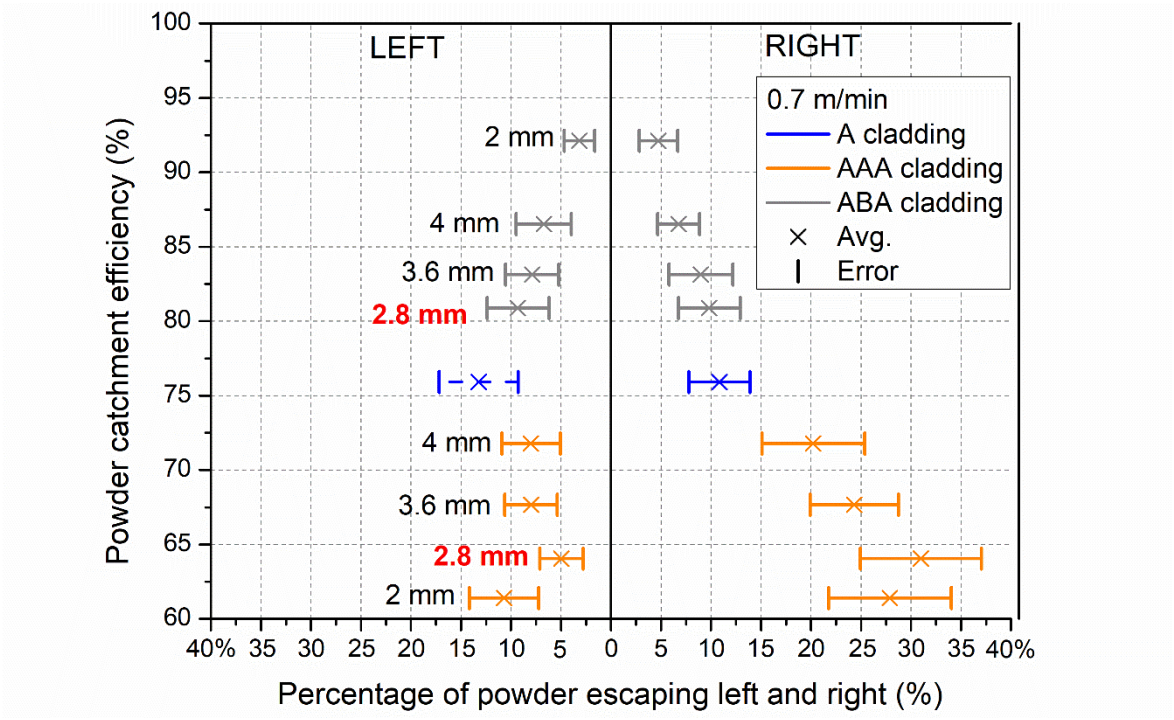

Figure 8.7 Measurements of the powder catchment efficiency of single track A, traditional AAA and new ABA cladding as a function of cladding speed and inter-track distance, and the proportions of particles escaping from the cladding zone in the general left and right directions.

8.4.2 Analysis of the melt pool powder catchment behaviour

In laser cladding the area coverage rate of the process can be improved by increasing the process speed or by decreasing the number of tracks per unit area, which involves an increase in inter-track distance. There is therefore a desire to determine whether an increase in inter-track distance can improve powder catchment efficiency. Figure 8.8 and Figure 8.9 show melt pool maps for AAA and ABA cladding at a process speed of 0.7 m/min with inter-track distances of 2, 2.8, 3.6 and 4mm.

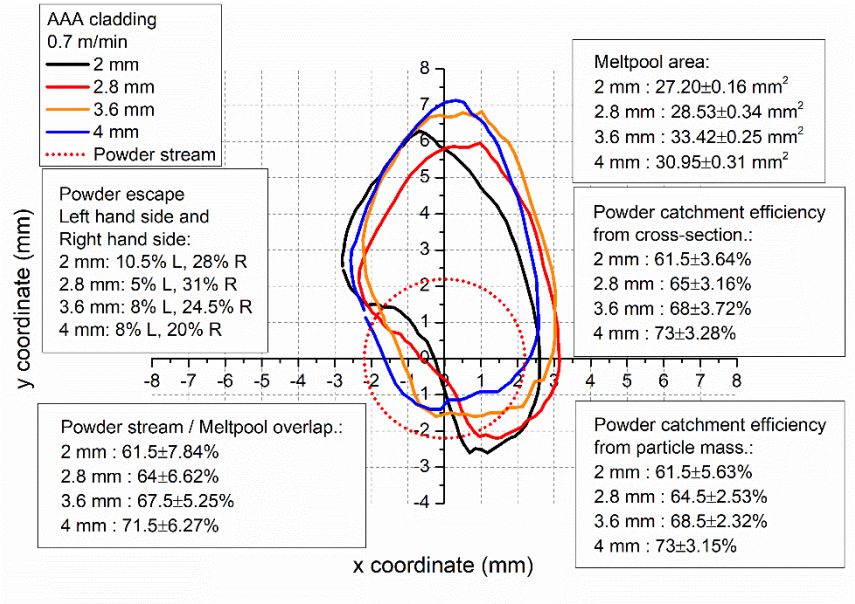

Figure 8.8 Melt pool maps for AAA cladding concerning increasing inter-track distance.

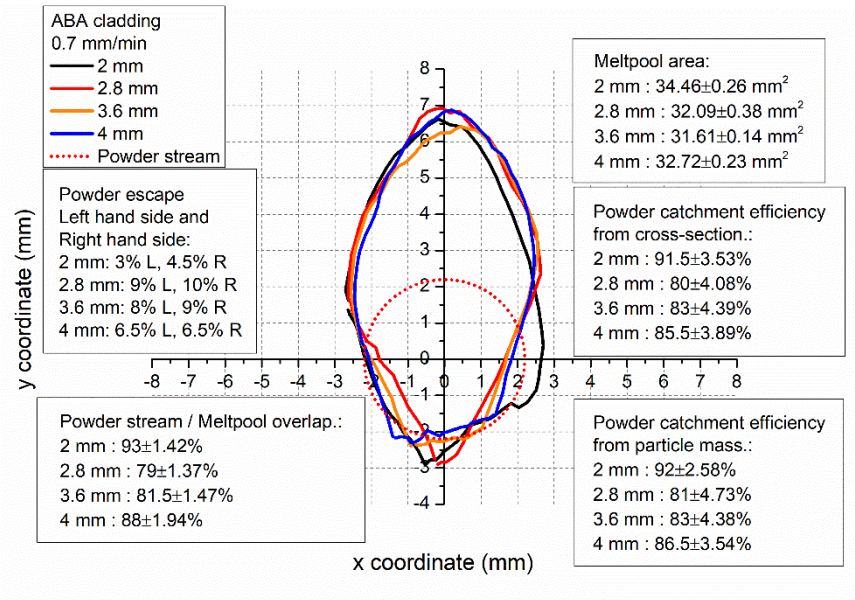

Figure 8.9 Melt pool maps for ABA cladding concerning increasing inter-track distance.

According to AAA melt pool maps, the late start of the melt front on the track overlap side of the pool is most pronounced at smaller inter-track distances. As the inter-track spacing is increased, this effect is diminished because more of the flat substrate surface is exposed to the melt pool, which resembles a solo 'A' track. ABA melt pool maps present similar information regarding the late start of the melt on both sides of the leading edge.

According to the AAA cladding process, the melt pool area gradually increases as the inter-track distance increases and the melt pool initiation delay due to slope of the previous track diminishes. In the case of the ABA clad B pools, there is no clear trend in pool size with increasing inter-track distance, despite the fact that B pools are generally larger than AAA pools. In addition, the B tracks of this data set have better deposition rates than the initial or subsequent A tracks.

Using the same processing parameters, Figure 8.10 represents a comparison of melt pool shapes in single A, traditional AAA and new ABA cladding.

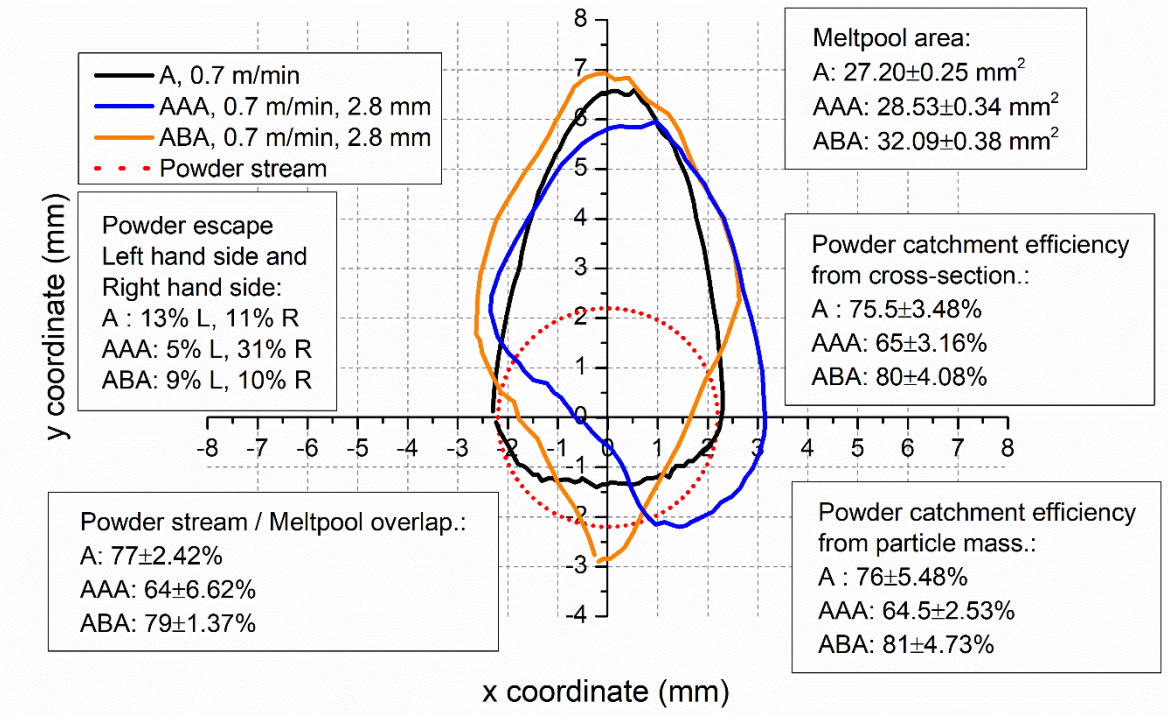

Figure 8.10 A comparison of melt pool shapes for different laser cladding interaction types using the same processing parameter.

In AAA cladding, there is a considerable difference in melt pool shape and powder catchment efficiency between the initial track and subsequent tracks. Based on the geometries and positions of the melt pools and surrounding solid material in each case, ABA cladding had significantly greater powder catchment efficiency than AAA cladding.

8.5 Further enhancement of productivity by utilizing different parameters for A and B parameters in ABA cladding

The previous section focused on the comparison of AAA and ABA cladding in terms of process efficiency, in particular powder catchment efficiency. A potential advantage of ABA laser cladding in comparison with traditional AAA cladding is investigated by increasing the speed of the B clad process in order to further improve powder catchment efficiency. Particularly, this section compares the two methods in terms of powder catchment efficiency, deposition and coverage rates, surface waviness, and total material waste. The process speed of the B clads was varied from a value of 1.0 m m/min to 2.0 m/min. Samples were created with a variety of inter-track spacings.

The Figure 8.11 illustrates a comparison of powder catchment efficiency for AAA and ABA claddings with the same A and B clad speeds as well as with increased B clad speeds.

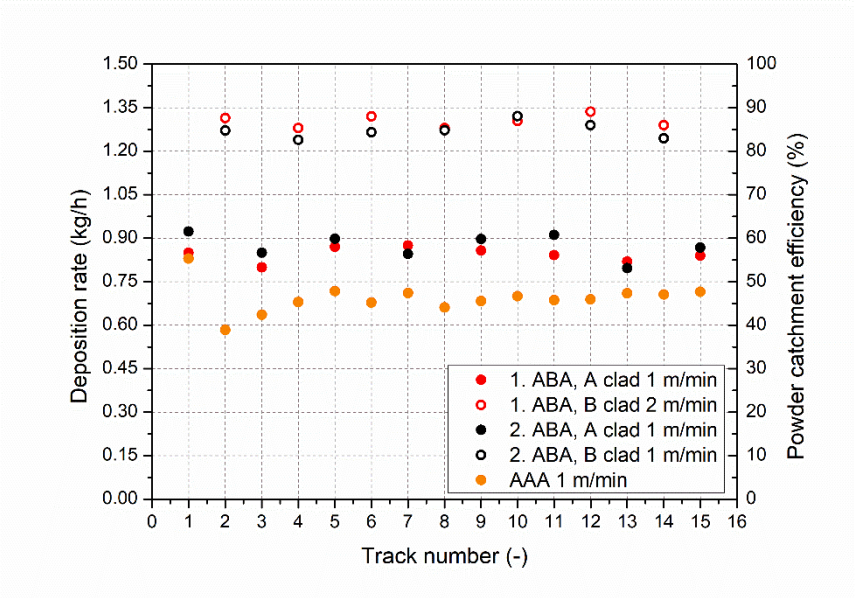

Figure 8.11 A comparison of powder catchment efficiency for AAA and ABA cladding with the same A and B clad speeds as well as with increased B clad speeds.

The initial 'A' track of the 'AAA' cladding has a greater powder catchment efficiency of 57% than any of the subsequent ‘AAA’ tracks. In the second track, the efficiency of the powder catchment is only 35%, while after the first four tracks, the process becomes stable, with an average efficiency of 45%. Using same parameters for the 'A' tracks, the powder catchment efficiency of the AAA cladding was considerably less than that of the 'ABA' cladding. Because all 'A' tracks have the same melt pool geometry, there is no need to establish a build-up to a stable track geometry for ABA cladding. Furthermore, in almost all cases of 'ABA'

cladding, it has been found that the powder catchment efficiency when laying down the 'B' tracks is much higher than when laying down the 'A' tracks. As a result, ABA cladding has always had a greater overall powder catchment efficiency than AAA cladding. As the melt pool is effectively held in a valley between two previously deposited 'A' tracks, the 'ABA' cladding creates a very effective powder catchment geometry for the 'B' tracks.

8.5.1 Deposition rate and powder catchment

As shown in the Figure 8.12, the overall deposition rate and powder catchment efficiency in AAA and ABA cladding are calculated using different inter-track distances and different cladding speeds (in ABA, the average cladding speed of the A and the B). On the basis of the graphs, it can be concluded that the average cladding speed (or an increase in B clad speed in ABA) does not have any effect on the overall deposition rate or the powder catchment efficiency. In the case of narrow inter-track spacing, melt pool geometry can change; as a result, the melt front flow towards the cladding direction. Thus, the powder particles that escape the front of the meltpool will now be directed to the meltpool, which would positively impact powder capture efficiency. In previous sections in 8.4.1 and 8.4.2, we discussed how different inter-track distances affect powder catchment efficiency. Nevertheless, the increased speed of B clads and the optimized intertrack distances may further improve the overall coverage rate of the process by altering the clad cross section geometry in a manner that makes the clad surface uniformly flat. As a result, less post-processing machining is required on the clad surface, and a higher B clad speed can result in a shorter process time.

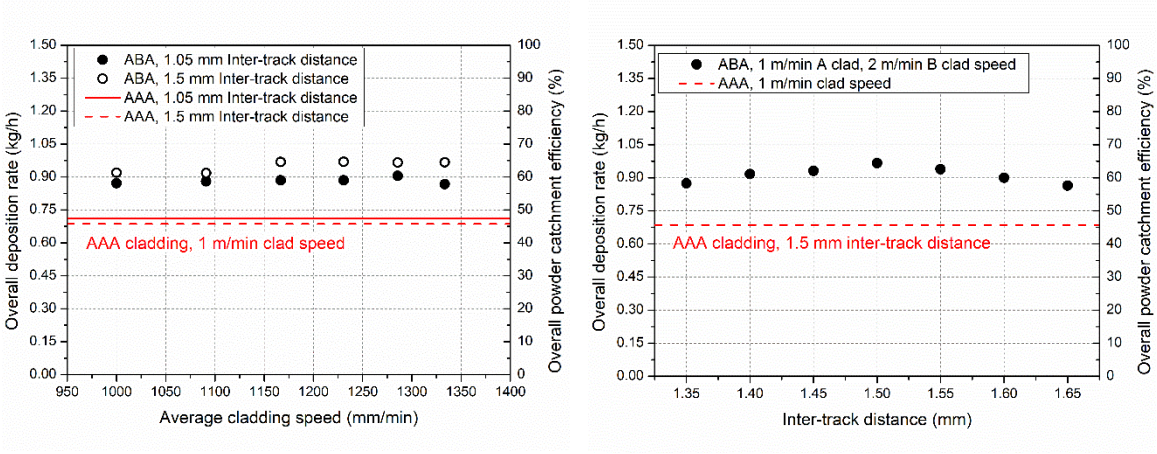

Different cladding speed **Different inter-track distance**

Figure 8.12 Comparing AAA and ABA cladding, the overall deposition rate and powder catchment efficiency were examined with respect to different B clad speeds and different intertrack distances.

8.5.2 Surface waviness

As a result of the improved powder catchment of the 'B' tracks of the ABA cladding, 'B' tracks will have a larger cross-section than 'A' tracks if the same process parameters are used for both types of tracks. Consequently, the clad surface may become uneven and ridged. An optimized cladding process can result in a flat surface, thus minimizing post-processing costs. Two factors are responsible for determining the post-processing cost, namely the surface waviness (the amount of material that needs to be removed in order to produce a flat surface) and powder loss efficiency during deposition (powder particles which does not enter the melt pool). The cladding speed for the 'B' tracks has been increased in order to level out the surface. Additionally, this strategy increases the overall coverage rate as well. The Figure 8.13 represents the surface waviness with different cladding speeds (in ABA cladding, the average cladding speed of the A and B clad) and different inter-track distances. According to the figure, using the same processing parameters as for A and B clad in ABA cladding results in a higher surface waviness (527 µm) than AAA (308 µm) cladding. The anomaly can be explained, in part, by the higher powder catchment efficiency and deposit rate, which is caused by the advanced meltpool geometry of the B clad, which results in a larger cross-section geometry, which results in a more concave surface. Nevertheless, it is possible to change the concave shape by increasing the speed of the B clad and thereby producing a more even surface (89 µm) between the previously laid A clad tracks. This makes the ABA cladding process a more beneficial application due to improved powder capture efficiency and reduced surface waviness (material waste). An alternative approach would be to change the inter-track distance between the A tracks in order to change the B clad cross-section geometry. In addition, this can result in a flat clad surface or it could result in a convex form, which is not beneficial.

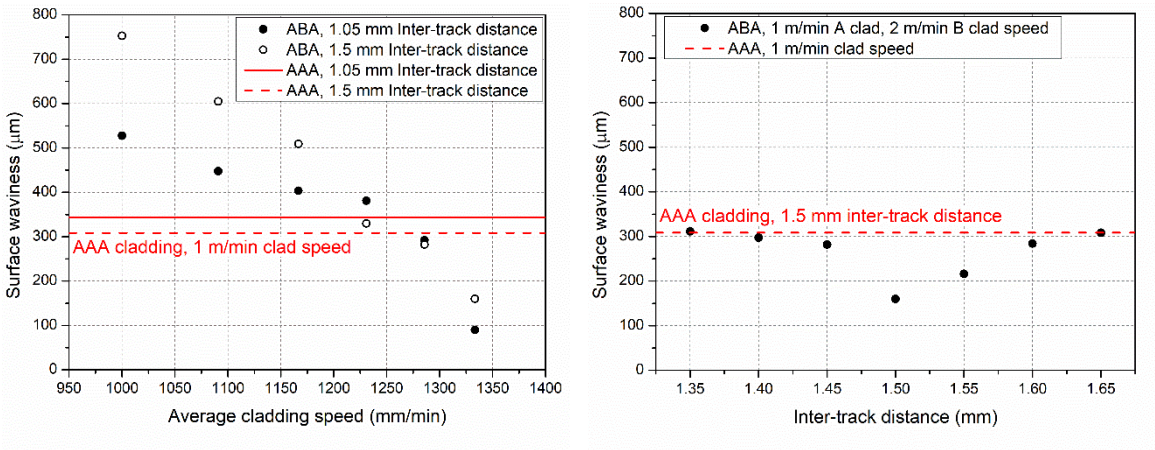

Different cladding speed **Different inter-track distance**

Figure 8.13 The surface waviness for different cladding speeds (in ABA cladding, the average cladding speed between A and B cladding) and different inter-track distances in AAA and ABA cladding.

8.5.3 Useful volumetric coverage rate

The Figure 8.14 illustrates the useful volumetric coverage rate in AAA and ABA cladding for different cladding speeds (average cladding speed for A and B in ABA cladding) and different inter-track distances. Based on inter-track distance, average cladding speed, and useful clad thickness (clad layer after post-processing), the useful volumetric coverage rate was derived. In the figure, it can be seen that the use of the same processing parameters in AAA and ABA cladding, ABA produces higher coverage rates, although, as was mentioned earlier, ABA cladding exhibits a greater degree of surface waviness than AAA cladding. Several factors could explain this phenomenon, including a higher deposition rate and powder catchment efficiency, which resulted in a higher concentration of B clad deposition, which led to a greater height of the clad layers (1.9 mm) as well as an increase in surface roughness (520 µm). However, after post-machining, the final layer thickness (1.37 mm) of the ABA clad was higher than that of the AAA clad (1.24 mm), where the clad height was 1.58 mm, and the surface roughness was 343 µm only. As a consequence of increasing the B clad speed from 1 m/min to 2 m/min, the coverage rate could be increased from 21 mm^3/s to 33 mm^3/s, increasing the process productivity by 1.5 times. It is possible to increase the coverage rate by applying different inter-track distances as well. The efficiency of the process could also be enhanced by the fact that "ABA" cladding involves a wider spacing between the tracks than "AAA" cladding, due to the nature of the process. This could result in fewer tracks being required to cover a particular area.

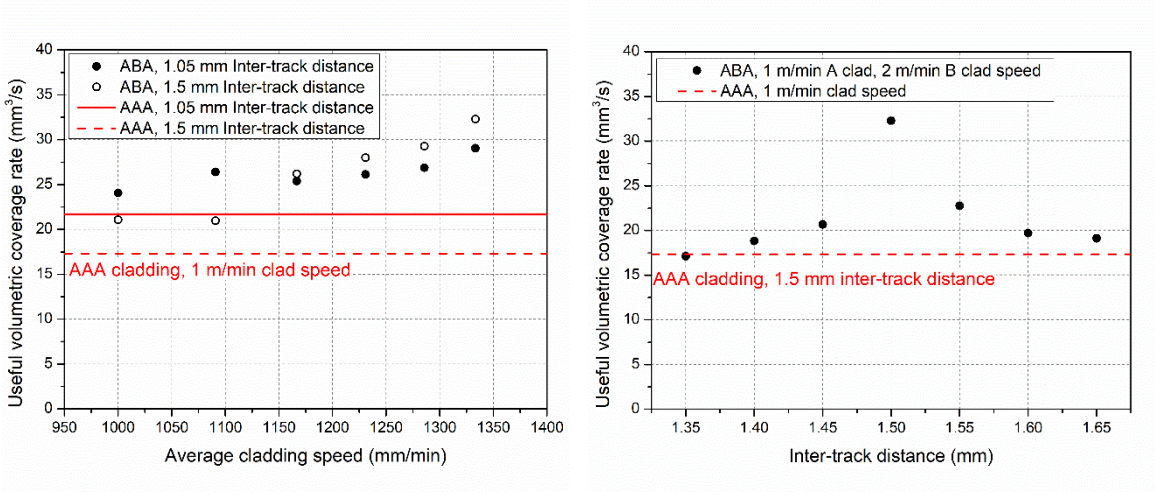

Different cladding speed **Different inter-track distance**

Figure 8.14 The useful volumetric coverage rate in AAA and ABA cladding for different cladding speeds (average cladding speeds for A and B in ABA cladding) and different inter-track distances.

8.5.4 Total material waste

Based on the different cladding speeds (average A and B cladding speeds in ABA) and different intertrack distances, the Figure 8.15 represents the total material wasted during the deposition of AAA and ABA cladding. Total material waste was calculated from waste from post processing waste (the material waste which needs to be removed to achieve the final layer thickness) and the waste from powder escape. In each laser cladding technique, the total material waste gives information regarding the quantity of material wasted in kg per square meter. Due to the higher powder catchment in ABA cladding compared to AAA cladding, less powder is escaping from the interaction zone, resulting in less powder waste. Furthermore, the effective thickness of the ABA cladding was greater than that of the AAA cladding, resulting in less material being removed during the post-processing process. Therefore, it can be concluded that ABA cladding has a lower total amount of material wasted during deposition. A significant benefit of this improvement would be that it could reduce the powder recycling and minimize the amount of expensive alloy powder being wasted. Considering the results of AAA and ABA cladding with the same intertrack distance of 1.5 mm and the same cladding speed of 1 m/min. AAA cladding resulted in a total material waste of 13.6 kg/m^2 whereas ABA cladding resulted in a total material waste of 12.1 kg/m^2. This means that if the same process conditions are applied, but only the cladding type is changed from traditional cladding to ABA cladding, the total material waste can be reduced by around 1 kg per square meter.

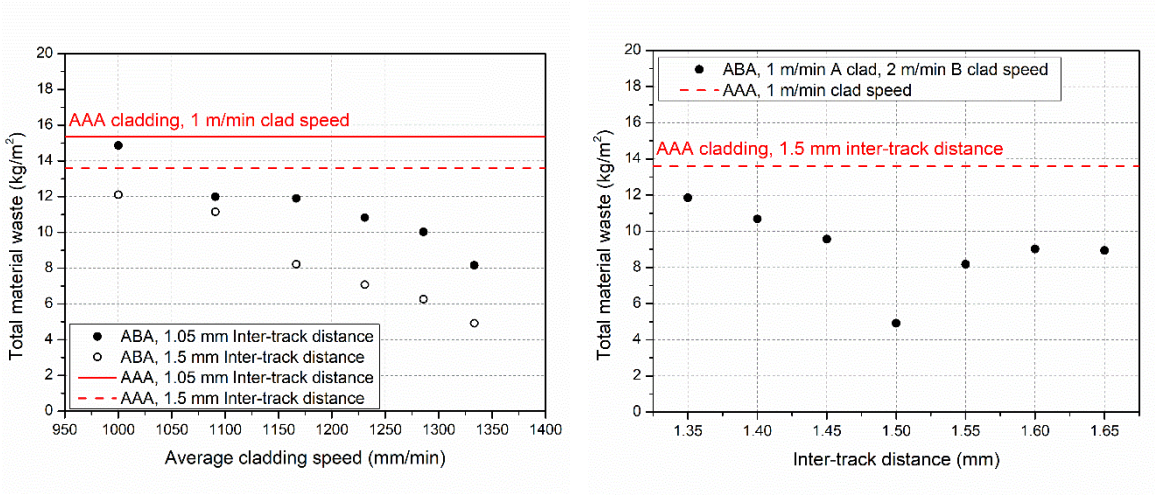

Different cladding speed **Different inter-track distance**

Figure 8.15 The amount of material wasted during the deposition of AAA and ABA cladding is related to cladding speed (average A and B cladding speeds in ABA) and intertrack distances.

It has been shown that increasing the speed of the B clad from 1 m/min to 2 m/min (using an average cladding speed of 1.3 m/min) can reduce the total material waste from 12.1 kg/m^2 to 4.4 kg/m^2. It not only results in significant reductions in the amount of expensive materials that will be removed/escaped, but also in a reduction in the overall processing time as a result of the high cladding speed of B clads. ABA cladding enhances the volumetric coverage rate while reducing waste material and processing time, which enhances the overall productivity of the process by making it a viable cladding technique for industrial applications.

8.5.5 Cross section geometry

Industry attempts to produce an ideal clad track geometry in industrial applications. For an ideal clad track shape, the clad should have low dilution but enough adhesion, sufficient clad height (application dependent), wide clad, flat top surface geometry that does not require further post-processing, and perpendicular sides. While these factors are considered ideal, it is not possible to produce the ideal clad track. The principal research question is what sort of clad geometry can we achieve that is close to the ideal clad geometry. In real life circumstances, it may be possible to achieve low dilution, a suitable clad height, and wide clad tracks by modifying the processing parameters; however, the actual real clad requires post-processing work in order to achieve the desired final product. In the engineering field, these factors are extremely important since there is an ongoing effort to reduce the cost of engineering parts. The purpose of this section is to provide further information on the ABA cladding in regarding of the cross section geometry of the clad. In the Figure 8.16, an illustration is shown of single and overlapped clads in their ideal and actual states.

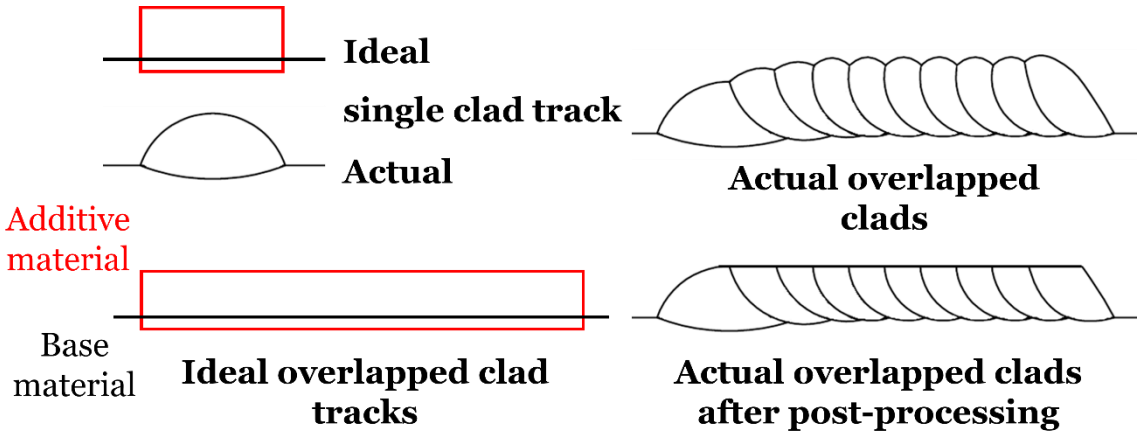

Figure 8.16 An illustration of the ideal and actual situation of single and overlapped clads

8.5.5.1 Effect of the cladding speed

The Figure 8.17 depicts the traditional AAA cladding with A clad speed of 1 m/min, ABA with A and B clad speed of 1 m/min, and ABA with A 1 m/min and B 2 m/min. The samples were conducted at a distance of 1.05 mm between tracks. According to the figure, during the traditional AAA cladding, the deposition rate was low at 0.71 kg/h, the catchment efficiency was low at 47.36 %, and the surface waviness was moderate at 343 µm, which was close to being flat. The volumetric coverage rate was 24.6 mm3/sec and the total material waste was 15.37 kg/m^2. Comparing AAA and ABA with the same process parameters, increased deposition rate to 0.87 kg/h, increased powder catchment efficiency to 58.13 %, and high surface waviness of 527 µm with a convex B clad shape geometry. When the same process conditions are used in both AAA and ABA, volumetric coverage rates were 30.27 mm^3/sec, which indicates an increase in coverage rates. Increasing the B clad speed from 1 m/min to 2 m/min, faster average cladding speed, overall deposition rate at 0.86 kg/h and overall powder catchment efficiency 57.8 % remained constant and higher than AAA cladding. With an increased B clad speed, there is a significant reduction in surface waviness at 89 µm. Despite the fact that the total volumetric coverage rate remained constant (from 30.27 mm^3/sec to 30.1 mm^3/sec), the total material waste decreased from 14.86 kg/m^2 to 8.16 kg/m^2, indicating that with increased B clad speed the same volume of clad can be deposited with saving 50% of material.

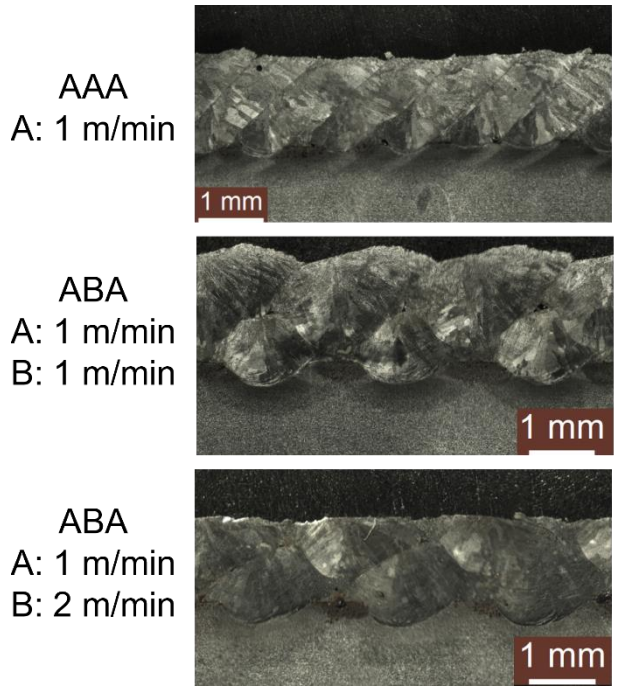

	AAA	ABA	ABA
Average speed (m/min)	1	1	1.3
Deposition rate (kg/h)	0.71	0.87	0.86
Powder catchment efficiency (%)	47.36	58.12	57.8
Surface waviness (micron)	343	527	89
Surface profile	Flat	Convex	Flat
Volumetric coverage rate (mm^3/sec)	24.6	30.27	30.1
Total material waste (kg/m^2)	15.37	14.86	8.16
Process time (h/m^2)	15.87	15.87	11.9

Figure 8.17 The cross-section images of AAA and ABA cladding with same and increased B clad speed. The productivity factors listed in the table.

8.5.5.2 Effect of the inter-track distance

The Figure 8.18 illustrates cross-sectional images of ABA cladding with different inter-track distances with the same average cladding speed. The productivity factors are listed in the table below. As can be seen in the figure, the B clad surface profile has a convex shape when the distance between the tracks is narrow. By increasing the inter-track distance, a flat surface profile can be achieved with a decrease in surface waviness, process time, and a reduction in total material waste. However, as the intertrack distance is increased further, the surface profile geometry changes from flat to concave, resulting in increased surface waviness and increased total material waste.

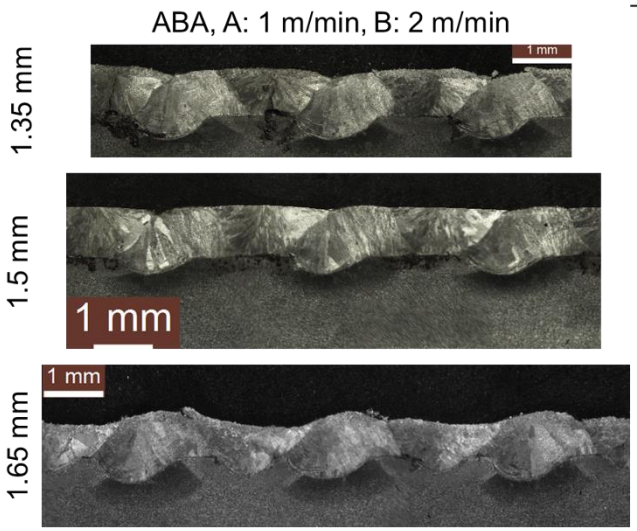

Inter-track distance (mm)	1.35	1.5	1.65
Average speed (m/min)	1.3	1.3	1.3
Deposition rate (kg/h)	0.87	0.96	0.86
Powder catchment efficiency (%)	64.44	58.35	57.63
Surface waviness (micron)	311	120	307
Surface profile	Convex	Flat	Concave
Volumetric coverage rate (mm^3/sec)	30.39	33.56	30
Total material waste (kg/m^2)	11.84	4.42	8.93
Process time (h/m^2)	9.25	8.33	7.57

Figure 8.18 The cross-section images of ABA cladding with different inter-track distances. The productivity factors listed in the table.

8.6 Corrections for chapter VI and VII.

A subchapter has been added to the general discussion chapter where updated versions of graphs are included and explained, which were not included in previous papers. This is due to the fact that the last paper contains the correlation position of meltpool and powder stream / laser beam. The papers have, however, already been published and have been accepted by journal editors who are professionals in the field.

8.6.1 Corrections in chapter VI.

8.6.1.1 Correction for Figure 6.5

The liquid flows forward in AAA and ABA cladding, whereas in single A cladding, the liquid lags behind the laser beam. Figure 6.5 solely represents the differences in meltpool shapes among A, AAA, and ABA cladding. It does not include the location of the laser beam and meltpool shapes. The corrected version of the graph illustrated in Figure 8.19.

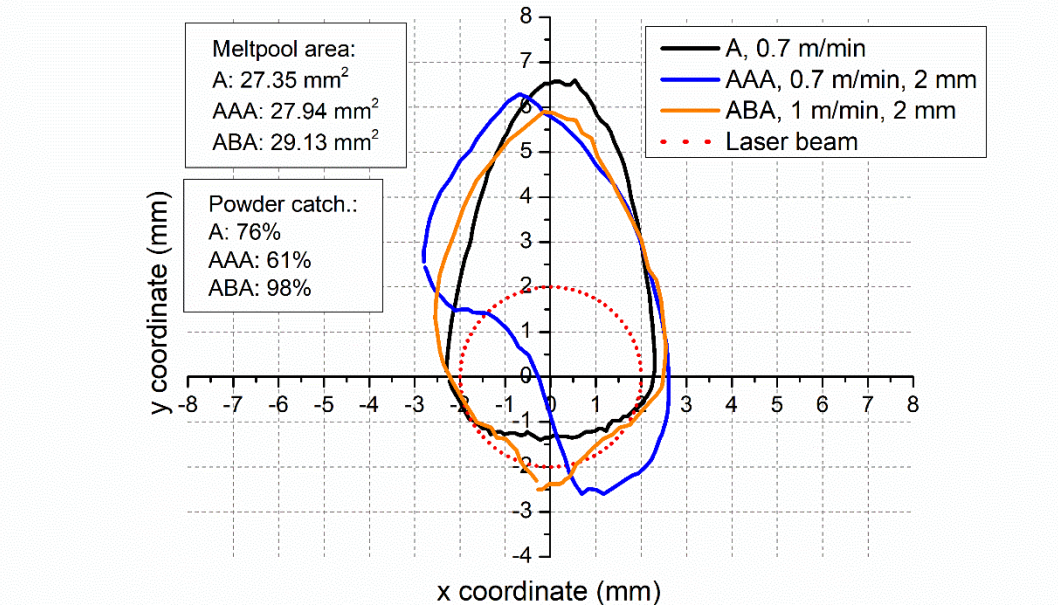

Figure 8.19 Melt pool shapes (plan, or top view i.e. mapped in the plane parallel to the substrate surface) for different laser cladding interaction types. In these maps the part of the melt pool at the bottom of the figure is the front, or leading edge, of the melt pool. (i.e.. The melt pool is portrayed as moving downwards along the y axis in this figure). The laser beam (shown as a dotted circle) is centred on the x,y 0,0 point. The information on the top right gives details of the process speed and inter-track separation distance.

8.6.1.2 Correction for Figure 6.6 and Figure 6.7

Figure 8.20 shows the meltpool and laser beam positions for Figure 6.6 and Figure 6.7 Furthermore, a-b) High speed image frames, c-d) plain view of the meltpool and laser beam in AAA and ABA Cladding

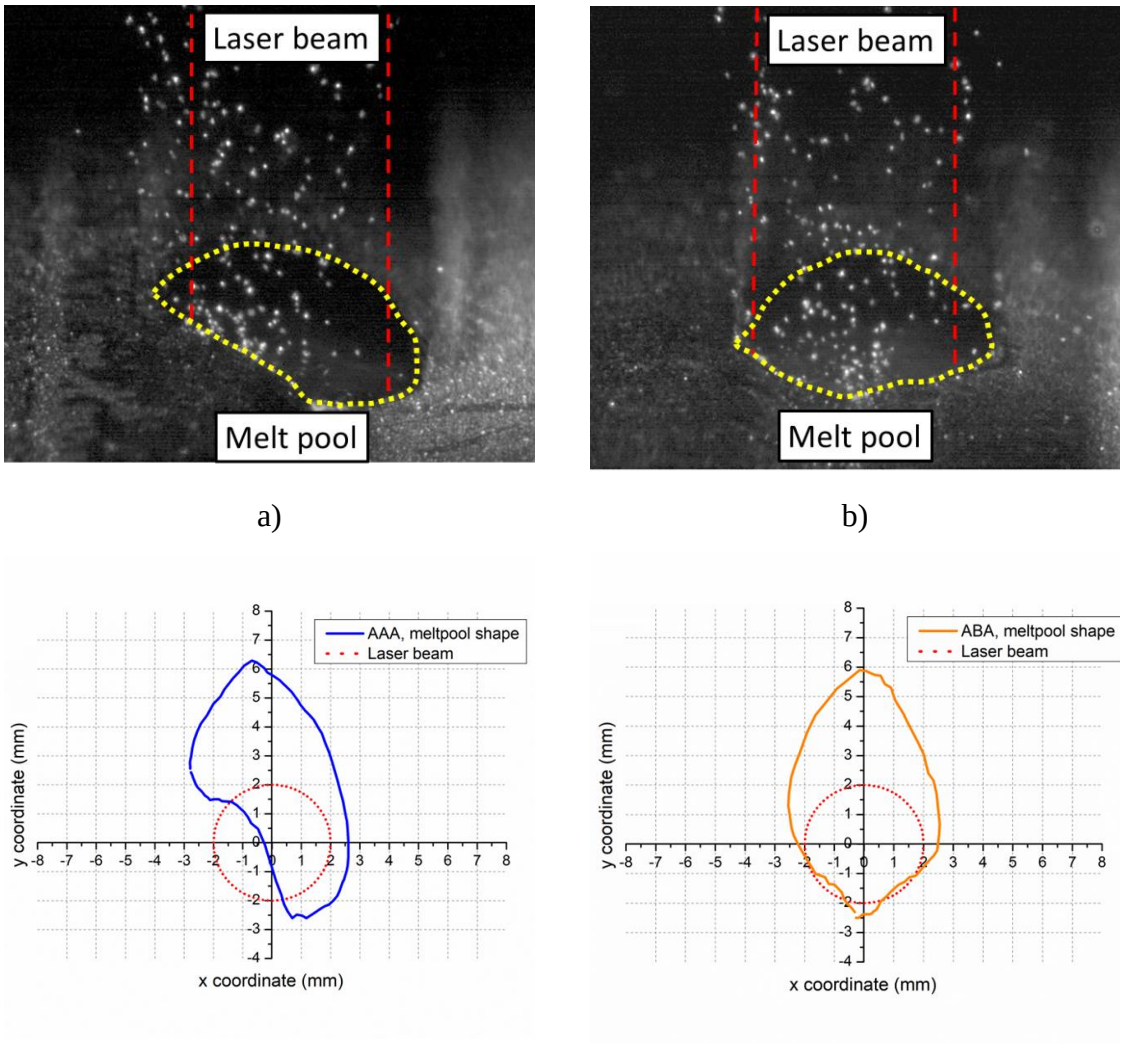

Figure 8.20Interaction Between the Laser Beam and Meltpool in AAA and ABA Cladding, a-b) High speed image frames, c-d) plain view of the meltpool and laser beam.

8.6.1.3 Correction for Figure 6.8

Figure 8.21 shows the corrected meltpool locations and laser beam position for Figure 6.8. Melt pool maps for AAA and ABA cladding with increasing inter-track distances.

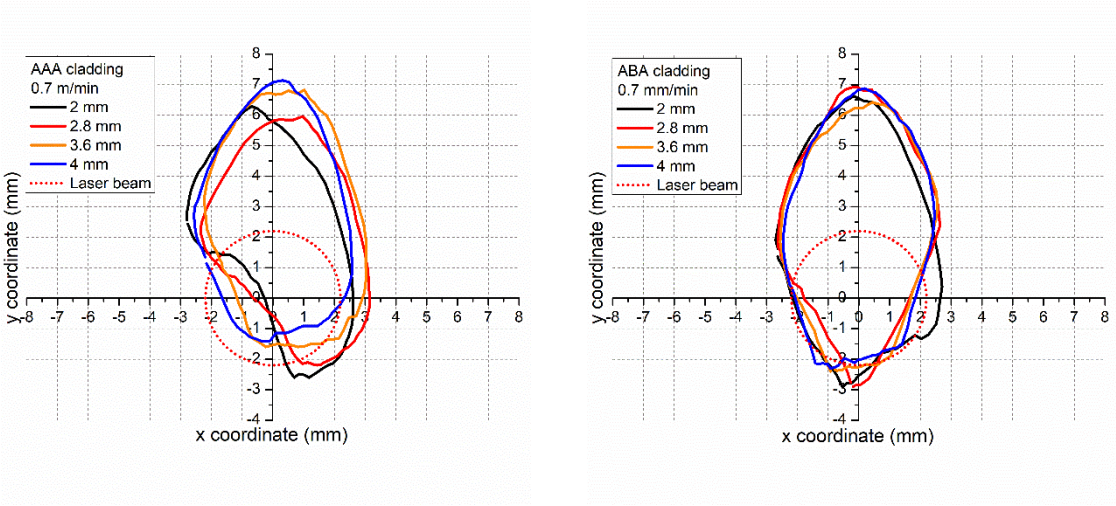

a) b)

Figure 8.21 Melt pool maps for AAA and ABA cladding with increasing inter-track distance.

8.6.1.4 Correction for Figure 6.11

Figure 8.22shows the corrected meltpool locations and laser beam position for Figure 6.11. Melt (plan view) for 'A' tracks as a function of process speed.

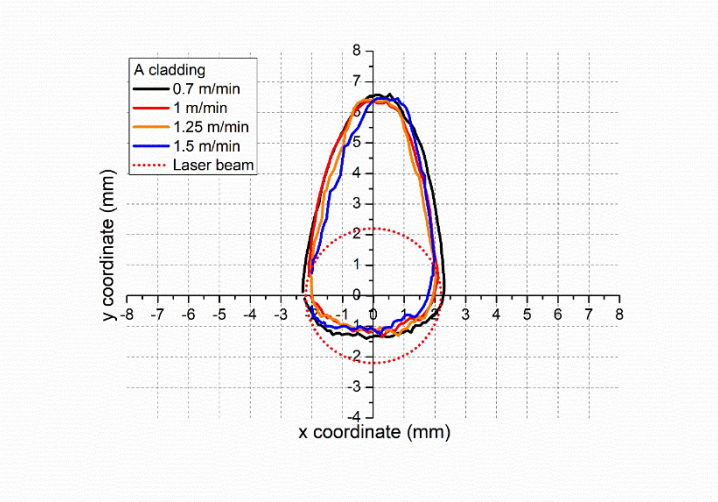

Figure 8.22 Melt (plan view) for 'A' tracks as a function of process speed

8.6.1.5 Correction for Figure 6.14

I excluded the laser beam from the graph to emphasize the correlation between meltpool shapes rather than their relationship to the laser beam. The graph only illustrates shape differences, not the meltpool's location relative to the laser beam. It's important to note that the meltpool isn't smaller than the laser beam; instead, it flows forward.

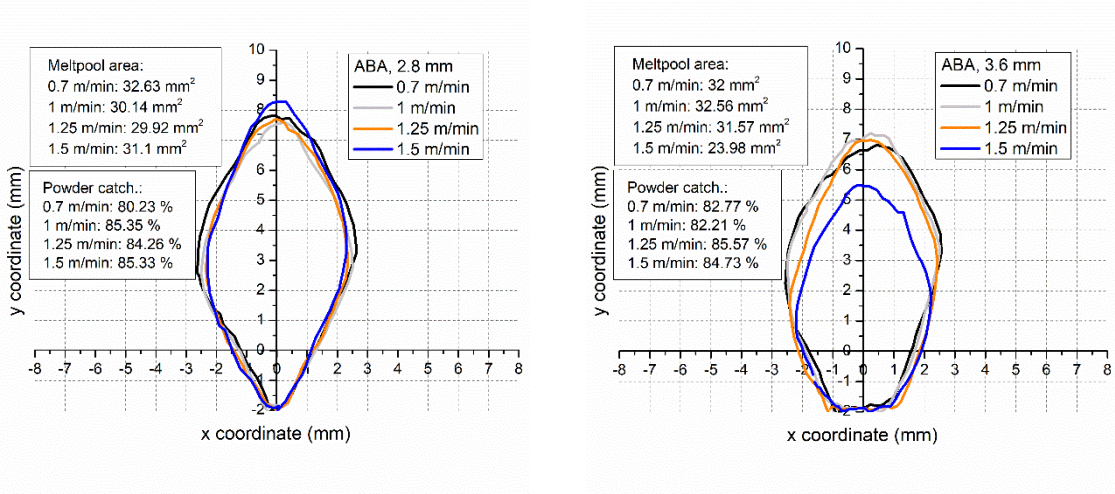

a) b)

Figure 8.23 The melt pool shapes, areas and powder catchment efficiencies for the samples shown in Figure 6.12 and Figure 6.13.

8.6.2 Explanations in chapter VII.

8.6.2.1 Explanation for Figure 7.3

In Figure 7.3 plan views of melt pools in single track ‘A’ cladding as a function of cladding speed. The position and size of the powder stream is indicated as a dotted circle. ‘Powder catchment efficiency from particle mass’ figures is taken from the HSI video analysis.

An illustrative example of a high-speed image frame from A cladding, at a speed of 700mm/min, is provided. In Figure 8.24-a, Frame 1 is displayed, Figure 8.24-b represents Frame 10, and Figure 8.24-c depicts Frame 20. In these frames, three distinct particles are highlighted with different colors (red, yellow, and blue) for easy identification. These images clearly show that these particles come into contact with the substrate in front of the meltpool and are deflected in various directions.

a)

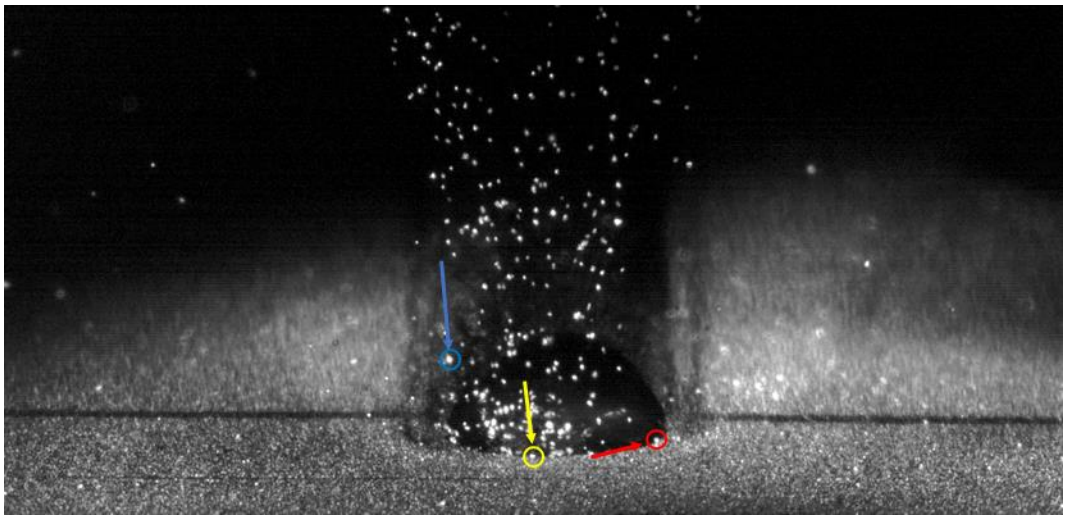

b)

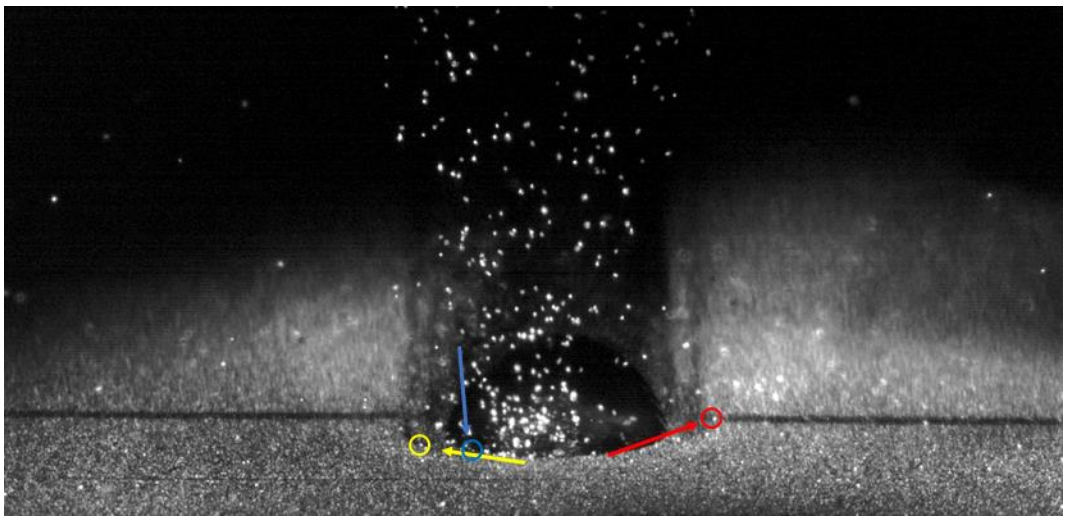

c)

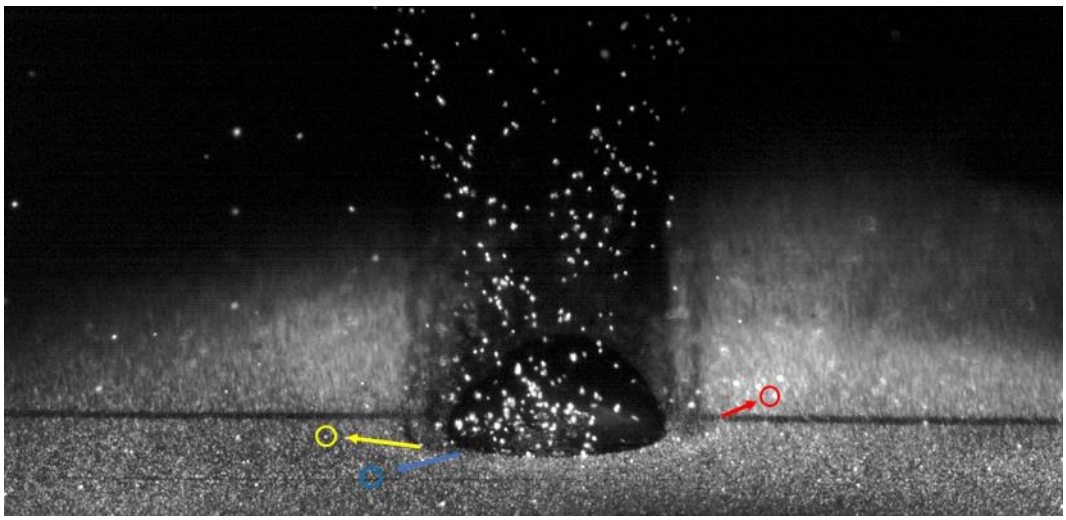

Figure 8.24 An illustrative example of a high-speed image frame from A cladding, with a speed of 700mm/min, is presented. In Figure a, Frame 1 is shown, Figure b corresponds to Frame 10, and Figure c illustrates Frame 20.

8.6.2.2 Explanation for Figure 7.7

In Figure 7.7 plan views of melt pools for ‘AAA’ cladding as a function of inter-track distance. The position and size of the powder stream is indicated as a dotted circle.

According to what was previously stated:

From Figure 7.3 and Figure 7.6 it is clear that the powder catchment efficiency of the ‘AAA’ process (61.5% - 73%) is lower than that of single track ‘A’ cladding (75.5% - 76%) at the same cladding speed (0.7m/min). It can also be seen in Figure 7.7 that the direction of travel of the ‘wasted’ powder particles is heavily biased towards the right-hand side. This makes sense because the ‘shoulder’ of the previous solidified track is an inclined surface will tend to deflect particles towards the right.

An illustrative example of a high-speed image frame from AAA cladding, featuring an inter-track distance of 2 mm and a speed of 700mm/min, is provided. In Figure 8.25-a, frame 1 is displayed, Figure 8.25-b represents frame 10, and Figure 8.25-c depicts frame 20. Within these frames, three distinct particles are highlighted with varying colors (red, yellow, and blue) to facilitate ease of identification. The images clearly demonstrate that these particles make contact with the previously deposited A track shoulder and subsequently rebound in the rightward direction.

When we initially wrote the paper, our primary assumption was that in ABA cladding, powder particles would reflect back to the meltpool from the A-clad shoulders. However, after conducting a more detailed analysis of the data and videos in the subsequent chapter and publishing our next paper, we came to the realization that the primary factor explaining the improvement in powder catchment efficiency in ABA cladding is the meltpool pouring forward, creating a greater overlap between the powder stream and the meltpool. Therefore, the initial statement is no longer accurate in light of our latest research findings.

a)

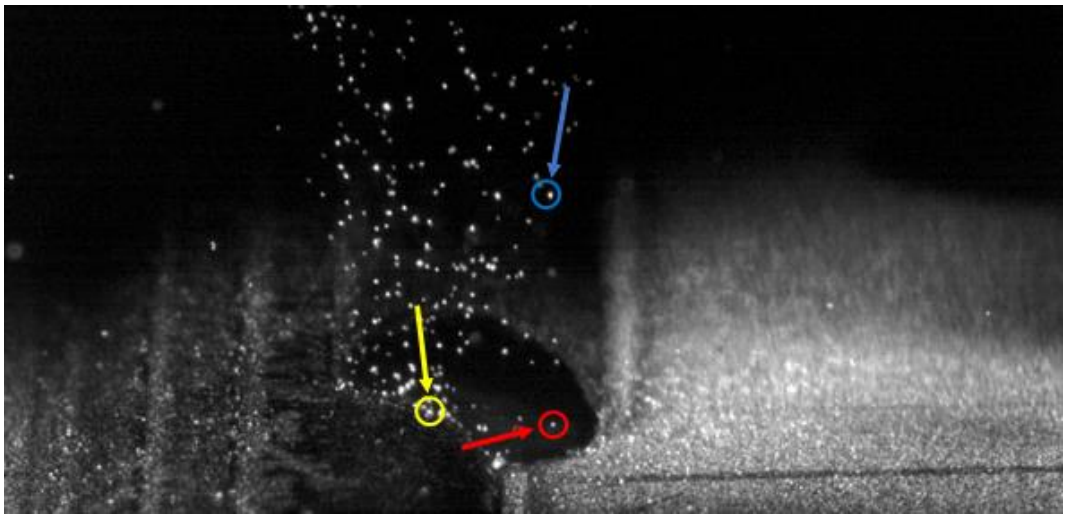

b)

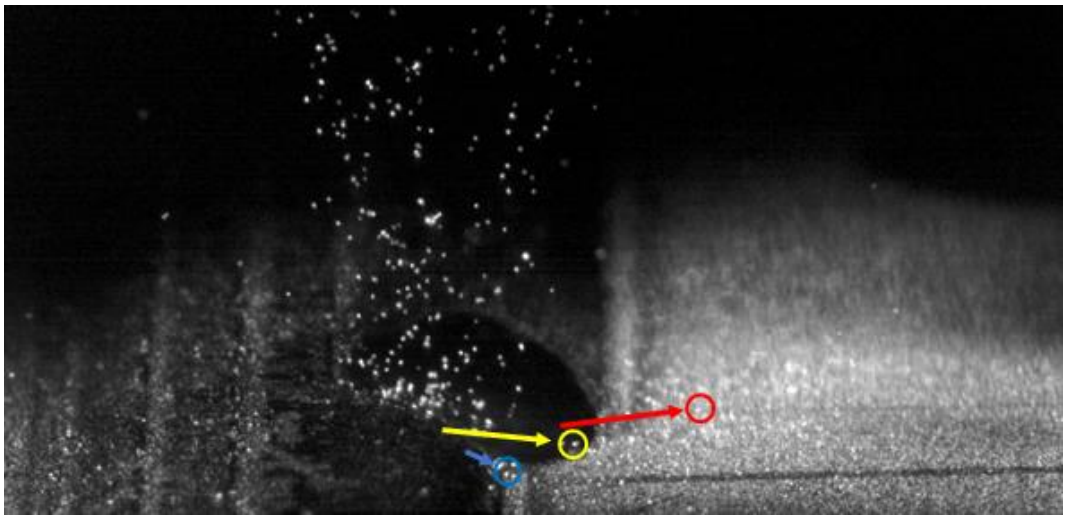

c)

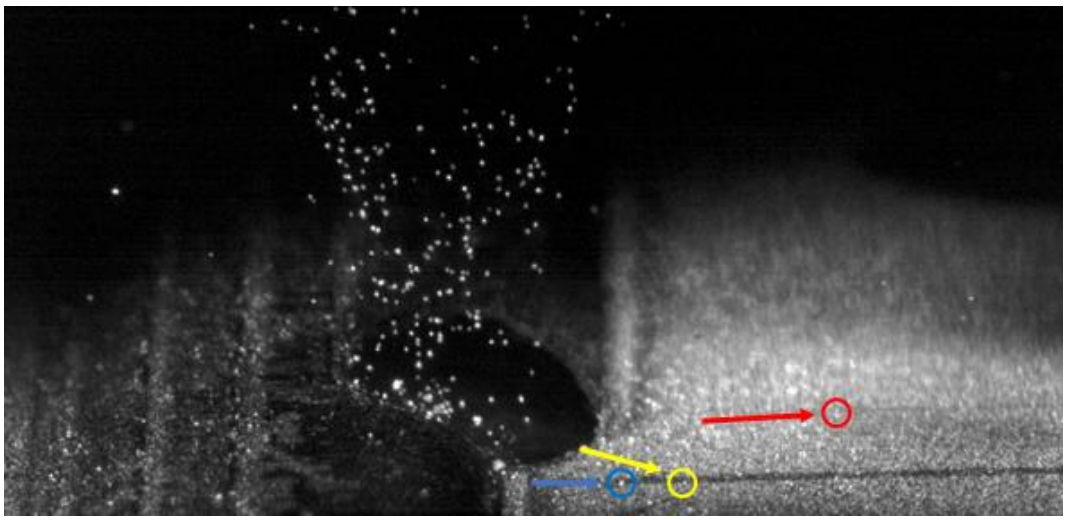

Figure 8.25 An illustrative example of a high-speed image frame from AAA cladding, with an inter-track distance of 2mm and a speed of 700mm/min, is presented. Figure a) displays frame 1, b) corresponds to frame 10, and c) illustrates frame 20.

9 Chapter IX. General conclusion and Future work

9.1 General conclusions

This thesis is primarily concerned with blown powder laser cladding. A major objective of the PhD was to reduce the cost (high productivity) of engineering parts with the required surface characteristics (high quality). The information can be summarised and consolidated into the below key findings:

The thesis provides guidelines and advice for researchers and engineers in the field of laser cladding and related Direct Energy Deposition (DED) techniques, to help establish a standardised approach to quality assessment and productivity metrics. Factors considered are; deposit geometry, porosity, cracking, dilution, build-up/coverage rate and powder catchment efficiency. The following guidelines were addressed for laser cladding and related DED processes. (1) Research into individual clad tracks is of minimal industrial relevance. (2) Fluctuations in clad surface height should be as small as possible to minimise post-cladding machining and areas with insufficient clad material. Height fluctuations should be measured in two orthogonal directions to find the waviness (Rw). (3) Porosity should be minimised and, if possible, eliminated. (4) Cracks should be eliminated (small cracks are generally no better than large cracks). (5) Measure average dilution by the area method. (6) Average dilution should usually be in the target range 3-5% but there are case-specific exceptions. (7) Production time should be minimised within the constraints of adequate quality. (8) Coverage or build-up rate should be maximised within the constraints of required clad thickness. (9) Coverage rates should be given as a compound metric of the form X mm^2/unit time x Y mm (thickness). (10) Powder capture efficiency (Epc) should be maximised and should be a major metric for industrial process validity.

Furthermore, the thesis provides quantitative information about the paths taken by powder particles which enter and do not enter the laser generated melt pool during laser cladding (DED). A proportion of the powder is ‘wasted’ by bouncing off the solid areas surrounding the melt pool. This wastage reduces the productivity of the process. Specially developed software was used to analyse High Speed Imaging videos of the cladding process, to monitor the directions of powder particle flight towards and away from the melt pool area. In both these techniques the melt pool surface is the collection area for the cladding powder and the shape of this pool can be affected by several parameters including cladding speed, inter-track spacing and type of cladding technique.

This information has been correlated to the geometry and position of the melt pool zone for three different cladding techniques; single track cladding (A tracks), standard overlapping track cladding (AAA cladding) and a recently developed technique called ABA cladding. The experimental and analytical work presented here confirms the following conclusions within the parameter set used; (1) Powder catchment efficiency is an important metric for laser cladding and associated DED processes. (2) There is a substantial difference between the melt pool shape and the powder catchment efficiency of the initial track and subsequent tracks in AAA cladding. (3) The 'subsequent' tracks in AAA cladding have an asymmetrical melt pool shape as a result of the overlap of one track with the previous one. This asymmetry exposes more solid material to the incoming powder stream which decreases the powder catchment efficiency of the process. (4) The results show that the melt pool geometry, and particularly the overlap between the melt pool and the incoming powder stream, have a strong influence on powder catchment efficiency. (5) An increase in inter-track distance can improve powder catchment for AAA cladding but has no clear effect on ABA cladding powder catchment. (6) Increasing cladding speed has a surprisingly small effect on weld pool size or powder catchment efficiency, although it has a substantial effect on clad layer cross section (reduced speeds result in thicker clad layers). (7) ABA cladding offers a substantial improvement in powder catchment efficiency over AAA cladding and also eliminates the initiation anomalies common to AAA cladding. (8) ABA cladding was found to have considerably better powder catchment efficiency than standard AAA cladding and this improvement can explained by consideration of the geometries and positions of the melt pools and surrounding solid material in each case. (9) As powder costs are an important factor in industrial laser cladding, the adaption of the ABA technique, and/or control of pool/powder stream overlap (for example by making the powder stream not coaxial with the laser beam) could have a beneficial effect on the profitability of the process.

Additionally, the thesis provides quantitative information regarding ABA cladding with altered B cladding speeds and inter-track distances. Based on the experimental and analytical results presented here, the following conclusions can be drawn:

(1) Increasing the B clad speed in ABA cladding does not affect the deposition rate or powder catchment efficiency.

(2) A narrow inter-track spacing could result in a floatable meltpool geometry, which would improve powder catchment efficiency and deposit rate.

(3) By increasing B clad speed, a significant reduction in surface waviness can be achieved, resulting in a uniformly flat clad surface. It is evident from the results that the total volumetric coverage rate remained constant, but the total material waste decreased significantly, indicating that with increased B clad speed the same volume of clad can be deposited with significant material savings, thereby making ABA an appropriate cladding technique for industrial applications.

According to the results presented above, the powder catchment efficiency is completely determined by the overlap between the powder cloud and the melt pool. The laser cladding industry should maximize this overlap since powder catchment efficiency is a significant factor in laser cladding profitability. In order to achieve higher power catchment efficiency, it may be beneficial to use side powder feeders that apply powder directly to the meltpool by adjusting the position of the powder stream.

9.2 Future work and industrial applications

It would be beneficial in the future to address some of the questions raised by the research presented in this thesis. To summarize, the following research directions are suggested:

According to the results presented above, the powder catchment efficiency is completely determined by the overlap between the powder cloud and the melt pool. The laser cladding industry should maximize this overlap since powder catchment efficiency is a significant factor in laser cladding profitability. In order to achieve higher power catchment efficiency, it may be beneficial to use side powder feeders that apply powder directly to the meltpool by adjusting the position of the powder stream. It may also be possible to adjust the powder cloud position in order to ensure that every particle is directed into the melting pool in addition to developing different coaxial feeder geometries. The Figure 9.1 below represents the traditional AAA cladding with a coaxial powder feeder and a modified side powder feeder.

The ABA technique has this effect without question; however, it may also be beneficial to introduce a spatial lag between the front of the laser beam and the powder cloud. Lags are not appropriate in all cases because they interfere with the ability to perform equally well in all directions of x and y. Although this is the case, a great deal of industrial cladding is arranged in overlapping straight lines which are or may be arranged in the same direction (e.g., spiral overlaps on tubes or parallel lines on flat surfaces). There is also potential to use different beam shapes to optimise the overlap between powder cloud and melt pool.

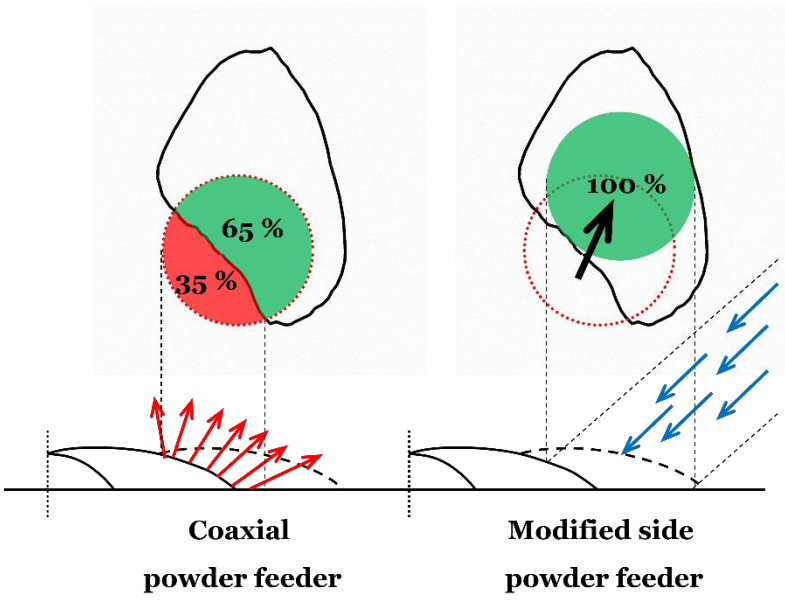

Figure 9.1 Traditional AAA cladding with a coaxial and with modified side powder feeder.

Further exploration could be made into the use of ABA cladding for the purpose of cladding a structure using multiple materials (more predictable local metallurgy). By using a cheaper first or inner layer, production costs can be reduced. Using an inner material, it is possible to combine incompatible clads and substrates. This Figure 9.2 illustrates the multi-material laser cladding with different alloys, resulting in a sandwich structure.

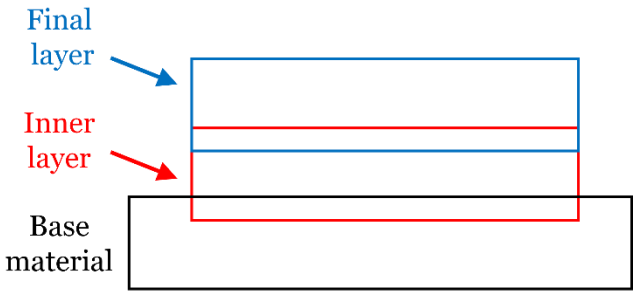

Figure 9.2 An illustration of the sandwich structure resulting from the multi-material laser cladding with different alloys.

In addition to saving costs on expensive superalloys, this technique could also be used to clad incompatible clad/substrate combinations where an intermediate layer of 'A' material separates tracks of 'B' material from the substrate.

Further investigation will be conducted into possible improvements in dilution effects (dilution uniformity) using ABA cladding.

10 References

1. Dwivedi, Dheerendra Kumar. Surface Engineering: Enhancing Life of Tribological Components. Springer India, 2018.
2. J. Powell, *Laser Cladding*. Imperial College of Science and Technology, 1983.
3. Davis, J.R. Surface Engineering for Corrosion and Wear Resistance. IOM Communications, 2001.
4. Holmberg, Kenneth, and Allan Matthews. Coatings Tribology: Properties, Techniques and Applications in Surfaces Engineering. Elsevier, 1994.
5. Alam, N., and Ion, J. C., "Extending the Life of Components by Laser Beam Cladding", Australian Welding Journal, Volume 47, 2nd Quarter, 2002, Pages 26 – 27
6. Cotell, Catherine Mary, et al. ASM Handbook: Surface Engineering. ASM International, 1994.
7. Rickerby, D. S., and A. Matthews. Advanced Surface Coatings: A Handbook of Surface Engineering. Blackie, 1991.
8. ASM Handbook. Heat Treating. ASM International, 1998.
9. A. Singh and S. P. Harimkar. Laser Surface Engineering of Magnesium Alloys: A Review. JOM Journal of the Minerals, Metals and Materials Society, 64(6): 716{733, 2012.
10. S.V. Joshi and G. Sundararajan. Lasers for Metallic and Intermetallic Coatings. ASM International, Materials Park, OH, 1998.
11. J.C. Ion. Laser Processing of Engineering Materials, Principle, Procedure and Industrial Application. Elsevier Butterworth Heinemann, Linacre House,Jordan Hill, Oxford, UK, 2005.

12. Malakondaiah, G., and T. Nicholas. “The Influence of Laser Glazing on Fatigue Crack Growth in Ti-24ai-11nb.” Metallurgical and Materials Transactions A, vol. 25, no. 1, 1994, pp. 183–192., https://doi.org/10.1007/bf02646686.

13. Singh, Subhash C., and Chunlei Guo. “Laser Material Processing: Section Introduction.” Handbook of Laser Technology and Applications, 2021, pp. 1–2., https://doi.org/10.1201/9781315310855-1.

14. Chen, Z., Lim, L.C., Qian, M., Laser cladding of WC-Ni composite. Journal of Materials Processing Technology, 1996. 62(4): p. 321-323.

15. Xu, P., Lin, C., Zhou, C., Yi, X., Wear and corrosion resistance of laser cladding AISI 304 stainless steel/Al2O3 composite coatings. Surface and Coatings Technology, 2014. 238: p. 9-14.

16. Desale, G.R., Paul, C. P., Gandhi, B. K., Jain, S. C., Erosion wear behavior of laser clad surfaces of low carbon austenitic steel. Wear, 2009. 266(9-10): p. 975-987.

17. Huang, Y., Characterization of dilution action in laser-induction hybrid cladding. Optics & Laser Technology, 2011. 43(5): p. 965-973.

18. Sexton, L., Lavin, S., Byrne, G., Kennedy, A., Laser cladding of aerospace materials. Journal of Materials Processing Technology, 2002. 122(1): p. 63-68.

19. Ion, J.C., Laser Processing of Engineering Materials. Principles, Procedure and Industrial Applications. 2005, Biddles Limited, King's Lynn: Oxford.

20. Canning, J., Fibre lasers and related technologies. Optics and Lasers in Engineering, 2006. 44(7): p. 647-676.

21. Dominic, V., MacCormack, S., Waarts, R., Sanders, S., Bicknese, S., Dohle, R., Wolak, E., Yeh, P.S., Zucker, E., 110 W fibre laser. Journal of Electronics Letters, 1999. 35(14): p. 1158-1160.

22. Liu J, Jiang H, Lei Z, Bai R, Yu S. Analysis of the residual stress in additive manufacturing of Ti-6Al-4V. InJournal of Physics: Conference Series 2022 Feb 1 (Vol. 2206, No. 1, p. 012011). IOP Publishing.

23. Zhuang W, Liu Q, Djugum R, Sharp PK, Paradowska A. Deep surface rolling for fatigue life enhancement of laser clad aircraft aluminium alloy. Applied Surface Science. 2014 Nov 30;320:558-62.

24. Shah K, Pinkerton AJ, Salman A, Li L. Effects of melt pool variables and process parameters in laser direct metal deposition of aerospace alloys. Materials and Manufacturing Processes. 2010 Dec 3;25(12):1372-80.

25. Chen, J., and L. Xue. "Laser Cladding of CPM Tool Steels on Hardened H13 Hot-Work Steel for Low-Cost High-Performance Automotive Tooling." JOM, vol. 64, no. 6, 2012, pp. 688–693., https://doi.org/10.1007/s11837-012-0332-2.

26. Piscopo, Gabriele, and Luca Iuliano. "Current Research and Industrial Application of Laser Powder Directed Energy Deposition." The International Journal of Advanced Manufacturing Technology, vol. 119, no. 11-12, 2022, pp. 6893–6917., https://doi.org/10.1007/s00170-021-08596-w.

27. Chen ZD, Mai TA, Lim GC. Rapid tooling by laser cladding. InInternational Congress on Applications of Lasers & Electro-Optics 1998 Nov 1 (Vol. 1998, No. 1, pp. E8-E14). Laser Institute of America.

28. Costa L, Vilar R, Reti T, Deus AM. Rapid tooling by laser powder deposition: Process simulation using finite element analysis. Acta Materialia. 2005 Aug 1;53(14):3987-99.

29. Li X, Zhang CH, Zhang S, Wu CL, Liu Y, Zhang JB, Shahzad MB. Manufacturing of Ti3SiC2 lubricated Co-based alloy coatings using laser cladding technology. Optics & Laser Technology. 2019 Jun 1;114:209-15.

30. Smurov, Igor. “Laser Cladding and Laser Assisted Direct Manufacturing.” Surface and Coatings Technology, vol. 202, no. 18, 2008, pp. 4496–4502., https://doi.org/10.1016/j.surfcoat.2008.04.033.

31. Sun F, Cai K, Li X, Pang M. Research on laser cladding Co-based alloy on the surface of vermicular graphite cast iron. Coatings. 2021 Oct 13;11(10):1241.

32. Liu Q, Janardhana M, Hinton B, Brandt M, Sharp K. Laser cladding as a potential repair technology for damaged aircraft components. International Journal of Structural Integrity. 2011 Aug 30;2(3):314-31.

33. Paydas H, Mertens A, Carrus R, Lecomte-Beckers J, Tchuindjang JT. Laser cladding as repair technology for Ti–6Al–4V alloy: Influence of building strategy on microstructure and hardness. Materials & Design. 2015 Nov 15;85:497-510.

34. Kotoban D, Aramov A, Tarasova T. Possibility of multi-material laser cladding fabrication of nickel alloy and stainless steel. Physics Procedia. 2016 Jan 1;83:634-46.

35. Masanta M, Ganesh P, Kaul R, Nath AK, Choudhury AR. Development of a hard nano-structured multi-component ceramic coating by laser cladding. Materials Science and Engineering: A. 2009 May 20;508(1-2):134-40.

36. Atamert, S., and H. K. Bhadeshia. “Comparison of the Microstructures and Abrasive Wear Properties of Stellite Hardfacing Alloys Deposited by Arc Welding and Laser Cladding.” Metallurgical Transactions A, vol. 20, no. 6, 1989, pp. 1037–1054., https://doi.org/10.1007/bf02650140.

37. Ren ZY, Hu YL, Tong Y, Cai ZH, Liu J, Wang HD, Liao JZ, Xu S, Li LK. Wear-resistant NbMoTaWTi high entropy alloy coating prepared by laser cladding on TC4 titanium alloy. Tribology International. 2023 Apr 1;182:108366.

38. Yan Y, Li J, Li R, Shao M, Li J. Investigation into Corrosive Wear of the CoCrFeNiTax Laser-Clad Coatings on TC4 in the Neutral and Alkaline Circumstance. Coatings. 2023 Jan 5;13(1):105.

39. Subramanian R, Sircar S, Mazumder J. Laser cladding of zirconium on magnesium for improved corrosion properties. Journal of Materials science. 1991 Feb;26:951-6.

40. Przybylowicz, J., and J. Kusinski. “Laser Cladding and Erosive Wear of Co–Mo–Cr–Si Coatings.” Surface and Coatings Technology, vol. 125, no. 1-3, 2000, pp. 13–18., https://doi.org/10.1016/s0257-8972(99)00563-0.

41. Zhang, Zhe, and Radovan Kovacevic. “Laser Cladding of Iron-Based Erosion Resistant Metal Matrix Composites.” Journal of Manufacturing Processes, vol. 38, 2019, pp. 63–75., https://doi.org/10.1016/j.jmapro.2019.01.001.

42. S. H. Mok, G. Bi, J. Folkes, and I. Pashby, "Deposition of Ti-6A1-4V using a high power diode laser and wire, part I: Investigation on the process characteristics, " Surface & Coatings Technology, vol. 202, pp. 3933-3939,2008.

43. A. Heralic, A. K. Christiansson, M. Ottosson, and B. Lennartson, "Increased stability in laser metal wire deposition through feedback from optical measurements, " Optics and Lasers in Engineering, vol. 48, pp. 478-485,2010.

44. Kanishka, Kumar, and Bappa Acherjee. “A Systematic Review of Additive Manufacturing-Based Remanufacturing Techniques for Component Repair and Restoration.” Journal of Manufacturing Processes, vol. 89, 2023, pp. 220–283., https://doi.org/10.1016/j.jmapro.2023.01.034.

45. Wang K, Liu W, Hong Y, Sohan HS, Tong Y, Hu Y, Zhang M, Zhang J, Xiang D, Fu H, Ju J. An overview of technological parameter optimization in the case of laser cladding. Coatings. 2023 Feb 23;13(3):496.

46. Qi, Kang, and Yong Yang. “Microstructure, Wear, and Corrosion Resistance of NB-Modified Magnetic Field-Assisted Co-Based Laser Cladding Layers.” Surface and Coatings Technology, vol. 434, 2022, p. 128195., https://doi.org/10.1016/j.surfcoat.2022.128195.

47. Das, Anil Kumar. “Recent Trends in Laser Cladding and Alloying on Magnesium Alloys: A Review.” Materials Today: Proceedings, vol. 51, 2022, pp. 723–727., https://doi.org/10.1016/j.matpr.2021.06.217.

48. Liu Y, Ding Y, Yang L, Sun R, Zhang T, Yang X. Research and progress of laser cladding on engineering alloys: A review. Journal of Manufacturing Processes. 2021 Jun 1;66:341-63.

49. PICASSO, M., and M. RAPPAZ. “Laser-Powder-Material Interactions in the Laser Cladding Process.” Le Journal De Physique IV, vol. 04, no. C4, 1994, https://doi.org/10.1051/jp4:1994404.

50. Peng S, Li T, Zhao J, Lv S, Tan GZ, Dong M, Zhang H. Towards energy and material efficient laser cladding process: Modeling and optimization using a hybrid TS-GEP algorithm and the NSGA-II. Journal of Cleaner Production. 2019 Aug 1;227:58-69.

51. Wang D, Hu Q, Zheng Y, Xie Y, Zeng X. Study on deposition rate and laser energy efficiency of Laser-Induction Hybrid Cladding. Optics & Laser Technology. 2016 Mar 1;77:16-22.

52. Prasad HS, Brueckner F, Kaplan AF. Powder catchment in laser metal deposition. InInternational Congress on Applications of Lasers & Electro-Optics 2018 Oct 1. AIP Publishing.

53. Li Y, Ma J. Study on overlapping in the laser cladding process. Surface and Coatings Technology. 1997 Mar 15;90(1-2):1-5

54. Gao W, Zhao S, Liu F, Wang Y, Zhou C, Lin X. Effect of defocus manner on laser cladding of Fe-based alloy powder. Surface and Coatings Technology. 2014 Jun 15;248:54-62.

55. Nenadl O, Ocelík V, Palavra A, De Hosson JT. The prediction of coating geometry from main processing parameters in laser cladding. Physics Procedia. 2014 Jan 1;56:220-7.

56. Li G, Wang Z, Yao L, Ding J, Gao J. Component mixing in laser cladding processes: From single-track to single-layer multi-track and multi-layer multi-track. Surface and Coatings Technology. 2023 Feb 25;455:129233.

57. Ya W, Pathiraj B, Matthews DT, Bright M, Melzer S. Cladding of Tribaloy T400 on steel substrates using a high power Nd: YAG laser. Surface and coatings technology. 2018 Sep 25;350:323-33

58. Imam HZ, Al-Musaibeli H, Zheng Y, Martinez P, Ahmad R. Vision-based spatial damage localization method for autonomous robotic laser cladding repair processes. Robotics and Computer-Integrated Manufacturing. 2023 Apr 1;80:102452.

59. Koch, J. L., and J. Mazumder. “Rapid Prototyping by Laser Cladding.” International Congress on Applications of Lasers & Electro-Optics, 1993, https://doi.org/10.2351/1.5058617.

60. Tomlinson K, Fletcher DI, Lewis R. Evaluation of laser cladding as an in-situ repair method on rail steel. Tribology International. 2023 Feb 1;180:108210.

61. Shepeleva L, Medres B, Kaplan WD, Bamberger M, Weisheit A. Laser cladding of turbine blades. Surface and coatings technology. 2000 Mar 1;125(1-3):45-8.

62. Galun R, Weisheit A, Mordike BL. Laser surface alloying of magnesium base alloys. Journal of Laser Applications. 1996 Dec 1;8(6):299-305.

63. Sexton L, Lavin S, Byrne G, Kennedy A. Laser cladding of aerospace materials. Journal of Materials Processing Technology. 2002 Mar 5;122(1):63-8.

64. Babu PD, Buvanashekaran G, Balasubramanian KR. Experimental studies on the microstructure and hardness of laser transformation hardening of low alloy steel. Transactions of the Canadian Society for Mechanical Engineering. 2012;36(3):241-58.

65. Muthukumaran, G., and P. Dinesh Babu. "Laser Transformation Hardening of Various Steel Grades Using Different Laser Types." Journal of the Brazilian Society of Mechanical Sciences and Engineering, vol. 43, no. 2, 2021, https://doi.org/10.1007/s40430-021-02854-4.

66. Mazumder, J. Laser Processing: Surface Treatment and Film Deposition. Kluwer Academic Publishers, 1996.

67. Chen ZD, West DR, Steen WM. Laser melting of alloy cast irons. InInternational Congress on Applications of Lasers & Electro-Optics 1986 Nov 1 (pp. 27-35). AIP Publishing.

68. Colaço, R., and R. Vilar. "Laser Surface Melting of Bearing Steels." Laser Applications for Mechanical Industry, 1993, pp. 305–314., https://doi.org/10.1007/978-94-011-1990-0_19.

69. Man HC, Cui ZD, Yue TM. Surface characteristics and corrosion behavior of laser surface nitrided NiTi shape memory alloy for biomedical applications. Journal of laser applications. 2002 Nov 1;14(4):242-7.

70. Marsden C, West DR, Steen WM. Laser surface alloying of stainless steel with carbon. Laser Surface Treatment of Metals. 1986:461-73..

71. Riabkina-Fishman, M., and J. Zahavi. “Laser Alloying and Cladding for Improving Surface Properties.” Applied Surface Science, vol. 106, 1996, pp. 263–267., https://doi.org/10.1016/s0169-4332(96)00408-4.

72. Gao Q, Liu H, Chen P, Liu X, Yang H, Hao J. Multi-objective optimization for laser cladding refractory MoNbTiZr high-entropy alloy coating on Ti6Al4V. Optics & Laser Technology. 2023 Jun 1;161:109220.

73. Costa, Lino, and Rui Vilar. “Laser Powder Deposition.” Rapid Prototyping Journal, vol. 15, no. 4, 2009, pp. 264–279., https://doi.org/10.1108/13552540910979785.

74. Ion, John C. “Cladding.” Laser Processing of Engineering Materials, 2005, pp. 296–326., https://doi.org/10.1016/b978-075066079-2/50015-5.

75. Bruck, G. J. “Fundamentals and Industrial Applications of High Power Laser Beam Cladding.” SPIE Proceedings, 1988, https://doi.org/10.1117/12.947699.

76. Liang Y, Liao ZY, Zhang LL, Cai MW, Wei XS, Shen J. A review on coatings deposited by extreme high-speed laser cladding: processes, materials, and properties. Optics & Laser Technology. 2023 Sep 1;164:109472.

77. Chryssolouris G, Zannis S, Tsirbas K, Lalas C. An experimental investigation of laser cladding. CIRP Annals. 2002 Jan 1;51(1):145-8.

78. Van Acker K, Vanhoyweghen D, Persoons R, Vangrunderbeek J. Influence of tungsten carbide particle size and distribution on the wear resistance of laser clad WC/Ni coatings. wear. 2005 Jan 1;258(1-4):194-202.

79. Desale GR, Paul CP, Gandhi BK, Jain SC. Erosion wear behavior of laser clad surfaces of low carbon austenitic steel. Wear. 2009 Apr 24;266(9-10):975-87.

80. Li XZ, Li HC, Wang YT, Li B. Investigations on the behavior of laser cladding Ni–Cr–Mo alloy coating on TP347H stainless steel tube in HCl rich environment. Surface and Coatings Technology. 2013 Oct 15;232:627-39.

81. Hofman JT, De Lange DF, Pathiraj B, Meijer J. FEM modeling and experimental verification for dilution control in laser cladding. Journal of Materials Processing Technology. 2011 Feb 1;211(2):187-96.

82. Huang, Yongjun. “Characterization of Dilution Action in Laser-Induction Hybrid Cladding.” Optics & Laser Technology, vol. 43, no. 5, 2011, pp. 965–973., https://doi.org/10.1016/j.optlastec.2010.12.005.

83. Cao X, Xiao M, Jahazi M, Fournier J, Alain M. Optimization of processing parameters during laser cladding of ZE41A-T5 magnesium alloy castings using Taguchi method. Materials and Manufacturing Processes. 2008 Apr 4;23(4):413-8.

84. Huang SW, Samandi M, Brandt M. Abrasive wear performance and microstructure of laser clad WC/Ni layers. wear. 2004 Jun 1;256(11-12):1095-105.

85. Wang C, Zhou J, Zhang T, Meng X, Li P, Huang S. Numerical simulation and solidification characteristics for laser cladding of Inconel 718. Optics & Laser Technology. 2022 May 1;149:107843.

86. Zhu YY, Li ZG, Li RF, Li M, Feng K, Wu YX, Wada T, Kato H. High power diode laser cladding of Fe–Co–B–Si–C–Nb amorphous coating: Layered microstructure and properties. Surface and Coatings Technology. 2013 Nov 25;235:699-705.

87. Tong X, Li FH, Liu M, Dai MJ, Zhou H. Thermal fatigue resistance of non-smooth cast iron treated by laser cladding with different self-fluxing alloys. Optics & Laser Technology. 2010 Oct 1;42(7):1154-61.

88. Wang G, Zhang J, Shu R, Yang S. High temperature wear resistance and thermal fatigue behavior of Stellite-6/WC coatings produced by laser cladding with Co-coated WC powder. International Journal of Refractory Metals and Hard Materials. 2019 Jun 1;81:63-70.

89. Kerschbaumer M, Ernst G, O'Leary P. Tool path generation for 3D laser cladding using adaptive slicing technology. InInternational Congress on Applications of Lasers & Electro-Optics 2005 Oct 1 (Vol. 2005, No. 1, p. 604). Laser Institute of America.

90. Zheng H, Cong M, Dong H, Liu Y, Liu D. CAD-based automatic path generation and optimization for laser cladding robot in additive manufacturing. The International Journal of Advanced Manufacturing Technology. 2017 Oct;92:3605-14.

91. Powell J, Henry PS, Steen WM. Laser cladding with preplaced powder: analysis of thermal cycling and dilution effects. Surface engineering. 1988 Jan 1;4(2):141-9.

92. Li J, Li HN, Liao Z, Axinte D. Overlapped wire-fed laser cladding on inclined surfaces: An analytical model considering gravity and a model application. Journal of Materials Processing Technology. 2022 Jun 1;304:117559.

93. Li J, Gu J, Zhang Y, Wang Z, Zhang G. Study on laser cladding process and friction characteristics of friction pairs of copper-based powder metallurgy materials. Tribology International. 2023 Jan 1;177:107953.

94. Lugscheider E, Bolender H, Krappitz H. Laser cladding of paste bound hardfacing alloys. Surface Engineering. 1991 Jan 1;7(4):341-4.

95. Uenishi, Keisuke, and Kojiro F. Kobayashi. "Formation of Surface Layer Based on al3ti on Aluminum by Laser Cladding and Its Compatibility with Ceramics." Intermetallics, vol. 7, no. 5, 1999, pp. 553–559., https://doi.org/10.1016/s0966-9795(98)00071-5.

96. Zhao S, Xu S, Huang Y, Yang L. Laser hot-wire cladding of Ni/WC composite coatings with a tubular cored wire. Journal of Materials Processing Technology. 2021 Dec 1;298:117273.

97. Eboo, G. M., and A. G. Blake. “Laser Cladding of Gas Turbine Components.” Volume 5: Manufacturing Materials and Metallurgy; Ceramics; Structures and Dynamics; Controls, Diagnostics and Instrumentation; Education; Process Industries, 1986, https://doi.org/10.1115/86-gt-298.

98. Gedda H, Kaplan A, Powell J. Melt-solid interactions in laser cladding and laser casting. Metallurgical and materials transactions B. 2005 Oct;36:683-9.

99. Kar, A., and J. Mazumder. “Modeling in Laser Materials Processing: Melting, Alloying, Cladding.” Laser Processing: Surface Treatment and Film Deposition, 1996, pp. 129–155., https://doi.org/10.1007/978-94-009-0197-1_7.

100. Contin A, de Vasconcelos G, Barquete DM, Campos RA, Trava-Airoldi VJ, Corat EJ. Laser cladding of SiC multilayers for diamond deposition on steel substrates. Diamond and Related Materials. 2016 May 1;65:105-14.

101. Xiong YJ, Qiu ZL, Li RD, Yuan TC, Hong WU, Liu JH. Preparation of ultra-fine grain Ni–Al–WC coating with interlocking bonding on austenitic stainless steel by laser clad and friction stir processing. Transactions of Nonferrous Metals Society of China. 2015 Nov 1;25(11):3685-93.

102. Wang W, Huang L, Zhang F, Hu X, Lin H, Xie J. Remanufacturing of Aero-engine Components by Laser Cladding. In2014 International Conference on Mechatronics, Control and Electronic Engineering (MCE-14) 2014 Mar (pp. 598-601). Atlantis Press.

103. Chen L, Zhao Y, Chen X, Yu T, Xu P. Repair of spline shaft by laser-cladding coarse TiC reinforced Ni-based coating: Process, microstructure and properties. Ceramics International. 2021 Nov 1;47(21):30113-28.

104. Miao, Hong Bin, and Wen Qiang Zhao. “Research of Fiber Laser Cladding Technology on Shaft-Parts.” Applied Mechanics and Materials, vol. 217-219, 2012, pp. 2238–2241., https://doi.org/10.4028/www.scientific.net/amm.217-219.2238.

105. Ding Y, Liu R, Yao J, Zhang Q, Wang L. Stellite alloy mixture hardfacing via laser cladding for control valve seat sealing surfaces. Surface and Coatings Technology. 2017 Nov 25;329:97-108.

106. Aihua W, Zengyi T, Beidi Z. Laser beam cladding of seating surfaces on exhaust valves. Welding Research Supplement. 1991 Apr 1;4:106S-9S.

107. Roshchin, M. “Laser Cladding of the Coating on the Shroud Flanges of the Turbine Blades.” VII INTERNATIONAL CONFERENCE “SAFETY PROBLEMS OF CIVIL ENGINEERING CRITICAL INFRASTRUCTURES” (SPCECI2021), 2023, https://doi.org/10.1063/5.0124942.

108. Hu D, Kovacevic R, Valant M. Solid freeform fabrication of metal parts by 3d laser cladding. InASME International Mechanical Engineering Congress and Exposition 2000 Nov 5 (Vol. 19166, pp. 365-371). American Society of Mechanical Engineers.

109. Keshav K, Alya S, Singh RK, Gupta A. Laser cladding for 3D deposition and Free-form repair. In2016 IEEE International Conference on Industrial Technology (ICIT) 2016 Mar 14 (pp. 898-903). IEEE.

110. Qi C, Zhan X, Gao Q, Liu L, Song Y, Li Y. The influence of the pre-placed powder layers on the morphology, microscopic characteristics and microhardness of Ti-6Al-4V/WC MMC coatings during laser cladding. Optics & Laser Technology. 2019 Nov 1;119:105572.

111. Wang W, Wang M, Jie Z, Sun F, Huang D. Research on the microstructure and wear resistance of titanium alloy structural members repaired by laser cladding. Optics and Lasers in Engineering. 2008 Nov 1;46(11):810-6.

112. Del Val J, López-Cancelos R, Riveiro A, Badaoui A, Lusquiños F, Quintero F, Comesaña R, Boutinguiza M, Pou J. On the fabrication of bioactive glass implants for bone regeneration by laser assisted rapid prototyping based on laser cladding. Ceramics International. 2016 Jan 1;42(1):2021-35.

113. Laeng J, Stewart JG, Liou FW. Laser metal forming processes for rapid prototyping-A review. International Journal of Production Research. 2000 Nov 1;38(16):3973-96.

114. Fujimagari H, Hagiwara M, Kojima T. Laser cladding technology to small diameter pipes. Nuclear engineering and design. 2000 Feb 2;195(3):289-98.

115. Gedda H, Powell J, Wahlström G, Li WB, Engström H, Magnusson C. Energy redistribution during CO2 laser cladding. InInternational Congress on Applications of Lasers & Electro-Optics 2001 Oct 1 (pp. 549-558). AIP Publishing.

116. Eboo, G. M., and A. E. Lindemanis. “Advances in Laser Cladding Process Technology.” SPIE Proceedings, 1985, https://doi.org/10.1117/12.946399.

117. Liu Y, Xiang D, Wang K, Yu T. Corrosion of Laser Cladding High-Entropy Alloy Coatings: A Review. Coatings. 2022 Nov 3;12(11):1669.

118. Mazumder, J., and L. J. Li. A Study of the Mechanism of Laser Cladding Processes. University of Illinois, 1984.

119. Chen, H., Liu, S., Jiang, S., Zhao, W. and Zhang, H., 2024. Effect of CeO2 on the Microstructure and Properties of In Situ Nano-VC Reinforced Sub-micron Fe-Based Laser Cladding Layers. Journal of Materials Engineering and Performance, pp.1-11.

120. Chen, B., Zhang, G., Zhang, Z., Wang, X., Gao, L. and Song, X., 2024. Effect of niobium content on microstructure and wear and corrosion resistance of laser-clad FeCo0. 5CrNi1. 5B0. 5Nbx coatings on ductile iron. Surface and Coatings Technology, 476, p.130210.

121. Zhu, H., Lin, X., Xue, X., Zhang, Y., Wang, L., Ning, Y., Dong, Y. and Fang, X., 2024. Laser cladding of stainless-steel ball valves by a high-power diode laser source with a rectangular beam spot. Optics & Laser Technology, 169, p.110123.

122. Ghorbani, H., Khorrami, M.S., Geranmayeh, A. and Sohi, M.H., 2024. In-situ synthesis of TiC/Ti alloyed layer via pulsed Nd: YAG laser melting of Ti-6Al-4V titanium with preplaced carbon-based powder. Optics and Lasers in Engineering, 172, p.107864.

123. Hua, K., Ding, H., Sun, L., Cao, Y., Li, X., Wu, H. and Wang, H., 2024. Enhancing high-temperature fretting wear resistance of TC21 titanium alloys by laser cladding self-lubricating composite coatings. Journal of Alloys and Compounds, p.173360.

124. Zhang, B., 2024. Microstructure and wear resistance of laser cladding a novel nickel-based alloy coating. Materials Letters, 357, p.135695.

125. Li, Y.J., Hsieh, Y.H., Lin, W.T., Tran, H.C., Huang, J.W. and Chien, C.S., 2024. Comparison of laser cladding properties of tantalum and tantalum pentoxide powders on titanium substrates.

126. Feng, M., Ma, Y., Tian, Y. and Cao, H., 2024. Microstructure and Wear Resistance of Ti6Al4V Titanium Alloy Laser-Clad Ni60/WC Composite Coating. Materials, 17(1), p.264.

127. Iceland, William F. "." SPIE Proceedings, 1976, https://doi.org/10.1117/12.954963.

128. Ding D, Pan Z, Cuiuri D, Li H. Wire-feed additive manufacturing of metal components: technologies, developments and future interests. The International Journal of Advanced Manufacturing Technology. 2015 Oct;81:465-81.

129. Nurminen J, Riihimäki J, Näkki J, Vuoristo P. Hot-wire cladding process studies. InInternational Congress on Applications of Lasers & Electro-Optics 2007 Oct 1 (Vol. 2007, No. 1, p. 1702). Laser Institute of America.

130. Mohammed S, Zhang Z, Kovacevic R. Optimization of processing parameters in fiber laser cladding. The International Journal of Advanced Manufacturing Technology. 2020 Dec;111:2553-68.

131. Moures F, Cicală E, Sallamand P, Grevey D, Vannes B, Ignat S. Optimisation of refractory coatings realised with cored wire addition using a high-power diode laser. Surface and Coatings Technology. 2005 Dec 21;200(7):2283-92.

132. Syed, Waheed Ul, and Lin Li. "Effects of Wire Feeding Direction and Location in Multiple Layer Diode Laser Direct Metal Deposition." Applied Surface Science, vol. 248, no. 1-4, 2005, pp. 518–524., https://doi.org/10.1016/j.apsusc.2005.03.039.

133. Mok SH, Bi G, Folkes J, Pashby I. Deposition of Ti–6Al–4V using a high power diode laser and wire, Part I: Investigation on the process characteristics. Surface and Coatings Technology. 2008 May 15;202(16):3933-9.

134. Syed WU, Pinkerton AJ, Li L. A comparative study of wire feeding and powder feeding in direct diode laser deposition for rapid prototyping. Applied surface science. 2005 Jul 15;247(1-4):268-76.

135. Rodrigues MB, Silva RG, Pereira M, Teichmann EW. Effect of dynamic wire feeding on deposition quality in laser cladding process. Journal of Laser Applications. 2020 May 1;32(2).

136. Medrano A, Folkes J, Segal J, Pashby I. Fibre laser metal deposition with wire: parameters study and temperature monitoring system. InXVII International Symposium on Gas Flow, Chemical Lasers, and High-Power Lasers 2009 Apr 21 (Vol. 7131, pp. 539-545). SPIE.

137. Ahn, Young-Nam, and Cheolhee Kim. "Comparison of Powder Feeding and Wire Feeding in Laser Cladding." Journal of Welding and Joining, vol. 31, no. 4, 2013, pp. 13–16., https://doi.org/10.5781/kwjs.2013.31.4.13.

138. Li W, Sugio K, Liu X, Yamamoto M, Guo Y, Zhu S, Sasaki G. Microstructure evolution and mechanical properties of 308L stainless steel coatings fabricated by laser hot wire cladding. Materials Science and Engineering: A. 2021 Sep 8;824:141825.

139. Shen Q, Xue J, Yu X, Zheng Z, Ou N. Triple-wire plasma arc cladding of Cr-Fe-Ni-Tix high-entropy alloy coatings. Surface and Coatings Technology. 2022 Aug 15;443:128638.

140. Lian G, Xiao S, Zhang Y, Jiang J, Zhan Y. Multi-objective optimization of coating properties and cladding efficiency in 316L/WC composite laser cladding based on grey relational analysis. The International Journal of Advanced Manufacturing Technology. 2021 Jan;112:1449-59.

141. Williams SW, Martina F, Addison AC, Ding J, Pardal G, Colegrove P. Wire+ arc additive manufacturing. Materials science and technology. 2016 May 2;32(7):641-7.

142. Heralić A, Christiansson AK, Lennartson B. Height control of laser metal-wire deposition based on iterative learning control and 3D scanning. Optics and lasers in engineering. 2012 Sep 1;50(9):1230-41.

143. Tabernero I, Lamikiz A, Martínez S, Ukar E, Figueras J. Evaluation of the mechanical properties of Inconel 718 components built by laser cladding. International Journal of Machine Tools and Manufacture. 2011 Jun 1;51(6):465-70.

144. Yan Q, Yang K, Wang ZD, Chen MZ, Sun GF, Ni ZH. Surface roughness optimization and high-temperature wear performance of H13 coating fabricated by extreme high-speed laser cladding. Optics & Laser Technology. 2022 May 1;149:107823.

145. Abioye TE, Farayibi PK, Clare AT. A comparative study of Inconel 625 laser cladding by wire and powder feedstock. Materials and Manufacturing Processes. 2017 Oct 26;32(14):1653-9.

146. Zhou S, Xu T, Hu C, Wu H, Liu H, Ma X. Utilizing carbon nanotubes in ceramic particle reinforced MMC coatings deposited by laser cladding with Inconel 625 wire. Journal of Materials Research and Technology. 2021 Jul 1;13:2026-42.

147. A., Yelistratov, and Sciammarella F. "Laser Surfacing with Wire Feeding." Welding Journal, 2005, pp. 36–39.

148. Haemers TA, Rickerby DG, Lanza F, Geiger F, Mittemeijer EJ. Laser cladding of stainless steel with Hastelloy. Advanced Engineering Materials. 2001 Apr 1;3.

149. Zhuang DD, Du B, Zhang SH, Tao WW, Wang Q, Shen HB. Effect and action mechanism of ultrasonic assistance on microstructure and mechanical performance of laser cladding 316L stainless steel coating. Surface and Coatings Technology. 2022 Mar 15;433:128122.

150. Chen W, Peng Y, Wang Y, Cao P, Zhu Y, Guo Y. Research on high-temperature friction and wear performances of Stellite 12 laser cladding layer against coated boron steels. Wear. 2023 May 15;520:204665.

151. Chang SS, Wu HC, Chen C. Impact wear resistance of stellite 6 hardfaced valve seats with laser cladding. Materials and Manufacturing processes. 2008 Sep 4;23(7):708-13.

152. Rezayat M, Aboutorabi Sani A, Talafi Noghani M, Saghafi Yazdi M, Taheri M, Moghanian A, Mohammadi MA, Moradi M, Mateo García AM, Besharatloo H. Effect of Lateral Laser-Cladding Process on the Corrosion Performance of Inconel 625. Metals. 2023 Feb 11;13(2):367.

153. Xu X, Mi G, Chen L, Xiong L, Jiang P, Shao X, Wang C. Research on microstructures and properties of Inconel 625 coatings obtained by laser cladding with wire. Journal of alloys and Compounds. 2017 Aug 25;715:362-73.

154. Adak B, Nash P, Chen D, Swiglo A. Microstructural characterization of laser cladding of Cu-30Ni. Journal of materials science. 2005 Apr 1;40(8):2051-4.

155. Farayibi PK, Abioye TE, Clare AT. A parametric study on laser cladding of Ti-6Al-4V wire and WC/W 2 C powder. The International Journal of Advanced Manufacturing Technology. 2016 Dec;87:3349-58.

156. Ganjali M, Ganjali M, Sadrnezhaad SK, Pakzad Y. Laser cladding of Ti alloys for biomedical applications. Laser Cladding of Metals. 2021:265-92.

157. Cheng Q, Guo N, Fu Y, Wang G, Yu M, He J. Investigation on in-situ laser cladding 5356 aluminum alloy coating on 5052 aluminum alloy substrate in water environment. Journal of Materials Research and Technology. 2021 Nov 1;15:4343-52.

158. Guo N, Wu D, Wang G, Cheng Q, Fu Y, Yu M. Investigation on underwater wire-feed laser deposition of 5052 aluminum alloy. Journal of Manufacturing Processes. 2022 Apr 1;76:687-94.

159. Liu R, Wang Z, Sparks T, Liou F, Newkirk J. Aerospace applications of laser additive manufacturing. InLaser additive manufacturing 2017 Jan 1 (pp. 351-371). Woodhead Publishing.

160. Zhang, Sam, and Dongliang Zhao. Aerospace Materials Handbook. CRC Press, 2016.

161. Findik F. Laser cladding and applications. Sustainable Engineering and Innovation. 2023 Feb 28;5(1):1-4.

162. Capello, Edoardo, and Barbara Previtali. “The Influence of Operator Skills, Process Parameters and Materials on Clad Shape in Repair Using Laser Cladding by Wire.” Journal of Materials Processing Technology, vol. 174, no. 1-3, 2006, pp. 223–232., https://doi.org/10.1016/j.jmatprotec.2006.01.005.

163. Huebner J, Kata D, Kusiński J, Rutkowski P, Lis J. Microstructure of laser cladded carbide reinforced Inconel 625 alloy for turbine blade application. Ceramics International. 2017 Aug 15;43(12):8677-84.

164. Rottwinkel B, Nölke C, Kaierle S, Wesling V. Laser cladding for crack repair of CMSX-4 single-crystalline turbine parts. Lasers in Manufacturing and Materials Processing. 2017 Mar;4:13-23.

165. Santo, Loredana. “Laser Cladding of Metals: A Review.” International Journal of Surface Science and Engineering, vol. 2, no. 5, 2008, p. 327., https://doi.org/10.1504/ijsurfse.2008.021345.

166. Kim, Jae-Do, and Yun Peng. “Melt Pool Shape and Dilution of Laser Cladding with Wire Feeding.” Journal of Materials Processing Technology, vol. 104, no. 3, 2000, pp. 284–293., https://doi.org/10.1016/s0924-0136(00)00528-8.

167. Nasiri MT, Movahhedy MR. A new design of continuous coaxial nozzle for direct metal deposition process to overcome the gravity effect. Progress in Additive Manufacturing. 2022:1-4.

168. Lamikiz A, Tabernero I, Ukar E, Martinez S, N Lopez de Lacalle L. Current designs of coaxial nozzles for laser cladding. Recent Patents on Mechanical Engineering. 2011 Jan 1;4(1):29-36.

169. Shi T, Lu B, Shi S, Meng W, Fu G. Laser metal deposition with spatial variable orientation based on hollow-laser beam with internal powder feeding technology. Optics & Laser Technology. 2017 Feb 1;88:234-41.

170. Microstructure and properties of lightweight Al0.2CrNbTiV refractory high entropy alloy coating with different dilutions deposited by high speed laser cladding

171. Wang J, Zhang B, Tang H, Wei X, Hao W, Wang J. Development of Integrated Automatic System of Laser Cladding for Repairing of Polycrystalline Diamond Compact Bits. Electronics. 2023 Feb 10;12(4):900..

172. Huang K, Wu K, Li S, Zhang Z, Li M, Wang L, Tan H, Yi X. Microstructure and properties evaluation of vacuum and laser cladding Ni-base composite coatings. Applied Physics A. 2023 Feb;129(2):161.

173. Lewis, Gary K, and Eric Schlienger. “Practical Considerations and Capabilities for Laser Assisted Direct Metal Deposition.” Materials & Design, vol. 21, no. 4, 2000, pp. 417–423., https://doi.org/10.1016/s0261-3069(99)00078-3.

174. Toyserkani E, Khajepour A, Corbin S. 3-D finite element modeling of laser cladding by powder injection: effects of laser pulse shaping on the process. Optics and lasers in engineering. 2004 Jun 1;41(6):849-67.

175. Lin, Jehnming. "A simple model of powder catchment in coaxial laser cladding." Optics & Laser Technology 31, no. 3 (1999): 233-238.

176. Picasso, M., and M. Rappaz. "Laser-powder-material interactions in the laser cladding process." Le Journal de Physique IV 4, no. C4 (1994): C4-27.

177. Amara, E. H., L. Achab, and O. Boumia. "Numerical modelling of the laser cladding process using a dynamic mesh approach." In Proceedings of CAOL 2005. Second International Conference on Advanced Optoelectronics and Lasers, 2005., vol. 1, pp. 142-145. IEEE, 2005.

178. Hoadley, A. F. A., A. Frenk, and C. F. Marsden. "A process overview of laser hardfacing." In Surface Engineering, pp. 171-186. Routledge, 2018.

179. Picasso, M., C. F. Marsden, J. D. Wagniere, A. Frenk, and M. Rappaz. "A simple but realistic model for laser cladding." Metallurgical and materials transactions B 25 (1994): 281-291.

180. Becker, R., and G. Sepold. "Micro-coating by a laser powder feed process." Advanced Powder Technology 2, no. 3 (1991): 181-189.

181. Liu, Chang-Yi, and Jehnming Lin. "Thermal processes of a powder particle in coaxial laser cladding." Optics & Laser Technology 35, no. 2 (2003): 81-86.

182. Haferkamp, H., H. Schmidt, J. Gerken, and T. Püster. "Application of laser powder cladding and the risk of residual powder." DVS BERICHTE 163 (1994): 475-475.

183. Marsden, C. F., A. Frenk, J. D. Wagniere, and R. Dekumbis. "Effects of injection geometry on laser cladding." In Proc. ECLAT, vol. 90, pp. 535-542. 1990.

184. Migliore, Leonard R. Laser materials processing. CRC Press, 2018.

185. Wang K, Zhang Z, Xiang D, Ju J. Research and Progress of Laser Cladding: Process, Materials and Applications. Coatings. 2022 Sep 22;12(10):1382.

186. Hoadley AF, Frenk A, Marsden CF. A process overview of laser hardfacing. InSurface Engineering 2018 Dec 12 (pp. 171-186). Routledge.

187. Migliore, Leonard. Laser Materials Processing. Dekker, 1996.

188. Marsden, C.F., A. Frenk, J.D. Wagniere, and R. Dekumbis, Effects of injection geometry on laser cladding. in Proceedings of ECLAT. 1990. Coburg,

189. Chen, H., Liu, S., Jiang, S., Zhao, W. and Zhang, H., 2024. Effect of CeO2 on the Microstructure and Properties of In Situ Nano-VC Reinforced Sub-micron Fe-Based Laser Cladding Layers. Journal of Materials Engineering and Performance, pp.1-11.

190. Feng, M., Lin, T., Lian, G., Chen, C. and Huang, X., 2024. Effects of Nb content on the microstructure and properties of CoCrFeMnNiNbx high-entropy alloy coatings by laser cladding. Journal of Materials Research and Technology.

191. Jeong, J., Webster, S., Zha, R., Mogonye, J.E., Ehmann, K. and Cao, J., 2024. Effects of Laser-Powder Alignment on Clad Dimension and Melt Pool Temperature in Directed Energy Deposition. Journal of Manufacturing Science and Engineering, 146(1).

192. Yang, C., Jing, C., Fu, T., Lin, T., Guo, W. and Liu, N., 2024. Effect of CeO2 on the microstructure and properties of AlCoCrFeNi2. 1 laser cladding coatings. Journal of Alloys and Compounds, 976, p.172948.

193. Bruck, G. J. "High-Power Laser Beam Cladding." JOM, vol. 39, no. 2, 1987, pp. 10–13., https://doi.org/10.1007/bf03259463.

194. Volz, R., Reichelt, U., Wolf, S., Pei, Y. T. and Zuo, T. C., Laser processing of aluminium automobile parts with powder technologies, Proceedings of the 30th ISATA: Rapid prototyping/laser applications in the automotive industries, Croydon, England: Automotive Automation Ltd., edited by D. Roller, 1997, 393-400

195. Weisheit, A., Backes, G., Stromeyer, R., Gasser, A., Wissenbach, K., and Poprawe, R., " Powder Injection: The Key to Reconditioning and Generating Components Using Laser Cladding", Proceedings, International Congress on Advanced Materials and Processes, Materials Week 2001, Munich, Germany, 1 – 4 October, 2001, https://publica.fraunhofer.de/entities/publication/8a368f18-ab9c-4e7a-ad18-6f470de22e5a/fullmeta

196. Li, W.-B., Engström, H., Powell, J., Tan, Z., and Magnusson, C., "Modelling of the Laser Cladding Process – Preheating of the Blown Powder Material", Lasers in Engineering, Volume 4, 1995, Pages 329 – 341, https://www.researchgate.net/publication/313085834_Modeling_of_the_laser_cladding_process_-_Pre-heating_of_the_blown_powder_material

197. Liu H, Tan CK, Dong X, Meng TL, Cao J, Wei Y. Laser-cladding and robotic hammer peening of stainless steel 431 on low alloy steel 4140 for surface enhancement and corrosion protections. Journal of Adhesion Science and Technology. 2022 Nov 2;36(21):2313-27.

198. M. Gaumann, H. Rusterholz, R. Baumann D.J.Wagniere, andW. Kurz, "Single crystal turbine components repaired by epitaxial laser metal forming," Materials for Advanced Powder Engineering, vol. 1479, pp. 1—6, 1998.

199. M.T. Ensz and M.L. Griffth, "Critical issues for functionally graded material deposition by laser engineered net shaping" in Proceedings of the 2002 MPIF Laser Metal Deposition Conference. 2002.

200. Li, W.-B., Engström, H., Powell, J., Tan, Z., and Magnusson, C., "Redistribution of the Beam Power in Laser Cladding by Powder Injection", Lasers in Engineering, Volume 5, 1996, Pages 175 – 183, https://www.diva-portal.org/smash/record.jsf?pid=diva2%3A980026&dswid=3471

201. Hayhurst P, Tuominen J, Vuoristo P, Mäntylä T. Coaxial laser cladding nozzle for use with a high power diode laser. InInternational Congress on Applications of Lasers & Electro-Optics 2002 Oct 1 (Vol. 2002, No. 1, p. 156745). Laser Institute of America.

202. Weerasinghe, V.M. and W.M. Steen, LASER CLADDING WITH BLOWN POWDER. Vol. 19. 1987. 581-585.

203. Doubenskaia M, Kulish A, Sova A, Petrovskiy P, Smurov I. Experimental and numerical study of gas-powder flux in coaxial laser cladding nozzles of Precitec. Surface and Coatings Technology. 2021 Jan 25;406:126672.

204. Tabernero I, Lamikiz A, Ukar E, De Lacalle LL, Angulo C, Urbikain G. Numerical simulation and experimental validation of powder flux distribution in coaxial laser

cladding. Journal of Materials Processing Technology. 2010 Nov 19;210(15):2125-34.

205. Audebert F, Colaco R, Vilar R, Sirkin H. Production of glassy metallic layers by laser surface treatment. Scripta materialia. 2003 Feb 1;48(3):281-6.

206. Doubenskaia M, Bertrand P, Smurov I. Optical monitoring of Nd: YAG laser cladding. Thin Solid Films. 2004 Apr 1;453:477-85.

207. Arrizubieta JI, Lamikiz A, Klocke F, Martínez S, Arntz K, Ukar E. Evaluation of the relevance of melt pool dynamics in Laser Material Deposition process modeling. International Journal of Heat and Mass Transfer. 2017 Dec 1;115:80-91.

208. Arrizubieta JI, Martínez S, Lamikiz A, Ukar E, Arntz K, Klocke F. Instantaneous powder flux regulation system for Laser Metal Deposition. Journal of Manufacturing Processes. 2017 Oct 1;29:242-51.

209. Bi G, Schürmann B, Gasser A, Wissenbach K, Poprawe R. Development and qualification of a novel laser-cladding head with integrated sensors. International Journal of Machine Tools and Manufacture. 2007 Mar 1;47(3-4):555-61.

210. Wetzig A, Brenner B, Fux V, Beyer E. Induction assisted laser-cladding a new and effective method for producing high wear resistant coatings on steel components. InInternational Congress on Applications of Lasers & Electro-Optics 1998 Nov 1 (pp. D20-D28). AIP Publishing..

211. Zhang Y, Yu G, He X. Numerical study of thermal history in laser aided direct metal deposition process. Science China Physics, Mechanics and Astronomy. 2012 Aug;55:1431-8.

212. Wang J, Ai C, Guo F, Yun X, Zhu X. Research of On-Line Monitoring Technology Based on Laser Triangulation for Surface Morphology of Extreme High-Speed Laser Cladding Coating. Coatings. 2023 Mar 16;13(3):625.

213. Lin, Jehnming. “Concentration Mode of the Powder Stream in Coaxial Laser Cladding.” Optics & Laser Technology, vol. 31, no. 3, 1999, pp. 251–257., https://doi.org/10.1016/s0030-3992(99)00049-3.

214. Lemoine, F., Grevey, and D.F., Vannes, A.B., “Indirect Determination of the Absorptance During Nd:YAG Laser-Matter Interaction”, Lasers in Engineering, Volume 4, 1995, Pages 273 – 279

215. Vetter, P.-A., Engel, T., and Fontaine, J., “Laser Cladding: The Relevant Parameters for Process Control”, Proceedings. Laser Materials Processing: Industrial and Microelectronics Applications, SPIE, 1994, Volume 2207, Pages 452 – 462

216. Jouvard JM, Grevey DF, Lemoine F, Vannes AB. Continuous wave Nd: YAG laser cladding modeling: a physical study of track creation during low power processing. Journal of Laser Applications. 1997 Feb 1;9(1):43-50.

217. Miah MH, Chand DS, Malhi GS, Khan S, al Muin A. Research on Surface Treatment Coating on Titanium Alloy Based on Laser Cladding Technology. SAE Technical Paper; 2023 Mar 7.

218. Gibson I, Rosen DW, Stucker B, Khorasani M, Rosen D, Stucker B, Khorasani M. Additive manufacturing technologies. Cham, Switzerland: Springer; 2021.

219. Zhu G, Li D, Zhang A, Tang Y. Numerical simulation of metallic powder flow in a coaxial nozzle in laser direct metal deposition. Optics & Laser Technology. 2011 Feb 1;43(1):106-13.

220. Roata IC, Croitoru C, Stanciu EM, Pascu A. Cladding under the spotlight: between performance materials and occupational health hazards. Materials Today: Proceedings. 2019 Jan 1;19:1051-8.

221. Liu C, Liu Z, Gao Y, Wang X, Zheng C. Effect of Cr Content on Corrosion Resistance of Ni–xCr–Mo Laser-Cladding Coatings under H2S-Induced High-Temperature Corrosion Atmosphere. Materials. 2022 Mar 3;15(5):1885.

222. Liu C, Liu Z, Gao Y, Zheng C, Wang X. Investigation on the corrosion behavior of Ni-Cr-Mo-W-xSi laser cladding coating in H2S corrosion environment. Applied Surface Science. 2022 Mar 15;578:152061.

223. Liu H, Gao Q, Dai J, Chen P, Gao W, Hao J, Yang H. Microstructure and high-temperature wear behavior of CoCrFeNiWx high-entropy alloy coatings fabricated by laser cladding. Tribology International. 2022 Aug 1;172:107574.

224. Mortazavian E, Wang Z, Teng H. Finite element investigation of thermal-kinetic-mechanical evolutions during laser powder deposition as an innovative technique for rail repair. The International Journal of Advanced Manufacturing Technology. 2021:1-24.

225. Wang K, Zhao J, Xie D, Lv F, Zhang Z, Wang H. Improved mechanical properties of laser-repaired 15-5PH stainless steel by in-situ heat treatment and grain refinement. Optics & Laser Technology. 2022 Jun 1;150:107999.

226. Chen L, Yu T, Chen X, Zhao Y, Guan C. Process optimization, microstructure and microhardness of coaxial laser cladding TiC reinforced Ni-based composite coatings. Optics & Laser Technology. 2022 Aug 1;152:108129.

227. Yu J, Ho H, Chen J. Effect of Ti content on the microstructure and mechanical properties of laser clad Ti/B4C/dr40-based composite coatings on shaft parts surface. Ceramics International. 2022 May 15;48(10):13551-62.

228. Naesstroem, Himani. “Phenomena in Laser Based Material Deposition.” Luleå University of Technology, 2021.

229. M.U. Islam, L. Xue, and G. McGregor, “Process for manufacturing or repairing turbine engine or compressor components,” U.S. Patent Number 6269540, August 7 2001.

230. P.F. Jeantette, D.M Keicher, J.A. Romero, and L.P Schanwald, “Mutiple and system for producing complex-shape objects,” U.S. Patent Number 6046426, April 2000.

231. D.M. Keicher andW.D. Miller, “Multiple beams and nozzles to increase deposition rate,” U.S. Patent Number 6268584, July 31 2001.

232. Kruth JP, Leu MC, Nakagawa T. Progress in additive manufacturing and rapid prototyping. Cirp Annals. 1998 Jan 1;47(2):525-40.

233. Comesaña R, Lusquiños F, Del Val J, López-Álvarez M, Quintero F, Riveiro A, Boutinguiza M, De Carlos A, Jones JR, Hill RG, Pou J. Three-dimensional bioactive glass implants fabricated by rapid prototyping based on CO2 laser cladding. Acta Biomaterialia. 2011 Sep 1;7(9):3476-87.

234. Resch M, Kaplan AF, Schuoecker D. Laser-assisted generating of three-dimensional parts by the blown powder process. InXIII International Symposium on Gas Flow and Chemical Lasers and High-Power Laser Conference 2001 Jan 25 (Vol. 4184, pp. 555-558). SPIE.

235. Chiumenti M, Lin X, Cervera M, Lei W, Zheng Y, Huang W. Numerical simulation and experimental calibration of additive manufacturing by blown powder technology. Part I: thermal analysis. Rapid Prototyping Journal. 2017 Mar 20;23(2):448-63.

236. Kumar S, Roy S, Paul CP, Nath AK. Three-dimensional conduction heat transfer model for laser cladding process. Numerical Heat Transfer, Part B: Fundamentals. 2008 Jan 9;53(3):271-87.

237. Zavala-Arredondo M, Boone N, Willmott J, Childs DT, Ivanov P, Groom KM, Mumtaz K. Laser diode area melting for high speed additive manufacturing of metallic components. Materials & Design. 2017 Mar 5;117:305-15.

238. Bidare P, Bitharas I, Ward RM, Attallah MM, Moore AJ. Fluid and particle dynamics in laser powder bed fusion. Acta Materialia. 2018 Jan 1;142:107-20.

239. Xiang Z, Yin M, Dong G, Mei X, Yin G. Modeling of the thermal physical process and study on the reliability of linear energy density for selective laser melting. Results in Physics. 2018 Jun 1;9:939-46.

240. Nurminen J, Riihimäki J, Näkki J, Vuoristo P. Comparison of laser cladding with powder and hot and cold wire techniques. InInternational Congress on Applications of Lasers & Electro-Optics 2006 Oct (Vol. 2006, No. 1, p. 1006). Laser Institute of America.

241. Webber, T. "Material processing using a CW Nd: YAG laser." Industrial Laser Review 7, no. 11 (1992): 5-9.

242. Denney, Paul, and Al Grubowski. "Using fiber optics for laser cladding." Journal of ship production 8, no. 03 (1992): 157-162.

243. Steen, W. M. "Surface engineering with lasers." In Applied Laser Tooling, pp. 131-181. Springer, Dordrecht, 1987.

244. Ion, John C. “Engineering Materials.” Laser Processing of Engineering Materials, 2005, pp. 139–177., https://doi.org/10.1016/b978-075066079-2/50008-8.

245. Nowotny, Steffen. "Current use of laser technology for build-up welding applications." Surface engineering 27, no. 4 (2011): 231-233.

246. Steen, William M. "Laser cladding, alloying and melting." Industrial Laser Annual Handbook (1986): 158-174.

247. Liu, Jichang, and Lijun Li. “Study on Cross-Section Clad Profile in Coaxial Single-Pass Cladding with a Low-Power Laser.” Optics & Laser Technology, vol. 37, no. 6, 2005, pp. 478–482., https://doi.org/10.1016/j.optlastec.2004.07.010.

248. Huang Y, Zeng X, Hu Q. Analysis of laser-induction hybrid cladding processing conditions. In3rd International Symposium on Advanced Optical Manufacturing and Testing Technologies: Advanced Optical Manufacturing Technologies 2007 Nov 14 (Vol. 6722, pp. 329-336). SPIE.

249. Huang, Yongjun, and Xiaoyan Zeng. “Investigation on Cracking Behavior of Ni-Based Coating by Laser-Induction Hybrid Cladding.” Applied Surface Science, vol. 256, no. 20, 2010, pp. 5985–5992., https://doi.org/10.1016/j.apsusc.2010.03.106.

250. Schopphoven T, Gasser A, Wissenbach K, Poprawe R. Investigations on ultra-high-speed laser material deposition as alternative for hard chrome plating and thermal spraying. Journal of Laser Applications. 2016 May 1;28(2).

251. Xiao M, Gao H, Sun L, Wang Z, Jiang G, Zhao Q, Guo C, Li L, Jiang F. Microstructure and mechanical properties of Fe-based amorphous alloy coatings prepared by ultra-high speed laser cladding. Materials Letters. 2021 Aug 15;297:130002.

252. Cui Z, Qin Z, Dong P, Mi Y, Gong D, Li W. Microstructure and corrosion properties of FeCoNiCrMn high entropy alloy coatings prepared by high speed laser cladding and ultrasonic surface mechanical rolling treatment. Materials Letters. 2020 Jan 15;259:126769.

253. Xu QL, Zhang Y, Liu SH, Li CJ, Li CX. High-temperature oxidation behavior of CuAlNiCrFe high-entropy alloy bond coats deposited using high-speed laser cladding process. Surface and Coatings Technology. 2020 Sep 25;398:126093.

254. Li L, Shen F, Zhou Y, Tao W. Comparative study of stainless steel AISI 431 coatings prepared by extreme-high-speed and conventional laser cladding. Journal of Laser Applications. 2019 Nov 1;31(4).

255. Schopphoven T, Gasser A, Backes G. EHLA: Extreme High-Speed Laser Material Deposition: Economical and effective protection against corrosion and wear. Laser Technik Journal. 2017 Sep;14(4):26-9.

256. Toyserkani E, Khajepour A, Corbin SF. Laser cladding. CRC press; 2004 Aug 12.

257. S., William M., and J. Mazumder. Laser Material Processing. Springer, 2010.

258. Jinoop AN, Paul CP, Bindra KS. Laser assisted direct energy deposition of Hastelloy-X. Optics & Laser Technology. 2019 Jan 1;109:14-9.

259. Jeantette, Francisco P, Keicher, David M, Romero, Joseph A, and Schanwald, Lee P. 2000. "Method and system for producing complex-shape objects". United States. https://www.osti.gov/servlets/purl/872939.

260. Carvalho PA, Braz N, Pontinha MM, Ferreira MG, Steen WM, Vilar R, Watkins KG. Automated workstation for variable composition laser cladding—its use for rapid alloy scanning. Surface and Coatings Technology. 1995 May 1;72(1-2):62-70.

261. Mazumder J, Dutta D, Kikuchi N, Ghosh A. Closed loop direct metal deposition: art to part. Optics and lasers in engineering. 2000 Oct 1;34(4-6):397-414.

262. R.G. Landers, M. Hilgers, F.W. Liou, and B. McMillin, “Object oriented modeling and fault detection of a powder feeder for a laser metal deposition system,” in 13th Annual Solid Freeform Fabrication Symposium. Austin, Texas, 2002., https://core.ac.uk/display/237202367

263. Li, L., and W. M. Steen. “Sensing, Modelling and Closed Loop Control of Powder Feeder for Laser Surface Modification.” International Congress on Applications of Lasers & Electro-Optics, 1993, https://doi.org/10.2351/1.5058663.

264. Corbin SF, Toyserkani E, Khajepour A. Cladding of an Fe-aluminide coating on mild steel using pulsed laser assisted powder deposition. Materials Science and Engineering: A. 2003 Aug 15;354(1-2):48-57.

265. Xue, L., and M. Islam. “Free-Form Laser Consolidation for Producing Functional Metallic Components.” International Congress on Applications of Lasers & Electro-Optics, 1998, https://doi.org/10.2351/1.5059143.

266. Bayode, A. Advanced Material Development: Functionally Graded Stainless Steel Alloy Composites. 2018. http://hdl.handle.net/10210/284879

267. Siddiqui AA, Dubey AK, Paul CP. A study of metallurgy and erosion in laser surface alloying of AlxCu0. 5FeNiTi high entropy alloy. Surface and Coatings Technology. 2019 Mar 15;361:27-34.

268. Fogagnolo JB, Rodrigues AV, Sallica-Leva E, Lima MS, Caram R. Surface stiffness gradient in Ti parts obtained by laser surface alloying with Cu and Nb. Surface and Coatings Technology. 2016 Jul 15;297:34-42.

269. Wen X, Cui X, Jin G, Zhang X, Zhang Y, Zhang D, Fang Y. Design and characterization of FeCrCoAlMn0. 5Mo0. 1 high-entropy alloy coating by ultrasonic assisted laser cladding. Journal of Alloys and Compounds. 2020 Sep 15;835:155449.

270. Abe N, Tanigawa D, Tsukamoto M, Hayashi Y, Yamazaki H, Tatsumi Y, Yoneyama M. Dynamic observation of formation process in laser cladding using high speed video camera. InInternational Congress on Applications of Lasers & Electro-Optics 2013 Oct 1 (pp. 448-452). AIP Publishing.

271. Aghakhani, M. “Parametric Optimization of Gas Metal Arc Welding Process by Taguchi Method on Weld Dilution.” International Journal of Modeling and Optimization, 2011, pp. 216–220., doi:10.7763/ijmo.2011.v1.38.

272. Alizadeh-Sh M, Marashi SP, Ranjbarnodeh E, Shoja-Razavi R, Oliveira JP. Prediction of solidification cracking by an empirical-statistical analysis for laser cladding of Inconel 718 powder on a non-weldable substrate. Optics & Laser Technology. 2020 Aug 1;128:106244.

273. Amado JM, Tobar MJ, Alvarez JC, Lamas J, Yáñez A. Laser cladding of tungsten carbides (Spherotene®) hardfacing alloys for the mining and mineral industry. Applied Surface Science. 2009 Mar 1;255(10):5553-6.

274. Apolinario LH, Wallerstein D, Montealegre MA, Urtiga Filho SL, Torres EA, Hermenegildo TF, Santos TF. Predominant solidification modes of 316 austenitic stainless steel coatings deposited by laser cladding on 304 stainless steel substrates. Metallurgical and materials transactions A. 2019 Aug 15;50:3617-28.

275. Banovic SW, DuPont IN, Marder AR. Dilution control in gas-tungsten-arc welds involving superaustenitic stainless steels and nickel-based alloys. Metallurgical and Materials Transactions B. 2001 Dec;32:1171-6.

276. Bax B, Rajput R, Kellet R, Reisacher M. Systematic evaluation of process parameter maps for laser cladding and directed energy deposition. Additive Manufacturing. 2018 May 1;21:487-94.

277. Bin L, Heping L, Xingbin J, Yuxin L, Peikang B. The effect of laser process parameters on microstructure and dilution rate of cladding coatings. InIOP Conference Series: Materials Science and Engineering 2018 Feb 1 (Vol. 307, No. 1, p. 012035). IOP Publishing.

278. Caneda CM, Fogagnolo JB, Kiminami CS, Afonso CR. Ultrafine eutectic coatings from Fe-Nb-B powder using laser cladding. Materials characterization. 2020 Feb 1;160:110080.

279. Chakraborty, Shitanshu Shekhar, and Samik Dutta. “Estimation of Dilution in Laser Cladding Based on Energy Balance Approach Using Regression Analysis.” Sādhanā, vol. 44, no. 6, 2019, doi:10.1007/s12046-019-1134-9.

280. Chen JL, Li J, Song R, Bai LL, Shao JZ, Qu CC. Effect of the scanning speed on microstructural evolution and wear behaviors of laser cladding NiCrBSi composite coatings. Optics & Laser Technology. 2015 Sep 1;72:86-99.

281. Chen Y, Wang X, Zhao Y, Song B, Yu T. Interactive optimization of process parameters and coating analysis of laser cladding JG-3 powder. The International Journal of Advanced Manufacturing Technology. 2020 Mar;107:2623-33.

282. Cheng FT, Lo KH, Man HC. A preliminary study of laser cladding of AISI 316 stainless steel using preplaced NiTi wire. Materials Science and Engineering: A. 2004 Aug 25;380(1-2):20-9.

283. Chiu KY, Cheng FT, Man HC. Laser cladding of austenitic stainless steel using NiTi strips for resisting cavitation erosion. Materials Science and Engineering: A. 2005 Aug 15;402(1-2):126-34.

284. Coniglio N, Cross CE, Michael T, Lammers M. Defining a critical weld dilution to avoid solidification cracking in aluminum. Welding Journal. 2008 Sep 1;87(8):237s-47s.

285. De Oliveira U, Ocelik V, De Hosson JT. Analysis of coaxial laser cladding processing conditions. Surface and Coatings Technology. 2005 Jul 22;197(2-3):127-36.

286. Fathi A, Toyserkani E, Khajepour A, Durali M. Prediction of melt pool depth and dilution in laser powder deposition. Journal of Physics D: Applied Physics. 2006 Jun 2;39(12):2613.

287. Figueredo EW, Apolinario LH, Santos MV, Silva AC, Avila JA, Lima MS, Santos TF. Influence of laser beam power and scanning speed on the macrostructural characteristics of AISI 316L and AISI 431 stainless steel depositions produced by laser cladding process. Journal of Materials Engineering and Performance. 2021 May;30:3298-312.

288. Rebouças Filho PP, da Silveira Cavalcante T, de Albuquerque VH, Tavares JM, Cortez PC. Measurement of welding dilution from images using active contours. InSEECCM 2009-2nd South-East European Conference on Computational Mechanics 2009.

289. Golyshev AA, Orishich AM, Filippov AA. Similarity laws in laser cladding of cermet coatings. Journal of Applied Mechanics and Technical Physics. 2019 Jul;60:758-67.

290. Goodarzi DM, Pekkarinen J, Salminen A. Effect of process parameters in laser cladding on substrate melted areas and the substrate melted shape. Journal of Laser Applications. 2015 Feb 1;27(S2).

291. Gowtham A, Chaitanya G, Katiyar JK, Chandak A, Gupta TV. Experimental investigations on laser cladding of NiCrBSi+ WC coating on SS410. Materials Today: Proceedings. 2020 Jan 1;27:1984-9.

292. Powell J, Koti D, Garmendia X, Voisey KT. Assessing the quality and productivity of laser cladding and direct energy deposition: Guidelines for researchers. Journal of Laser Applications. 2023 Feb 14;35(1):012024.

293. Hemmati I, Ocelík V, De Hosson JT. Dilution effects in laser cladding of Ni–Cr–B–Si–C hardfacing alloys. Materials Letters. 2012 Oct 1;84:69-72.

294. Henri P, Sebastian T, Jari T, Steffen N, Petri V. Laser cladding with coaxial wire feeding. InInternational Congress on Applications of Lasers & Electro-Optics 2012 Sep 1 (Vol. 2012, No. 1, pp. 1196-1201). Laser Institute of America.

295. Hofman, J.T. "Development of an Observation and Control System for Industrial Laser Cladding." Proefschrift Universiteit Twente, Enschede, S.n., 2009.

296. Hofman JT, Pathiraj B, Van Dijk J, De Lange DF, Meijer J. A camera based feedback control strategy for the laser cladding process. Journal of Materials Processing Technology. 2012 Nov 1;212(11):2455-62.

297. Huang FX, Jiang ZH, Liu XM, Lian JS, Chen L. Effects of process parameters on microstructure and hardness of layers by laser cladding. ISIJ international. 2011 Mar 15;51(3):441-7.

298. Huang, Yongjun. "Characterization of Dilution Action in Laser-Induction Hybrid Cladding." Optics & Laser Technology, vol. 43, no. 5, 2011, pp. 965–973., doi:10.1016/j.optlastec.2010.12.005.

299. Ju H, Zhang ZJ, Lin CX, Liu ZJ, Jiang HL. Design optimization and experimental study of coaxial powder-feeding nozzle in the laser cladding process. InIOP Conference Series: Materials Science and Engineering 2019 (Vol. 474, No. 1, p. 012008). IOP Publishing.

300. Kathuria, Y.P. "Some Aspects of Laser Surface Cladding in the Turbine Industry." Surface and Coatings Technology, vol. 132, no. 2-3, 2000, pp. 262–269., doi:10.1016/s0257-8972(00)00735-0.

301. Khorram A, Jamaloei AD, Paidar M, Cao X. Laser cladding of Inconel 718 with 75Cr3C2+ 25 (80Ni20Cr) powder: Statistical modeling and optimization. Surface and Coatings Technology. 2019 Nov 25;378:124933.

302. Kim CK, Choi SG, Kim JH, Jo HJ, Jo YC, Choi SP, Cho YT. Characterization of surface modification by laser cladding using low melting point metal. Journal of Industrial and Engineering Chemistry. 2020 Jul 25;87:54-9.

303. Kim JD, Kang KH, Kim JN. Nd: YAG laser cladding of marine propeller with hastelloy C-22. Applied Physics A. 2004 Sep;79:1583-5.

304. Kim, Jae-Do, and Yun Peng. “Plunging Method for Nd:YAG Laser Cladding with Wire Feeding.” Optics and Lasers in Engineering, vol. 33, no. 4, 2000, pp. 299–309., doi:10.1016/s0143-8166(00)00046-4.

305. Kim, Jae-Do, and Yun Peng. “Time-Dependent FEM Simulation of Dilution Control of Laser Cladding by Adaptive Mesh Method.” KSME International Journal, vol. 14, no. 2, 2000, pp. 177–187., doi:10.1007/bf03184784.

306. Kumar, Amitesh, and Subhransu Roy. “Effect of Three-Dimensional Melt Pool Convection on Process Characteristics during Laser Cladding.” Computational Materials Science, vol. 46, no. 2, 2009, pp. 495–506., doi:10.1016/j.commatsci.2009.04.002.

307. Li M, Huang J, Zhu YY, Li ZG. Effect of heat input on the microstructure of in-situ synthesized TiN–TiB/Ti based composite coating by laser cladding. Surface and Coatings Technology. 2012 May 25;206(19-20):4021-6.

308. Li R, Li Z, Huang J, Zhu Y. Dilution effect on the formation of amorphous phase in the laser cladded Ni–Fe–B–Si–Nb coatings after laser remelting process. Applied surface science. 2012 Aug 1;258(20):7956-61.

309. Li Y, Su K, Bai P, Wu L. Microstructure and property characterization of Ti/TiBCN reinforced Ti based composite coatings fabricated by laser cladding with different scanning speed. Materials Characterization. 2020 Jan 1;159:110023.

310. Lian G, Yao M, Zhang Y, Chen C. Analysis and prediction on geometric characteristics of multi-track overlapping laser cladding. The International Journal of Advanced Manufacturing Technology. 2018 Jul;97:2397-407.

311. Liu H, Qin X, Huang S, Hu Z, Ni M. Geometry modeling of single track cladding deposited by high power diode laser with rectangular beam spot. Optics and Lasers in Engineering. 2018 Jan 1;100:38-46.

312. Liu H, Hu Z, Qin X, Wang Y, Zhang J, Huang S. Parameter optimization and experimental study of the sprocket repairing using laser cladding. The International Journal of Advanced Manufacturing Technology. 2017 Aug;91:3967-75.

313. Liu J, Li J, Cheng X, Wang H. Effect of dilution and macrosegregation on corrosion resistance of laser clad AerMet100 steel coating on 300M steel substrate. Surface and Coatings Technology. 2017 Sep 25;325:352-9.

314. Liu J, Liu H, Tian X, Yang H, Hao J. Microstructural evolution and corrosion properties of Ni-based alloy coatings fabricated by multi-layer laser cladding on cast iron. Journal of Alloys and Compounds. 2020 May 5;822:153708.

315. Liu J, Yu H, Chen C, Weng F, Dai J. Research and development status of laser cladding on magnesium alloys: A review. Optics and Lasers in Engineering. 2017 Jun 1;93:195-210.

316. Liu K, Li Y, Wang J, Ma Q. Effect of high dilution on the in situ synthesis of Ni–Zr/Zr–Si (B, C) reinforced composite coating on zirconium alloy substrate by laser cladding. Materials & Design. 2015 Dec 15;87:66-74.

317. Liu S, Liu W, Kovacevic R. Experimental investigation of laser hot-wire cladding. Proceedings of the Institution of Mechanical Engineers, Part B: Journal of Engineering Manufacture. 2017 May;231(6):1007-20.

318. Liu WW, Tang ZJ, Liu XY, Wang HJ, Zhang HC. A review on in-situ monitoring and adaptive control technology for laser cladding remanufacturing. Procedia Cirp. 2017 Jan 1;61:235-40.

319. Miná ÉM, Da Silva YC, Dille J, Silva CC. The effect of dilution on microsegregation in AWS ER NiCrMo-14 alloy welding claddings. Metallurgical and Materials Transactions A. 2016 Dec;47:6138-47.

320. Ming Q, Lim LC, Chen ZD. Laser cladding of nickel-based hardfacing alloys. Surface and coatings technology. 1998 Aug 4;106(2-3):174-82.

321. Miyamoto I, Fujimori S, Itakura K. Mechanism of dilution in laser cladding with powder feeding. InInternational Congress on Applications of Lasers & Electro-Optics 1997 Nov 1 (pp. F1-F10). AIP Publishing.

322. Moosa AA, Kadhim MJ, Subhi AD. Dilution effect during laser cladding of Inconel 617 with Ni-Al powders. Modern Applied Science. 2011 Feb 1;5(1):50.

323. Näkki J, Tuominen J, Vuoristo P. Effect of minor elements on solidification cracking and dilution of alloy 625 powders in laser cladding. Journal of Laser Applications. 2017 Feb 1;29(1).

324. Ocelík, V., and J.T.M. De Hosson. “Thick Metallic Coatings Produced by Coaxial and Side Laser Cladding: Processing and Properties.” Advances in Laser Materials Processing, 2010, pp. 426–457., doi:10.1533/9781845699819.5.426.

325. Ocelík V, De Oliveira U, De Boer M, De Hosson JT. Thick Co-based coating on cast iron by side laser cladding: Analysis of processing conditions and coating properties. Surface and Coatings Technology. 2007 Mar 5;201(12):5875-83.

326. Pajukoski H, Näkki J, Thieme S, Tuominen J, Nowotny S, Vuoristo P. High performance corrosion resistant coatings by novel coaxial cold-and hot-wire laser cladding methods. Journal of Laser Applications. 2016 Feb 1;28(1)..

327. Pekkarinen J, Salminen A, Kujanpää V. Laser cladding with scanning optics: Effect of scanning frequency and laser beam power density on cladding process. Journal of Laser Applications. 2014 Aug 1;26(3)..

328. Qian M, Lim LC, Chen ZD, Chen WI. Parametric studies of laser cladding processes. Journal of Materials Processing Technology. 1997 Jan 1;63(1-3):590-3.

329. Riquelme A, Rodrigo P, Escalera-Rodríguez MD, Rams J. Analysis and optimization of process parameters in Al–SiCp laser cladding. Optics and Lasers in Engineering. 2016 Mar 1;78:165-73.

330. Riquelme A, Escalera-Rodriguez MD, Rodrigo P, Rams J. Role of laser cladding parameters in composite coating (Al-SiC) on aluminum alloy. Journal of Thermal Spray Technology. 2016 Aug;25:1177-91.

331. Rivero LE, Pizzatto A, Teixeira MF, Rabelo A, Falcade T, Scheid A. Effect of Laser Power and Substrate on the Hastelloy C276 TM Coatings Features Deposited by Laser Cladding. Materials Research. 2020 Jun 1;23..

332. Salehi, Dariush Seyed. “Sensing and Control of Nd:YAG Laser Cladding Process.” Swinburne University of Technology, Industrial Research Institute Swinburne -, Melbourne, Australia 2005.

333. Sampedro J, Pérez I, Carcel B, Ramos JA, Amigó V. Laser cladding of TiC for better titanium components. Physics Procedia. 2011 Jan 1;12:313-22.

334. Saqib S, Urbanic RJ, Aggarwal K. Analysis of laser cladding bead morphology for developing additive manufacturing travel paths. Procedia Cirp. 2014 Jan 1;17:824-9..

335. Singh R, Kumar D, Mishra SK, Tiwari SK. Laser cladding of Stellite 6 on stainless steel to enhance solid particle erosion and cavitation resistance. Surface and Coatings Technology. 2014 Jul 25;251:87-97.

336. Sobiyi, Kehinde, and Esther Akinlabi. “Microstructural Investigation Of Ti Coating On Ti6al4v By Laser Cladding.” Materials Today: Proceedings, vol. 4, no. 2, 2017, pp. 244–249., doi:10.1016/j.matpr.2017.01.018.

337. Song B, Hussain T, Voisey KT. Laser cladding of Ni50Cr: A parametric and dilution study. Physics Procedia. 2016 Jan 1;83:706-15.

338. de Sousa JM, Ratusznei F, Pereira M, de Medeiros Castro R, Curi EI. Abrasion resistance of Ni-Cr-B-Si coating deposited by laser cladding process. Tribology International. 2020 Mar 1;143:106002.

339. Sun RL, Yang DZ, Guo LX, Dong SL. Laser cladding of Ti-6Al-4V alloy with TiC and TiC+ NiCrBSi powders. Surface and Coatings Technology. 2001 Jan 15;135(2-3):307-12..

340. Tanigawa D, Funada Y, Abe N, Tsukamoto M, Hayashi Y, Yamazaki H, Tatsumi Y, Yoneyama M. Suppression of dilution in Ni-Cr-Si-B alloy cladding layer by controlling diode laser beam profile. Optics & Laser Technology. 2018 Feb 1;99:326-32.

341. Tanigawa D, Abe N, Tsukamoto M, Hayashi Y, Yamazaki H, Tatsumi Y, Yoneyama M. The effect of particle size on the heat affected zone during laser cladding of Ni–Cr–Si–B alloy on C45 carbon steel. Optics and Lasers in Engineering. 2018 Feb 1;101:23-7.

342. Tian H, Chen X, Yan Z, Zhi X, Yang Q, Yuan Z. Finite-element simulation of melt pool geometry and dilution ratio during laser cladding. Applied Physics A. 2019 Jul;125:1-9.

343. Toyserkani E, Khajepour A, Corbin S. Application of experimental-based modeling to laser cladding. Journal of Laser Applications. 2002 Aug 1;14(3):165-73.

344. Tuominen, J. “Engineering Coatings by Laser Cladding - the Study of Wear and Corrosion Properties.” Trepo Etusivu, Tampere University of Technology, 1 Jan. 2009, trepo.tuni.fi/handle/10024/115193.

345. Wen P, Feng Z, Zheng S. Formation quality optimization of laser hot wire cladding for repairing martensite precipitation hardening stainless steel. Optics & Laser Technology. 2015 Jan 1;65:180-8.

346. Wen X, Cui X, Jin G, Zhang X, Zhang Y, Zhang D, Fang Y. Design and characterization of FeCrCoAlMn0. 5Mo0. 1 high-entropy alloy coating by ultrasonic assisted laser cladding. Journal of Alloys and Compounds. 2020 Sep 15;835:155449.

347. Wirth, Florian, and Konrad Wegener. “A Physical Modeling and Predictive Simulation of the Laser Cladding Process.” Additive Manufacturing, vol. 22, 2018, pp. 307–319., doi:10.1016/j.addma.2018.05.017.

348. Xi W, Song B, Zhao Y, Yu T, Wang J. Geometry and dilution rate analysis and prediction of laser cladding. The International Journal of Advanced Manufacturing Technology. 2019 Aug 1;103:4695-702.

349. Xu G, Kutsuna M, Liu Z, Yamada K. Comparison between diode laser and TIG cladding of Co-based alloys on the SUS403 stainless steel. Surface and Coatings Technology. 2006 Oct 5;201(3-4):1138-44.

350. Ya, W. “Laser Materials Interactions during Cladding: Analyses on Clad Formation, Thermal Cycles, Residual Stress and Defects.” Dissertation University of Twente in order to obtain the degree of doctor in the year, 2015.

351. Yu T, Yang L, Zhao Y, Sun J, Li B. Experimental research and multi-response multi-parameter optimization of laser cladding Fe313. Optics & Laser Technology. 2018 Dec 1;108:321-32.

352. Zanzarin, Simone. “Laser Cladding with Metallic Powders.” Thesis / Dissertation ETD, University of Trento, 2015.

353. Zhang H, Shi Y, Kutsuna M, Xu GJ. Laser cladding of Colmonoy 6 powder on AISI316L austenitic stainless steel. Nuclear engineering and design. 2010 Oct 1;240(10):2691-6.

354. Zhao G, Cho C, Kim JD. Application of 3-D finite element method using Lagrangian formulation to dilution control in laser cladding process. International Journal of Mechanical Sciences. 2003 May 1;45(5):777-96.

355. Zhong M, Liu W, Yao K, Goussain JC, Mayer C, Becker A. Microstructural evolution in high power laser cladding of Stellite 6+ WC layers. Surface and Coatings Technology. 2002 Aug 22;157(2-3):128-37.

356. Zhu S, Chen W, Ding L, Zhan X, Chen Q. A mathematical model of laser cladding repair. The International Journal of Advanced Manufacturing Technology. 2019 Aug 1;103:3265-78.

357. Zhu S, Chen W, Zhan X, Ding L, Wang E. Optimization of dilution rate of laser cladding repair based on deep learning. The International Journal of Advanced Manufacturing Technology. 2020 Sep;110:1471-84.

358. Aghili, S.E., and M. Shamanian. “Investigation of Powder Fed Laser Cladding of NiCr-Chromium Carbides Single-Tracks on Titanium Aluminide Substrate.” Optics & Laser Technology, vol. 119, 2019, p. 105652., doi:10.1016/j.optlastec.2019.105652.

359. Al-Sayed Ali SR, Hussein AH, Nofal AA, Hasseb Elnaby SE, Elgazzar HA, Sabour HA. Laser powder cladding of Ti-6Al-4V α/β alloy. Materials. 2017 Oct 15;10(10):1178.

360. Alvarez P, Montealegre MÁ, Pulido-Jiménez JF, Arrizubieta JI. Analysis of the process parameter influence in laser cladding of 316L stainless steel. Journal of Manufacturing and Materials Processing. 2018 Aug 15;2(3):55.

361. Ansari M, Razavi RS, Barekat M. An empirical-statistical model for coaxial laser cladding of NiCrAlY powder on Inconel 738 superalloy. Optics & Laser Technology. 2016 Dec 1;86:136-44.

362. Barekat M, Razavi RS, Ghasemi A. Nd: YAG laser cladding of Co–Cr–Mo alloy on γ-TiAl substrate. Optics & Laser Technology. 2016 Jun 1;80:145-52.

363. Bourahima F, Helbert AL, Rege M, Ji V, Solas D, Baudin T. Laser cladding of Ni based powder on a Cu-Ni-Al glassmold: Influence of the process parameters on bonding quality and coating geometry. Journal of Alloys and Compounds. 2019 Jan 15;771:1018-28.

364. Cai Y, Chen Y, Manladan SM, Luo Z, Gao F, Li L. Influence of dilution rate on the microstructure and properties of FeCrCoNi high-entropy alloy coating. Materials & Design. 2018 Mar 15;142:124-37.

365. Capello E, Colombo D, Previtali B. Repairing of sintered tools using laser cladding by wire. Journal of materials processing technology. 2005 May 15;164:990-1000..

366. Cho C, Zhao G, Kwak SY, Kim CB. Computational mechanics of laser cladding process. Journal of materials processing technology. 2004 Nov 10;153:494-500.

367. Choi J, Han L, Hua Y. “Modeling and Experiments of Laser Cladding With Droplet Injection.” Journal of Heat Transfer, vol. 127, no. 9, 2005, pp. 978–986., doi:10.1115/1.2005273.

368. Colaco R, Carvalho T, Vilar R. Laser cladding of stellite 6 on steel substrates. High Temp. Chem. Processes. 1994;3(1):21-9.

369. Del Val J, Comesaña R, Lusquiños F, Boutinguiza M, Riveiro A, Quintero F, Pou J. Laser cladding of Co-based superalloy coatings: Comparative study between Nd: YAG laser and fibre laser. Surface and Coatings Technology. 2010 Mar 15;204(12-13):1957-61.

370. Erfanmanesh M, Abdollah-Pour H, Mohammadian-Semnani H, Shoja-Razavi R. An empirical-statistical model for laser cladding of WC-12Co powder on AISI 321 stainless steel. Optics & Laser Technology. 2017 Dec 1;97:180-6.

371. Erfanmanesh M, Shoja-Razavi R, Abdollah-Pour H, Mohammadian-Semnani H. Influence of using electroless Ni-P coated WC-Co powder on laser cladding of stainless steel. Surface and Coatings Technology. 2018 Aug 25;348:41-54.

372. Fan, Pengfei, and Guan Zhang. “Study on Process Optimization of WC-Co50 Cermet Composite Coating by Laser Cladding.” International Journal of Refractory Metals and Hard Materials, vol. 87, 2020, p. 105133., doi:10.1016/j.ijrmhm.2019.105133.

373. Farahmand, Parisa, and Radovan Kovacevic. “Parametric Study and Multi-Criteria Optimization in Laser Cladding by a High Power Direct Diode Laser.” Lasers in Manufacturing and Materials Processing, vol. 1, no. 1-4, 2014, pp. 1–20., doi:10.1007/s40516-014-0001-0.

374. Guo LF, Yue TM, Man HC. A finite element method approach for thermal analysis of laser cladding of magnesium alloy with preplaced Al–Si powder. Journal of Laser Applications. 2004 Nov 1;16(4):229-35.

375. Guo S, Chen Z, Cai D, Zhang Q, Kovalenko V, Yao J. Prediction of simulating and experiments for Co-based alloy laser cladding by HPDL. Physics Procedia. 2013 Jan 1;50:375-82.

376. He X, Song RG, Kong DJ. Microstructures and properties of Ni/TiC/La2O3 reinforced Al based composite coatings by laser cladding. Optics & Laser Technology. 2019 Sep 1;117:18-27.

377. Javid, Y. “Multi-Response Optimization in Laser Cladding Process of WC Powder on Inconel 718.” CIRP Journal of Manufacturing Science and Technology, vol. 31, 2020, pp. 406–417., doi:10.1016/j.cirpj.2020.07.003.

378. Javid, Y., and M. Ghoreishi. “Thermo-Mechanical Analysis in Pulsed Laser Cladding of WC Powder on Inconel 718.” The International Journal of Advanced Manufacturing Technology, vol. 92, no. 1-4, 2017, pp. 69–79., doi:10.1007/s00170-017-0117-4.

379. Kai-ming W, Han-guang F, Yu-long L, Yong-ping L, Shi-zhong W, Zhen-qing S. Effect of power on microstructure and properties of laser cladding NiCrBSi composite coating. Transactions of the IMF. 2017 Nov 2;95(6):328-36.

380. Kumar, S., S. Roy, C.P. Paul, and A.K. Nath, Three-dimensional conduction heat transfer model for laser cladding process. Numerical Heat Transfer, Part B, 2008. 53: p. 271-287.

381. Kumar, Subrata, and Subhransu Roy. “Development of a Theoretical Process Map for Laser Cladding Using Two-Dimensional Conduction Heat Transfer Model.” Computational Materials Science, vol. 41, no. 4, 2008, pp. 457–466., doi:10.1016/j.commatsci.2007.05.002.

382. Li Y, Zhang P, Bai P, Su K, Su H. TiBCN-ceramic-reinforced Ti-based coating by laser cladding: Analysis of processing conditions and coating properties. Coatings. 2019 Jun 24;9(6):407.

383. Luo X, Li J, Li GJ. Effect of NiCrBSi content on microstructural evolution, cracking susceptibility and wear behaviors of laser cladding WC/Ni–NiCrBSi composite coatings. Journal of Alloys and Compounds. 2015 Mar 25;626:102-11.

384. Ma M, Xiong W, Lian Y, Han D, Zhao C, Zhang J. Modeling and optimization for laser cladding via multi-objective quantum-behaved particle swarm optimization algorithm. Surface and Coatings Technology. 2020 Jan 15;381:125129.

385. Marzban J, Ghaseminejad P, Ahmadzadeh MH, Teimouri R. Experimental investigation and statistical optimization of laser surface cladding parameters. The International Journal of Advanced Manufacturing Technology. 2015 Feb;76:1163-72.

386. Mirzade FK, Niziev VG, Panchenko VY, Khomenko MD, Grishaev RV, Pityana S, van Rooyen C. Kinetic approach in numerical modeling of melting and crystallization at laser cladding with powder injection. Physica B: Condensed Matter. 2013 Aug 15;423:69-76.

387. Pan F, Zhu Q, Li S, Xiang M, Du Z. Decomposition-carbonization of ammonium paratungstate in a fluidized bed. International Journal of Refractory Metals and Hard Materials. 2018 Apr 1;72:315-22.

388. Nabhani M, Razavi RS, Barekat M. An empirical-statistical model for laser cladding of Ti-6Al-4V powder on Ti-6Al-4V substrate. Optics & Laser Technology. 2018 Mar 1;100:265-71.

389. Fesharaki MN, Shoja-Razavi R, Mansouri HA, Jamali H. Microstructure investigation of Inconel 625 coating obtained by laser cladding and TIG cladding methods. Surface and Coatings Technology. 2018 Nov 15;353:25-31.

390. Palumbo G, Pinto S, Tricarico L. Numerical finite element investigation on laser cladding treatment of ring geometries. Journal of materials processing technology. 2004 Nov 30;155:1443-50.

391. Partes, K., and G. Sepold. “Modulation of Power Density Distribution in Time and Space for High Speed Laser Cladding.” Journal of Materials Processing Technology, vol. 195, no. 1-3, 2008, pp. 27–33., doi:10.1016/j.jmatprotec.2007.05.052.

392. Pekkarinen IJ, Kujanpää V, Salminen A. Laser cladding using scanning optics. Journal of Laser Applications. 2012 Nov 1;24(5).

393. Pekkarinen J, Kujanpää V, Salminen A. Laser cladding with scanning optics: Effect of power adjustment. Journal of Laser Applications. 2012 Aug 1;24(3).

394. Riveiro A, Mejías A, Lusquiños F, Del Val J, Comesaña R, Pardo J, Pou J. Optimization of laser cladding for Al coating production. Physics Procedia. 2013 Jan 1;41:327-34.

395. Santhanakrishnan S, Kong F, Kovacevic R. An experimentally based thermo-kinetic hardening model for high power direct diode laser cladding. Journal of Materials Processing Technology. 2011 Jul 1;211(7):1247-59.

396. Shayanfar P, Daneshmanesh H, Janghorban K. Parameters optimization for laser cladding of inconel 625 on ASTM A592 steel. Journal of Materials Research and Technology. 2020 Jul 1;9(4):8258-65.

397. Siddiqui, Anas Ahmad, and Avanish Kumar Dubey. “Recent Trends in Laser Cladding and Surface Alloying.” Optics & Laser Technology, vol. 134, 2021, p. 106619., doi:10.1016/j.optlastec.2020.106619.

398. Smurov I, Doubenskaia M, Zaitsev A. Comprehensive analysis of laser cladding by means of optical diagnostics and numerical simulation. Surface and Coatings Technology. 2013 Apr 15;220:112-21.

399. Sun, Yuwen, and Mingzhong Hao. “Statistical Analysis and Optimization of Process Parameters in Ti6Al4V Laser Cladding Using Nd:YAG Laser.” Optics and Lasers in Engineering, vol. 50, no. 7, 2012, pp. 985–995., doi:10.1016/j.optlaseng.2012.01.018.

400. Tseng, W.C., and J.N. Aoh. “Simulation Study on Laser Cladding on Preplaced Powder Layer with a Tailored Laser Heat Source.” Optics & Laser Technology, vol. 48, 2013, pp. 141–152., doi:10.1016/j.optlastec.2012.09.014.

401. Wang H, Zhang W, Peng Y, Zhang M, Liu S, Liu Y. Microstructures and wear resistance of FeCoCrNi-Mo high entropy alloy/diamond composite coatings by high speed laser cladding. Coatings. 2020 Mar 24;10(3):300.

402. Weng F, Chen C, Yu H. Research status of laser cladding on titanium and its alloys: A review. Materials & Design. 2014 Jun 1;58:412-25.

403. Wu X, Zhu B, Zeng X, Hu X, Cui K. Critical state of laser cladding with powder auto-feeding. Surface and Coatings technology. 1996 Feb 1;79(1-3):200-4.

404. Wu D, Guo M, Ma G, Niu F. Dilution characteristics of ultrasonic assisted laser clad yttria-stabilized zirconia coating. Materials Letters. 2015 Feb 15;141:207-9.

405. Xu G, Kutsuna M, Liu Z, Zhang H. Characteristics of Ni-based coating layer formed by laser and plasma cladding processes. Materials Science and Engineering: A. 2006 Feb 15;417(1-2):63-72.

406. Yang S, Liu W, Zhong M, Wang Z. TiC reinforced composite coating produced by powder feeding laser cladding. Materials Letters. 2004 Sep 1;58(24):2958-62.

407. Yang Y, Jiang ZP, Li HZ. Effect of co-based alloy on properties of laser cladding layer. InIOP Conference Series: Materials Science and Engineering 2017 Nov 1 (Vol. 265, No. 1, p. 012021). IOP Publishing.

408. Yong Y, Fu W, Deng Q, Chen D. A comparative study of vision detection and numerical simulation for laser cladding of nickel-based alloy. Journal of Manufacturing Processes. 2017 Aug 1;28:364-72.

409. Zhai L, Ban C, Zhang J, Yao X. Characteristics of dilution and microstructure in laser cladding Ni-Cr-B-Si coating assisted by electromagnetic compound field. Materials Letters. 2019 May 15;243:195-8.

410. Zhao HY, Zhang HT, Xu CH, Yang XQ. Temperature and stress fields of multi-track laser cladding. Transactions of Nonferrous Metals Society of China. 2009 Sep 1;19:s495-501.

411. Zhou S, Dai X, Zeng X. Effects of processing parameters on structure of Ni-based WC composite coatings during laser induction hybrid rapid cladding. Applied Surface Science. 2009 Jul 30;255(20):8494-500.

412. Zhu L, Xue P, Lan Q, Meng G, Ren Y, Yang Z, Xu P, Liu Z. Recent research and development status of laser cladding: A review. Optics & Laser Technology. 2021 Jun 1;138:106915.

413. Abioye TE, McCartney DG, Clare AT. Laser cladding of Inconel 625 wire for corrosion protection. Journal of Materials Processing Technology. 2015 Mar 1;217:232-40.

414. Abioye TE, Folkes J, Clare AT. A parametric study of Inconel 625 wire laser deposition. Journal of Materials Processing Technology. 2013 Dec 1;213(12):2145-51.

415. Aghasibeig, Maniya, and Hasse Fredriksson. “Laser Cladding of a Featureless Iron-Based Alloy.” Surface and Coatings Technology, vol. 209, 2012, pp. 32–37., doi:10.1016/j.surfcoat.2012.08.013.

416. Chiang, K.A., and Y.C. Chen. “Microstructural Characterization and Microscopy Analysis of Laser Cladding Stellite12 and Tungsten Carbide.” Journal of Materials Processing Technology, vol. 182, no. 1-3, 2007, pp. 297–302., doi:10.1016/j.jmatprotec.2006.08.007.

417. Feng K, Chen Y, Deng P, Li Y, Zhao H, Lu F, Li R, Huang J, Li Z. Improved high-temperature hardness and wear resistance of Inconel 625 coatings fabricated by laser cladding. Journal of Materials Processing Technology. 2017 May 1;243:82-91.

418. Lai Q, Abrahams R, Yan W, Qiu C, Mutton P, Paradowska A, Fang X, Soodi M, Wu X. Effects of preheating and carbon dilution on material characteristics of laser-cladded hypereutectoid rail steels. Materials Science and Engineering: A. 2018 Jan 17;712:548-63.

419. Nowotny S, Brueckner F, Thieme S, Leyens C, Beyer E. High-performance laser cladding with combined energy sources. Journal of Laser Applications. 2015 Feb 1;27(S1).

420. Nurminen J, Riihimäki J, Näkki J, Vuoristo P. Comparison of laser cladding with powder and hot and cold wire techniques. InPacific International Conference on Applications of Lasers and Optics 2006 Oct 1. AIP Publishing.

421. Pereira JC, Zambrano JC, Rayón E, Yañez A, Amigó V. Mechanical and microstructural characterization of MCrAlY coatings produced by laser cladding: The influence of the Ni, Co and Al content. Surface and Coatings Technology. 2018 Mar 25;338:22-31.

422. Sexton CL, Byrne G, Watkins KG. Alloy development by laser cladding: an overview. Journal of Laser Applications. 2001 Feb 1;13(1):2-11.

423. St-Georges, L. “Development and Characterization of Composite Ni–Cr+WC Laser Cladding.” Wear, vol. 263, no. 1-6, 2007, pp. 562–566., doi:10.1016/j.wear.2007.02.023.

424. Sun, S., Y. Durandet, and M. Brandt, Correlation between melt pool temperature and clad formation in pulsed and continuous wave Nd:YAG laser cladding of Stellite 6. Proceedings of PICALO. 2004. Melbourne.

425. Tabernero, I., Lamikiz, A., Martínez, S., Ukar, E. and Figueras, J., 2011. Evaluation of the mechanical properties of Inconel 718 components built by laser cladding. International Journal of Machine Tools and Manufacture, 51(6), pp.465-470.

426. Zhu, L., Wang, S., Pan, H., Yuan, C. and Chen, X., 2020. Research on remanufacturing strategy for 45 steel gear using H13 steel powder based on laser cladding technology. Journal of Manufacturing Processes, 49, pp.344-354.

427. Weng F, Yu H, Chen C, Liu J, Zhao L, Dai J, Zhao Z. Effect of process parameters on the microstructure evolution and wear property of the laser cladding coatings on Ti-6Al-4V alloy. Journal of alloys and compounds. 2017 Jan 25;692:989-96.

428. Brandt M, Scott DA, Emms SB, Yellup JM. Laser cladding with a pulsed Nd: YAG laser and optical fibers. Journal of Laser Applications. 1997 Apr 1;9(2):67-75.

429. Candel JJ, Amigó V, Ramos JA, Busquets D. Sliding wear resistance of TiCp reinforced titanium composite coating produced by laser cladding. Surface and Coatings Technology. 2010 Jul 15;204(20):3161-6.

430. Kattire P, Paul S, Singh R, Yan W. Experimental characterization of laser cladding of CPM 9V on H13 tool steel for die repair applications. Journal of Manufacturing Processes. 2015 Oct 1;20:492-9.

431. Yellup, J.M. “Laser Cladding Using the Powder Blowing Technique.” Surface and Coatings Technology, vol. 71, no. 2, 1995, pp. 121–128., doi:10.1016/0257-8972(94)01010-g.

432. Harooni A, Nasiri AM, Gerlich AP, Khajepour A, Khalifa A, King JM. Processing window development for laser cladding of zirconium on zirconium alloy. Journal of Materials Processing Technology. 2016 Apr 1;230:263-71.

433. Pinkerton, Andrew J., and Lin Li. “The Significance of Deposition Point Standoff Variations in Multiple-Layer Coaxial Laser Cladding (Coaxial Cladding Standoff Effects).” International Journal of Machine Tools and Manufacture, vol. 44, no. 6, 2004, pp. 573–584., https://doi.org/10.1016/j.ijmachtools.2004.01.001.

434. Chen L, Zhao Y, Song B, Yu T, Liu Z. Modeling and simulation of 3D geometry prediction and dynamic solidification behavior of Fe-based coatings by laser cladding. Optics & Laser Technology. 2021 Jul 1;139:107009.

435. Partes, Knut. “Analytical Model of the Catchment Efficiency in High Speed Laser Cladding.” Surface and Coatings Technology, vol. 204, no. 3, 2009, pp. 366–371., https://doi.org/10.1016/j.surfcoat.2009.07.041.

436. Donadello S, Furlan V, Demir AG, Previtali B. Interplay between powder catchment efficiency and layer height in self-stabilized laser metal deposition. Optics and Lasers in Engineering. 2022 Feb 1;149:106817.

437. Lin, J., and W.M. Steen. “An in-Process Method for the Inverse Estimation of the Powder Catchment Efficiency during Laser Cladding.” Optics & Laser Technology, vol. 30, no. 2, 1998, pp. 77–84., https://doi.org/10.1016/s0030-3992(98)00007-3.

438. da Silva MD, Partes K, Seefeld T, Vollertsen F. Comparison of coaxial and off-axis nozzle configurations in one step process laser cladding on aluminum substrate. Journal of Materials Processing Technology. 2012 Nov 1;212(11):2514-9.

439. Paul CP, Ganesh P, Mishra SK, Bhargava P, Negi JA, Nath AK. Investigating laser rapid manufacturing for Inconel-625 components. Optics & Laser Technology. 2007 Jun 1;39(4):800-5.

440. Liu S, Zhang Y, Kovacevic R. Numerical simulation and experimental study of powder flow distribution in high power direct diode laser cladding process. Lasers in Manufacturing and Materials Processing. 2015 Dec;2:199-218.

441. Lee, Y. S., M. Nordin, S. S. Babu, and D. F. Farson. "Influence of fluid convection on weld pool formation in laser cladding." Weld. J 93, no. 8 (2014): 292-300.

442. Dalaee M, Cerrutti E, Dey I, Leinenbach C, Wegener K. Parameters development for optimum deposition rate in laser Dmd of stainless steel En x3crnimo13-4. Lasers in Manufacturing and Materials Processing. 2021 Dec:1-7.

443. Bloemer PR, Pacheco JT, Cunha A, Veiga MT, Filho OC, Meura VH, Teixeira MF. Laser cladding of Inconel 625 on AISI 316L: Microstructural and mechanical evaluation of parameters estimated by empirical-statistical model. Journal of Materials Engineering and Performance. 2022 Jan;31(1):211-20.

444. Meng L, Sheng P, Zeng X. Comparative studies on the NI60 coatings deposited by conventional and induction heating assisted extreme-high-speed laser cladding technology: Formability, microstructure and hardness. Journal of Materials Research and Technology. 2022 Jan 1;16:1732-46.

445. Ocelík V, Eekma M, Hemmati I, De Hosson JT. Elimination of Start/Stop defects in laser cladding. Surface and Coatings Technology. 2012 Jan 15;206(8-9):2403-9.

446. Liu, Shuang, and Radovan Kovacevic. “Statistical Analysis and Optimization of Processing Parameters in High-Power Direct Diode Laser Cladding.” The International Journal of Advanced Manufacturing Technology, vol. 74, no. 5-8, 2014, pp. 867–878., https://doi.org/10.1007/s00170-014-6041-y.

447. Sohrabpoor, Hamed. “Analysis of Laser Powder Deposition Parameters: ANFIS Modeling and ICA Optimization.” Optik, vol. 127, no. 8, 2016, pp. 4031–4038., https://doi.org/10.1016/j.ijleo.2016.01.070.

448. Bergant Z, Batič BŠ, Felde I, Šturm R, Sedlaček M. Tribological properties of solid solution strengthened laser cladded NiCrBSi/WC-12Co metal matrix composite coatings. Materials. 2022 Jan 4;15(1):342.

449. Tabernero I, Calleja A, Lamikiz A, De Lacalle LL. Optimal parameters for 5-axis laser cladding. Procedia Engineering. 2013 Jan 1;63:45-52.

450. Zhou C, Zhao S, Wang Y, Liu F, Gao W, Lin X. Mitigation of pores generation at overlapping zone during laser cladding. Journal of materials processing technology. 2015 Feb 1;216:369-74.

451. Gao W, Zhao S, Liu F, Wang Y, Zhou C, Lin X. Effect of defocus manner on laser cladding of Fe-based alloy powder. Surface and Coatings Technology. 2014 Jun 15;248:54-62.

452. Liu S, Farahmand P, Kovacevic R. Optical monitoring of high power direct diode laser cladding. Optics & Laser Technology. 2014 Dec 1;64:363-76.

453. Heigel JC, Gouge MF, Michaleris P, Palmer TA. Selection of powder or wire feedstock material for the laser cladding of Inconel® 625. Journal of Materials Processing Technology. 2016 May 1;231:357-65.

454. Shen F, Tao W, Li L, Zhou Y, Wang W, Wang S. Effect of microstructure on the corrosion resistance of coatings by extreme high speed laser cladding. Applied Surface Science. 2020 Jul 1;517:146085.

455. Lin, Jehnming. “A Simple Model of Powder Catchment in Coaxial Laser Cladding.” Optics & Laser Technology, vol. 31, no. 3, 1999, pp. 233–238., https://doi.org/10.1016/s0030-3992(99)00046-8.

456. Calleja A, Tabernero I, Fernández A, Celaya A, Lamikiz A, De Lacalle LL. Improvement of strategies and parameters for multi-axis laser cladding operations. Optics and Lasers in Engineering. 2014 May 1;56:113-20.

457. Cárcel B, Serrano A, Zambrano J, Amigó V, Cárcel AC. Laser cladding of TiAl intermetallic alloy on Ti6Al4V-process optimization and properties. Physics Procedia. 2014 Jan 1;56:284-93.

458. Tuominen, Jari, Jonne Näkki, Henri Pajukoski, T. Peltola, Petri Vuoristo, M. Kuznetsov, and G. Turichin. "Laser cladding with 15 kW fiber laser." In Proceedings of the 13th NOLAMP Conference in Trondheim, pp. 27-29. Trondheim: Norwegian University of Science and Technology, 2011.

459. Tuominen J, Näkki J, Pajukoski H, Peltola T, Vuoristo P. Recent developments in high power laser cladding techniques. InInternational Congress on Applications of Lasers & Electro-Optics 2012 Sep 1 (Vol. 2012, No. 1, pp. 192-196). Laser Institute of America.

460. Ignat S, Sallamand P, Nichici A, Vannes B, Grevey D, Cicalã E. MoSi2 laser cladding—elaboration, characterisation and addition of non-stabilized ZrO2 powder particles. Intermetallics. 2003 Sep 1;11(9):931-8.

461. Yang L, Yang X, Zhang T, Sun R. Optimization of microstructure and properties of composite coatings by laser cladding on titanium alloy. ceramics International. 2021 Jan 15;47(2):2230-43.

462. Pellizzari M, Zhao Z, Bosetti P, Perini M. Optimizing direct laser metal deposition of H13 cladding on cube alloy substrate. Surface and Coatings Technology. 2022 Feb 25;432:128084.

463. Turichin GA, Zemlyakov EV, Pozdeeva EY, Tuominen J, Vuoristo P. Technological possibilities of laser cladding with the help of powerful fiber lasers. Metal Science and Heat Treatment. 2012 Jul;54:139-44.

464. Govekar E, Jeromen A, Kuznetsov A, Levy G, Fujishima M. Study of an annular laser beam based axially-fed powder cladding process. CIRP annals. 2018 Jan 1;67(1):241-4.

465. Sun S, Durandet Y, Brandt M. Parametric investigation of pulsed Nd: YAG laser cladding of stellite 6 on stainless steel. Surface and Coatings Technology. 2005 May 1;194(2-3):225-31.

466. Kim JD, Lee EJ, Whang JG. Comparison of clad layer characteristics with overlapping criterion in multi pass laser cladding. Journal of Advanced Marine Engineering and Technology. 2016;40(9):768-73.

467. Tuominen J, Näkki J, Pajukoski H, Peltola T, Vuoristo P, Kuznetsov M, Turichin G. Laser cladding with 15 kW fiber laser. InProceedings of the 13th NOLAMP Conference in Trondheim 2011 Jun (pp. 27-29). Trondheim: Norwegian University of Science and Technology.

468. Ge T, Chen L, Gu P, Ren X, Chen X. Microstructure and corrosion resistance of TiC/Inconel 625 composite coatings by extreme high speed laser cladding. Optics & Laser Technology. 2022 Jun 1;150:107919.

469. Barr C, Da Sun S, Easton M, Orchowski N, Matthews N, Brandt M. Influence of macrosegregation on solidification cracking in laser clad ultra-high strength steels. Surface and Coatings Technology. 2018 Apr 25;340:126-36.

470. Han B, Chen Y, Tan C, Jiang M, Bi J, Feng J, Chen X, Chen L, Zhang L, Liu X, Cao L. Microstructure and wear behavior of laser clad interstitial CoCrFeNi high entropy alloy coating reinforced by carbon nanotubes. Surface and Coatings Technology. 2022 Mar 25;434:128241.

471. Ya W, Pathiraj B, Matthews DT, Bright M, Melzer S. Cladding of Tribaloy T400 on steel substrates using a high power Nd: YAG laser. Surface and coatings technology. 2018 Sep 25;350:323-33.

472. Kim, Jong Do, Eun Jin Lee, and Cheol Gyu Kim. "Study on Laser Cladding of Heat Resisting Steel Using EuTroLoy 16006 Powder (II)-Characteristics of Alloying Elements Distribution of Multi Pass Clad Layer." Transactions of the Korean Society of Mechanical Engineers A 41, no. 4 (2017): 307-312.

473. Salehi, D., and M. Brandt. “Melt Pool Temperature Control Using Labview in Nd:YAG Laser Blown Powder Cladding Process.” The International Journal of Advanced Manufacturing Technology, vol. 29, no. 3-4, 2005, pp. 273–278., https://doi.org/10.1007/s00170-005-2514-3.

474. Zhong C, Pirch N, Gasser A, Poprawe R, Schleifenbaum JH. The influence of the powder stream on high-deposition-rate laser metal deposition with inconel 718. Metals. 2017 Oct 20;7(10):443.

475. DebRoy T, Wei HL, Zuback JS, Mukherjee T, Elmer JW, Milewski JO, Beese AM, Wilson-Heid AD, De A, Zhang W. Additive manufacturing of metallic components–process, structure and properties. Progress in Materials Science. 2018 Mar 1;92:112-224.

476. Riveiro A, Mejías A, Lusquiños F, Del Val J, Comesaña R, Pardo J, Pou J. Laser cladding of aluminium on AISI 304 stainless steel with high-power diode lasers. Surface and Coatings Technology. 2014 Aug 25;253:214-20.

477. Vetter PA, Engel T, Fontaine J. Laser cladding: the relevant parameters for process control. InLaser Materials Processing: Industrial and Microelectronics Applications 1994 Sep 7 (Vol. 2207, pp. 452-462). SPIE.

478. Vetter, P. A., J. Fontaine, Th Engel, L. Lagrange, and T. Marchione. "Characterization of laser-material interaction during laser cladding process." WIT Transactions on Engineering Sciences 2 (1970).

479. Li, W-B., Hans Engström, John Powell, Z. Tan, and Claes Magnusson. "Redistribution of the beam power in laser cladding by powder injection." Lasers in engineering (Print) 5, no. 3 (1996): 175-183.

480. Brenner SS, Wriedt HA, Oriani RA. Impact adhesion of iron at elevated temperatures. Wear. 1981 May 1;68(2):169-90.

481. Hoadley, A. F., and M. Rappaz. “A Thermal Model of Laser Cladding by Powder Injection.” Metallurgical Transactions B, vol. 23, no. 5, 1992, pp. 631–642., https://doi.org/10.1007/bf02649723.

482. Jones, H. “Cooling, Freezing and Substrate Impact of Droplets Formed by Rotary Atomization.” Journal of Physics D: Applied Physics, vol. 4, no. 11, 1971, pp. 1657–1660., https://doi.org/10.1088/0022-3727/4/11/206.

483. Picasso M, Marsden CF, Wagniere JD, Frenk A, Rappaz M. A simple but realistic model for laser cladding. Metallurgical and materials transactions B. 1994 Apr;25:281-91.

484. Trapaga, Gerardo, and Julian Szekely. “Mathematical Modeling of the Isothermal Impingement of Liquid Droplets in Spraying Processes.” Metallurgical and Materials

Transactions B, vol. 22, no. 6, 1991, pp. 901–914., https://doi.org/10.1007/bf02651166.

485. Zimon, Anatolii D. “Adhesion of Dust and Powder.” 1982, https://doi.org/10.1007/978-1-4615-8576-3.

486. Chacón JM, Caminero MA, García-Plaza E, Núnez PJ. Additive manufacturing of PLA structures using fused deposition modelling: Effect of process parameters on mechanical properties and their optimal selection. Materials & Design. 2017 Jun 15;124:143-57.

487. Johnson L, Mahmoudi M, Zhang B, Seede R, Huang X, Maier JT, Maier HJ, Karaman I, Elwany A, Arróyave R. Assessing printability maps in additive manufacturing of metal alloys. Acta Materialia. 2019 Sep 1;176:199-210.

488. Khorasani AM, Gibson I, Ghasemi A, Ghaderi A. A comprehensive study on variability of relative density in selective laser melting of Ti-6Al-4V. Virtual and Physical Prototyping. 2019 Oct 2;14(4):349-59.

489. Moghaddam AO, Shaburova NA, Samodurova MN, Abdollahzadeh A, Trofimov EA. Additive manufacturing of high entropy alloys: A practical review. Journal of Materials Science & Technology. 2021 Jun 30;77:131-62.

490. Carty S, Owen I, Steen WM, Bastow B, Spencer JT. Catchment efficiency for novel nozzle designs used in laser cladding and alloying. Laser processing: surface treatment and film deposition. 1996:395-410.

491. Cacace S, Furlan V, Sorci R, Semeraro Q, Boccadoro M. Using recycled material to produce gas-atomized metal powders for additive manufacturing processes. Journal of Cleaner Production. 2020 Sep 20;268:122218.

492. Li T, Zhang L, Bultel GG, Schopphoven T, Gasser A, Schleifenbaum JH, Poprawe R. Extreme high-speed laser material deposition (EHLA) of AISI 4340 steel. Coatings. 2019 Nov 21;9(12):778.

493. Al-Hamdani KS, Murray JW, Hussain T, Clare AT. Controlling ceramic-reinforcement distribution in laser cladding of MMCs. Surface and Coatings Technology. 2020 Jan 15;381:125128.

494. Ya W, Pathiraj B, Liu S. 2D modelling of clad geometry and resulting thermal cycles during laser cladding. Journal of materials processing technology. 2016 Apr 1;230:217-32.

495. Huang Y, Khamesee MB, Toyserkani E. A comprehensive analytical model for laser powder-fed additive manufacturing. Additive Manufacturing. 2016 Oct 1;12:90-9.

496. Panda BK, Sarkar S, Nath AK. 2D thermal model of laser cladding process of Inconel 718. Materials Today: Proceedings. 2021 Jan 1;41:286-91.

497. Chai Q, Wang Z, Fang C, Xing Y, Qiu X, Zhou Z. Numerical and experimental study on the profile of metal alloys formed on the inclined substrate by laser cladding. Surface and Coatings Technology. 2021 Sep 25;422:127494.

498. Lin, Jehnming, and Bor-Chyang Hwang. “Coaxial Laser Cladding on an Inclined Substrate.” Optics & Laser Technology, vol. 31, no. 8, 1999, pp. 571–578., https://doi.org/10.1016/s0030-3992(99)00116-4.

499. Farahmand, Parisa, and Radovan Kovacevic. “Laser Cladding Assisted with an Induction Heater (LCAIH) of Ni–60%Wc Coating.” Journal of Materials Processing Technology, vol. 222, 2015, pp. 244–258., https://doi.org/10.1016/j.jmatprotec.2015.02.026.

500. Lin, J., and W. M. Steen. “Design Characteristics and Development of a Nozzle for Coaxial Laser Cladding.” Journal of Laser Applications, vol. 10, no. 2, 1998, pp. 55–63., https://doi.org/10.2351/1.521821.

501. Yan J, Battiato I, Fadel G. Design of injection nozzle in direct metal deposition (DMD) manufacturing of thin-walled structures based on 3D models. The International Journal of Advanced Manufacturing Technology. 2017 Jul;91:605-16.

502. Cortina M, Arrizubieta JI, Ruiz JE, Lamikiz A, Ukar E. Design and manufacturing of a protective nozzle for highly reactive materials processing via Laser Material Deposition. Procedia Cirp. 2018 Jan 1;68:387-92.

503. Leunda J, Sanz C, Soriano C. Laser cladding strategies for producing WC reinforced NiCr coatings inside twin barrels. Surface and Coatings Technology. 2016 Dec 15;307:720-7.

504. Zhang K, Liu W, Shang X. Research on the processing experiments of laser metal deposition shaping. Optics & Laser Technology. 2007 Apr 1;39(3):549-57.

505. Sun SD, Leary M, Liu Q, Brandt M. Evaluation of microstructure and fatigue properties in laser cladding repair of ultrahigh strength AerMet® 100 steel. Journal of Laser Applications. 2015 Feb 1;27(S2).

506. Arias-González F, Del Val J, Comesaña R, Penide J, Lusquiños F, Quintero F, Riveiro A, Boutinguiza M, Pou J. Fiber laser cladding of nickel-based alloy on cast iron. Applied Surface Science. 2016 Jun 30;374:197-205.

507. Calleja A, Urbikain G, González H, Cerrillo I, Polvorosa R, Lamikiz A. Inconel® 718 superalloy machinability evaluation after laser cladding additive manufacturing process. The International Journal of Advanced Manufacturing Technology. 2018 Jul;97:2873-85.

508. Brandt, M., D. A. Scott, S. B. Emms, and J. M. Yellup. "Laser cladding with a pulsed Nd: YAG laser and optical fibers." Journal of Laser Applications 9, no. 2 (1997): 67-75.

509. Ocelík V, Nenadl O, Palavra A, De Hosson JT. On the geometry of coating layers formed by overlap. Surface and Coatings Technology. 2014 Mar 15;242:54-61.

510. Arias-González F, del Val J, Comesaña R, Penide J, Lusquiños F, Quintero F, Riveiro A, Boutinguiza M, Pou J. Production of phosphor bronze coatings by laser cladding. Procedia Manufacturing. 2017 Jan 1;13:177-82.

511. Frenk A, Vandyoussefi M, Wagnière JD, Kurz W, Zryd A. Analysis of the laser-cladding process for stellite on steel. Metallurgical and Materials transactions B. 1997 Jun;28:501-8.

512. Yuan W, Li R, Chen Z, Gu J, Tian Y. A comparative study on microstructure and properties of traditional laser cladding and high-speed laser cladding of Ni45 alloy coatings. Surface and Coatings Technology. 2021 Jan 15;405:126582.

513. Yang J, Bai B, Ke H, Cui Z, Liu Z, Zhou Z, Xu H, Xiao J, Liu Q, Li H. Effect of metallurgical behavior on microstructure and properties of FeCrMoMn coatings prepared by high-speed laser cladding. Optics & Laser Technology. 2021 Dec 1;144:107431.

514. Chen C, Lian G, Jiang J, Wang Q. Simplification and experimental investigation of geometrical surface smoothness model for multi-track laser cladding processes. Journal of Manufacturing Processes. 2018 Dec 1;36:621-8.

515. Zhang, Peirong, and Zhanqiang Liu. “Effect of Sequential Turning and Burnishing on the Surface Integrity of Cr–Ni-Based Stainless Steel Formed by Laser Cladding Process.” Surface and Coatings Technology, vol. 276, 2015, pp. 327–335., https://doi.org/10.1016/j.surfcoat.2015.07.026.

516. Chen L, Zhang X, Wu Y, Chen C, Li Y, Zhou W, Ren X. Effect of surface morphology and microstructure on the hot corrosion behavior of TiC/IN625 coatings prepared by extreme high-speed laser cladding. Corrosion Science. 2022 Jun 1;201:110271.

517. LUBASZKA, PIOTR, and BERND BAUFELD. "Study on powder blown laser cladding of vertical surfaces." The Laser User 87 (2018): 18-19.

518. LUBASZKA, PIOTR, and BERND BAUFELD. "Powder Blown Laser Cladding of Vertical Surfaces." Lasers in Engineering (Old City Publishing) 39 (2018).

519. Tuominen, Jari. "Engineering coatings by laser cladding-the study of wear and corrosion properties." (2009).

520. Hongnan Zhang, Tuominen, Jari, Marc Kaubisch, Sebastian Thieme, Jonne Näkki, Steffen Nowotny, and Petri Vuoristo. "Laser strip cladding for large area metal deposition." Additive Manufacturing 27 (2019): 208-216.

521. Du C, Hu L, Ren X, Li Y, Zhang F, Liu P, Li Y. Cracking mechanism of brittle FeCoNiCrAl HEA coating using extreme high-speed laser cladding. Surface and Coatings Technology. 2021 Oct 25;424:127617.

522. Ren Y, Li L, Zhou Y, Wang S. In situ synthesized VC reinforced Fe-based coating by using extreme high-speed laser cladding. Materials Letters. 2022 May 15;315:131962.

523. Tuominen J, Näkki J, Pajukoski H, Peltola T, Vuoristo P, Kuznetsov M, Turichin G. Laser cladding with 15 kW fiber laser. In Proceedings of the 13th NOLAMP Conference in Trondheim 2011 Jun (pp. 27-29). Trondheim: Norwegian University of Science and Technology.

11 Appendix A

11.1 High speed image processing code

```
# -*- coding: utf-8 -*-

"""

Created on Tue Jun 28 09:52:06 2022


@author: dkoti

"""



#----------------------------------------------------------------load packages

import matplotlib.pyplot as plt

import numpy as np

import cv2


from scipy import ndimage as ndi

from skimage import filters

from scipy.ndimage.filters import gaussian_filter

from openpiv import tools, pyprocess, validation, filters, scaling

#import math


#------------------------------------------------------------------------------#


plt.close("all")
```

```
#-----------------------------------------------------create high pass filter zz (don't delete the next 5 lines)
rows, cols =616, 1280
crow,ccol = np.int_(rows/2) , np.int_(cols/2)
zz=np.zeros((rows, cols))
zz[crow-150:crow+150, ccol-300:ccol+300] = 1
zz= gaussian_filter(zz, sigma=13)



min_size = 6



# The video feed is read in as a VideoCapture object
cap = cv2.VideoCapture('C:/Users/dkoti/Desktop/Cladding/project3.avi')
param=np.loadtxt ('test1.txt')

count = 0
# ret = a boolean return value from getting the frame
ret, first_frame = cap.read()

#-----------------------------------------------------load image 0 and label it as imageA
prev_gray = cv2.cvtColor(first_frame, cv2.COLOR_BGR2GRAY)
imageA=np.copy(prev_gray)
```

```
#-------------------------------image preprocessing (step 1 but only with one image just to see how it works)


neighborhood = ndi.morphology.generate_binary_structure(2,2)

local_max = ndi.filters.maximum_filter(np.copy(prev_gray) , footprint=neighborhood)

# plt.figure()

# plt.imshow(prev_gray, cmap='gray', vmin=0, vmax=200)

# plt.figure()

# plt.imshow(prev_gray[400:660,400:600], cmap='gray', vmin=0, vmax=200)

# plt.figure()

# plt.imshow(local_max , cmap='gray', vmin=0, vmax=200)

# plt.figure()

# plt.imshow(local_max[400:660,400:600] , cmap='gray', vmin=0, vmax=200)

# pg=np.copy(prev_gray)


#compute background intensity distribution and subtract it

bl0=cv2.blur(np.copy(prev_gray), (3,3)) #denoised(maybe replace with wavelet decomp)

bl0=bl0.astype('float32')

bl1=cv2.blur(np.copy(bl0), (45,45)) #treshold map

bl1=bl1.astype('float32')

# plt.figure()

# plt.imshow(bl1 , cmap='gray', vmin=0, vmax=120)

# plt.figure()
```

```
# plt.imshow(bl1[400:660,400:600] , cmap='gray', vmin=0, vmax=120)
B=bl0-bl1
# plt.figure()
# plt.imshow(B , cmap='gray', vmin=0, vmax=60)
# plt.figure()
# plt.imshow(B[400:660,400:600] , cmap='gray', vmin=0, vmax=60)

# fft to convert the image to freq domain
f = np.fft.fft2(B)
# shift the center
fshift = np.fft.fftshift(f)
# apply high pass filter and shift back(we shifted the center before)
f_ishift = np.fft.ifftshift(fshift*zz)

# inverse fft to get the image back hopefully without noise
img_back = np.fft.ifft2(f_ishift)
img_back = np.abs(img_back)

# plt.figure()
# plt.imshow(zz,cmap='gray')
# plt.figure()
# plt.imshow(img_back , cmap='gray', vmin=10, vmax=60)
# plt.figure()
# plt.imshow(img_back[400:660,400:600] , cmap='gray', vmin=10, vmax=60)
```

```
#compute background intensity, second round
bl0=cv2.blur(np.copy(img_back), (3,3)) #denoised
bl0=bl0.astype('float32')
bl1=cv2.blur(np.copy(bl0), (85,85)) #treshold map
bl1=bl1.astype('float32')

#use threshold value to create particle binary image
pg=np.copy(img_back)
pg[pg>=10*bl1]=255
pg[pg<10*bl1]=0
pg=pg.astype('uint8')



# plt.figure()
# plt.imshow(pg , cmap='gray', vmin=0, vmax=60)
# plt.figure()
# plt.imshow(pg[400:660,400:600] , cmap='gray', vmin=0, vmax=60)

#counting particles as in:
#https://stackoverflow.com/questions/72118665/particle-detection-with-python-opencv
nb_components, output, stats, centroids = cv2.connectedComponentsWithStats(pg.astype('uint8'), connectivity=8)
sizes = stats[1:, -1]
nb_components = nb_components - 1
```

```
# # for every component in the image, you keep it only if it's above min_size
min_size = 6
for i in range(0, nb_components):
    if sizes[i] < min_size:
        pg[output == i + 1] = 0
nb_components, output, stats, centroids = cv2.connectedComponentsWithStats(pg, connectivity=8)
sizes = stats[1:, -1]
nb_components = nb_components - 1
print(nb_components)



#------------------------------ ----------END OF IMAGE PREPROCESSING EXAMPLE
# make sure to not delete imageA!!




# the code starts here (think how to name the processing code)
#------------------------------ ----------------------------------------------functions used along the code


###now write the preprocessing lines as function and check computaion is ok
def twolevelblur(im,c1,c2):
```

```
    bl0=cv2.blur(np.copy(im), (c1,c1)) #denoised(maybe replace with wavelet decomp)
    bl0=bl0.astype('float32')
    bl1=cv2.blur(np.copy(bl0), (c2,c2)) #treshold map
    bl1=bl1.astype('float32')
    return bl0,bl1


def countdrops(im,minsize):
    nb_components, output, stats, centroids = cv2.connectedComponentsWithStats(im.astype('uint8'), connectivity=8)
    sizes = stats[1:, -1]
    nb_components = nb_components - 1
    for i in range(0, nb_components):
        if sizes[i] < min_size:
            im[output == i + 1] = 0
    nb_components, output, stats, centroids = cv2.connectedComponentsWithStats(im.astype('uint8'), connectivity=8)
    sizes = stats[1:, -1]
    nb_components = nb_components - 1
    return(nb_components)


def find_metal_droplets(inputim, freqfilter, g1,g2,g3,th,minsize):
    im=np.copy(inputim)
    bl0,bl1=twolevelblur(im,g1,g2)
    f = np.fft.fft2(bl0-bl1)
    fshift = np.fft.fftshift(f)
```

```
    f_ishift = np.fft.ifftshift(fshift*zz)
    img_back = np.fft.ifft2(f_ishift)
    img_back = np.abs(img_back)
    bl0,bl1=twolevelblur(img_back ,g1,g3)
    drops=np.copy(bl0)
    #local_max = ndi.filters.maximum_filter(np.copy(drops) , footprint=neighborhood)
    drops[drops >=th*bl1]=255
    drops[drops <th*bl1]=0
    dnumber=countdrops(np.copy(drops),minsize)
    #print(dnumber)
    return(drops,dnumber)



#------------------------------  ----------------------------------------------parameters needed for step 1
thresh=10
g1=3
g2=45
g3=85
thsize=6

#check if functions work
#drops,dnumber=find_metal_droplets(prev_gray, zz, g1,g2,g3,thresh,thsize)
#print(dnumber)
#plt.figure()
```

```
#plt.imshow(drops)


#------------------------------  ----------------------------------------------parameters needed for step 2



#Optical FLow
of_win=24
mask = np.zeros_like(first_frame)
mask[..., 1] = 255

#PIV
winsize = 100 # pixels, interrogation window size in frame A
searchsize = 120  # pixels, search in image B
overlap = 50 # pixels, 50% overlap
dt_piv = 1 # sec, time interval between pulses
x, y = pyprocess.get_coordinates(prev_gray.shape, searchsize,overlap )
not_physical_value=45 #not physical displacemnt in pixels



#variables to store results
particle_number_list=[]
velocity_u_list=[]
velocity_v_list=[]
particle_size_list=[]
```

```
particle_av=np.zeros(np.shape(imageA))
OF_u_av=np.zeros(np.shape(imageA))
OF_v_av=np.zeros(np.shape(imageA))
mask_of_av=np.zeros(np.shape(imageA))

u2_av=np.zeros(np.shape(imageA))
v2_av=np.zeros(np.shape(imageA))
exclude_av=np.zeros(np.shape(imageA))

OF_u_av_no_filter=np.zeros(np.shape(imageA))
OF_v_av_no_filter=np.zeros(np.shape(imageA))



while(cap.isOpened()):

    ret, frame = cap.read()
    if ret:
        cv2.imshow("input", frame)
        count = count + 1
        print(count)
        gray = cv2.cvtColor(frame, cv2.COLOR_BGR2GRAY)
```

```
        imageB=np.copy(gray)

    ##### ----------------------------------------------------------------------STEP1 find droplet
        drops,dnumber=find_metal_droplets(imageB, zz, g1,g2,g3,thresh,thsize)

    # Opens a new window and check results
        cv2.imshow("only droplets", drops)

    ##### ----------------------------------------------------------------------STEP2 optical flow
    ### the results of optical flow computation are used for the velocity of escaping particles

        flow = cv2.calcOpticalFlowFarneback(imageA, imageB, None, 0.5, 3, of_win, 3, 5, 1.2,
0)
    # Computes the magnitude and angle of the 2D vectors
        OF_u=np.copy(flow[..., 0]) #pixels
        OF_v=np.copy(flow[..., 1]) #pixels
        magnitude, angle = cv2.cartToPolar(flow[..., 0], flow[..., 1])
        mask[..., 0] = angle * 180/np.pi
        mask[..., 2] = cv2.normalize(magnitude, None, 0, 255, cv2.NORM_MINMAX)
        # Converts HSV to RGB (BGR) color representation
        rgb = cv2.cvtColor(mask, cv2.COLOR_HSV2BGR)
        gim_of=cv2.cvtColor(rgb, cv2.COLOR_BGR2GRAY)
        mask_of=np.copy(gim_of)
        mask_of[gim_of<=2]=0
        mask_of[gim_of>2]=255
```

```
        #draw results
        # drawof=np.copy(OF_u)
        # drawof[mask_of==0]=0
        # plt.figure()
        # plt.imshow( drawof,cmap='gray', vmin=-10, vmax=10)
        # plt.colorbar()



    # Opens a new window and check results
        #cv2.imshow("dense optical flow", rgb)


    ##### ----------------------------------------------------------------------STEP2 PIV
    ### the results of PIV computation are used for the velocity of central jet


        #compute vectors
        u0, v0, sig2noise = pyprocess.extended_search_area_piv(imageA.astype(np.int32), imageB.astype(np.int32),
                                                window_size=winsize, overlap=overlap, dt=dt_piv,
                                                search_area_size=searchsize, sig2noise_method='peak2peak')
        u1, v1, maskp = validation.sig2noise_val( u0, v0, sig2noise,  threshold = 1.05 )
        u2, v2 = filters.replace_outliers( u1, v1, method='localmean', max_iter=3, kernel_size=3)
        #x, y, u3, v3 = scaling.uniform(x, y, u1, v1, scaling_factor = 1 )
        # plt.figure()
```

```
        # plt.imshow(v2)


        # drawpv=np.copy(v2)
        # plt.figure()
        # plt.imshow( drawpv,cmap='gray', vmin=-40, vmax=0)
        # plt.colorbar()


    #####----------------------------------------------------------------------------STEP 3: velocity vectors to particles


        OF_v_neg=np.copy(OF_v)*(-1)
        ## right side  (using OF)
        mask_right=np.zeros(imageA.shape)
        mask_right[:,np.int_(param[1]):imageA.shape[1]]=255

drops_right=cv2.bitwise_and(mask_right.astype('uint8'),np.copy(drops).astype('uint8'))
        #plt.imshow(drops_right)
        drops_right=cv2.bitwise_and(drops_right.astype('uint8'),mask_of.astype('uint8'))
        #plt.imshow(drops_right)
        drops_right[drops_right>0]=1
        drops_right_u=drops_right*OF_u
        drops_right_v=drops_right*OF_v_neg


        ## left side (using OF)
        mask_left=np.zeros(imageA.shape)
```

```
mask_left[:,0:np.int_(param[0])]=255
drops_left=cv2.bitwise_and(mask_left.astype('uint8'),np.copy(drops).astype('uint8'))
drops_left=cv2.bitwise_and(drops_left.astype('uint8'),mask_of.astype('uint8'))
drops_left[drops_left>0]=1
drops_left_u=drops_left*OF_u
drops_left_v=drops_left*OF_v_neg


##mask center
H=np.int_(param[2])
mask_center=np.zeros(imageA.shape)
# points to be cropped
roi_corners = np.array([[(np.int_(param[0]), 0), (np.int_(param[3]), H), (np.int_(param[4]), H), (np.int_(param[1]), 0) ]], dtype=np.int32) #change this
# fill the ROI into the mask
cv2.fillPoly(mask_center, roi_corners, 255)


## center (using PIV)
dim=(imageA.shape[1],imageA.shape[0])
u2 = cv2.resize(u2, dim, interpolation = cv2.INTER_AREA)*0.5
v2 = cv2.resize(v2, dim, interpolation = cv2.INTER_AREA)*0.5
exclude=1+np.zeros(imageA.shape)
exclude[abs(u2)>not_physical_value]=0
exclude[abs(v2)>not_physical_value]=0
```

```
drops_center=cv2.bitwise_and(mask_center.astype('uint8'),np.copy(drops).astype('uint8'))
        drops_center[drops_center>0]=1
        drops_center_u=drops_center*u2*exclude
        drops_center_v=drops_center*v2*exclude
        # drawpv=np.copy(v2)
        # plt.figure()
        # plt.imshow( drawpv,cmap='gray', vmin=-40, vmax=0)
        # plt.colorbar()



        ## center (using OF)
        #
drops_center=cv2.bitwise_and(mask_center.astype('uint8'),np.copy(drops).astype('uint8'))
        # drops_center=cv2.bitwise_and(drops_center.astype('uint8'),mask_of.astype('uint8'))
        # drops_center[drops_center>0]=1
        # drops_center_u=drops_center*OF_u
        # drops_center_v=drops_center*OF_v



        #merge left, right, center info
        mask_drops=drops_left+drops_right+drops_center
        drops_U=drops_right_u+drops_left_u+drops_center_u
        drops_V=drops_right_v+drops_left_v+drops_center_v
```

```
    #find unique value u,v for each particle
    drops_U_1val=np.zeros(np.copy(drops_U).shape)
    drops_V_1val=np.zeros(np.copy(drops_V).shape)
    numLabels, labels, stats, centroids = cv2.connectedComponentsWithStats(mask_drops, connectivity=8)
    x_list=[]
    y_list=[]
    v_list=[]
    u_list=[]

    for i in range(1, numLabels):
       #print(i)
       component_mask=np.zeros(labels.shape)
       component_mask[labels==i]=1

       u_values=np.copy(drops_U)*(component_mask)
       av_u =  u_values[np.nonzero(u_values)].mean()
       drops_U_1val=drops_U_1val+av_u*component_mask

       v_values=np.copy(drops_V)*component_mask
       av_v = v_values[np.nonzero(v_values)].mean()
       drops_V_1val=drops_V_1val+av_v*component_mask
```

```
    x_list.append(centroids[i,0])
    y_list.append(centroids[i,1])
    u_list.append(av_u )
    v_list.append(av_v )

alpha=0.5
blend= drops_V*alpha+mask_drops*( 1.0 - alpha )

# plt.figure()
# imp=plt.imshow(blend)
# vep=plt.quiver(x_list,y_list, u_list, v_list,color=['red'], scale=160)
# plt.show()
# plt.figure()
# imp=plt.imshow(gray,cmap='gray', )
# vep=plt.quiver(x_list,y_list, u_list, v_list,color=['red'], scale=120)
# plt.show()


##### ----------------------------------------------------------------------STEP 4 mass rate
#minimum size in pixel to consider a particle
p_size=2

#  number of particles and average velocity in kozpont
```

```
N=countdrops(drops_center,p_size)

N_size=np.count_nonzero(drops_center)

N_u=drops_center_u[np.nonzero(drops_center_u)].mean()

N_v=drops_center_v[np.nonzero(drops_center_v)].mean()


#  number of particles and average velocity  jobbra

n_right=countdrops(drops_right,p_size)

n_right_size=np.count_nonzero(drops_right)

n_right_u=drops_right_u[np.nonzero(drops_right_u)].mean()

n_right_v=drops_right_v[np.nonzero(drops_right_v)].mean()


#  number of particles and average velocity  balra

n_left=countdrops(drops_left,p_size)

n_left_size=np.count_nonzero(drops_left)

n_left_u=drops_right_u[np.nonzero(drops_right_u)].mean()

n_left_v=drops_right_v[np.nonzero(drops_right_v)].mean()



#record particle number for each area and for each image in a unique array

particle_array=N,n_right,n_left

print(particle_array)

particle_number_list.append(np.array(particle_array))


#record  particle size
```

```
size_array=N_size,n_right_size,n_left_size
particle_size_list.append(np.array(size_array))

#record average velocity for each area and for each image in a unique array
velocity_u_array=N_u,n_right_u,n_left_u
velocity_v_array=N_v,n_right_v,n_left_v
velocity_u_list.append(np.array(velocity_u_array))
velocity_v_list.append(np.array(velocity_v_array))



#### FINAL PART: average of velocity



#summing up particles
particle_av=particle_av+mask_drops

#left and right, Optical Flow velocities
OF_u_av_no_filter=OF_u_av_no_filter+OF_u
OF_v_av_no_filter=OF_v_av_no_filter+OF_v

OF_u_av=OF_u_av+OF_u*(mask_left/255+mask_right/255)*mask_of/255
OF_v_av=OF_v_av+OF_v_neg*(mask_left/255+mask_right/255)*mask_of/255
mask_of_av=mask_of_av+(mask_left/255+mask_right/255)*mask_of/255
```

```
        #to use for average: center values, PIV velocities
        u2_av=u2_av+u2*(mask_center/255)*exclude
        v2_av=v2_av+v2*(mask_center/255)*exclude
        exclude_av=exclude_av+exclude*(mask_center/255)



        # Updates previous frame
        imageA=np.copy(imageB)

        #delete images every 10, to not crash RAM
        if count % 10 ==0:
            plt.close("all")

        if cv2.waitKey(1) & 0xFF == ord('q'):
            break
    else:
        break
## np.array(particle_number_list)

cap.release()
cv2.destroyAllWindows()

## compute averaged quantities
```

```
#conversion factors
M= 0.0175 #mm/px
dt= 1/102400 # seconds
density=8000 #kg/m3
density_air=1 #kg/m3

#velcity in central area
velocity_u_list=np.array(velocity_u_list)*M/(dt*1000) #m/s
velocity_v_list=np.array(velocity_v_list)*M/(dt*1000) #m/s
#average velocity
V=velocity_v_list[:,0].mean()


#volume of cylinder
r=0.002 #m
h=H*M/1000  #m
vol=np.pi*r*r*h   #m^3


#density inside cilinder
P=np.array(particle_number_list)
NN=P[:,0].mean() # average number of particles
particle_size_list=np.array(particle_size_list)
```

```
S=particle_size_list[:,0].mean()/NN # average particle size in pixel (area on image)

r_particle=(M/1000)*pow((S/np.pi),0.5) # radius of particle in meters

particle_average_volume=(4/3)*np.pi*pow(r_particle,3) #m3, assuming particle is spherical

particle_total_volume=particle_average_volume*NN   #m^3

particle_volume_fraction=particle_total_volume/vol

air_volume_fraction=(vol-particle_total_volume)/vol

density_av=particle_volume_fraction*density+air_volume_fraction*density_air


#mass flow rate in kilogram per seconds

A=np.pi*pow(r,2)

mass_rate=1000* density_av*A*(-V)  #  grams per second

print('mass rate = ' , mass_rate, '  g/s')



#compute averages, visualize particles



#Optical Flow (left, right)

Uesc=OF_u_av/mask_of_av

Vesc=OF_v_av/mask_of_av
```

```
#PIV (center)

Ujet=u2_av/exclude_av

Vjet=v2_av/exclude_av


#overal U and V

Uesc[np.isnan(Uesc)]=0

Vesc[np.isnan(Vesc)]=0

Ujet[np.isnan(Ujet)]=0

Vjet[np.isnan(Vjet)]=0



U=Uesc+Ujet

V=Vesc+Vjet


#velocity magnitude

VM= (U**2+V**2)**0.5


xl = np.linspace(0, VM.shape[1], VM.shape[1])

yl = np.linspace(0, VM.shape[0], VM.shape[0])

xv, yv = np.meshgrid(xl, yl, indexing='xy')
```

```
#VISUALIZATION ################

# option 1

#this one is simply plotting the sum of all optical flow computayions.
# it doesn't have a quantitative meaning, but it is usefull to see where particles go for every configaration

OF_VM= (OF_u_av_no_filter**2+OF_v_av_no_filter**2)**0.5
plt.figure()
plt.imshow(OF_VM,cmap='gray')

#option 2

#this one plots all the particles found during the processing of the video in one image only.

plt.figure()
plt.imshow(particle_av,cmap='gray',vmin=0, vmax=count/10)

#VECTOR FIELD ################

#option 1
#this one overlap average vector field and velocity magnitude
plt.figure()
```

```
plt.imshow(VM)

skip=20

plt.quiver(xv[::skip,::skip],yv[::skip,::skip],U[::skip,::skip],V[::skip,::skip],color=['red'])


#option 2

#this one overlap average vector field and particles

plt.figure()

plt.imshow(particle_av,cmap='gray',vmin=0, vmax=count/10)

skip=20

plt.quiver(xv[::skip,::skip],yv[::skip,::skip],U[::skip,::skip],V[::skip,::skip],color=['red'])



#option 3

#this one overlap average vector field and sum of Optical Flow results (again, only qualitative)

plt.figure()

plt.imshow(OF_VM)

skip=30

plt.quiver(xv[::skip,::skip],yv[::skip,::skip],U[::skip,::skip],V[::skip,::skip],color=['red'])



#option 4

#this one overlap average vector field (without zero vectors) and velocity magnitude


mask_z=np.copy(particle_av)
```

```
mask_z[mask_z>0]=1


Xf = xv[mask_z.astype(bool)]

Yf = yv[mask_z.astype(bool)]

Uf = U[mask_z.astype(bool)]

Vf = V[mask_z.astype(bool)]


plt.figure()

plt.imshow(particle_av, cmap='gray',vmin=0, vmax=count/10)

skip=40

plt.quiver(Xf[::skip],Yf[::skip],Uf[::skip],Vf[::skip],color=['red'],scale=120)# width=0.001, headwidth=4)

#parameter explanation for quiver plot

#https://matplotlib.org/stable/api/_as_gen/matplotlib.pyplot.quiver.html


plt.figure()

plt.imshow(particle_av, cmap='gray',vmin=0, vmax=count/10)

skip=40

plt.quiver(Xf[::skip],Yf[::skip],Uf[::skip],Vf[::skip], np.arctan2(Uf[::skip], Vf[::skip]), scale=120)

plt.colorbar()

#coloring vectors with angle values: https://stackoverflow.com/questions/40026718/different-colours-for-arrows-in-quiver-plot
```